ANALYSIS OF RESIDUAL STRESS AND FATIGUE CRACK PROPAGATION BEHAVIOUR IN LASER WELDED AEROSPACE ALUMINIUM T-JOINTS

Vom Promotionsausschuss der
Technischen Universität Hamburg-Harburg
zur Erlangung des Akademischen Grades
Doktor-Ingenieurin
genehmigte Dissertation

von
Funda Şeniz Bayraktar

aus
Ankara, Türkei

2011

1. Gutachter: Prof. Dr.-Ing. Norbert Huber
2. Gutachter: Prof. Dr. Andreas Schreyer

Tag der Mündlichen Prüfung: 02. November 2011

Acknowledgement

This PhD work was conducted at the GKSS Research Centre using the aluminium alloys and laser beam welded materials which were generated within the framework of two projects, namely EU funded project "WEL-AIR – Development of Short Distance Welding Concepts for Airframes" and "HGF Virtual Institute PNAM – Photon and Neutron Research on Advanced Engineering Materials".

I would like to express my sincere gratitute to Dr. Mustafa Koçak for his invaluable guidance to establish scientific and experimental framework of this study as well as for his advice and comments on the thesis.

I am grateful to Prof. A. Schreyer, Dr. P. Staron for their invaluable advice and guidance during this work. I wish to express my thanks to Prof. N. Huber for his continuous support during this study.

I wish also to thank my colleagues Mr. M. Horstmann, Mr. S. Riekehr, Mr. H. Tek and Mr. R. Dinse for their technical supports in fatigue tests and laser welds.

Last but not least my special thanks go to my husband Mehmet and my sweet son Doruk who showed great patient and were source of continuous support and encouragement throughout the entire time of this work.

Funda Şeniz Bayraktar, November 2011

Table of Content

1 Introduction

The aerospace industry traditionally uses riveting technology to join metallic materials to fabricate airframe structures. This well-established design and fabrication technology is accompanied by many years of experience on damage tolerance behaviour of riveted/fastened aircraft structures. Fatigue crack initiation, and growth, as well as fracture resistance and corrosion issues associated with riveted structures are well understood. However, recent developments in Al-alloys and welding technologies have led to the use of advanced welding technologies to reduce weight and fabrication costs [1]-[8]. Laser beam welding (LBW) has been successfully applied for manufacturing of skin-stringer curved panels for various civilian aircrafts in Europe. Friction stir welding (FSW) is also considered as a prospective welding process for butt-joint applications in fuselage and wing structures [3]-[5]. It is obvious that optimization of the welding processes and joint design are requisite to achieve damage tolerance properties equal to or even better than riveted structures.

Currently, the LBW process has been successfully applied to the fabrication of stiffened panels to join skin-stringer (T-joint) parts for integral airframe structures made of 2xxx and/or 6xxx series weldable Al-alloys [6], [9], [10]. This technological development will eventually lead to use of LBW process in joining of further components such as “skin-clip”, “clip-frame” or “frame-skin” applications to achieve further weight and cost savings as well as part-count reductions in future metallic airframes, Figure 1.1. Certainly, such a step should be developed together with optimization of the joint design while maintaining the superior damage tolerance behaviour of weld joints (local engineering).

One of the advantages of LBW of aerospace Al-alloys is that the residual stresses and distortion due to welding are low. However, even low levels of residual stress will affect fatigue crack initiation and fatigue crack propagation (FCP) properties of thin-walled welded components. Hence, the prediction, control, and full understanding of the roles of residual stresses on crack initiation and FCP are essential to avoid their critical effects. Reduced tensile residual stress within the weld can reduce crack propagation rate and by this method the service life of the welded components can be improved.

While substantial research has been carried out on the damage tolerance behaviour of conventional riveted airframe structures, the effects of LBW on damage tolerance behaviour have not been widely reported. A limited number of investigations have been conducted in recent years to understand damage tolerance (fatigue and fracture) properties of advanced welding processes, including laser beam and friction stir welding [7], [9]-[13]. Principally, the majority of the reported studies on welded airframes have dealt with the “skin-stringer” LBW joints and butt-joint (skin-skin) configuration in the case of FSW. However, no work has been undertaken to investigate the LBW of clips to the skin (Figure 1.1) and their joint design optimisation, residual stress as well as fatigue and fracture performance. The European Community funded collaborative project WEL-AIR (Short Distance Welding Concepts for Airframes) has been developed to investigate the welding process and damage tolerance aspects of such welds and start/end (run-in/run-out) locations of the skin-stringer welds for future applications. However, main attention was given to the start/end issues of the skin-stringer joints.

Differential cooling due to the inhomogeneous temperature fields during the welding process knowingly create residual stresses in the welded area, and their levels and distributions depend on numerous factors. During the cooling process after welding, the shrinkage of the

weld material and any hindrance of this, leads to residual stresses in the welded region. The weld length, joint type as well as start (run-in) and end (run-out) locations of the welding process inevitably play a role in the evolution of the residual stresses. LBW of clip-skin joints, Figure 1.1b, is short (approx. 120 mm to 160 mm) and hence can be considered as "short distance welds". Residual stress state in short distance weld seams can be affected by varying the start and end locations of the LBW process relative to the weld geometry.

In order to develop an optimum joint design for short distance welds, it was essential to investigate the residual stress magnitude and distribution for a variety of welding configurations, in which the positions of run-ins and run-outs change. Furthermore, to investigate the evolution of the residual stresses and their effects on the FCP behaviour of the skin-clip joints, systematic study (including both experimental testing and numerical simulation) need to be undertaken. Therefore, both aspects have been investigated within this Ph.D programme.

It is known that tensile residual stresses can have detrimental effects on fatigue life, whereas compressive residual stresses can be beneficial. Therefore, one of the goals was to control the residual stresses via proper selection of welding process to obtain lower tensile residual stresses and if possible to generate compressive residual stresses, which contribute to the lower crack growth rate along the weld seam.

For this purpose, a clip was welded to two different Al-alloy base plates (skin) from one side using a 3.3 kW Nd:YAG laser to investigate the residual stresses and fatigue crack propagation, including weldability and joint properties. Residual stress measurements on these short distance welded fillet welds of aluminium alloys were conducted using neutron diffraction and partly reported in previous publications [14]-[17].

a) 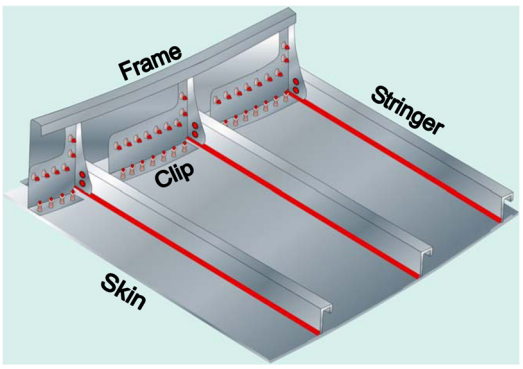

b) 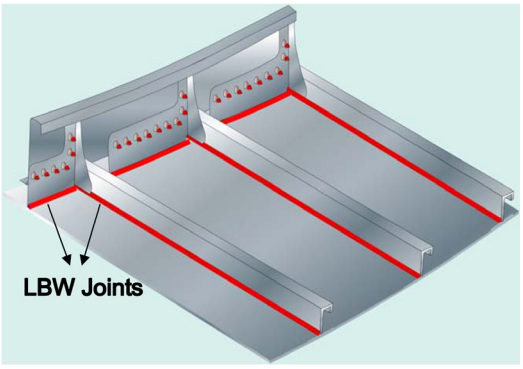

Figure 1.1: Schematic drawing showing a) the application of LBW to the currently used panels with welded skin-stringer joints, b) possible future application of welding for clip-skin joints. Note the riveted clip-frame joints, which may provide further potential location for use of laser beam welding or simply joining frames to skin using LBW process.

Numerical finite element (FE) simulation of LBW processes was performed using the commercial code SYSWELD to determine the residual stress distribution for various clip welds. Substantial amount of work had to be conducted to generate data on the temperature field around the clip weld seam and compared with the thermal simulation data.

The 400 mm wide panels with single central clip were notched at the weld toe to conduct FCP tests under constant amplitude cyclic loading at room temperature. Fatigue crack propagation data and crack path development were carefully monitored to capture any possible effect of the welding process, residual stress state and local geometry of the weld seam area.

Airframe panels should be fabricated in light-weight manner. Hence, any excessive material is usually removed for example with chemical milling method. To resemble this practise as well as to provide "local strengthening" to the weld areas, the panels were machined from one side by reducing the panel thickness locally (see section 3.1). Principally, the weld area was supported by leaving the skin thickness at original sheet thickness (socket) while reducing sheet thickness of far-field areas between stringers (pocket), the FCP tests were carried out on such panels.

In this study the following goals were achieved:

- The beneficial effect of the LBW process optimisation on the residual stress evolution around the short distance skin-clip welds was successfully demonstrated.
- A change of start (run-in) and end (run-out) locations of the welding process were shown to be effective for modifications of residual stress states.
- The use of the neutron diffraction method on thin-walled skin-clip LB welded Al-alloy panels was successfully demonstrated and detailed residual stress profiles were obtained for various weldments.
- Complex temperature field data for the clip welded panel has been experimentally obtained to be able to explain the residual stress behaviours (experimental measurements) of the welded configurations and to compare with the temperature field results of the numerical simulations.
- The commercial FE-code SYSWELD was successfully applied to describe the residual stress distribution for panels containing a central LBW clip weld.
- The fatigue crack propagation rate of a propagating crack along the clip weld was found to be higher than the un-welded base material for both 6156 and 2139 Al-alloys.
- An introduction of compressive transverse residual stresses was shown to be very effective to increase the fatigue life of the clip welds analysed in the form of "one-bay-crack" panels under tension.

2 State of the art

2.1 Laser beam welding (LBW) process

Laser welding has been widely used in recent years in similar and dissimilar joints because of its high intensity, small heat affected zone, higher welding speed and precision, etc. During laser welding, the dynamics of heat transfer, fluid flow and mass transfer affect the characteristic and quality of the fabricated product. Owing to the small size of the weld pool and the presence of plasma in its vicinity the measurements of the temperature and the velocity fields in the pool are not easy tasks. There have been numerous experimental and numerical simulation studies to improve the understanding of the beam-material interaction, coupling pore formation and solidification process of various metallic materials. In order to provide some insight, selected studies will briefly be covered. Paul et al. [18] studied the essential physicals features of the process by mathematically modelling to develop an understanding of the transport processes. Milewski et al. [19] performed a study on modelling of laser energy concentration by 3D simulation to determine the effects of angle dependent absorption and diffuse reflections on beam transport. Tsukamoto et al. [20] investigated the behaviour of the laser induced plasma and the correlation to the penetration depth for various welding conditions in CO_2 laser welding. It is proven that the plasma was formed in the region where the power density of the laser beam exceeds the critical value. That value is found to be dependent on the composition and flow rate of the shielding gas, but independent of the laser power and beam focussing condition. Kazemi et al. [21] studied on a development of 3D finite element (FE) model to dynamically simulate the full penetration laser welding process. The parametric design capabilities of the FE code ANSYS were employed for this purpose. The heat source was parameterized by the combination of a circular disk source with a Gaussian distribution of thermal flux. It is presented that this modified heat source model could predict the weld cross section in deep penetration laser welding, especially in the case of full penetration welding. Furthermore, various values of conductivity were examined for different welding speeds. The results suggested that for different welding speeds, an effective conductivity for material must be used to predict the weld cross section.

Reynolds et al. [22] investigated another issue, hot cracking in pulsed laser welds in austenitic stainless steels, some Ni-based alloys and combinations of the two types using single and overlapping welds. Kujanpää et al. [23] also studied on hot cracking of laser welds in X20CrMoV121 heat-resisting steel. Biela et al. [24] searched for the effects of process variables on cracking of pulsed laser welds in nickel-chromium-iron based alloy Inconel 600. Shibahara et al. [25] worked on numerical prediction of welding hot cracking of SM490 steel using 3D FEM with temperature dependent interface element. Furthermore, keyhole instability and liquid flow induced by evaporation enhances the generation of bubbles and pores including a shielding gas. Katayama et al. [26] investigated keyhole behaviour and molten flow as well as bubble and porosity formation mechanism during welding of AA 5083 aluminium alloys and 304 austenitic stainless steels with YAG and CO_2 lasers by using X-ray transmission real-time observation system. Similarly, Kawaguchi et al. [27] studied on suppression of porosity formation in CO_2 laser welding by power modulation with the modified waveform.

For the Al-alloys, the LBW process is now well-established and well-understood to weld crack and porosity-free conditions.Vitek et al. [28] developed a model to predict the weld pool shape in pulsed Nd:YAG laser welds of aluminium alloy 5754. The model utilized

neural network analysis to relate the weld process conditions to four pool shape parameters: penetration, width, width at half-penetration, and cross-sectional area. The predicted weld shape parameters were converted into predicted weld profiles utilizing the actual experimental weld pool profiles as templates. The feasibility of successfully predicting weld pool shapes by means of neural network analysis was clearly demonstrated. The effect of the mechanical and material inhomogeneity on the deformation and failure behaviour of laser beam welded aluminium joints was investigated by Blauel et al. [29] experimentally and numerically. Small scale tensile and fracture mechanics specimen were extracted from butt and overlap laser beam welds in AlMgSi-alloys and were tested to characterize the local strength, toughness and damage properties. Finite element structural models were generated using the material data and were evaluated to predict the integral behaviour of differently fabricated joints. The calculations were compared to experiments and the results were used to derive criteria for the qualification of laser beam welds in aluminium structures under service conditions. Leigh et al. [30] discussed some of the potential defects in aluminium laser welds and presented the results of the examination of some early weldments made with aluminium alloy 6013 and several filler alloys. Braun et al. [31], [32], [33] also studied the same aluminium alloy. Microstructure, hardness, tensile properties and corrosion behaviour were investigated in the as-welded and in the post-weld heat treated T6 temper. Vaidya et al. [34] investigated microstructural and mechanical properties of butt joints of 6013 and 6056 aluminium alloys and referred to fatigue and fracture performance.

Cicală et al. [35] investigated hot cracking issue in laser welded AA 6056 (Al–Mg–Si–Cu) alloy taking into account not only the individual, but also the interactive, influences of various parameters. It is confirmed that the most influential factors in avoiding hot cracking were the welding speed, fastening system and wire parameters. The best results were given by low welding speeds and a uniform compression fastening system. High wire feed rates produced instabilities, whereas low feed rates did not sufficiently modify the chemical composition of the molten pool. Welding stability was also found to be important, as instability generated crack and vitiated the weld's mechanical properties. It is also concluded that the information related to the stability of the process could be gained from the temperature dispersion. Using the polynomial model, that was created by multiple regression technique enabled by the experimental model results, tensile strength could be estimated as a function of the welding speed and filler wire quantitiy.

Fabrègue et al. [36] also studied hot tearing phenomenon during solidification of AA 6056 alloy. He developed an experimental set-up to study the fracture behaviour of the alloy during non-isothermal tensile tests carried out in the mushy state during solidification. The mush exhibited a viscoplastic behaviour and showed a transition between fracture in the solid state and fracture in the semi-solid state when the imposed displacement speed was decreased. It is found that that critical speed for the occurrence of rupture in the mushy state depends on the composition of the alloy and on the cooling rate. Decreasing the Si content, increasing the cooling rate, or adding a grain refiner leads to an increase of the critical speed. These experiments also showed that the displacement to fracture did not depend on the displacement speed but was a function of the cooling rate and the composition. Moreover, the mechanical behaviour of the mush was successfully modelled using a creep-type law in which the fraction of grain boundaries wetted by the liquid was taken into account. Simulation could predict the occurrence of hot tearing. It was also remarked that some remaining liquid could feed the hot tears and heal them during laser welding. In addition, the addition of filler wire during welding could also change the physical properties of the mush, and therefore affects the occurrence of hot tearing. Nevertheless, the study was thought to

constitute a step towards the understanding of the behaviour of a mush under non-isothermal conditions with a high cooling rate and the conditions of the occurrence of hot tearing during laser welding processes. In his further study [37], hot tears in AA 6056 aluminium alloy laser weld were characterized using both scanning electron microscopy and three-dimensional X-ray tomography. Hot tears were shown to be intergranular, originated from fracture of liquid films without plasticity of the surrounding grains. It is demonstrated that the hot tear initiated on both sides of the fusion zone, followed the liquid films between the columnar grains of the weld line and then propagated around the equiaxed grains of the fusion zone centre. He investigated further [38] the mechanical properties of the same material as a function of the silicon content in the fusion zone which depends on the amount of the Al-12% filler wire used during welding. It is established that an increase of the silicon content in the fusion zone induced an improvement of the mechanical properties of the weld in tension, not only in terms of fracture strength but also in terms of fracture strain. This behaviour was explained by a better homogeneous strain distribution in the weld during tensile deformation when the silicon content increased. Finite element simulations of the weld tensile deformation using code Abaqus were conducted to evaluate the distribution of local strains from the local properties and to predict the macroscopic mechanical response of the weld. Simulations were shown to reproduce the experimental load/displacement curves.

Ancona et al. [39] evaluated the mechanical properties of CO_2 laser beam butt welds of AA 5083 alloy. Tensile tests, hardness profiles across the weld sections, porosity measurements and EDX analyses were performed. The influence of the welding speed and laser power on the response variables that were considered to be representative for the weld quality (tensile strength, porosity, microhardness), were evaluated. Two levels of incident laser power (2000, 2500 W) and four levels of welding speed (60, 80, 100 and 120 mm/s) were investigated, with several repetitions for each set of process parameters. Best performances were obtained by operating at 2500 W and 100 mm/s where it was found a tensile strength of more than 90 % with respect to the native material, a porosity level less than 3% and just a small hardening across the weld zone. The process was demonstrated to be robust and reliable under those conditions. Partial or discontinuous penetrations were achieved for lower laser powers or higher welding speeds, while for too high energy inputs weld dropout occurred. Overall result were very competitive in comparison to weld performances reported in literature on the same alloy with alternative techniques like friction stir welding or gas tungsten arc welding (GTAW). Sánchez-Amaya et al. [40] also investigated the influence of experimental variables, as the laser power and the linear welding rate, on the sizes and properties of the butt weld beads of AA 5083 TO and AA 6082 T6 aluminium alloys. In addition to measure the depths and widths of the weld beads, their microstructure, microhardness profile and corrosion resistance were analysed. The results obtained allow one to define the experimental conditions leading to good quality butt welds with higher penetration than those published in the recent literature under conduction regime. Additionally, a simple mathematical expression relating the weld depth (d) with the laser power (P) and the processing rate (v) was proposed: $d = (P - bb')/(av) - (ba')/a$, being a, a', b and b' constant values for each alloy and under the employed experimental conditions. The values of those coefficients were estimated from the fitting to the experimental depth values of 5083 and 6082 butt welds generated under conduction regime.

2.2 Light-weight aerospace structures and laser welding

Leight-weight welded components with high strength are of essential interest for all branches that produce moving masses [41], [42]. The goal is enhancing effective payload and property reliability of structures. These goals may be pursued through materials science, manufacturing techniques and design engineering. These three disciplines are mutually dependent and it is through their interaction that progress is achieved. LBW offers the possibility to manufacture joints of all light metals such as aluminium, titanium, magnesium and their combinations. The high potential of laser welding technologies has been proven through successful applications in the automotive, aeronautics and aerospace industries.

Aluminium alloys are major materials for light-weight constructions especially in the transportation industry due to their good mechanical properties and low density. An appropriate joining technology is the laser beam welding process, because of its low localised energy input resulting in low distortion and high processing speeds. This concentrated heat input leads to narrow but deep weld seams. Despite the numerous advantages, LBW may suffer from statistically occurring seam imperfections like notches or holes in the seam which reduce the mechanical properties of the joint. However, using optimum process parameters and filler wire adapted to the alloy and weld geometry, weld qualities are possible, which fulfil the requirements of the aircraft industry, where estimates of risks are normally done in a most conservative way. Currently, LBW of Al-alloys of 6xxx and 2xxx grades require use of filler wire with high Si-content. The most commonly used 4047 (12 % Si) filler wire is generally being used in high strength weldable Al-alloys such as used in this study [29]–[38]. The reason for this is to compensate the loss of strength due to partly loss of Mg (evaporation) in the weld zone and due to low viscosity of 4047 filler wire the decrease of the superficial tension of the molten pool. Therefore, the weld zones generally exhibit “strength undermatching” which causes difficulties for the designers to fulfil the strength requirements. To do this, current practise in airframes is locally strengthening of the joints by using “socket” concept which provides local skin thickening at the joint area.

The safe operation of many structures and components is ensured through the operation of damage tolerant design and evaluation, which intended to certify that fatigue, corrosion, or other mechanisms should cause crack to grow within the operational life of the system, so that the remaining structure can withstand reasonable loads without failure or excessive structural deformation until the damage is detected [43]. A critical element of damage tolerant design in many systems is the ability to predict the growth rate of fatigue cracks growing through the structure under known applied loading. Effective stress state of the welded components considering residual stress fields, in this context, is highly significant.

Residual stresses exist in many manufactured components, as a consequence of the thermal or mechanical processing applied during production. Local plastic deformation of a material will produce a residual stress variation; as will rapid cooling from elevated temperatures as in the case of fusion welding, where the material’s yield strength is usually significantly lower than at room temperature. It is crucial to predict quantitatively how a given residual stress field will enhance or degrade fatigue crack growth rates. When a residual stress field is present, a growing fatigue crack is likely to exhibit a different growth rate from a crack growing in residual stress free material. This has obvious implications for lifing components where a damage tolerant approach is adopted, assuming a known fatigue crack growth rate and load cycle characteristics. If not taken into account, a tensile stress field can lead to an overestimate of the component life, while a compressive residual stress could give a

conservative life. The aim is to design and manufacture components with compressive residual stresses which will lead to retardation of crack growth and hence improved damage tolerance performance. This was possible to a certain extent in conventional riveted structures and should also be possible for advanced welded integral Al-alloy components or sub-structures, such as stiffened panels.

2.3 Residual stresses in fusion welds

During the fusion welding processes, residual stresses are introduced by a rise in temperature during the melting or heating and by subsequent cooling of the weld and surrounding material. The volume contraction that takes place in the melt pool during solidification and during the subsequent cooling involves a tensile stress field in the welded joint. To understand the effect of residual stresses on the static and dynamic mechanical properties of the welded structures, the magnitude and distribution of the residual stresses should be known, and if possible should be controlled. There exist high amount of investigations related with residual stress determination using either destructive or non-destructive techniques, even for various type of high-strength Al-alloys. The selected studies are given here to figure out what kinds of investigations were conducted in this area.

The following studies are dealing with the LBW process of Al-alloys: Müller et al. [44] performed a study on determination of residual stresses of LB welded Aluminium alloy sheets of AA6016 using simple geometries as bead-on-plate and butt welding using X-ray diffraction technique. The effects of filler material and preliminary heat treatment on residual stresses were examined as well as the influence of different thermal and mechanical post-treatments. Reproducible and characteristic residual stress curves were obtained and explained by a simple model. It is proven that the influence of thermal pre- and post-treatments was obvious. Shot peening as an example of mechanical treatment produced compressive stresses close to the surface. Similarly, the influence of temper conditions before welding, sheet thickness and post weld heat treatment on residual stresses were examined by Staron et al. [45]. The residual stress determination in LB welded butt joints of AA 6056 aluminium sheets was performed using neutron diffraction and high-energy X-ray diffraction at a synchrotron source. It was found that for reduction of residual stresses, LBW in the underaged condition (T4) is beneficial. A further reduction by post-weld heat treatment was not possible at the temperature employed (190°C). Whereas residual stresses existed well below the yield stress in thin sheets (3.2 mm), they approached nearly the yield stress of LBW in thick sheets (6 mm).

Ramana et al. [46] studied the influence of parent metal heat treatment condition on the residual stress distribution in electron beam dissimilar metal butt welds of maraging steel to quenched and tempered medium alloy medium carbon steel. Residual stress measurement was carried out with X-ray stress analyser. It is found that if one of the parent metals was in soft condition, the magnitude of the residual stresses was lowered due to stress absorbing nature of the softer parent metal. The benefit of soft parent metal prevailed even after post-weld aging treatment. In addition, coarsening of martensite plates during aging enabled to reduce the stresses in quenched and tempered steel.

Another study to analyse the effect of thickness on residual stresses was carried out by Bruno et al. [47] in tungsten inert gas (TIG) butt welded Ti6Al4V curved plates using the neutron diffraction measurement technique. It was concluded that higher stresses were obtained at the transition region from fusion zone to heat affected zone. In addition, the far field stress level

was not zero for the two samples having thickness values of 6 mm and 2 mm, indicating a clear influence of the machining of the specimens. The weld stresses reached higher values of tensile stresses in those samples, which occurred probably due to overlap of the machining stresses. Lower tensile stresses were found in the thinnest sample with 1.6 mm thickness and zero values were reached far from the weld pool. Pearce et al. [48] investigated residual stresses in a thick cut section T-butt weld on a curved plate by neutron diffraction. The web to base plate welds were made by submerged arc welding (SAW). The parent material was BIS 812 Ema steel. The residual stress profile in the base plate below the weld showed that there was a large compressive region through the mid-section of the plate. It is confirmed that the weld residual stress field was dominated in the region close to weld and bending residual stresses were available far from weld. It is concluded that by determining which circumstances might warrant inclusion of pre-welding residual stress fields into an estimation of the welding residual stress profile, more accurate calculations for engineering assessments could be carried out. This would reduce unnecessary repairs of welds with flaws that are detected in zones of compressive stress.

Other investigations explaining comparative studies between different techniques are also given to demonstrate the reliability of the related techniques. Ganguly et al. [49] studied on 2024 T351 aluminium alloy. Residual strain measurements of variable polarity plasma arc (VPPA) butt welded plates were conducted by neutron and synchrotron X-ray diffraction methods. It has been demonstrated that the strain variation measured using two diffraction processes showed excellent comparability. He performed further study [50] on both metal inert gas (MIG) welded and VPPA welded specimen of 2024 T351 aluminium alloy using neutron and synchrotron X-ray diffraction. Specimens were double-V butt which welded in two pass. Analysis were performed both as-welded and following a post welding skim which served to remove the weld flash and reduce the plate thickness. A skimming treatment didn't cause any reduction of the peak stress for the MIG welded plate, although the stress pattern across the weld changed and the stress peak in the far heat affected zone was almost eliminated. This is contrary to the conventional belief that machining reduces the peak stress significantly. The longitudinal stress generation and its evolution during skimming were compared to data for the VPPA welding process. The stress generation in VPPA-welded plate showed a similar profile but the peak stress magnitude is less. This is attributed to the distortion associated with the welding process. The longitudinal stress in the skimmed VPPA plate followed closely the pattern and magnitude of the as-welded plate. Ya et al. [51] searched for residual stresses in an LB butt welded aluminium plate of 6056 material using ultrasonic technique for the macroscopic gradient and the Moiré interferometry incremental hole-drilling method for the local gradient. Former technique was used to measure the non-uniform residual stress distribution in transverse direction in a laser welded sample and latter to determine in-depth and in-plane residual stresses in the weld centre and heat-affected zone. It was shown that these two non-destructive ultrasonic and semi-destructive methods were effective for residual stress measurement of the welded components which have a high stress gradient. A comparative study by Albertini et al. [52] was conducted by using a neutron spallation source and X-ray diffraction methods. The selected material was VPPA butt welded material of AA 2219 T851. Residual stress agreement between surface X-ray and bulk neutron data was found, and the combined use of different sets of measurements allowed a clear overview of the stress field in the sample. It is shown that in the weld pool tensile bulk and compressive surface stresses were found, however reverse was the case in the heat affected zone (HAZ). Owen et al. [53] selected neutron diffraction, laboratory X-ray and high energy X-ray synchrotron radiation to investigate the residual stress field in tungsten inert gas (TIG) welded 2024 T3 aluminium bead-on plate joints. That was proven

that the results of each method compared well despite the differing penetration and sampling volumes associated with each technique. It was also found that the magnitudes of the tensile longitudinal stresses decreased along the weld due to progressive heating up during welding. The results were compared to that of a FE model and it has been concluded that softening of the HAZ region must be included to simulate the residual stress field. Kartal et al. [54] investigated longitudinal residual stresses within specially designed groove weld specimens fabricated using manual metal arc process. The comparison between residual stress fields arising from single and multi-pass weld beads were made by using neutron diffraction and the contour method for the measurement to validate FE simulation of the welding process. Good agreement was found between both techniques.

James et al. [55] provided insight into relationships between weld process conditions, weld zone metallurgy and mechanical properties. Residual strain and stress profiles were determined in MIG welded high strength steel butt joints by neutron diffraction technique. It was found that variations in terms of tensile region and peak magnitude values were at least partially explained by the cross section of the weld fusion zone and HAZ. The filler metal strength level was the predominant influence on the magnitude and position of peak strains in the weld metal and HAZ. In addition, an effect of plate thickness on the residual strain profile arose from the faster cooling rates that occur in a thinner plate.

Estefen et al. [56] studied surface residual stresses in double-electrode butt welded ASTM 131 grade A ferritic steel plates by portable X-ray diffraction equipment. The results were compared to single-electrode welded plates. Final stresses for the double-electrode case remained higher than equivalent values for single-electrode one, both for longitudinal and transverse directions. For the double-electrode case the maximum welding stress values were in both HAZ and base metal close to the fillet, while for the single electrode case the maximum values were located along the deposited material.

All these studies show the importance of the reliable analysis of residual stresses and provide information about the affecting factors. This knowledge will contribute to the understanding of fatigue behaviour of the welded structures.

2.4 Numerical simulation of weld residual stresses

The welding simulation has proven to be an efficient aid for the determination of the residual stress condition after the welding. This leads to the possibility of obtaining important statements about the residual stress condition in places where a measurement cannot be taken for geometrical reasons. Finite element analysis together with the equations of continuum-mechanics and irreversible thermodynamics (non-equilibrium thermodynamics) forms the basis for a successful analysis of welding processes. In thermodynamics, a change in the thermodynamic state of a system is irreversible if the system cannot be restored to its former state by infinitesimal changes in some property of the system without expenditure of energy. Most systems found in nature are not in thermodynamic equilibrium because they are not isolated from their environment and are therefore continuously sharing matter and energy with other systems. This sharing of matter and energy includes being driven by external energy sources as well as dissipating energy.

Goldak et al. [57] – [60] contributed to the development of welding analysis by developing a realistic heat source model to define the distribution of the flux on the surface of the bead-on plate weld and the power density throughout the volume of the weld. The analyses using

these models apply not only to quasi-steady state conditions but also to the transients on starting and stopping the weld. Transient computation is important because thermal strain and thermal stress are almost always more severe at the beginning and the end of the welding process. He also [61] performed a three dimensional (3D) transient computation of stress, strain, displacement, and temperature fields around a tack weld in a 12.7 mm thick butt joint of 1020 carbon steel with nonlinear thermo-elasto-plastic finite element analysis (FEA). In the present study, a 3D transient FE analysis was performed using commercial FE code SYSWELD to analyse the welding residual stresses of the various type of clip-skin weld. Since it is a short distance weld, where run-in and run-out positions would possess different residual stresses, a transient thermal analysis was necessary. Goldak's conical heat source model was used to model the LBW accurately. Temperature field data is experimentally obtained for comparison with that obtained by simulation and hence were used to modify the heat source model to calibrate the thermal simulation.

The complexity of welding FE analysis required some development stages by several studies using different FE codes. Some investigations are related here starting with Mok et al. [62], who studied the numerical prediction of the welding residual stresses in a thick (26 mm) T-joint of steel specimen with the FE code ABAQUS. The heat input from the electrode was simulated using a modified version of Goldak's double ellipsoidal heat source model. Two dimensional (2D) analyses were conducted with generalized plane strain elements. During the welding simulation, the specimen was not restrained and was free to distort. A time-independent, thermo-elastic-plastic constitutive model was assumed. Strain hardening and the Bauschinger effect were modelled by a kinematic hardening model. The effect of allotropic phase transformations was neglected. The predicted results agreed reasonably well (within 50 MPa) with neutron diffraction measurements. Also a through-thickness stress gradient was predicted which is contrary to some researchers' assumption of constant through-thickness stress. Another thermo-mechanical analysis using ABAQUS was conducted by Cañas et al. [63]. The residual stresses were determined in gas metal arc (GMAW) butt welded plates of the aluminium alloy AA 5083-O introducing simplified thermal hypotheses which, making use of an analytical thermal solution, omitting the actual ordering in time of the thermal actions. It was claimed that the use of the envelope of temperatures permitted the maximum reduction in the input data preparation, producing excellent results. The distribution of residual stresses obtained using a plane stress model was in very good accordance with the measurements obtained by means of the blind-hole technique. This agreement confirmed that it didn't seem necessary to include factors like the phase change, the creep or the modelling of the added metal. The plane strain model was unable to fit the distribution of experimental residual stresses. An uncoupled thermo-mechanical analysis approach was employed by Zain-ul Abdein et al. [64] using ABAQUS as well to predict the residual stresses in LB bead-on plate welded 6056 T4 aluminium alloy thin plate. A cone-shaped volumetric heat source with Gaussian distribution and an upper hollow sphere was used to attain the required weld pool size and temperature fields. A 3D symmetric model of the test plate and support was incorporated. A good correlation was found between experimental and simulation results.

Sarkani et al. [65] compared the residual stress fields in a welded T-joint computed by 3D models with those computed by 2D models. It was proven that the temperature distribution in the central zone of the joint could be captured successfully by a 2D finite element model by a technique that takes into account the heat transfer balance and welding speed. The residual stresses in the plane of the 2D model computed by that method showed fairly good agreement with those computed by the 3D model. All analyses were performed with

ABAQUS. Kim et al. [66] predicted the residual stress by a numerical simulation for modified 9Cr-1Mo steel multi-pass welds of V-butt and T-plate specimens induced by gas tungsten arc welding (GTAW) processes and compared the results with the experimentally determined residual stresses. Neutron diffraction technique is used to measure the residual stresses both on the surface and in the interiror of a thickness for the welded specimens. A finite element analysis using ABAQUS was carried out to calculate the residual stress distributions for the two types of welded specimens. Two dimensional idealization of a complex three dimensional geometry was assumed and 2D axisymmetric models were used. A transient thermal analysis was performed for a sequential addition of each weld bead. The weld passes were modelled to be added to the weld region just before a welding for each pass by using the "born and death" option in the software. The mechanical analysis was modelled similarly for a sequential addition of each weld bead. Loading was supplied from the temperature-time history of the thermal analysis. The predicted residual stresses had a close agreement with the measured data although there some differences, quantitatively.

Wu et al. [67] used the general purpose FE package ANSYS in a butt welded BS 4360 steel plate. A 2D FE analysis with a plane strain model was used to simulate the three dimensional welding process since a quasi-steady state was assumed to exist in certain long welds under a uniform welding speed. The model was validated by comparison of its predictions with published residual stresses from experiments and other numerical simulations. A thermal and stress analysis was performed sequentially. It was however concluded that a nonlinear transient thermal analysis was necessary to trace the rapid change of temperature with time while a static analysis could be adopted for the stress analysis. However, a significant number of time points, at which the temperature results were to be read into the stress analysis, should be defined to capture the temperature gradient and give accurate residual stress results using the load steps option. In addition, radiation and latent heat from phase transformations could be ignored to simplify the modelling procedure. In a further study [68], an FE simulation of fillet metal inert gas (MIG) welded T-joint of steel material was studied. The main features of the essentially 2D analysis by means of ANSYS were ramped heat input function, temperature dependent material properties and element death and rebirth technique. A parallel experimental investigation allowed the assessment of plastic properties variations in the welding area. The model was validated by temperature history data from the tests. The calculated longitudinal residual stress distributions along the surfaces of the plate were found to be good agreement with the experimentally determined patterns. Li et al. [69] investigated residual stresses in multi-pass welding of pipe-plate structure consisting of Q345 material. A 3D finite element analysis is performed using ANSYS code. The temperature distribution and its history in the welding model were computed by the heat conduction analysis. Then, the temperature history was employed as a thermal load in the subsequent mechanical elastic plastic calculation of the residual stress field. During the thermal analysis the model change option was used to simulate the weld metal deposition. After the completion of first welding pass, new elements were added to the model to simulate the weld metal deposition during the second welding pass. In the mechanical analysis, the kinematic hardening was taken into account. It is concluded that the maximum tensile radial and the hoop stress occurred in the weld bead, and the maximum tensile axial stress occurred in the weld toe.

Another comparative study is conducted by Keppas et al. [70] to determine residual stresses in a 3-bead letterbox-type repair weld on a $2\frac{1}{4}$ CrMo low alloy ferritic steel plate using a proposed simulation based on decoupled thermal and mechanical analyses and the "birth and death of elements" technique and by neutron diffraction. Parametric studies included

modelling aspects such as 2D plane strain versus 3D analysis, re-melting of weld material during sequential bead deposition, melting of base plate near the fusion line and annealing. Despite the large length of the 3-bead plates, 2D plane strain analysis is found to over-predict longitudinal stresses as compared to a full 3D simulation. Incorporating annealing in the analysis, the predicted transverse residual stresses were affected significantly however longitudinal stresses are not sensitive to this modelling aspect. Predicted stresses were compared with neutron diffraction testing data. It is concluded that numerical results were, in general, in satisfied agreement with the experimental data. Mousavi et al. [71] performed a 3D finite element analyses by element birth and death technique to analyze the residual stresses produced in the tungsten inert gas (TIG) grooved butt welding process of 304L stainless steel material. The effect of geometry configurations on the residual stress distributions were predicted from the 3D computer analysis using a thermoelastoplastic constitutive equation and compared with the results from X-ray diffraction analysis. Temperature dependent material properties were used and the effects of conduction, radiation and convection due to both air and inert gas flow rate were considered in the simulation. Simulation results showed that the peak of the tensile residual stress obtained for the u-grooved configuration was less than that predicted for the v-grooved configurations. The predicted residual stresses were in good agreements with those obtained by the X-ray diffraction experiments. The best agreement between the residual stress distributions and the X-ray experiments was obtained using the kinematic and isotropic hardening constitutive equations.

Preston et al. [72] developed an FE model taking into account the history-dependence of the yield stress-temperature response of TIG bead-on plate welded 2024 T3 aluminium alloy during welding. The FE predictions were validated against high resolution X-ray synchrotron diffraction measurements of residual strain. It was shown that the effect of the temperature history was weak for that alloy. The dominant requirement for that alloy was to use an appropriate short time-scale for softening of the material in selecting the yield stress-temperature response. It was anticipated that the effect of history could be greater in higher strength alloys and tempers, which suffer a greater degree of softening during welding. Cramer et al. [73] also studied the residual stresses in aluminium welded joints. The residual stresses were established on selected evaluation paths not only on the surface with the radiographic procedures but also across the plate thickness with the hole drilling procedures. MIG welded complex structure of the engine mounting from the automobile industry was investigated. An FE model of half the system was elaborated and hybrid meshing was carried out with volume and shell elements. The volume elements were used in the region around the weld so that the steep three-dimensional gradients of the temperature and the stresses could be portrayed. With regard to both the longitudinal and transverse residual stresses, it is showed that a comparison of the residual stresses from the radiographic measurement and the FE calculation resulted in very good congruence not only in the level of the residual tensile stress peaks but also in their qualitative course. In addition, hole drilling procedure offered the possibility of establishing courses across the depth.

Teng et al. [74] studied on residual stress analysis in T-joint fillet welds of SAE 1020 steel material by using thermal elasto-plastic analysis in the FEA. The technique of element birth and death was used to simulate the weld filler variation with time. Additionally the effects of flange thickness, welding penetration depth and restraint condition of welding on residual stresses were discussed. It is found that a high transverse stress and a very large stress were produced near the fillet weld toe. Moreover, the tensile residual stress near the fillet weld toe

increased with increasing flange thickness. With increasing penetration depth or heat input in fillet welding, the the tensile residual stress near the fillet weld toe decreased.

Lee et al. [75] investigated the circumferential variations of residual stresses in circumferential welds of KS SPPS 42 carbon steel pipes and the effects of diameter (thickness ratio ranging from 10 to 100) on residual stress distribution using a 3D uncoupled thermo-mechanical FE analysis. It is demonstrated that the axial and hoop residual stresses were generally influenced by the pipe diameter in the thin walled pipe welds. In the thick walled pipe welds similar tendency is expected to exist except for the complex residual stress distributions induced by the multi-pass welding, which was planned to be investigated in a future work.

As can be understood from the referred studies, the FE analyses of the welding process to yield residual stresses have been satisfactorily progressed being a powerful tool to enable the process and design optimization of the weld joints.

2.5 Fatigue crack propagation (FCP) behaviour of welds

The increasing tendency in the application of weld joints in structures such as airframe, ship, pipeline, offshore etc. led to investigation of the FCP behaviour of the welds for a couple of decades. Early studies concentrated on FCP behaviour of steel materials as performed by Dowse et al. [76]. FCP was investigated under constant, alternating and maximum stress intensity through the HAZ of two types of metal arc welded steel materials, one was Ducol W30 (a low alloy steel) and the other in mild steel. It is demonstrated that a hard HAZ reduced the crack propagation rate by a factor of two by restricting the size of the plastic zone around the crack tip. The plastic zone shape was found to influence the direction of crack propagation, which always deviated towards region of lower flow stress. Benoit et al. [77] investigated the influence of thickness and a load ratio on the FCP behaviour in the HAZ of butt welded joints in E 36 steel. Tests were performed on compact tension C(T) specimens with a constant load amplitude. It was shown that the presence of residual stresses following welding reduced the crack propagation rate by up to 6.7%, independent of the metallurgical structure being traversed. Braid et al. [78] investigated FCP in notched specimens of HY-80 steel containing bead-in-groove weld using constant applied loading and constant applied stress intensity. It was found that the crack grew faster in the parent-plate microstructure and progressed slowly as it passed through the HAZ and into the weld metal. It was also confirmed that microstructure and inclusion content had little effect on FCP rate at stress intensities near threshold. Therefore, the observed decrease in propagation rates was attributed to the presence of residual stresses. Lieurade et al. [79] demonstrated the influence of certain technological and mechanical parameters on fatigue strength of various types of welded joints. It is shown that weld fatigue characteristics could be improved by certain heat treatments or mechanical treatments. In order to examine the effect of the weld toe on fatigue crack initiation and propagation another study was performed by Itoh et al. [80]. Pulsating constant load controlled tests at various stresses were conducted on the gas metal arc (GMA) welded butt joints of C-Mn-Si steel specimens. The results demonstrated that shallow fatigue cracks, 0.5–1.0 mm initially grew rapidly under the influence of stress concentration at the weld toes, however the propagation behaviour of cracks more than that size was not affected by the weld toe.

Roberts et al. [81] discussed the various aspects of the influence of fatigue on the structural integrity of welded steel structures, including fatigue resistant design, inspection, monitoring,

assessment and repair. Difficulties in applying scientific theories and laboratory test data to real structures were highlighted. Oh et al. [82] studied the characteristics of fatigue strength and crack propagation behaviour of the Tailor Welded Blank SPCEN (KS D 3512) material sheet used for automobile body panel. Fatigue strength was found to be the highest when loading and welding direction was parallel and same thicknesses of the welded specimens. The fatigue strength was 8.5% less when plates with different thickness were welded together. There were signs of crack growth retardation around welding bead due to increased strength. As crack growed further, propagation speed increased and crack shape became narrower around welding bead due to decreased fracture toughness. Nakajima et al. [83] investigated fatigue behaviour of welded joints of a ferritic stainless steel, SUS444. Push-pull fatigue tests were conducted using plate specimens with the weld zone at the center of gauge section. FCP tests were also conducted using two types of CT-specimens with a starter notch in the HAZ and in the weld metal. Fatigue strength of the welded specimens decreased remarkably compared to that of the base material. Based on experimental results and 2D FEM analysis of the welded zone, it was concluded that the decrease in fatigue strength of the welded specimens was attributed to the stress concentration at the toe of weld. Crack initiation and growth in the welded specimens could not be measured owing to the geometry of the weld zone, thus crack growth was measured using the smooth welded specimens in which the excess weld was removed. In early crack growth region, the crack growth rates of the base specimens were faster than those of the smooth welded specimens. This result was correlated with the higher fatigue strength of the smooth welded specimens at high stress levels compared to base metal. With increasing crack size, the $da/dN - \Delta K$ relationships (between the crack growth rate and the stress intensity factor range) for small cracks gradually approached the $da/dN - \Delta K_{eff}$ relationships (between the crack growth rate and the efficient stress intensity factor range) for long cracks and then coincided with them.

Recent investigations concentrated more on the Aluminium alloys due to the increasing of application area. Hong et al. [84], [85] examined the FCP behaviour of friction stir welded (FSW) 6061 T651 Al–Mg–Si alloy with the fatigue crack growing either along the dynamically recrystallized zone (DXZ) at variable ΔK or perpendicular to DXZ at constant ΔK value of 7.5, 10 and 15 $MPa\sqrt{m}$. It was concluded that The FCP rates in the DXZ tended to be significantly lower than those in the BM particularly in low ΔK regime due to the compressive residual stress reducing effective ΔK; however, grain refinement caused intergranular fatigue failure. Moreover, the constant ΔK fatigue test across the weld zone showed that crack retardation occurred far beyond the HAZ at low ΔK regime. The residual stress measurement suggested that the crack retardation begun with the presence of compressive residual stress that existed in this region. Vaidya et al. [86] assessed the fracture and FCP behaviour of LB and FS welded Aluminium and Magnesium alloys for metallic airframes. It is confirmed in this study that strength undermatching caused by welding process of LB and FS welding of aluminium alloys could be protected and cracks could be deviated by increasing local thickness of the weld and by decreasing local thickness of the base metal under static loading. Large isolated pores introduced by LBW were found to induce a retardation during FCP, and this was attributed to the stress relaxation caused by the interaction with the crack growth. Contrary to Al-alloys, the Mg-alloy LB butt welded AZ31B did not exhibit any strength undermatching, consequently the FCP behaviour was nearly comparable to that of the base material. Moreira et al. [87] studied the fatigue behaviour of FS welded butt joints of 6082 T6 aluminium material by applying monotonic tensile and cyclic loading. It is verified that the FS welded material revealed lower yield and ultimate tensile stresses than the base material as well as lower elongation and hardness. In

contrary, an increase of the crack propagation resistance was detected for the welded material in comparison with the HAZ or even the base material. Balasubramanian et al. [88] investigated the influences of pulsed current welding and post weld aging treatment on FCP of AA7075 aluminium alloy joints. Four different welding techniques have been used to fabricate the joints, which are continuous current GTAW (Gas Tungsten Arc Welding), pulsed current GTAW, continuous current GMAW (Gas Metal Arc Welding) and pulsed current GMAW. FCP behaviour of the welded joints was evaluated by conducting tests under constant amplitude loading. Current pulsing leaded to relatively finer and equi-axed grain structure in GTA welds. Grain refinement was accompanied by an increase in fatigue crack growth resistance and fatigue life. A simple artificial aging treatment applied to the joints was found to be useful to enhance the fatigue crack growth resistance of welded joints. Nearly a 20-25 % increment in fatigue life was attained irrespective of welding techniques. The superior mechanical properties (higher yield strength and hardness), preferred microstructures in the weld metal region (very fine equi-axed grains with higher amount of precipitates) and favourable residual stress field in the weld metal region (large magnitude of compressive stress) were the reasons for better fatigue performance of the post weld aged joints.

The comparison of analytical and numerical methods was studied by Zhang et al. [89] on the growth of the fatigue cracks in welded structural steel members of floating production storage and offloading units. The effect of welding residual stresses was considered both in the analytical model and finite element model for long cracks. An analytical model was developed based on BS 7910 for the surface cracks and modified Dexter's analytical model for the long cracks in the stiffened plate. An analysis by the FE code ABAQUS was conducted using the J-integral approach to calculate the stress intensity factor at the crack tip during different stages of crack growth. It was shown that the FE results agreed well with the results from the analytical model. It is concluded that the amplitude of the compressive residual stress was highly variable and a conservative lower bound distribution should be used in the models. In addition, the influence of compressive residual stress was also quite sensitive to the applied stress ratio resulting from the external load. It is claimed that the residual stress might be relaxed due to external load or redistributed due to the propagating long crack itself, so the beneficial effect of compressive residual stress for the long cracks should normally be neglected. Another comparative work with experimental and numerical methods was performed by Fersini et al. [90] on FS welded aluminium alloy overlap joint. Two crack-like unwelded regions, which were present at the sides of the welded region, were subjected to mixed mode I/II loading conditions. The lifetime of these joints were defined as the number of cycles necessary to propagate this crack to failure. FE analysis with a code Franc2D were carried out to simulate the propogation and to determine the effective stress intensity factor at the crack tip.These K values were introduced in the software Afgrow to predict the duration. Constant load amplitude fatigue tests were performed at different load levels. The number of cycles to failure predicted numerically was lower than experimentally observed one. This difference was attributed mainly to an early stage of shear dominated (Mode II) propagation that was not accounted for in the numerical model. This type of propagation was detected experimentally and demonstrated to occur according to the "fatigue failure mechanism map". The simulation was then re-run taking into account that initial shear mode propagation and in that case good agreement was found between numerical and experimental results. Further studies related to the welded aluminium material investigated the fatigue crack propagation together with the residual stress effects, hence given in the next section.

2.6 Effect of residual stress on fatigue crack propagation behaviour of welds

The area of residual stress measurement, particularly at welds, and understanding of their influence on fatigue life has been a major challenge in research for many years. The most reliable method is having the knowledge of the magnitude and distribution of residual stresses by measurement. Most of the studies concentrated on the effect of residual stresses on fatigue crack initiation behaviour of the weld joints. Since there are limited amount of publications showing the effect of residual stresses on FCP behaviour, the concepts of the investigations are given in detail to understand the effect of residual stresses on FCP in different weld types and test sample geometries. Among the investigations related with the effect of residual stresses on FCP behaviour, different specimen geometries (e.g. compact tension, eccentrically loaded single edge and centre-crack tension) were used at different R ratios to understand the effect of the residual stresses on FCP behaviour.

John et al. [91] investigated the role of residual stresses on near-threshold FCP in friction stir welds (FSW) for the aluminium alloy 7050 T7451 and the titanium alloy Ti–6Al–4V. Tests were performed on weld coupons as a function of specimen geometry (compact tension, eccentrically loaded single edge and centre-crack tension) and stress ratio to understand the effects of residual stresses in the heat affected zone (HAZ) of the alloy. Residual stresses were measured on samples machined from the friction stir welded plates using X-ray diffraction technique prior to testing. The results showed that residual stresses play a key role in the crack growth parallel to the weld path in the HAZ. At low stress ratio ($R = 0.05$), the C(T) specimen showed significantly higher fatigue threshold and low crack growth rate compared to the M(T) specimen. At $R = 0.8$, the differences in the crack growth rate between the C(T) and M(T) geometry were considerably reduced. The analysis of $\Delta K - K_{\max}$ (the difference between stress intensity factor and the maximum stress intensity factor) behaviour near the threshold for various Al and Ti–6Al–4V alloys showed evidence of the dominant influence of residual stresses. A parametric analysis with an analytical model was conducted using uniform residual stress distributions along the crack plane. These analytical results suggested that the change in K_{res} (the stress intensity factor that is calculated including residual stress), which affects the total crack driving force is much higher for the C(T) geometry than that for the M(T). The fatigue threshold is significantly altered even in the presence of "low" residual stresses, sometimes leading to decreased threshold values. It is concluded that the M(T) specimen geometry is less susceptible to residual stresses and must be given due consideration while obtaining engineering design data for FS welded joints.

Kim et al. [92] studied on FCP behaviour of FS welded 5083 H32 and 6061 T651 specimens with fatigue crack growing either parallel to the dynamically recrystallized zone (DXZ) at variable ΔK values and an R ratio of 0.1 and 0.8, respectively, or perpendicular or 45° to the DXZ at various constant ΔK values. In the former case, FCP behaviour of the specimens was mainly determined by the beneficial compressive residual stress reducing effective ΔK. In the latter case, the presence of weld zone in front of propagating crack retarded the FCP rates of the specimens significantly in low and intermediate ΔK regimes due to the residual stress acting on the weld zone.

Pouget et al. [93] investigated FCP in FS welded AA 2050 C(T) specimens and the effects of FSW induced residual stresses. Longitudinal residual stresses were determined using the cut compliance technique. Fatigue tests were conducted with the crack propagating nominally

perpendicular to the weld and with decreasing $\Delta K_{applied}$ at various load ratios, $R = 0.1$, 0.4, and 0.65. It was demonstrated that FCP is strongly linked with the presence of residual stresses. Compressive residual stresses in the HAZ induced crack closure and were responsible for the apparent improvement of fatigue behaviour when the crack approached the weld. In the weld nugget, the FCP rates increased which is believed to be due, in part, to tensile residual stresses and, in part, to the microstructure. However, from the predictions of crack growth rates made from K_{res} and ΔK_{eff} profile determined with the opening method verified that the closure is mostly due to residual stresses in the HAZ and then other mechanisms, e.g. oxide-induced closure, are added once the crack tip is inside the weld.

Fratini et al. [94] examined the effect of longitudinal residual stress on FCP in friction stir welds of 2024 T351 aluminium alloy. FCP rate was attained through constant ΔK tests for notches at different distances from the weld centreline. Residual stresses were measured by cut-compliance method. Tensile residual stresses within the weld was determined, however the HAZs were subjected to compressive residual stresses. It was found that compressive residual stresses correspond to low crack growth rates outside the weld zone, depending on the position of the initial notch. However, the observed superior crack growth rate inside the weld compared to that of the base metal, was due to the low hardness values of the FSW in that region. Furthermore, weld residual stresses were mechanically relieved and effects on the crack propagation behaviour were observed. For the relieved joint, the crack growth rates approaching to the base material values explained that the reduction of the residual stress after stretching is responsible for the differences in the crack growth behaviour. The unchanged hardness values and microstructure after stretching confirmed the concluded case.

Galatolo et al. [95] investigated the FCP in residual stress fields of plasma welded aluminium 2219 T851 joints. He compared the FCP results of the two type of specimens, one being large centre cracked tension (CCT) (200 mm$\times$700 mm) and the other is the small compact tension (CT) ($W = 26$, the distance from the centerline of the holes to the lower end – perpendicular to the notch – of the specimen) specimens. The main difference between the two types of specimens concerned the residual stresses, which were not present in the CT specimens, due to their reduced dimensions. Initial notches were introduced as parallel and perpendicular to the welding directions for both of the specimens. The results of the tests were fully comparable in the case of a crack which propagates along the weld bead, as the residual stresses acting in this direction were quite low. In the case of a crack which propagates perpendicularly to the weld bead, the crack propagation rate measured on the CCT specimens was higher than that in the CT specimens, due to tensile residual stresses. Residual stresses were measured by instrumenting the plates with strain gauges, and then by sectioning them by milling, to produce the relaxation of residual stresses. Residual stresses in plasma-welded aluminium plates were measured in cracked and uncracked plates, so it was possible to evaluate the actual values of the stress ratio in the tests carried out on the CCT specimens. By taking into account these values, a close agreement between the results of the two sets of tests was observed.

Liljedahl et al. [96] studied the evolution of the residual stresses in a variable polarity plasma arc welded (VPPA) M(T) specimens of 2024 aluminium alloy with fatigue loading and subsequent crack growth. The residual stress measurements were performed at a time of flight instrument, at the Pulsed Neutron Source. FCP was conducted in situ and strain measurements averaged through the thickness of the specimen were made along two orthogonal directions as the crack grew. 2D finite element simulations of the evolution of the

initial residual stress field with crack growth, using an elastic model produced predictions that were in reasonable agreement with the experimental results. He found that some re-distribution of the residual stress field occurred due to crack tip plasticity associated with the fatigue loading. The magnitude of the stress field around the crack tip increased as the crack grew. In his further investigation [97], M(T) and C(T) specimens machined from a VPPA 2024 T351 plate were tested at three levels of applied constant stress intensity factor range. Crack closure was continuously monitored using an eddy current transducer and the residual stresses were measured with the same method as the previous work. To determine the effect of the residual stresses on the fatigue crack growth behaviour for both specimen geometries, two approaches were used: a crack closure approach where the effective stress intensity factor was computed; and a residual stress approach where the effect of the residual stresses on the stress ratio was considered. It is found that the initial residual stresses in a welded plate were redistributed with crack growth in both specimen geometries. The initial residual stress distributions in the M(T) and C(T) specimens were very different. The residual stresses accelerated the fatigue crack growth rate in the former specimen geometry whereas they decelerated the growth rate in the latter. This confirmed that FCP rates obtained from laboratory specimen, of which the exact residual stress field was not known might be misleading. Such factors should be taken into account when designing damage tolerant aerospace structures based on laboratory specimen data. A good correlation between the experimental results and the predictions were found for the effective stress intensity factor approach at a high stress intensity factor range whereas the residual stress approach yielded good predictions at low and moderate stress intensity factor ranges.

Lachmann et al. [98] researched the relaxation of residual stresses due to fatigue loading on gas-tungsten-arc (GTA) welded joints of structural steel S355J2G3. The fatigue testing was conducted with pure pulsating tension. After each decade of loading, residual stresses were measured with X-ray diffraction. For an evaluation of the deformation behaviour and the residual stress relaxation during the first load cycle (quasi-static load step) a 2D-FEM-simulation was conducted. A distribution of the transverse residual stresses measured by X-ray diffraction was taken as an input data for the initial residual stress state in the FEM-model. It was found that under quasi-static loading, the residual stresses within a weld relax dependent on the local plastic deformation in the respective weld zone. The calculated residual stress relaxation showed a good agreement with the results of an X-ray measurement and took place in correspondence with the calculated degree of plastic deformation in the FEM-model. After a significant change after the first load cycle, the residual stresses remained relatively constant during further loading until fracture.

Sarkani et al. [99] investigated the effect of residual stresses on fatigue damage accumulation in a welded T-joint subjected to stochastic loading. It was shown that welding residual stresses can significantly change the damage accumulation rates. The calculations using a simple approach based on an elastic-perfectly-plastic material model and the Gerber correction factor predicted that the residual stresses during stochastic loading randomly decayed to zero.

Goo et al. [100] studied the effect of welding residual stress on fatigue behaviour of a JIS SM 490 A steel C(T) specimen by a finite element analysis. Temperature, residual stress distributions, and residual stress redistribution with fatigue crack growth were calculated on the commercial package ABAQUS. FCP was simulated using a cohesive zone model along the symmetric line in the crack direction. To account for the damage accumulation due to fatigue, a law of damage evolution was included in the constitutive equation of the cohesive

zone model. The analysis was also applied to the specimen not welded and the prediction results of both specimens were compared to determine the influence of the residual stresses on fatigue behaviour. It was demonstrated that when compressive residual stress normal to the crack surface exists around the crack tip, the FCP rate was reduced. As the fatigue crack propagated, the welding residual stresses are redistributed. He also proposed a model [101] to evaluate fatigue life of the double V-grooved and the fillet welded structures considering notches and residual stress relaxation. The elastic-plastic finite element analysis of welding residual stress and stress relaxation due to applied loadings were performed on ABAQUS. Weld beads were generated by the element birth technique supplied on ABAQUS. It is found that the maximum tensile residual stress existing on the surface of the specimen decreased gradually and changed to compressive stress as the applied loading was larger than a certain value. He further proposed a procedure [102] to identify the fatigue properties from the Brinell hardness and Young's modulus based on a local strain approach. The last two studies demonstrated that due to residual stress change under applied loading, the locations of fatigue crack initiation depend on the magnitude of applied load. From the last investigation it was concluded that the effect of welding residual stress on fatigue life is more significant when the magnitude of the applied loading together with the residual stress is in the elastic range.

Gonçalves et al. [103] investigated the residual stresses behaviour of a API60X steel C(T) specimen under fatigue loading by a finite element analyses by the code LUSAS. Application and a release of high-intensity loads to the specimen were simulated to produce a residual stress field in transverse direction similar to that appear in butt joints, with multiple weld passes. The introduction of the crack produced a redistribution of the residual stresses. The stresses in the transverse direction, in the crack face became null, in the vicinities of the crack tip became high-intensity compression and, at a larger distance from the crack tip, became traction. The absolute values of the stresses, around the crack tip, increased with the number of cycles, for the specimen with residual stresses even for low intensity loads, inducing the fatigue fracture for a smaller number of cycles that is usually expected for the specimen without residual stresses. For more distant points, located inside the area of traction residual stresses, the variation happened in an opposed and weaker way.

As a conclusion, all these studies show that initial residual stresses are redistributed under the applied fatigue loading and are very effective especially at the early part of crack propagation.

2.7 Problem definition and adopted approaches

The aerospace industry traditionally uses riveting technology to join metallic materials to fabricate airframe structures. This well-established design and fabrication technology is accompanied by many years of experience on damage tolerance behaviour of riveted/fastened aircraft structures. Fatigue crack initiation and growth, as well as fracture resistance and corrosion issues associated with riveted structures are well understood.

Recent developments in Al-alloys and welding technologies have led to the use of advanced welding technologies to reduce weight and fabrication costs. Laser beam welding (LBW) has been successfully applied for manufacturing of "skin-stringer" panels for various civilian aircrafts in Europe. The fabrication of stiffened panels to join skin-stringer (T-joint) parts for integral airframe structures were made of 2xxx and/or 6xxx series weldable Al-alloys. This technological development will eventually lead to use of LBW process in joining of further components such as "skin-clip", "clip-frame" or "frame-skin" applications to achieve further

weight and cost savings as well as part-count reductions in future metallic airframes. Certainly, such a step should be developed together with optimization of the welding process and joint design while maintaining the superior damage tolerance behaviour of weld joints (local engineering).

As briefly summarised in section 2.6, it is known that residual stresses imposed by a welding process will affect fatigue crack initiation and fatigue crack propagation (FCP) properties of welded components. This is also true for thin-walled Al-alloy panels. Therefore, the investigation's goal was to control the residual stresses via proper selection of welding process to obtain lower tensile residual stresses and, if possible, to locally generate compressive residual stresses, which should contribute to the lower crack growth rate along the weld seam.

Therefore, residual stress states in such short distance fillet welds of two different aluminium alloys (3.2 and 4.5 mm thicknesses) as "clip-skin" joints were analysed for a various types of welding processes, in which the start and end locations of the LBW process were changed relative to the weld geometry. In addition, to resemble the practise in airframe panels, where any excessive material is usually removed, as well as to provide "local strengthening" to the weld areas, some of the panels were machined from one side by reducing panel thickness locally. Principally, the weld area was supported by leaving the skin thickness at original sheet thickness (socket) while reducing the sheet thickness of far-field areas between stringers (pocket).

Residual stress measurements on all type of welds and geometries were conducted using neutron diffraction. Residual stress analysis by numerical simulation of the LBW processes was performed for one of the panel containing no pocket using the commercial FE code SYSWELD and the results were compared to the experimental measurements.

Fatigue crack propagation and crack path development of notched middle tension panels with single central clip under constant amplitude cyclic loading were carefully monitored to capture any possible effect of the welding process, residual stress state and local geometry of the weld seam area.

3 Experimental procedures

3.1 Material and geometry of laser beam welded clips

The investigated panels were laser beam welded T-joint configurations with a thin sheet T-part (as clip) and a base plate (as skin). The geometries and the dimensions of the panels are given in (Figures 3.1 – 3.3). Two panel sizes of 275 mm × 160 mm and 400 mm × 625 mm were used, the former to establish the experimental methodology, the latter to be used as a M(T) 400 fatigue specimen to resemble clip-skin joints of an airframe. The 2 mm thick clip materials used were AA 6013 of T6 condition. Two different Al-alloy skin materials were studied, namely AA 6156 in T4 and in T6 conditions and AA 2139 T351, to investigate the sensitivity to hot cracking at the run-in and run-out locations of the clip welds. The thickness of 3.2 mm was used for the 2139 alloy and that for the 6156 alloy was 4.5 mm. The alloy selection was made due to their recent use and their improved properties with respect to ability to be strengthened by aging after forming and a good weldability, which depend on the chemical compositions and the heat treatment applied, see Tables 3.1 and 3.2. The total length of the welds was 120 mm and they were welded from one side only. The welding was carried out at GKSS using 4047 grade (12% Si) Al-alloy filler wire of ∅1.2 mm with a welding speed of 1.2 m/min by a 3.3 kW Nd:YAG LBW unit using He as a shielding gas. The use of a filler wire reduces the susceptibility of the alloy to hot tearing by increasing the solute content of the fusion zone above a critical value. In fact it is known that the hot cracking tendency for a binary aluminium alloy shows a maximum close to the solubility limit of the element and decreases rapidly beyond this limit [104]. The welding direction was parallel to the rolling direction of the skin sheet. No post-weld heat treatment was carried out after welding in any of the materials.

The welded configurations as shown in Figures 3.2 and 3.3 are referred to hereafter as “plain” and “machined” (pocketed) panels. Some areas of the panels near the weld were machined to a lower thickness (pockets) for weight reduction, similar to the practice in aircraft structures. Furthermore, the original thickness of the skin sheet has been kept (socket) at the weld area to provide higher local strength, since welded metal shows lower strength (undermatching) than the base metal. The panel thickness was reduced to 2.4 mm for the 3.2 mm thick panels and to 3 mm for the 4.5 mm thick panels. The thicker central area, in which the welded clip was placed, is called the “socket” (or sometimes called “pad-up” (Figure 3.3). Two socket widths of 11 mm and 20 mm were used to determine the role of the socket width in fatigue crack propagation and crack path deviation.

For the purpose of investigating the effects of different welding procedures – in which the location of the “start” and “end” positions changes – on the development of residual stresses and on the FCP behaviour, plain panels were welded in three different configurations, Figure 3.4. The first welding type was applied from one end of the clip and completed at the other end (called as “conventional” welding type, Figure 3.4a. The second welding type was started from the mid-clip position and finished at one end and the process was repeated for the other half of the clip (“two run-outs” welding type, Figure 3.4b). In contrast, the third welding type was started from one end of the clip and stopped at the mid-clip position, then started from the other end and finished again at the mid-clip position (“two run-ins” welding type, Figure 3.4c). The effect of the variation of the start and the end positions and the geometry through the introduction of pocketing on residual stress development and extension of the FCP performance of short distance laser welds are also investigated in this work.

Table 3.1: The chemical compositions of the Al alloys used in this study.

Element (wt %)	AA 6013	AA 6156	AA 2139	AA 4047 (Filler)
Si	0.60-1.0	0.86	0.06	11.0-13.0
Fe	---	0.08	0.07	0.80
Cu	0.60-1.10	1.02	4.90	
Mg	0.80-1.20	0.76	0.44	
Mn	0.20-0.80	0.45	0.29	
Cr	0.10	40 ppm	10 ppm	
Ni	---	52 ppm	<0.01	
Zn	0.25	0.15	<0.01	
Ti	0.10	0.02	0.05	
Zr	---	18 ppm	27 ppm	
Ag	---	---	0.31	

Table 3.2: The heat treatment conditions of the Al alloys used in this study.

	AA 6013	AA 6156	AA 2139
Heat Treatment	T6	T4/T6	T351

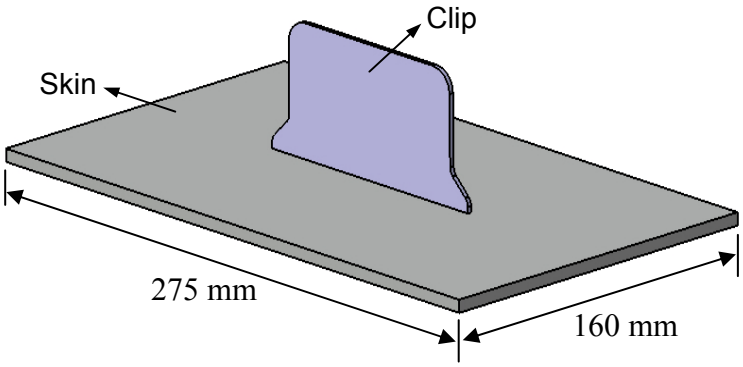

Figure 3.1: Geometry of the welded small panel (thickness of the base plate and the clip are 6 mm and 2 mm, respectively).

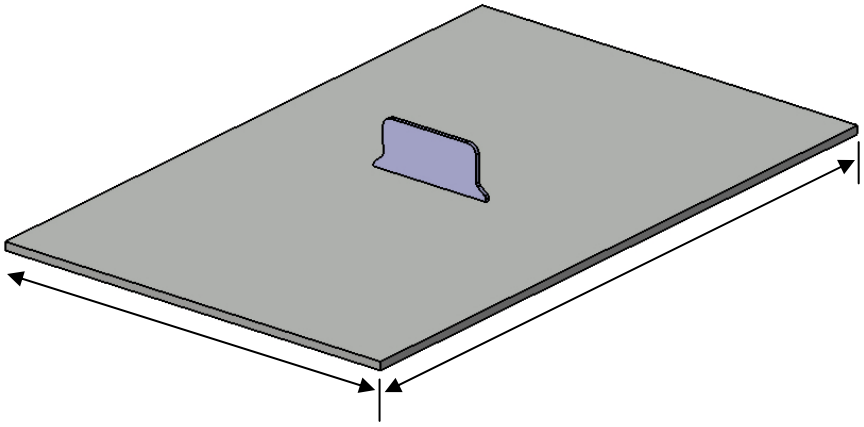

Figure 3.2: Geometry of the welded panel which would serve as a M(T) 400 panel (thickness of the base plate and the clip are 3.2 / 4.5 mm and 2 mm, respectively).

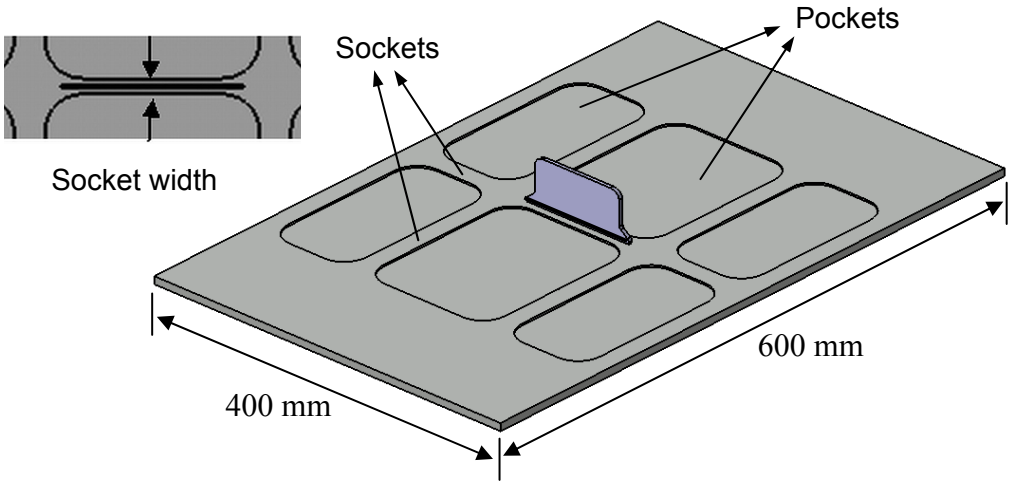

Figure 3.3: Geometry of the pocketed panel and tested as a M(T) 400 specimen (thickness of the base plate and the clip are 3.2 / 4.5 mm and 2 mm, respectively. Thickness of the pocketed area is 2.4 for 3.2 mm base plate and 3 mm for 4.5 mm thick base plate).

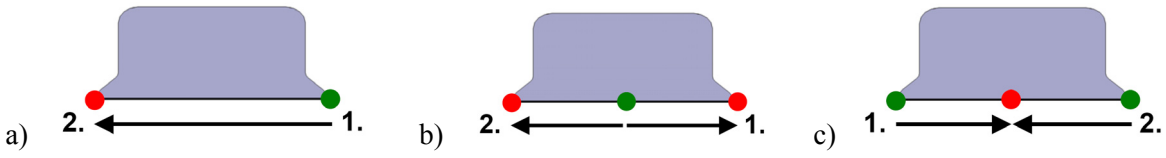

Figure 3.4: Welded clip types showing welding directions a) conventionally welded clip, b) welded clip including two run-outs at the ends, and c) welded clip including two run-ins at the ends.

3.2 Temperature field measurement

Temperature field measurements were performed in the framework of a Diploma Thesis [128]. The variation of the temperatures was measured in the 6156 T6 base panels of all three welding types (Figure 3.4) using K thermocouples (Ni-NiCr) with a diameter of 0.5 mm. All thermocouples were plugged into approximately 1 mm deep drilled holes (Figure 3.5).

The thermocouples were placed along three scan lines perpendicular to the clip (middle and clip ends). At each scan line two thermocouples were located on the front of the clip (laser side) and two on the back. Additionally one thermocouple was put at the bottom of the plate in the centre with a 3 mm deep hole (Figure 3.6). Thus, there were 13 measurement points in total for each sample. All data were read out by computer with a measurement frequency of 50 Hz. The total time passed until the temperature decreased to 30ºC was almost 90 seconds.

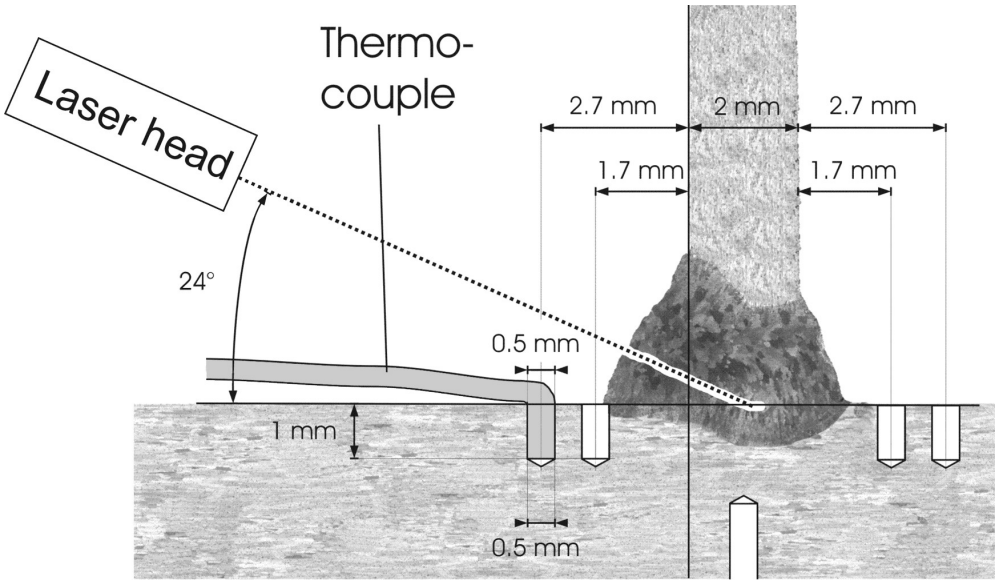

Figure 3.5: Positions of the thermocouples on the conventionally welded plain panel without pockets during thermal measurements – side view.

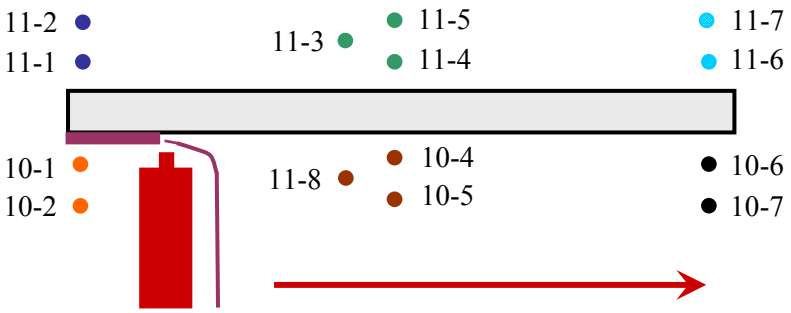

Figure 3.6: Positions of the thermocouples in reference to the position of clip during thermal measurements – top view (Red arrow shows the direction of the welding process for conventional welding, thermocouples numbered by 10–X are located on the front side and 11–X on the back side of the weld).

The measurements in the conventionally welded panel show that there exist big temperature differences between locations 1.7 mm and 2.7 mm from the clip axis on the front side of the weld at run-in (10–1 and 10–2) and run-out positions (10–6 and 10–7), see Figure 3.7. However, at the mid-clip position there is no significant temperature difference between different distances (1.7, 2.2 and 2.7 mm) from the clip axis on the front side of the weld.

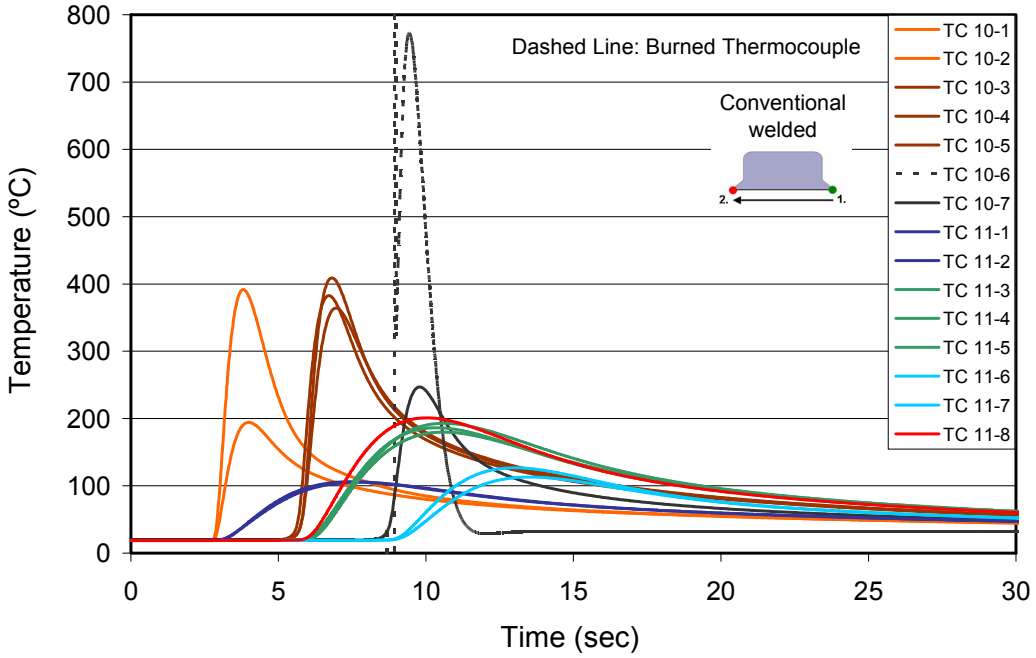

Figure 3.7: Cooling curves of the conventionally welded 6156 T6 panel during welding at each position of the thermocouples.

Figure 3.8 demonstrates the cooling curves of the welded plain panel containing two run-outs. The thermo couple position 10–1 (first run-out position of this welding type which is the run-in position of the conventionally welded panel) shows the same temperature level as in the conventionally welded panel (Figure 3.7). The thermo couple position 10–7 (the second run-out position of this welding type which is the run-out position of the conventionally welded panel) also possess the same temperature grade compared to the conventionally welded panel. First pass at mid-clip position (TC 10–3 and 10–4) show significantly higher values than the conventionally welded panel, however at the second pass comparable temperatures exist. The mid-clip position is the run-in position in this welding type and the comparison with the run-in position of the conventionally welded panel (TC10–1 and 10–2) reveals that much higher temperature levels were measured at the run-in position of the welded panel with two run-outs.

The cooling curves of the welded plain panel with two run-ins (Figure 3.9) also illustrate notably higher temperatures at the mid-clip position (TC 10–3 and 10–5) in comparison to the conventionally welded panel (Figure 3.7). The mid-clip position (the run-out position in this welding type) possesses much higher temperatures compared to the run-out position of the conventionally welded panel (TC10–7). At the first run-in position (TC 10–7) exists close temperature values compared to the run-out position of the conventionally welded panel (this position refers to the run-out position of the conventionally welded panel). At the second run-in position (TC10–2) very high temperatures with a peak value of approximately 700ºC exists (this position refers to the run-in position of the conventionally welded panel).

On the rear side of the welded panels (11–X), the temperatures reached were much lower than that on the front sides at run-in, run-out and mid-clip.

The different temperature fields occurred at mid-clip, run-in and run-out positions of each welded panel types led to different residual stress behaviours, see section 5.2.7.

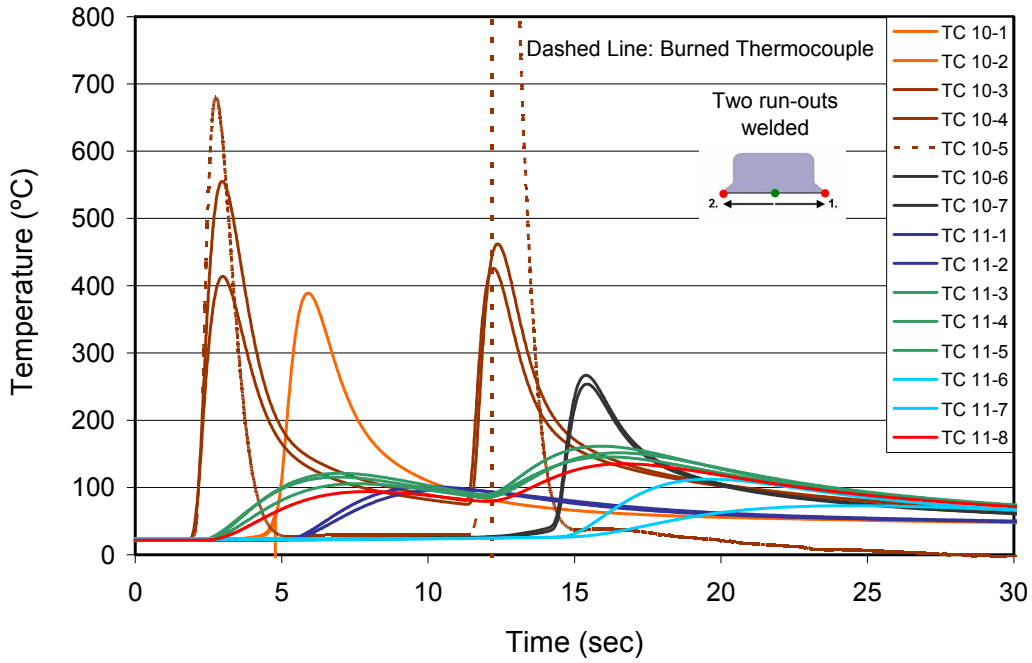

Figure 3.8: Cooling curves of the welded 6156 T6 panel which contains two run-outs during welding at each position of the thermocouples.

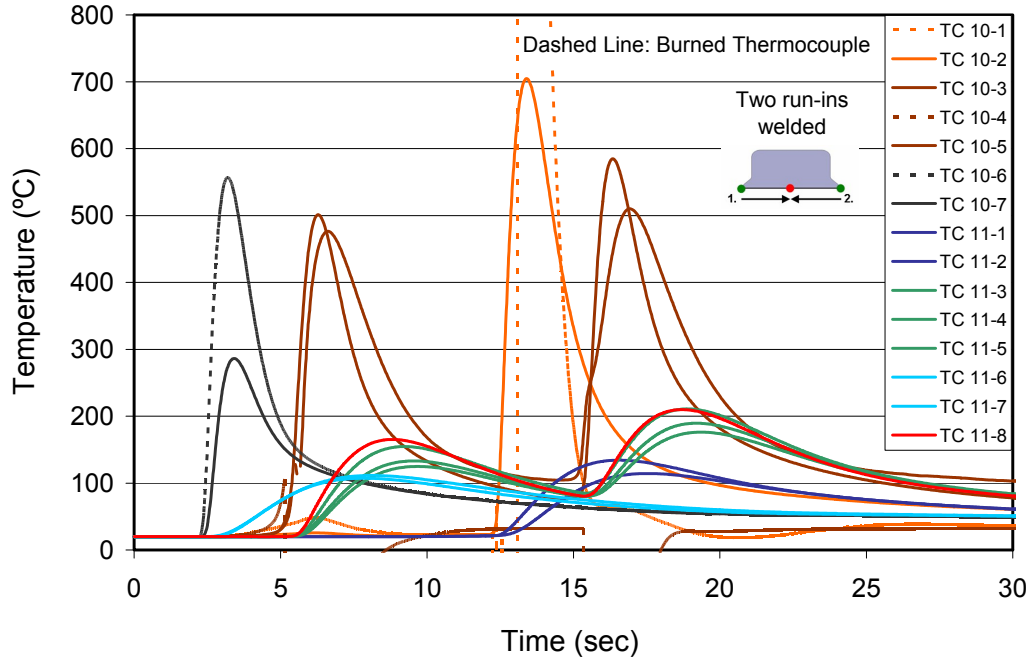

Figure 3.9: Cooling curves of the welded 6156 T6 panel which contains two run-ins during welding at each position of the thermocouples.

3.3 Mechanical testing of base material and welded specimens

Vickers microhardness measurements were performed on polished metallographic sections of the weld along a line, which is located 0.35 mm below from the surface of the skin plate (Figure 3.10) with a load of 444.82 N. Micro-hardness measurements ($HV_{0.2}$) were carried out across the weld zone part within the skin as shown by dashed lines. The zero position was selected as the centre of the clip position. The measurements were taken up to 9 mm on each side of the centre position.

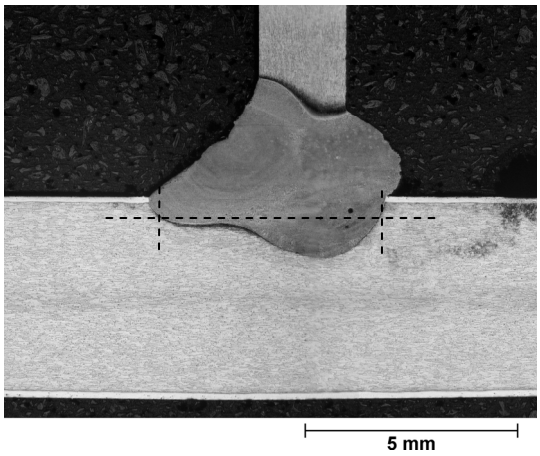

Figure 3.10: Representative cross-sectional view showing conventionally welded 6013 T6 clip on 6156 T4 skin material. The dashed line (located 0.35 mm below from the surface of the skin plate) shows across which the microhardness measurements were taken.

The tensile properties of the skin-clip joints (plain welds without socket or pocket) were determined by extracting flat transverse oriented specimens with original weld configuration (keeping part of the clip part on the specimens, as shown in Figure 3.11) at room temperature. The specimens had a gauge length of 50 mm and a width of 10 mm and were loaded transverse to the weld seam, as shown in Figure 3.11.

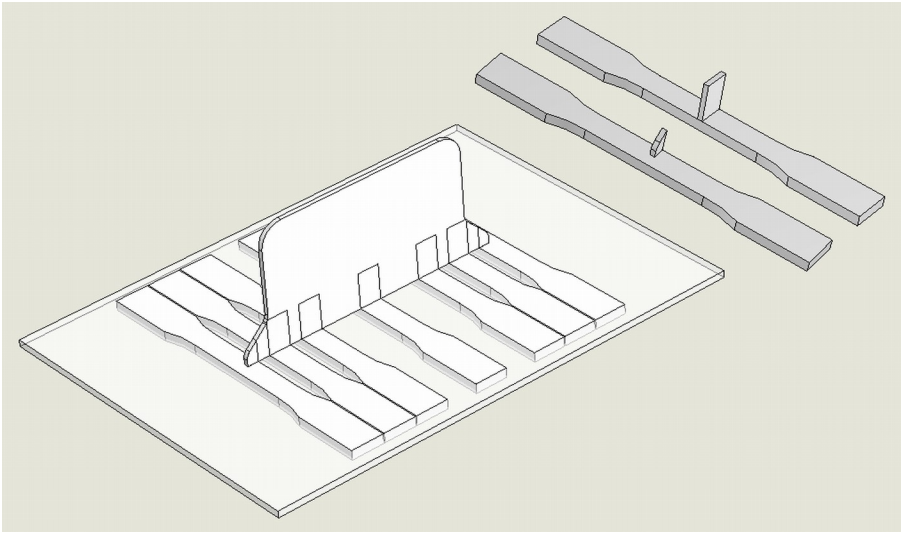

Figure 3.11: Sketch showing the locations of the extracted flat tensile specimens in the welded panel.

The fracture toughness properties of the skin-clip joints (plain welds) were determined by extracting C(T) 50 specimens from the base metal and from the weld with original weld configuration (keeping part of the clip part on the specimens, as shown in Figure 3.12).

The multiple specimen CTOD δ_5 (crack tip opening displacement) technique, which was developed at GKSS, consists of testing of several specimens which were unloaded at different CTOD levels. Corresponding Δa (crack length) values were measured for each CTOD value of the specimens. These non-standard specimens were tested to determine the role of weld and part of the clip presence on the crack tip deformation behaviour and consequently on the "apparent fracture toughness" values obtained.

a)

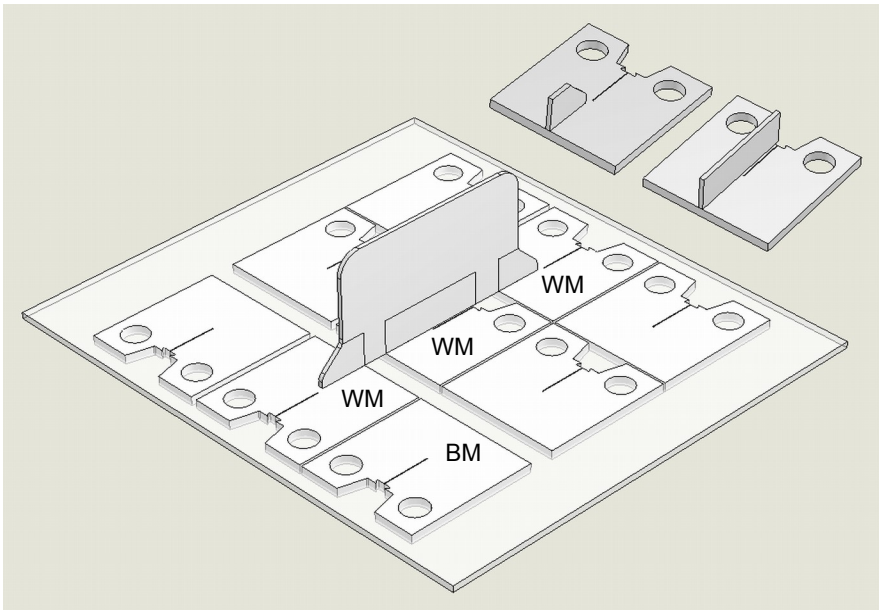

b)

Figure 3.12: Sketches showing a) the locations of the extracted C(T) 50 specimens in the welded panel, and b) welded and cut specimens.

3.4 Residual stress measurements on welded specimens

Residual stresses were determined using the neutron scattering technique at the mid-clip position in the middle of the base panel at different points through the scan line perpendicular to the weld. While longitudinal (x) residual stresses are stresses parallel to the weld line, transverse (y) stresses are perpendicular to the weld line. Normal stresses (z) act through the thickness direction of the base panel.

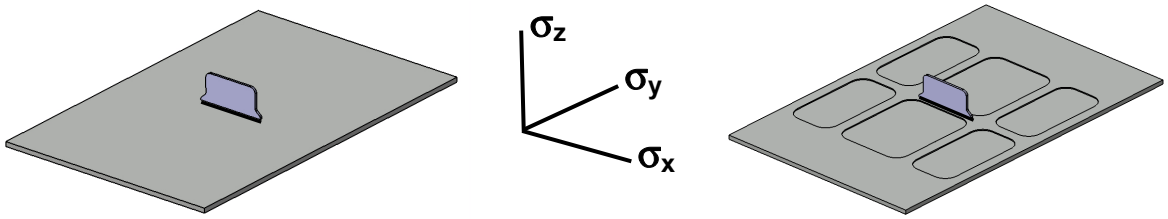

Figure 3.13: The directions of the measured residual stresses with respect to the welded plain and pocketed panels.

3.4.1 Methodology for stress determination

Residual strain measurements were performed with the neutron diffractometer ARES-2 at the Geesthacht Neutron facility (GeNF) at GKSS, see Figures 3.14 and 3.15 [105]. Neutrons of 0.1642 nm wavelength from an elastically bent perfect Silicon (311) monochromator were used. Triaxial residual stresses can be calculated from measured strains [106]. In general, diffraction elastic constants E and ν have to be used depending on the crystallographic plane (hkl) used for the strain measurement. However, the crystallographic anisotropy of the elastic constants is small for Al and therefore the macroscopic values of $E = 73$ GPa and $\nu = 0.33$ were used for the Al (311) reflection [107].

Assuming a plane stress state in a thin specimen, from the condition $\sigma_z = 0$, d_0 can be calculated for each point [52], [108]-[111]; the stresses σ_x and σ_y can be evaluated using the biaxial formula [106].

$$\sigma_X = (\varepsilon_X + \nu\varepsilon_Y)E/(1-\nu^2)$$
$$\sigma_Y = (\varepsilon_Y + \nu\varepsilon_X)E/(1-\nu^2) \qquad 3.1$$

and

$$\varepsilon_Z = -\nu(\varepsilon_X + \varepsilon_Y)/(1-\nu) \qquad 3.2$$

The plane stress assumptions used in the stress calculations was verified by FE simulations, the results are demonstrated in section 5.3.

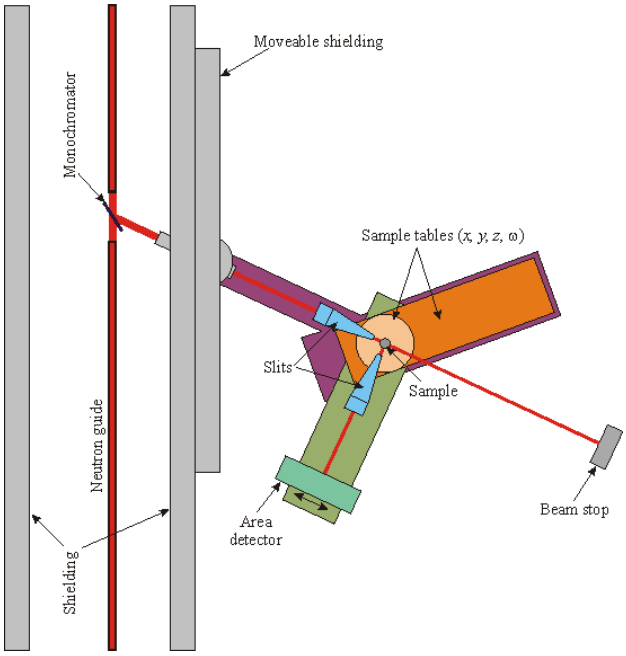

Figure 3.14: Setup of the neutron diffractometer ARES-2 at GKSS Research Centre.

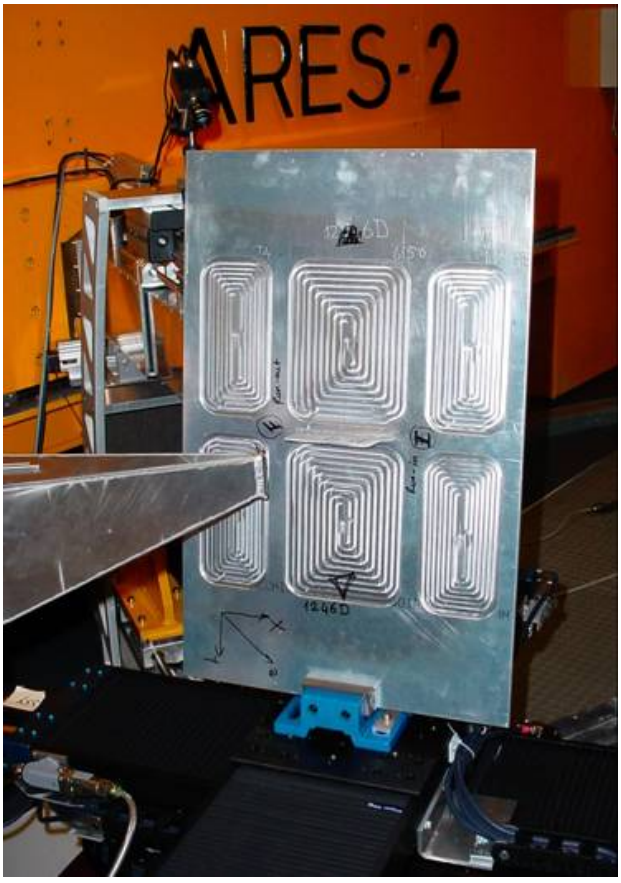

Figure 3.15: Strain measurement of the clip welded M(T) panel in which pockets were introduced.

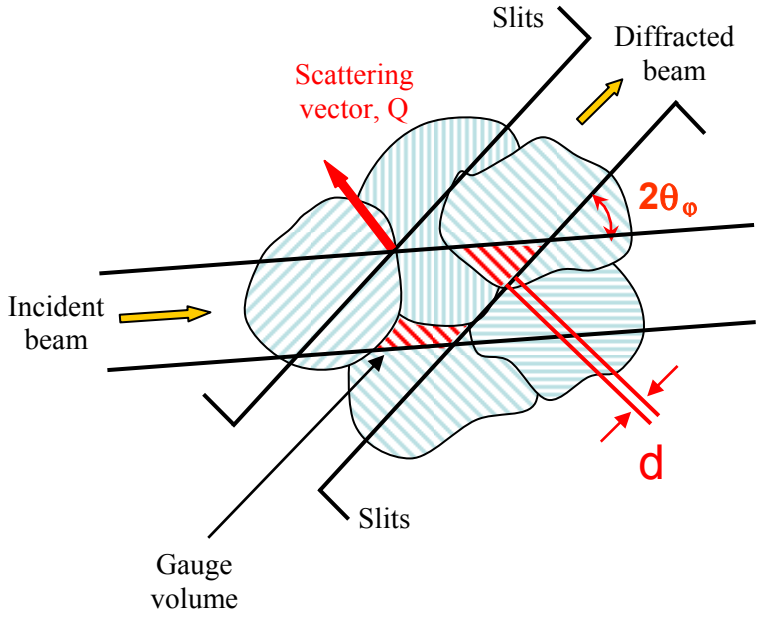

Figure 3.16: Principle of the neutron diffraction technique showing Bragg reflection from crystal planes with lattice parameter d .

3.4.2 Peak Fit

The principles of the neutron diffraction are illustrated in Figure 3.16. If d is the lattice spacing in the direction of Q and 2θ is the scattering angle then Bragg's law gives the positions of the coherent peaks [112], [113]

$$2d\sin\theta = \lambda \quad . \tag{3.3}$$

A small change in the lattice parameter Δd will result in a change $\Delta\theta$ in the angular position of the Bragg reflection given by

$$\Delta\theta = -\tan\theta\frac{\Delta d}{d} \quad . \tag{3.4}$$

The lattice strain ε, in the direction of the scattering vector is thus given explicitly as

$$\varepsilon = \frac{\Delta d}{d} = -\Delta\theta\cot\theta \quad . \tag{3.5}$$

To define the strain tensor at a point, and therefore the stress state, the d spacing shift must be determined as a function of sample orientation. For plane stress conditions or if the direction of the principle stresses are known, measurements in three, usually orthogonal, orientations are often sufficient for full definition.

The Bragg angles 2θ are detected by the centre of the diffraction peaks recorded for a certain location in the sample. The Gaussian function (Figure 3.17c) was chosen to fit all peaks of the samples. The lattice distances d_{hkl} of the planes are calculated from Braggs law.

Diffraction methods are sensitive to macro and microstresses, which can also lead to changes of the peak shape, which were, however, not observed here.

a) 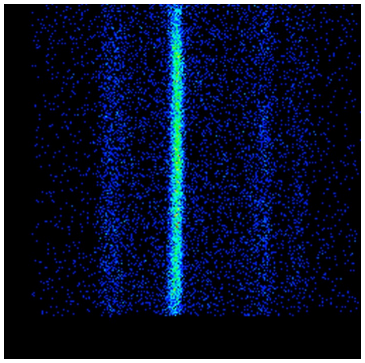 b) 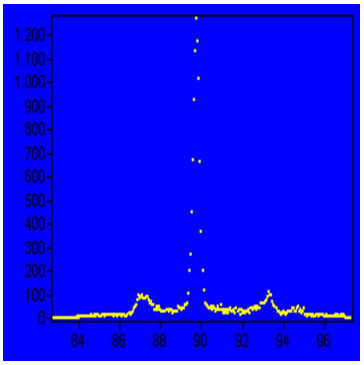

c) 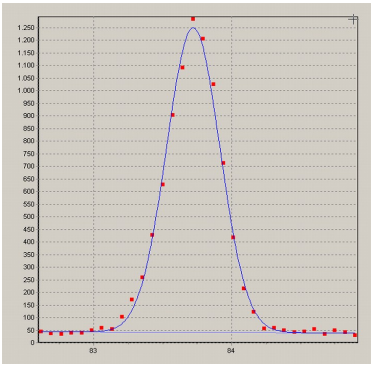

Figure 3.17: a) Detected part of Al (311) ring (detector image), b) integrated intensity and c) peak fit.

3.4.3 Positioning and strain measurement by ARES

The measurements were carried out in three perpendicular directions, which were chosen as the principal sample axes *x*, *y*, and *z* (Figure 3.13). Three scan lines were used perpendicular to the weld line (*y*-direction) in the base plate at mid-thickness. The zero position was the middle of the weld seam.

The gauge volumes were defined by Cadmium slits. A matchstick-like gauge volume of nominal size $2\times2\times10$ mm^3 was used for scanning ε_y and ε_z at the mid-clip position in the base metal for improving the intensity [114]–[119], assuming that the stresses are constant along *x* over the length of the volume element. A smaller volume size of $2\times2\times2$ mm^3 had to be used for scanning ε_x, because large stress gradients are present in the *y* direction. To increase the grain statistics in a measured volume, 5 measurements were carried out for scanning ε_x, each with 1.5 mm distances in the *x*-direction and the intensity of each were summed up to get a total intensity.

The Al (311) diffraction peak was recorded with an area detector at an angle of about 84°. This peak is recommended because the influence of micro-stresses on the stress results should be small, i.e. the (311) peak gives a good measure for the macro-stresses [107]. The peak centres, widths and intensities were obtained by least squares fitting of a Gaussian curve shape to the experimental data (Figure 3.17c).

3.4.4 Determination of the stress-free lattice parameter

For the determination of a triaxial stress state, the knowledge of the unstrained lattice parameter d_0 is required. Al-alloys 6156 and 6013 are heat treatable alloys in which the solute (Mg, Si mainly) concentration in the matrix can depend on the heat treatment. As the lattice parameter can change considerably with the solute content, the d_0-values can also depend on the heat treatment the materials were subjected to during welding [108]. To solve this problem, "comb" like structures (see Figure 3.18) with thin teeth (with 3 mm distance) were prepared by spark erosion from the weld regions of the 4.5 mm thick, conventionally welded 6156 T4 panel with pocket for all locations (run-in, middle and run-out, see Figure 3.19a) and two specimens from the on-going weld area of the 6156 T6 panel (without pocket) containing two run-ins (see Figure 3.19b). In such a cut specimen most of the macroscopic stresses are known to relax [109]. Such a comb could therefore serve as stress-free reference material [110].

Additionally, the measured lattice parameters "d" as a function of distances from the mid-clip position obtained from conventionally welded 6156 T4 panel with pocket at mid-clip position, run-in, and run-out are demonstrated in Figures 3.20a – 3.20c respectively. It can be seen that there are no significant variations of the lattice parameter for specimens from three locations. The average curve of three directions shows no significant variation in base metal as the position changes. The results (Figures 3.21a and 3.21b) taken from the specimens of the ongoing weld area of the 6156 T6 panel (without pocket) containing two run-ins also showed slight variation of the d values. Consequently, there is no need to make corrections for both specimens.

A slight asymmetry in the distribution of the d-values with respect to the mid-clip position (Figures 3.20 and 3.21) exist, since all samples were welded from one side.

a) 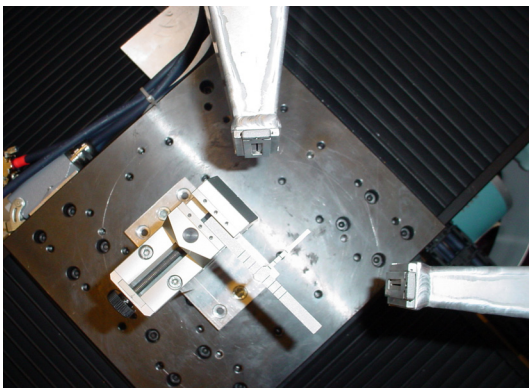 **b)** 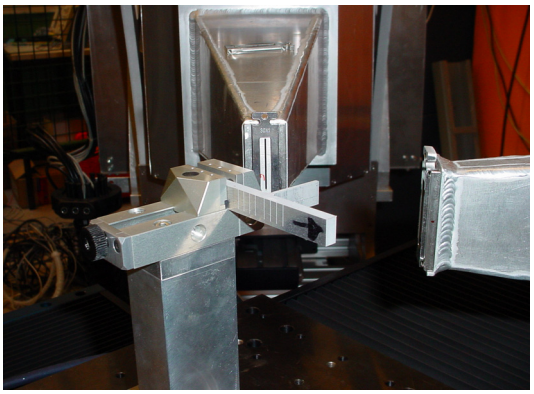

Figure 3.18: The installation of the "cut specimen" (comb-like specimen) for the residual stress measurement.

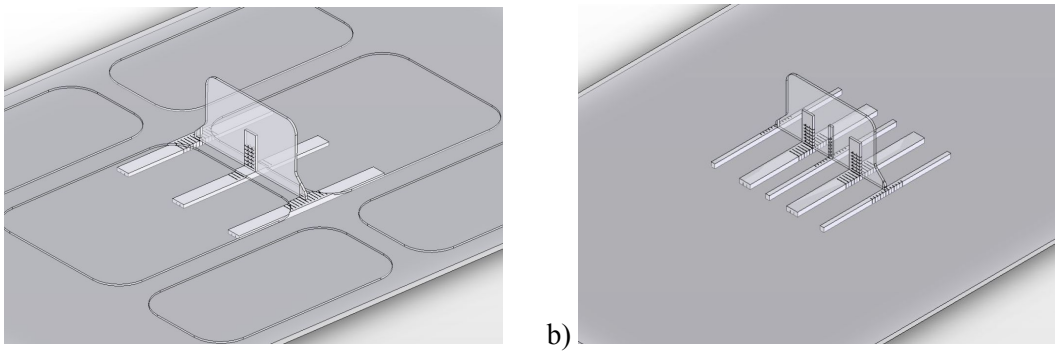

a) b)

Figure 3.19: The drawings show the locations of the extracted "comb-like" specimens from the 4.5 mm thick a) conventionally welded 6156 T4 panel with pocket, and b) 6156 T6 weld panel (without pocket) containing two run-ins.

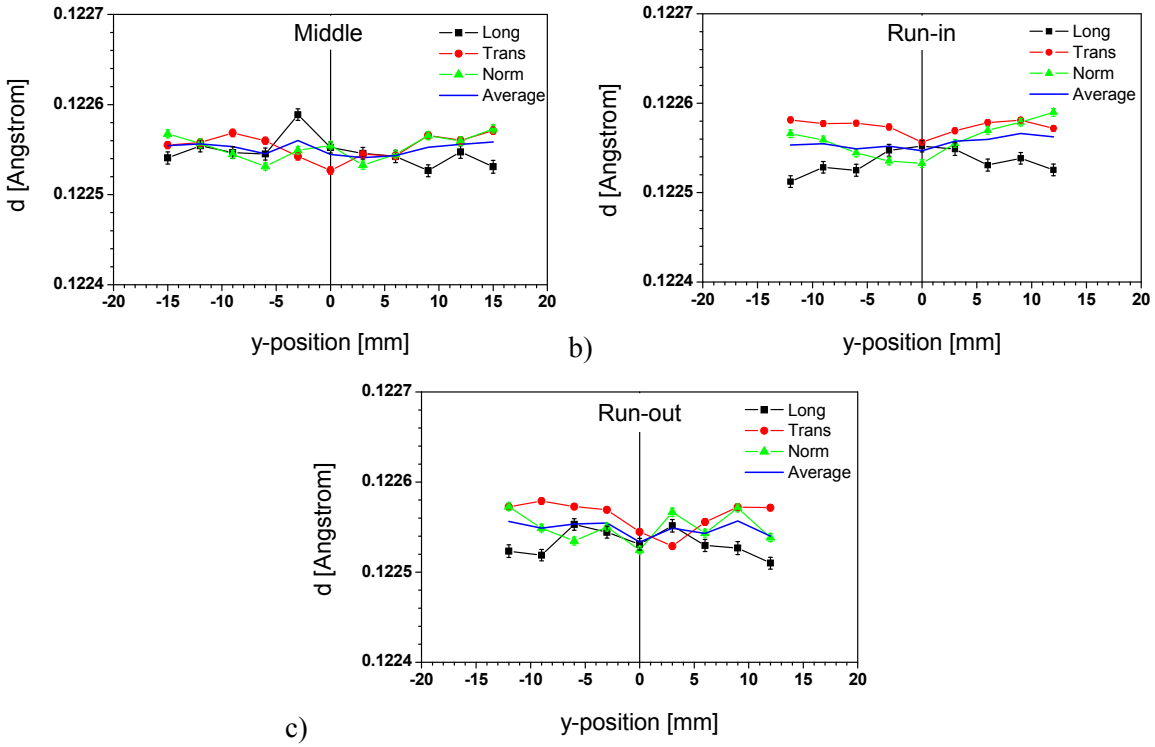

a) b) c)

Figure 3.20: Lattice parameters of the AA 6156 T4 comb specimens at a) mid-clip position of the base plate, b) run-in position of the base plate, c) run-out position of the base plate.

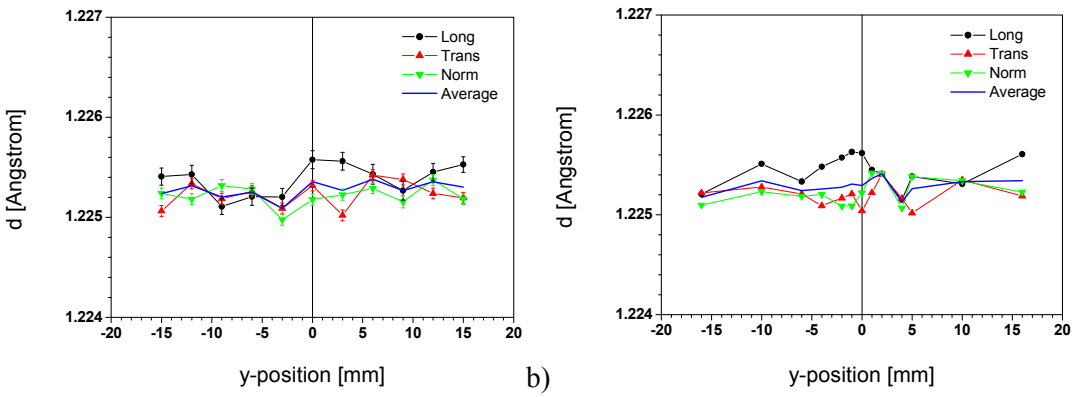

a) b)

Figure 3.21: Lattice parameters of the two AA 6156 T6 comb specimens at the on-going weld area of the base plate.

3.5 Fatigue crack propagation tests on welded middle tension specimens

Fatigue crack propagation (FCP) tests were performed at a stress ratio of $R = 0.1$ using a 400 kN capacity Instron servo-hydraulic fatigue machine operating at a frequency of 5 Hz at room temperature. Samples were subjected to constant-amplitude tensile sinusoidal loading, perpendicular to the welding line (Figures 3.22a and 3.22b), with a maximum applied load of 61 MPa. The initial central notch ($2a_0$), as shown in Figure 3.22a, has a circular hole with a diameter of 2 mm and a 0.2 mm thick electro-discharge machined notch of length 7 mm was placed at the mid-clip position adjacent to the weld toe on the root side (the rear side of the one-sided weld). The crack propagation length, Δa, was measured on the polished specimen surface using a travelling optical microscope on both sides (right and left sides). An average of both measurements was used to construct the FCP vs. crack length curves. Cyclic crack mouth opening displacement (CMOD) was also measured with a clip gauge at the backsides of the panels. The crack propagation rate, da/dN, was obtained by taking the derivative of the above crack length, a, versus cycles, N, curve by using an incremental polynomial method following the ASTM standard (E647) [120]–[124]. This method for computing da/dN involves fitting a second-order polynomial (parabola) to sets of $(2n+1)$ successive data points, where n is usually 1,2,3, or 4. The form of the equation for the local fit is as follows:

$$\hat{a}_i = b_0 + b_1\left(\frac{N_i - C_1}{C_2}\right) + b_2\left(\frac{N_i - C_1}{C_2}\right)^2 \quad , \tag{3.6}$$

where:

$$-1 \le \left(\frac{N_i - C_1}{C_2}\right) \le +1 \quad , \tag{3.7}$$

and b_0, b_1, and b_2 are the regression parameters that are determined by the least squares method (that is, minimization of the square of the deviations between observed and fitted values of crack size) over the range $a_{i-n} \le a \le a_{i+n}$. The value $\hat{a}_i$ is the fitted value of crack size at N_i. The parameters $C_1 = \frac{1}{2}(N_{i-n} + N_{i+n})$ and $C_2 = \frac{1}{2}(N_{i+n} - N_{i-n})$ are used to scale the input data, thus avoiding numerical difficulties in determining the regression parameters. The rate of crack growth at N_i is obtained from the derivative of the above parabola, which is given by the following expression:

$$(da/dN)_{\hat{a}_i} = (b_1)/(C_2) + 2b_2(N_i - C_1)/C_2^{\,2}. \tag{3.8}$$

The value of ΔK, stress intensity factor range associated with this da/dN value is calculated using the fitted crack size, $\hat{a}_i$, corresponding to N_i.

$$\Delta K = K_{\max} - K_{\min} = f(g)\Delta\sigma\sqrt{\pi a} \quad , \tag{3.9}$$

where $\Delta\sigma$ is the remote stress applied to the component and $f(g)$ is the geometrical function.

According to E647 [124], for M(T) specimens,

$$f(g) = \sqrt{\sec\frac{\pi a}{W}} \quad , \tag{3.10}$$

where W is the width of the panel.

The start and end locations of the weld are areas with high stress concentration due to the weld geometry of the T-joint. These locations may give rise to solidification cracking during welding and crack initiations under external loadings. Therefore, FCP behaviour along the weld seam and across these locations was carefully monitored.

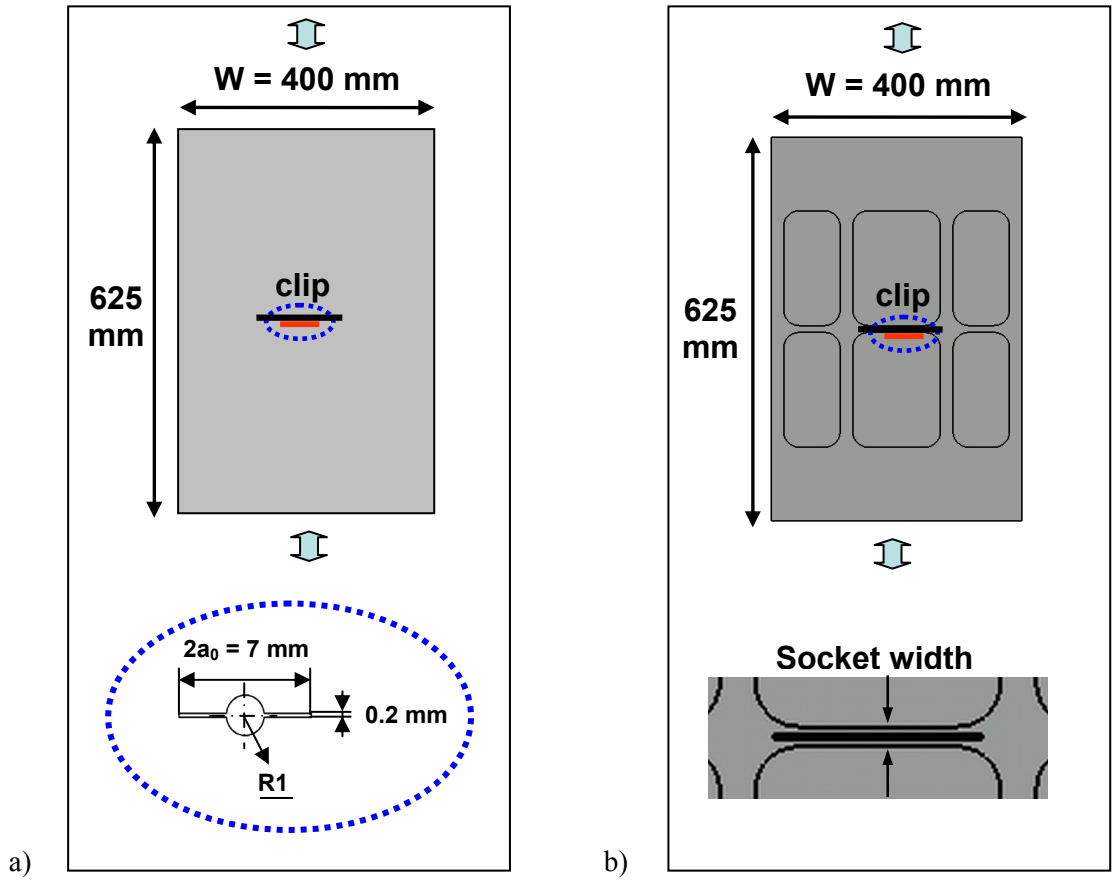

Figure 3.22: The panel types, dimensions, and details of the central through thickness notch introduced at the toe of the clip weld on the root side (indicated by the red line).

4 Finite element modelling of residual stresses

4.1 Methodology for FE modelling of residual stresses

Welding processes induce metallurgical and mechanical consequences, the evaluation of which requires the modelling of complex interactions between several physical phenomena such as thermics, metallurgy and mechanics [125]. Accurate prediction of the welding residual stresses is very difficult due to the complexity of welding process which includes localized heating, temperature dependence of material properties and moving heat source, etc [75]. In reality, important heat transfer effects are usually three–dimensional and therefore a 3D finite element (FE) analysis is required for most welding situations [60], [61].

In this study, a 3D FE model was developed to simulate the laser welding process for the 4.5 mm thick M(T) 400 clip welded panel without pocketing using the commercial code SYSWELD. Three types of interaction between thermal and metallurgical analyses are considered in the SYSWELD:

- phase transformations depending directly on the thermal history of the part,
- phase transformations accompanied by latent heat effects which modify temperature distribution,
- phase-dependent thermo-physical properties,
- A material is characterized at any moment by the proportions of its constitutive phases. Different models [LeD], [PBRF] are available within SYSWELD to describe the transformation kinetics of most materials. The models can deal with several transformations between several phases.

For the modelling of Aluminium alloys of 2xxx and 6xxx series, which can be hardened by heat treatment (precipitation), there exists a model allowing the simulation of precipitate dissolution kinetics. During welding, the heating at high temperature locally generates dissolution of precipitates for alloys hardened by precipitation. From a mechanical point of view, the generation of the new structure in the heat affected zone is accompanied by a strong decrease of properties. To model these phenomena in SYSWELD, two fictitious phases are considered: an initial hard phase and a generated soft phase. The hard phase corresponds to precipitation-hardened alloy. The soft phase corresponds to the “de-precipitated” structure. During the thermo-metallurgical analysis, a transformation from the hard to the soft phase is defined, depending on temperature and time. During the mechanical analysis, the mechanical properties of the hard and soft phases are different.

For welding processes simulation, the thermal analysis is computed under transient condition by solving the equations in the moving source frame. However, a significant number of time points, at which the temperature results were to be read into the metallurgical and mechanical analysis, were defined to capture the temperature gradient and give accurate residual stress results using the time steps option.

Figure 4.1 shows the inputs and steps of the welding simulation procedure [126]. First the geometry of the specimen was modelled and the mesh was generated as will be explained in the next section. Then the heat source was simulated as described in section 4.3. To perform the thermal analysis, the metallurgical transformations were subsequently defined and the

boundary and the initial conditions were applied in the form of heat loss and temperature of the environment, respectively [126], [127].

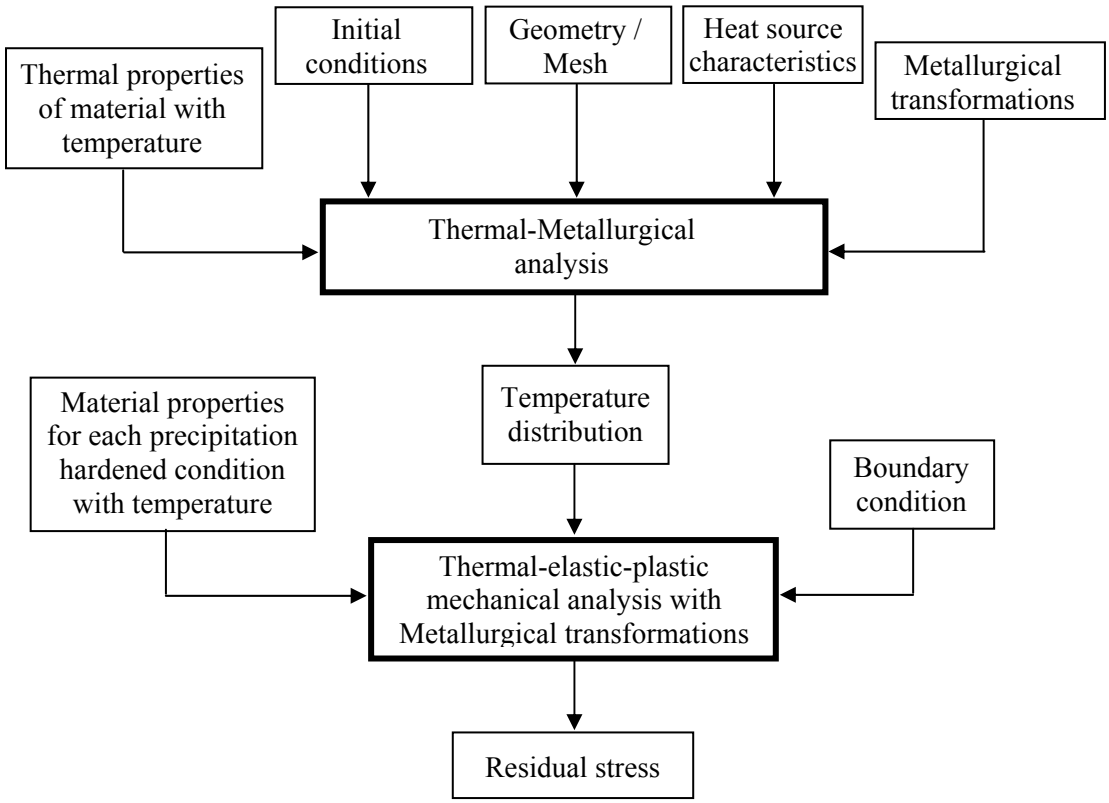

Figure 4.1: Flow chart of the welding simulation procedure [126].

4.2 Mesh preparation

The geometry of the welded clip structure, shown in Figure 3.2, was modelled using two types of elements; three-dimensional volume elements with eight nodes and two-dimensional membrane elements with four nodes. The three-dimensional elements were used for the basic body structure and two-dimensional elements for the surface of the welded parts in order to simulate the boundary between the structure and the environment. A dense mesh (element size of 0.75 mm×0.5 mm in x and y directions, longitudinal and transverse directions respectively) was used in the area along the weld line, as shown in Figure 4.2, and a coarser mesh (10 mm in x direction) for the rest of the structure. The final mesh was the result of compromise between computing time and accuracy.

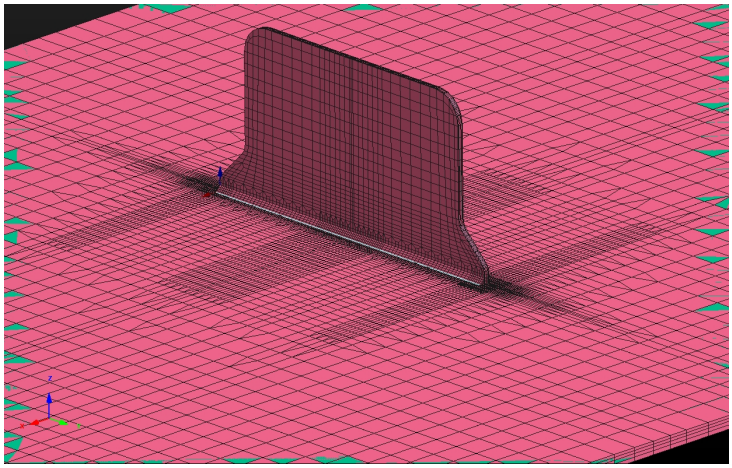

Figure 4.2: Three-dimensional FE model of the geometry.

4.3 Heat input

The heat input to the weld is generally calculated from the energy supplied. The heat input distribution will determine the size and shape of the weld pool. In order to simulate the heat distribution and flow in the welding direction, the laser beam is modelled as a three-dimensional moving heat source. The model of the heat source assumes a Gaussian heat flux distribution on the weld pool simulated by a cone. This model has the capability to be changed by the simple change of various geometrical parameters in order to simulate different weld pools that correspond to different welding parameters.

During laser welding, part of the energy generated by laser source is lost before absorption by the work-piece material. Energy loss is due to the reflection from specimen surface. The rest of energy was absorbed by the work-piece. It has to be mentioned that the maximum effective input power of heat source Q_{in} is 70% of the laser power Q_{laser} in case of Aluminium [58].

A cone-shaped volumetric heat source with Gaussian distribution of thermal flux [57], [59], [64] is used to attain the required weld pool size and temperature fields. The conical distribution of power density which has a Gaussian distribution radially and a linear distribution axially yields more accurate results in terms of capturing the effect of keyhole formation due to laser beam penetration. The heat flux of Gaussian distribution can be computed according to the formula

$$Q = \frac{2P}{\pi r_0^2 H} e^{1-(r/r_0)^2} (1 - \frac{z}{H}), \qquad 4.1$$

where P is the absorbed laser beam power, r_0 the initial radius (at the top of the keyhole), H the depth, r the current radius, i.e. the distance from the cone axis, and z is the current depth. The heat source parameters were given as an input to create the 3D conical Gaussion shape which was used during welding simulation with SYSWELD. Due to difficulties in the modelling of heat input, even with the aid of predefined source forms, heat source parameters were optimized by comparison of the thermally simulated and the experimentally observed weld pool geometry (see Figure 4.3).

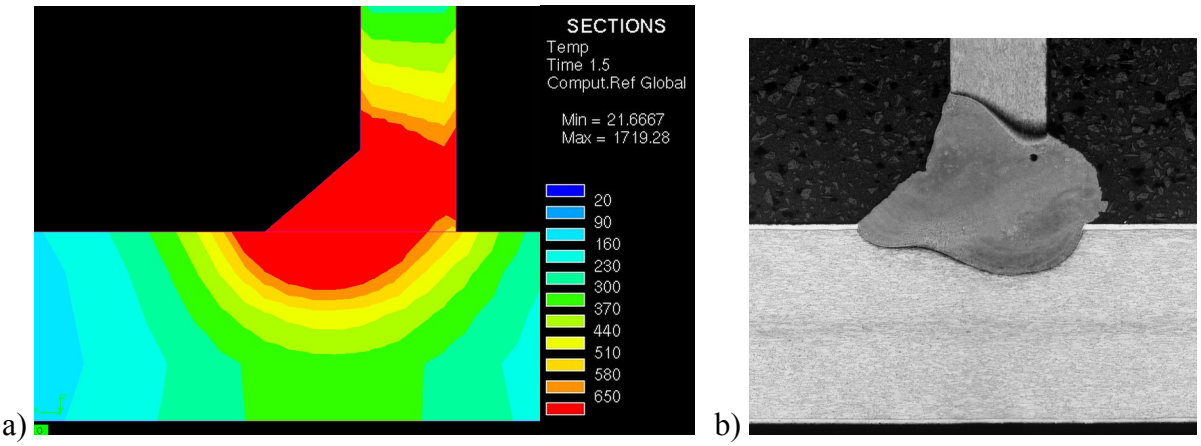

Figure 4.3: Comparison of the melted zone showing the a) thermal simulation result (red zone) and b) microstructure cross section.

The comparison of the cooling curves of the thermal measurement (Exp) and simulation (Pre) at thermocouple positions of mid-clip, run-in and run-out locations are given in Figures 4.4, 4.5 and 4.6 respectively. There exist discrepancies between experiment and simulation results, which resulted in higher residual stress calculations compared to experimental results (see section 5.3). Further improvement of the simulation with finer meshing within the weld area can be done, however the FE simulation results were satisfactory to predict the residual stresses qualitatively.

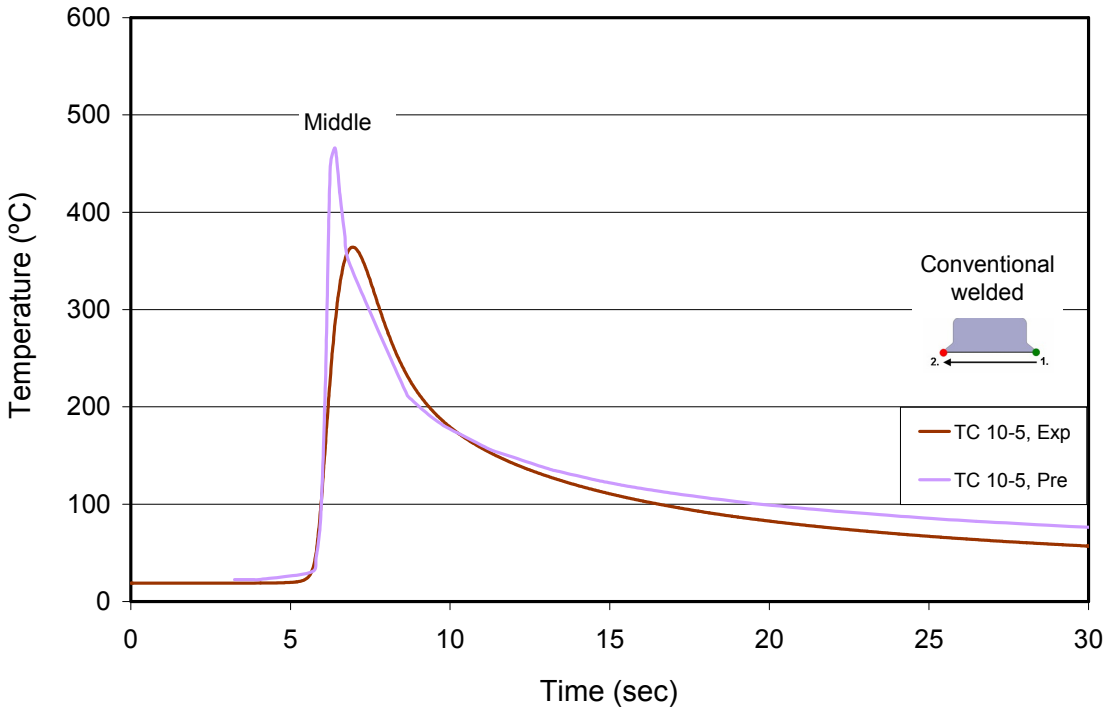

Figure 4.4: Comparison of cooling curves of the thermal measurement and simulation at the thermocouple position 10–5 (see Figure 3.6), which is giving the thermal history during conventional welding at mid-clip location in the 6156 T6 skin material.

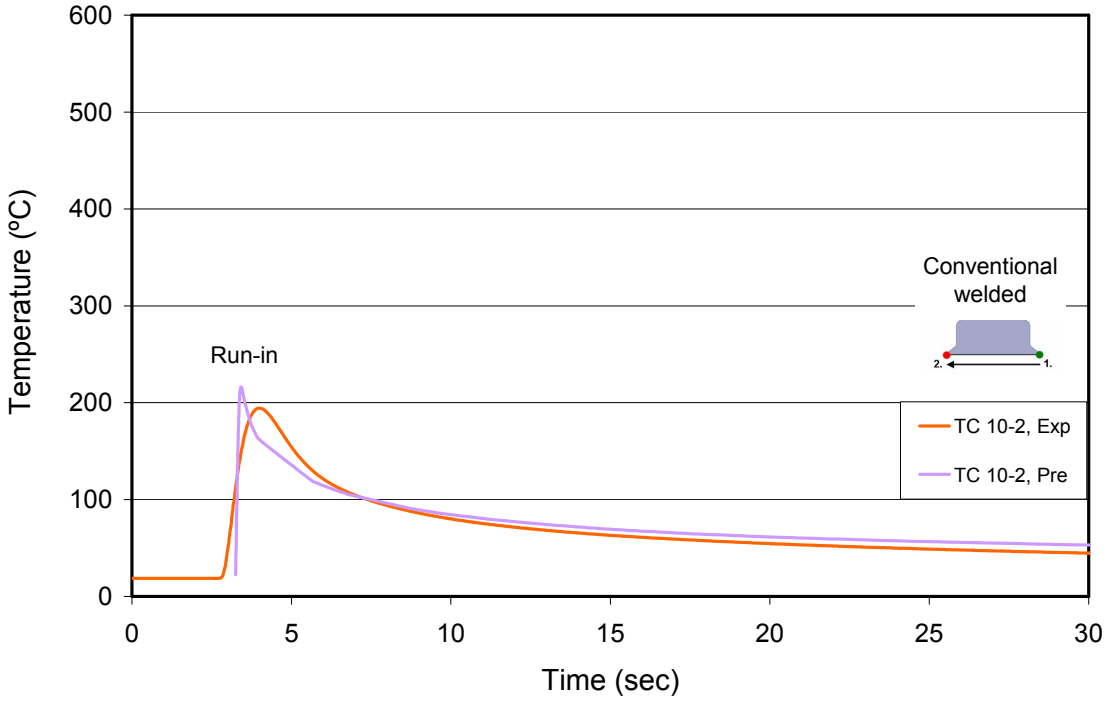

Figure 4.5: Comparison of cooling curves of the thermal measurement and simulation at the thermocouple position 10–2 (see Figure 3.6), which are giving the thermal history during conventional welding at run-in location in the 6156 T6 skin material.

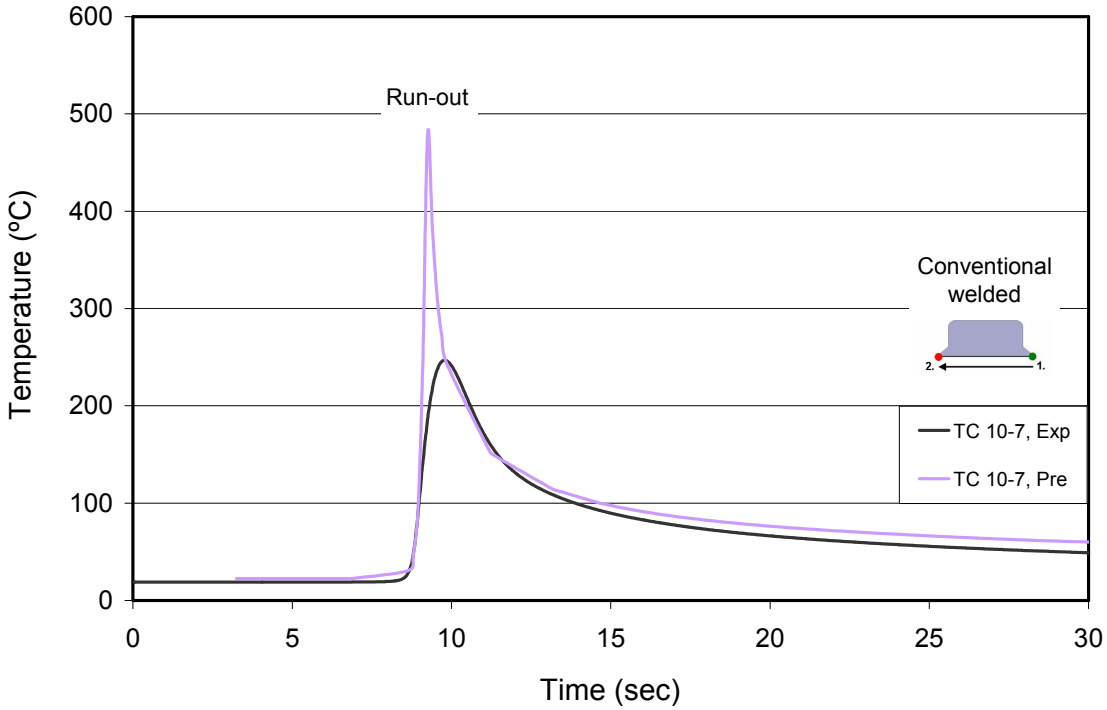

Figure 4.6: Comparison of cooling curves of the thermal measurement and simulation at the thermocouple position 10–7 (see Figure 3.6), which is giving the thermal history during conventional welding at run-out location in the 6156 T6 skin material.

4.4 Boundary and initial conditions

During the welding process, the heat was supplied to the weld pool by the laser beam. This heat is transferred to the metal by conduction and convection. A part of this heat energy is lost by free convection and radiation. In SYSWELD, the heat loss was implemented into the FE code by developing a FORTRAN subroutine. The heat loss by free convection follows Newton's law, where the coefficient of convective heat transfer was assumed to vary with both temperature and orientation of the boundary

$$q_c = \frac{kN_u}{L}(T - T_a), \tag{4.2}$$

where k is the thermal conductivity of the material, L the characteristic length of the plate (or surface), T_a the ambient temperature, and N_u the Nusselt number defined by;

$$N_u = 5.67 P_r^{\frac{1}{3}} G_r^{\frac{1}{3}}, \tag{4.3}$$

where P_r is the Prandtl number and G_r is the Grashof number, both of them being functions of ambient air properties and temperature differences between the surface and the environment

$$G_r = \frac{g\alpha(T_s - T)L^3}{\nu^2}, \tag{4.4}$$

where g is gravity, α is the thermal expansion coefficient, T_s is the surface temperature, L is the length, ν is the kinematic viscosity.

$$P_r = \frac{\nu}{\kappa}, \tag{4.5}$$

where ν is the kinematic viscosity, κ is the thermal diffusivity.

Heat losses due to thermal radiation between the weldments and environment are important when the temperature difference is high. This radiation was modelled by the standard Stefan–Boltzman relation

$$q_r = \varepsilon\sigma(T^4 - T_\alpha^4), \tag{4.6}$$

where ε is the heat emissivity and σ is the Stefan–Boltzman constant. Radiation is assumed from the surface to the surroundings. Prior to welding the material is assumed to be at room temperature.

4.5 Metallurgical transformation

A metallurgical analysis based on a precipitate dissolution kinetics was carried out in order to simulate dissolution of precipitates (β''–Mg_2Si) during welding. For the dissolution of the precipitations, under isothermal conditions, the reaction kinetics formula

$$t_1^* = t_{r_1}^* \exp\left[\left(\frac{Q'_{app}}{n_1 R} + \frac{Q_s}{R}\right)\left(\frac{1}{T} - \frac{1}{T_{r_1}}\right)\right] \quad \text{and} \quad f / f_0 = 1 - \left[t / t_1^*\right]^{n_1}, \tag{4.7}$$

was used where t_1^* is the time taken for complete reversion at $T(s)$, $t_{r_1}^*$ is that at $T_{r_1}(s)$, Q'_{app} is the enthalpy of apparent (metastable) solvus boundary, n_1 is the time exponent in dissolution model, R is the universal gas constant, Q_s is the activation energy for diffusion, f / f_0 is the ratio of particle volume fraction to the initial particle volume fraction, T is the temperature and T_{r_1} is the chosen reference temperature.

4.6 Thermal and mechanical solution

For the solution, a thermo-elasto-plastic analysis associated with metallurgical transformations was performed. The solution was conducted in two basic steps. First a transient heat transfer analysis with metallurgical transformations was carried out and the resulting temperature field was used on the second step as input to the mechanical analysis. A suitable time-stepping scheme was used for each analysis to realize fast convergence of the solution and reasonable accuracy.

The thermal analysis was performed using temperature dependent thermal material properties. The governing partial differential equation for the transient heat conduction is

$$k(T)\left\{\left(\frac{\partial^2 T}{\partial x^2}\right) + \left(\frac{\partial^2 T}{\partial y^2}\right) + \left(\frac{\partial^2 T}{\partial z^2}\right)\right\} + \dot{Q} = \rho(T) C_p(T)\left(\frac{\partial T}{\partial t}\right), \tag{4.8}$$

where x, y, z are the Cartesian coordinates, $\dot{Q}$ is the internal heat generation. In addition, ρ refers to the density, k to the thermal conductivity and C_p to the specific heat, which are all functions of temperature T.

The results of the thermal analysis (temperature distribution) were used as an input to the mechanical analysis, which requires the mechanical properties variation with temperature and the boundary conditions (clamping). The mechanical analysis was performed using an elastoplastic material formulation with von Mises yield criterion [129]

$$\sigma_v = \sqrt{\frac{1}{2}\left[(\sigma_1 - \sigma_2)^2 + (\sigma_2 - \sigma_3)^2 + (\sigma_3 - \sigma_1)^2\right]}, \tag{4.9}$$

with σ_1, σ_2 and σ_3 being the principal stresses and σ_v is the von Mises stress. Isotropic hardening has been considered in the model

$$F(\sigma_{ij}, \varepsilon_{eq}^{p}) = \sigma_{eq} - \sigma^{0}(\theta, \varepsilon_{eq}^{p}) \ , \qquad 4.10$$

where θ is the temperature and ε_{eq}^{p} is the cumulative equivalent plastic strain. Strain hardening was applied to the model by Ramberg-Osgood law

$$\sigma^{0}(\theta, \varepsilon_{eq}^{p}) = k(\theta) + K(\theta)\varepsilon_{eq}^{p^{n(\theta)}} \ , \qquad 4.11$$

where k is the internal variable, K and n describing the hardening behavior of the material.

Temperature dependent material properties used in FE simulation is given in Figure 4.7 for Al-Mg-Si alloy in T4 condition and in Figure 4.8 for T6 condition. The time required for the solution of the iterations was around 9 hours.

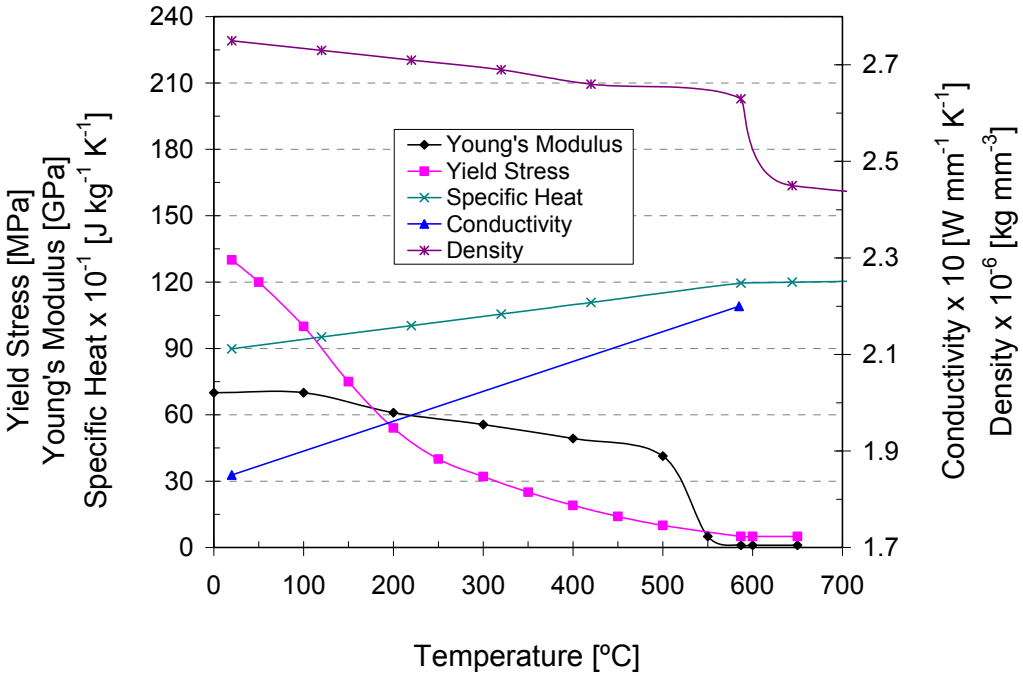

Figure 4.7: Material properties of Al-Mg-Si alloy in T4 condition used in FE simulation.

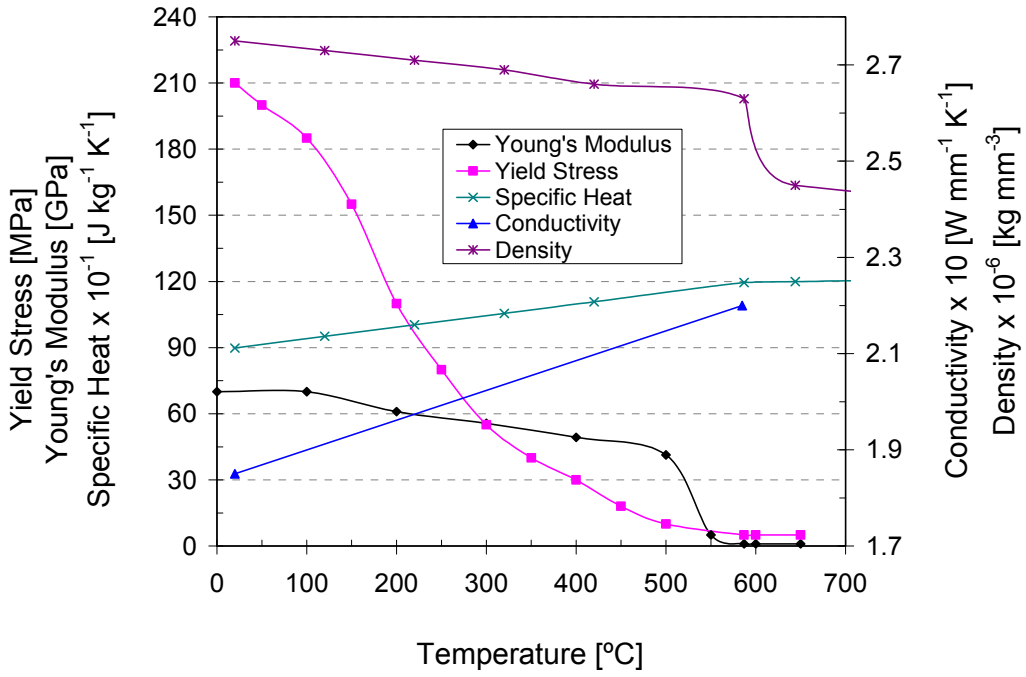

Figure 4.8: Material properties of Al-Mg-Si alloy in T6 condition used in FE simulation.

5 Results and Discussion

5.1 Microstructural and mechanical properties of weld joints

Microstructural characterization and hardness evaluation of the weld zones were conducted and detailed examinations were made at the run-in and run-out locations to reveal any hot cracking occurrence. However, no cracking was observed in all three skin materials used in this study. Tensile strength and fracture toughness of the base metal and welded panels were also determined. Additionally, post-test examinations were made to understand the fatigue crack propagation paths.

5.1.1 Microstructural features

A macrograph of the 4.5 mm thick 6156 T6 alloy, conventionally welded, is shown in Figure 5.1. The joint shapes and formation of root profiles as well as porosity formation can still be improved; however in this study, emphasis was not given to obtain a perfect weld, rather to focus on the residual stress control issues.

The 6xxx series aluminium alloys show a tendency to solidification cracking unless the weld metal composition includes appropriate filler metal additions. Hot cracking was avoided by using of filler wire of 4047 alloy containing high Si content (12%), see Figure 5.4. Due to a high solute level, the availability of sufficient eutectic liquid provides healing of tears during cooling [31].

Optical microscopy was used to characterize the microstructures of the base metal region, the heat affected zone (HAZ) and the weld metal (fusion zone), Figure 5.2 and 5.3. In literature [130], [131], particles for 6013 are given as a $Al_{12}(Fe,Mn)_3Si$ or as a $Al_{12}Mn_3Si$ for 6013 depending on the composition of the alloy. Former ($Al_{12}(Fe,Mn)_3Si$) is an intermetallic constituent particle formed during ingot casting. These constituent particles, especially when heterogeneously distributed and large in size, are detrimental for the fracture toughness and fatigue crack propagation resistance of the material as they create voids at particle/matrix interfaces ahead of the crack tip during crack growth. These form by a liquid-solid eutectic reaction during solidification, primarily from iron. Because the low solubility of iron in pure aluminium is reduced by alloying elements, constituent particles containing iron are insoluble. The size and size distribution of insoluble constituent particles are controlled by the rate of ingot solidification, the chemical composition, and the extent and nature of deformation. The particle size decreases with increasing solidification rate, as iron content decreases and as the amount of deformation increases. Constituents generally range in size from 1-30 μm. Latter ($Al_{12}Mn_3Si$) is dispersoid particle formed during the ingot preheat by precipitation of the transition element manganese. Their presence control grain structure and degree of recrystallization. Dispersoids normally range in size from 10-200 nm. Since they form from a solid-solid reaction, at least one of their interfaces with the matrix is coherent. The crystal structure of this type of dispersoid is non-cubic and stable unless thermal treatments much above the conventional solution treatment temperature are applied. Depending on their size and details of their interface with the matrix, dispersoids may also be detrimental, in that nucleation of fine voids at dispersoids may lead to the formation of void sheets and hence void coalescence between constituent particles may occur.

Strengthening of the 6156 alloy was promoted by T6 temper consisting in maintaining the alloy at 190 °C during 4 h. According to literature, aging results in the precipitation of intermetallic ternary and quaternary nanometric second phase particles. Copper is added to

6xxx series alloys to increase the peak aged strength above that achievable with Mg+Si alone. Sufficient copper changes the main precipitating species from Mg_2Si to a quaternary intermetallic, i.e. $Al_xMg_ySi_zCu_w$ [132]. The study of Olea et al. [133] demonstrated that the precipitation sequence in Al-Mg-Si-Cu alloy is as follows;

α (sss) $\rightarrow$GP zones $\rightarrow$ needle type ß´´ (Mg_5Si_6)$\rightarrow$ lath type Q´ $\rightarrow$ Q ($Al_5Cu_2Mg_8Si_6$) + Si.

Cabibbo et al. [134] also showed that friction stir welded 6056 parent metal contains a large number of GP zones and ß´´, together with Q phase. The morphology of precipitates obviously depends on their structure: needle or rod shaped particles correspond to a metastable ternary phase ß´ (rod type) or ß´´ (needle type, coherent) while laths correspond to the quaternary phase Q´ (AlMgSiCu) precursor of the stable Q phase. In the case of 6056 T6, the study of Delmas et al. [135] reports the precipitation of lath and needle shaped particles lying along ⟨100⟩ directions of the aluminium matrix. In the case of 6013 T6, Braun et al. [31] found fine needle-shaped ß´´ precipitates in the fusion zone of post-weld heat treated joints. In the study of Heinz et al. [136] also, Q´ and Q are not reported in 6013 T6. The precipitates normally range in size from 1-10 nm.

All the fusion zones (FZ) of different alloy welds displayed a very normal development of the solidification microstructure, which was generally consistent with previous observations of solidification structures in fusion welds. As is normal with weld solidification, freezing began with planar epitaxial growth from the solid, which broke down within about 2 microns into bundles of columnar cellular dendrites growing approximately normal to the local solid/liquid interface, see Figures 5.2 – 5.3 [132]. The dendritic cores are defined as a row of fine platelets of the dominant eutectic second phase, which is occurred from the filler alloying element silicon. The interdendritic regions should contain several eutectic phases (binary and ternary eutectics of Al, Si, Mg and Cu or probably eutectic formed by the alloying elements of the filler powders and the parent material) [31], [132], [32]. In inner parts of the welds, randomly oriented equiaxed grains were observed, which were nucleated and grown in the weld pool, see Figure 5.4. The equiaxed grains were clearly distinguishable from the columnar epitaxial grains as the former had coarser dendrite arm spacing and more dendrite side-branching. Porosity was detected as a main weld defect. Vaidya et al. [34] reported that the fusion zone of both 6056 and 6013 were free from hardening precipitates.

The weld interfaces in both the base metal part and T-part were sharp as can be seen from Figure 5.1 (fusion line). It was reported that, the composition of the weld metal within the fusion zone boundary, that is the planar part of the epitaxial growth zone in the current study (Figures 5.2d and 5.3d), may differ significantly from the fusion zone composition in aluminium alloys [131], [137]. This region melts and freezes without mixing with the rest of the fused metal when there is not enough time for mixing during cooling. Although the compositions of this unmixed zone is close to that of the base metal, it is much softer due to dissolution of the strengthening precipitates and dispersoids, which stayed in a solid solution upon fast cooling conditions of the power beam welding processes.

Adjacent to the fusion boundary within the HAZ, a partially melted zone (PMZ), which is caused by grain boundary liquation, with a width of two or three grains was observed. Transient melting followed grain boundaries in the solid and also tended to envelop dispersoids occurring within the grains in the zone [132], see also Figure 5.2. Grain boundary liquation is a result of eutectic reaction between the grain boundary phases and the matrix. If the peak temperature is higher than this eutectic reaction temperature close to the fusion

boundary, more α matrix dissolved in the eutectic GB liquid decreasing solute concentration. This hypoeutectic liquid resolidifies with a planar mode and with severe solute segregation. GB liquid solidified first as a soft and ductile solute depleted α band and last as a hard, brittle solute-rich eutectic at the new GB. Whereas a light-etching shows α band existed along the cold side of the boundary, a dark-etching represents eutectic GB (Figures 5.2d and 5.3d). This was confirmed in the study of Huang et al. [138] by both microsegregation measurements and microhardness testing after welding and also suggested by Leigh et al. [132]. Solidification of GB liquid was directional and upward and toward the weld because of the high temperature gradients in the PMZ.

GB liquation could lead to hot cracking if the material undergone tensile strains before the melt solidifies. However, no intergranular cracking was detected as can be seen from Figures 5.2d and 5.3d. Consequently, although the welding process markedly produces a transient liquated structure prone to rupture, the thermomechanical response of the solid material around the moving weld pool clearly generates little or no tensile strain field in the affected area until after the local temperature has decreased below the solidus [132]. No microstructural changes were detected in HAZ beyond the extent of the PMZ. Therefore, the full extent of the HAZ was studied by using microhardness data to estimate the nature of thermally induced metallurgical changes as a function of distance from the weld fusion zone. Vaidya et al. [34] reported that near to the fusion line and within HAZ, lenticular precipitates were available in the grain boundaries of the base metal and only dispersoids were present in the grain interior. Hence, such soft regions should be prone to plastic deformation under external stresses. Indeed, these softened locations have shown to be critical due to plastic strain localization which leads to damage initiation and rupture under high stresses.

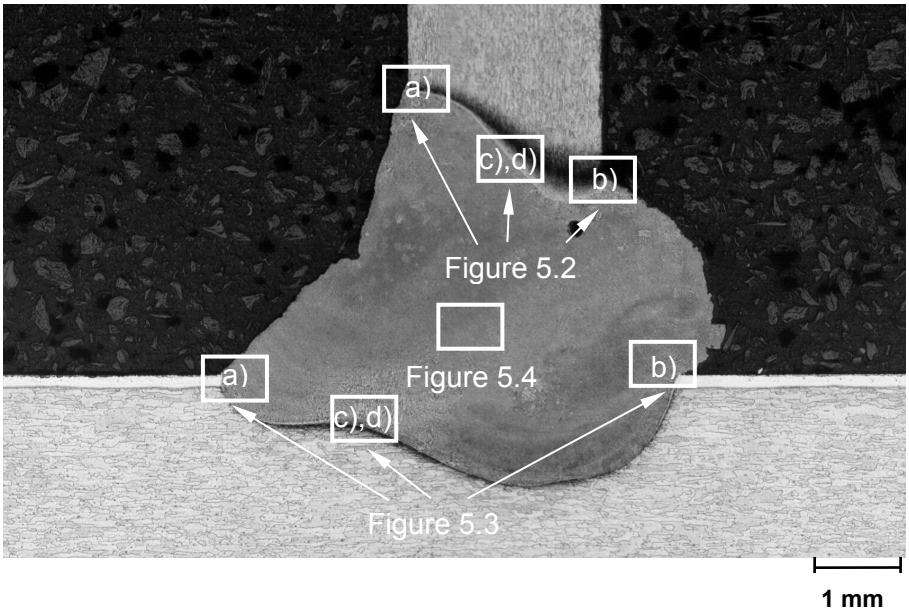

Figure 5.1: Representative cross-sectional view showing conventionally welded 6013 T6 clip on 6156 T6 skin material.

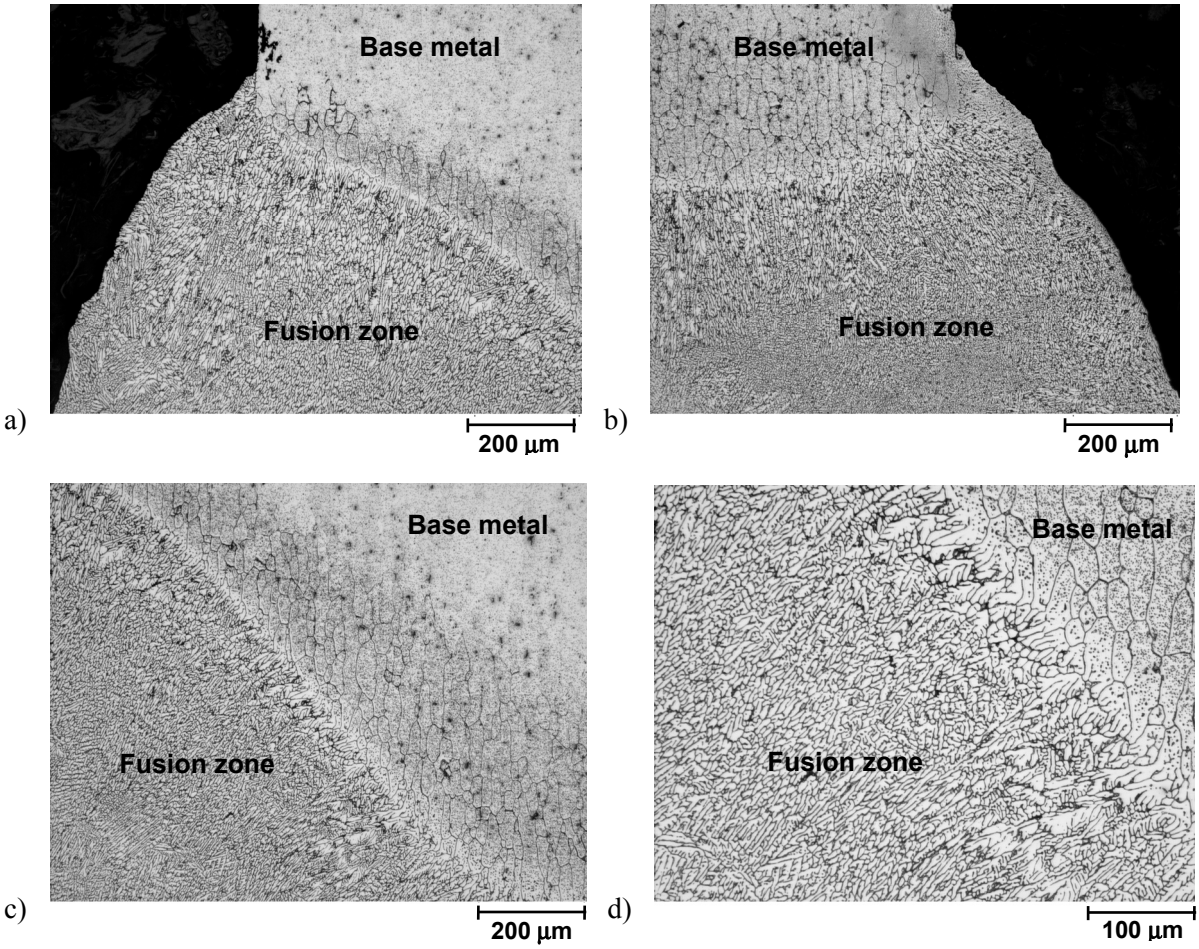

Figure 5.2: Detailed views taken from upper side (through the clip) of the clip weld illustrating FZ, HAZ, and BM. Grain boundary liquation is more apparent in larger magnification (see d).

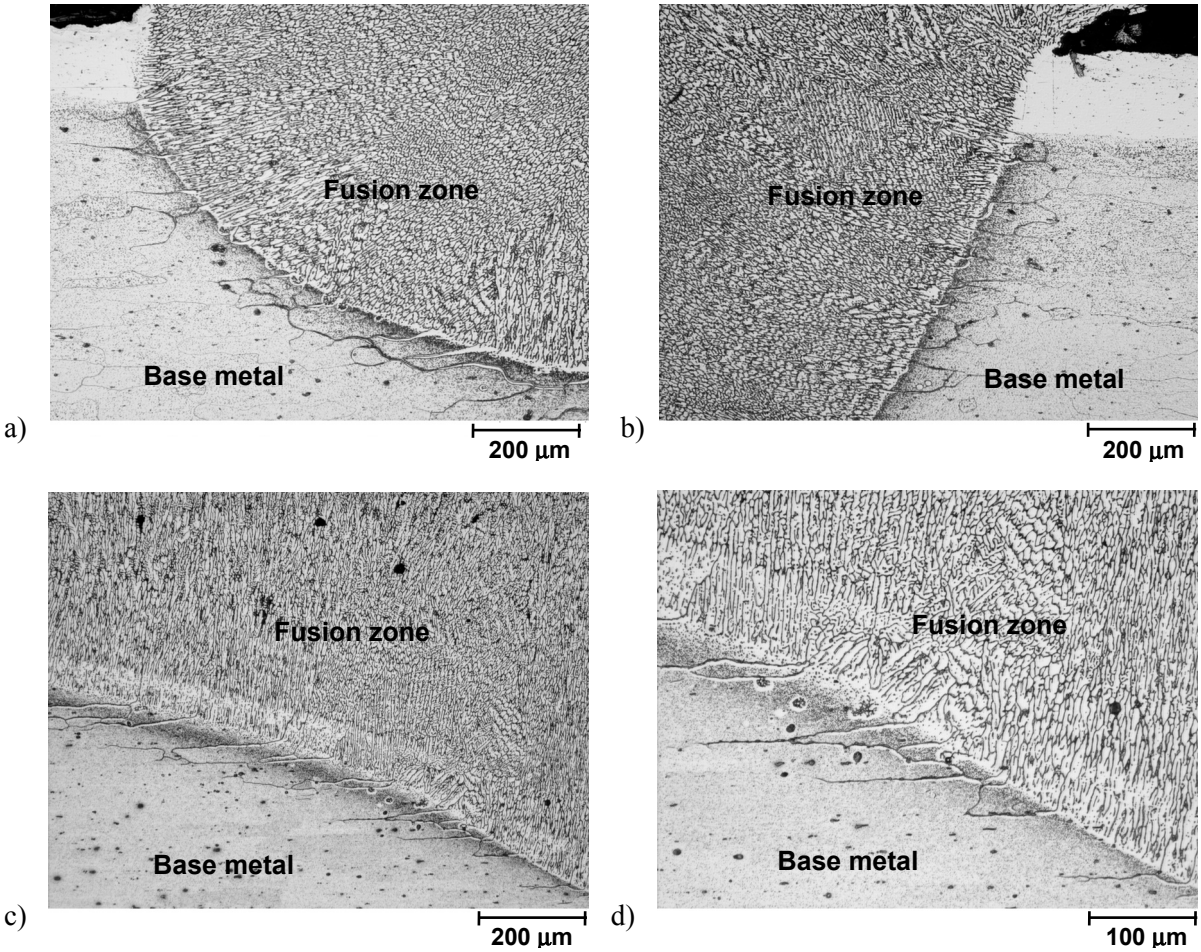

Figure 5.3: Detailed views taken from lower side (through the base metal) of the clip weld illustrating FZ, HAZ, and BM. Grain boundary liquation is more apparent in larger magnification (see d).

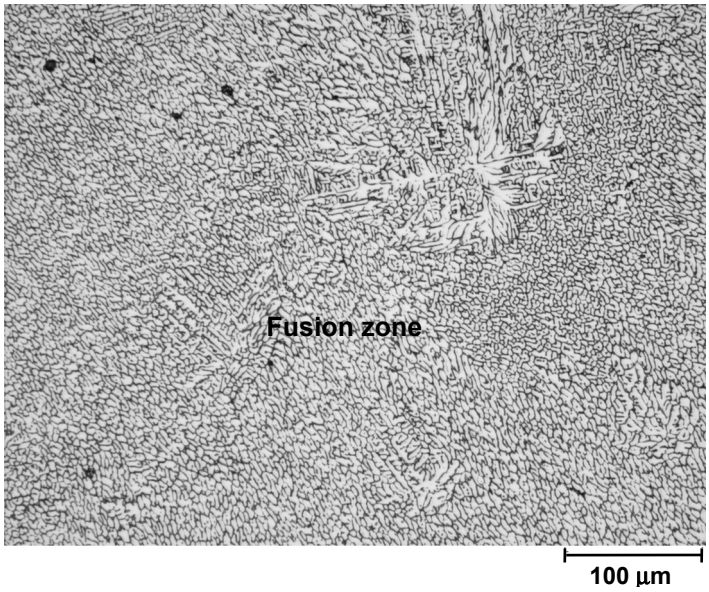

Figure 5.4: Centre of the fusion zone which shows randomly oriented dendrite colonies and equiaxed grains.

5.1.2 Microhardness

The microhardness profile of the conventionally welded clip on 4.5 mm thick 6156 T4 skin is plotted in Figure 5.5. The hardness value of the base plate varies between around 110 to 120 HV. The measured hardness values in the fusion zone range about 90 HV. There is no observed definite heat affected zone (HAZ). Figure 5.6 shows the measured hardness values of the conventionally welded clip on 3.2 mm thick 2139 T351 skin. Whereas base material hardness values keep on being approximately 140 HV, fusion zone hardness values are about 100 HV. Since there is no applied aging heat treatment, the tendency of the profiles shows similarity to the former material, in that no heat affected zone were defined.

The comparisons of micro-hardness profiles across the weld between different weld types of clip welds (Figure 3.4) are shown in Figure 5.7. The graphic contains the hardness profiles of three different weld types as conventionally welded, two run-outs welded and two run-ins welded. The base materials were 4.5 mm thick 6156 T6. The profiles and hardness values of different weld types show similarity. The similar degree of hardness loss was observed within the weld region (including heat affected zone) for all three types of welded panels. There exist transition regions (HAZs) between the base metal and fusion zone.

Hardness profiles of all welded panels revealed minima in the fusion zone, see Figures 5.5 – 5.7. This decrease can be attributed to dissolution of precipitates and to loss of Mg or to both. During welding the filler material and base metal combination are fused, leading to complete dissolution of the constituent elements. This is followed by a rapid solidification similar to the quench of a solution heat treatment. Mg is a major precipitate forming solute for $Al_xMg_ySi_zCu_w$ in the Cu containing 6xxx alloys and in case of loss of Mg by evaporation, restoration of hardness through post weld heat treatment is not possible. Therefore, the use of appropriate filler material to compensate this loss is essential. The investigation of Vaidya et al. [34] showed that nearly parallel shift in hardness profiles were obtained both for a fusion zone and base metal after peak hardening post weld heat treatment to T6 condition of the 6056 weld material, which was welded in T4 condition. As a result, Mg should have been available for precipitation, also in fusion zone. The filler material used was $AlSi_{12}$, which is the alternative designation of the 4047. The decrease in hardness values of the HAZ originate from overaging of the precipitates. Such soft zones (FZ and HAZ) become preferential sites for excessive strain localization. Since fracture is likely to occur in soft regions, solutions to reduce the difference in hardness between weld zone and the base metal need to be found. One can be a post weld heat treatment and the other possibility can be feeding of hardening elements through modified filler wires. Furthermore, local strengthening can be achieved using a “local engineering” concept and providing local thickening (socket) of the joint area to protect lower strength weld from applied strain.

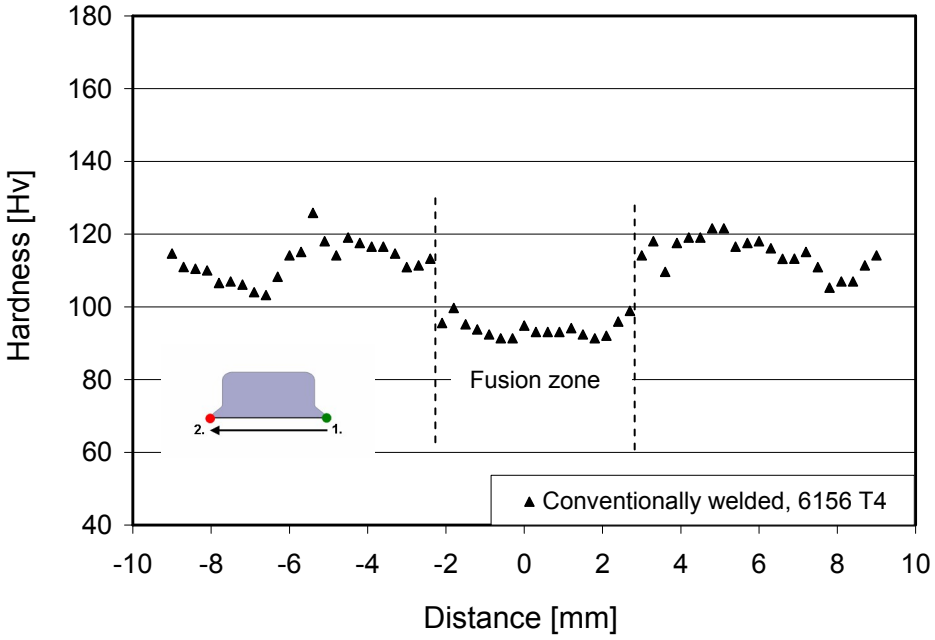

Figure 5.5: Hardness profile of the conventionally welded clip on 4.5 mm thick 6156 T4 skin material across the weld. (Zero position is the centre of the clip and measurements were made along a line which is located 0.35 mm below from the surface of the skin plate).

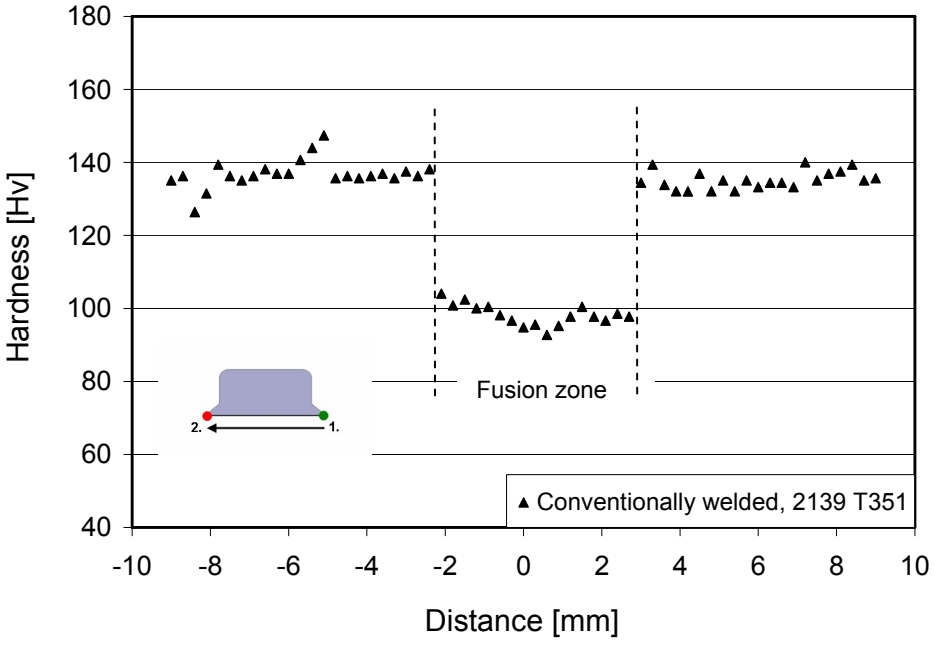

Figure 5.6: Hardness profile of the conventionally welded clip on 3.2 mm thick 2139 T351 skin material across the weld, which shows the "strength undermatched" nature of the fusion zone.

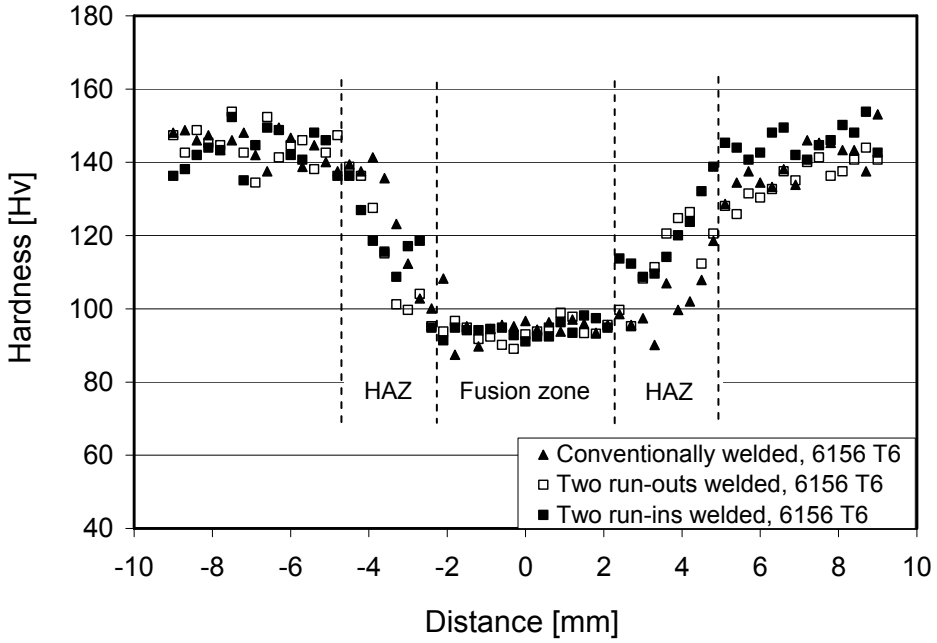

Figure 5.7: Comparison of hardness profiles of weld joint types of 4.5 mm thick 6156 T6 across the weld.

5.1.3 Tensile properties

Typical plots of stress versus strain are illustrated in Figure 5.8 for the 4.5 mm thick 6156 T4 base metal in L-T (rolling direction) and T-L (perpendicular to rolling direction) directions and the clip welded panel of the same skin material. The tensile properties of the base metal panel in L-T and T-L directions are very similar in yield strength, ultimate tensile strength (UTS) and % elongation values. The former has values as 209 MPa, 343 MPa, and 29% and the latter as 227 MPa, 339 MPa, and 30%, respectively. All of the tensile specimens prepared from clip welded panels are taken as T-L direction, since welding was applied parallel to the rolling directions. Tensile properties of the weld joints were determined on specimens extracted from clip welded panels as shown in Figure 3.11. Several clip welded specimens of the same skin material, which were welded as conventional type were tested, however one representative curve is shown in this figure. Nominal failure stress of the welded specimen was approximately 90% of the base metal UTS and approximately the same yield strength value as T-L direction of the base metal. Since a weld is a region of discontinuity between the base material(s) and has a lower strength than the base material, it becomes the site for preferential deformation under an applied load. This effect is known in the fracture community as “Undermatching” in a welded material [34]. The loss of strength and ductility of the joints are due to the lower strength of the weld area and notch effect. Internal porosity, which is an issue of the laser beam welds, should have been one of the factors affecting tensile properties, particularly when small pores are closely spaced and decrease the load bearing area. By controlling laser beam welding parameters, that is increasing laser input, increasing weld speed and by selection of appropriate filler wire, the amount of pores can be decreased and hence strength can be increased and undermatching effect can be decreased. However, it has not been given so much attention in this work to improve the weld quality, even tough the most appropriate filler wire was used in the welding process, rather residual stress control by changing the weld directions and hence the start and end positions with

respect to the clip geometry, was the main aim. The nominal elongation of the welded specimen was very low with a value of 9% (28% of that of the base metal), which proves that specimens fracture in an unstable manner, although this does not necessarily imply that welds were brittle. Since various zones in the tensile test specimen deform differently, the strain becomes localized, which induces constraint and fracture occurs at a low elongation. Strain localization occurrence has also been observed on the standard tensile specimens using a local strain measurement technique [136].

Stress-strain curve of a representative clip welded specimen of a 2139 T351 skin material was illustrated in Figure 5.9. The UTS, yield strength and % elongation values of the base metal are 440 MPa, 298 MPa, and 22%. The welded specimen test results give values of around 90% of UTS, 95% of yield strength and 33% elongation compared to the base metal.

A comparison of the tensile strengths between 4.5 mm skin material 6156 T6 and weld joint types is presented in Figure 5.10, as a representative result to all tested welded specimens. These curves also illustrate the strength undermatching of the weld joints compared to skin material by having lower strength and ductility. Base metal has a UTS value of 400 MPa, yield strength value of 351 MPa and elongation of 15%. The strength and ductility values of the different welding types as a percentage of base metal values are about 80% of UTS, 75% of yield strength and 29% of elongation for conventional welded sample, 87% of UTS, 95% of yield strength and 21% of elongation for two run-outs welded sample and 81% of UTS, 81% of yield strength and 21% of elongation for two run-ins welded panel.

All of the tensile fracture paths remained entirely within the weld fusion zone, mainly along the fusion line (interface between FZ and HAZ). However, it should be mentioned that all tested samples did not contain thickness increase (pad-up) of the skin under the clip.

It is usual design practise that weld areas are placed to the thicker skin locations to provide some degree of strengthening (local engineering) to the lower strength (undermatch) weld area. This approach was not used in these tests due to simplicity of the samples without pad-ups.

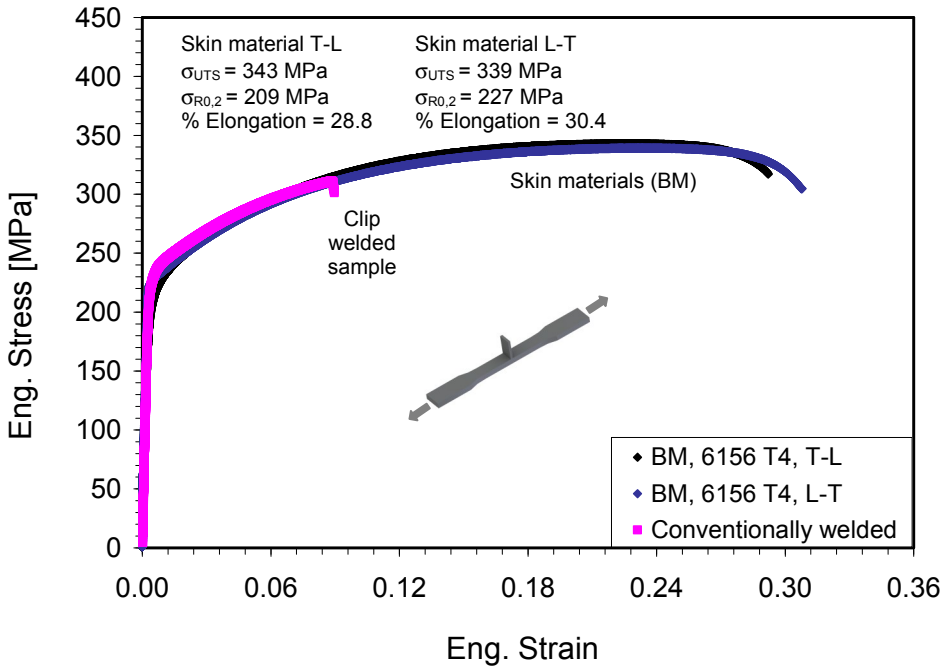

Figure 5.8: Stress vs. strain curves of the skin material (6156 T4, 4.5 mm thick) and conventionally welded clip panel tested transverse to the weld seam without pad-up (thickness increase) at the weld area.

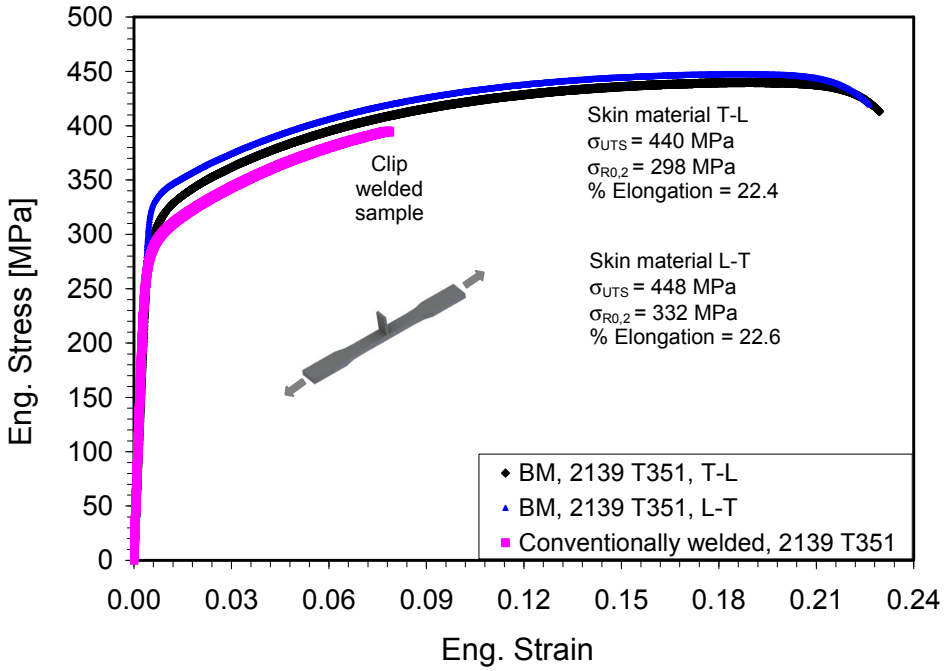

Figure 5.9: Stress vs. strain curve of the conventionally welded clip on 3.2 mm thick 2139 T351 skin material tested transverse to the weld seam without pad-up (thickness increase) at the weld area.

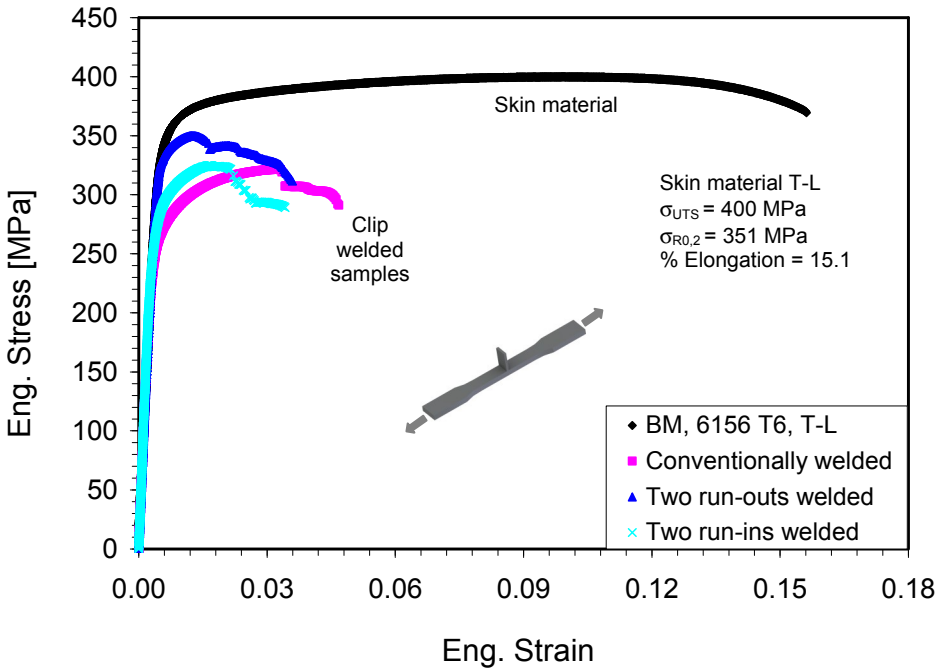

Figure 5.10: Comparison of the stress vs. strain curves of the skin material (6156 T6, 4.5 mm thick) and weld joint types tested transverse to the weld seam without pad-up (thickness increase) at the weld area.

5.1.4 Fracture toughness properties

As stated before, the weld area in Al alloys is undermatched and shall be exposed to preferential and localized plastic deformation. Under such condition and if the cracks are present in the weld or likely to be developed from the defects, sufficient fracture toughness ensures ductile crack growth under static loading and avoids unstable fracture [139]. Materials with low strength and low hardness generally reveal good fracture toughness. Uz et al. [140] confirmed the same trend for 6056 material having better fracture toughness in T4 condition than in T6 condition. He showed that ductile crack growth in the form of transcrystalline occurred for the materials at T4 condition whereas intercrystalline at T6. He also found out that in T6 condition, 6156 material had better fracture toughness than 6013 material. Such a trend was also confirmed by Dawes et al. [141], von Strombeck et al. [142] and Vaidya et al. [34] for friction stir welded (FSW) Al-alloys. However for LBW, Seib et al. [10] demonstrated that fracture toughness is lower than that of base metal for initially age hardened 6013 T6 material. It is also to be expected that being soft (Figures 5.5 – 5.7), the fusion zone shall undergo the extensive deformation and properties of the filler in the fusion zone shall determine fracture toughness. As high toughness is desired, welded components should also possess high load carrying capacity. However, for undermatched welds, factors which may enhance the load carrying capacity (for example narrow weld zone) may degenerate fracture toughness behaviour, since this leads to an increase of crack tip constraint.

AA 2139 is a very new material and its fracture toughness properties were determined for the complete material characterization purpose. The CTOD fracture toughness tests were carried out using CT(50) specimens of 2139 T351 material. The welded samples were extracted as shown in Figure 3.12 to determine the “apparent fracture toughness” values of the clip welds,

since specimens are not standard. The CTOD versus Δa curves were plotted in a diagram which gives the crack resistance curves (R-curves). A representative Load versus CTOD curves were also shown in Figure 5.11 for base metal and conventionally welded specimens for 2139 T351. The load carrying capacities of the base and welded samples are very similar.

The R-curve (crack resistance curve) results based on multiple specimen CTOD (δ_5) technique [143] are presented in Figure 5.12 for 3.2 mm thick 2139 T351. The curve is expressed in terms of equation $\delta_5 = f(\Delta a)$ and shown on the graphic. This kind of description is needed for conducting residual strength (fracture) analysis, using fitness-for-service procedures such as FITNET. The measured fracture toughness values for the welded specimens of the 2139 material are also included in the diagrams. The results of the welded specimens, independent of the welding type, were within the scatter of the corresponding base materials.

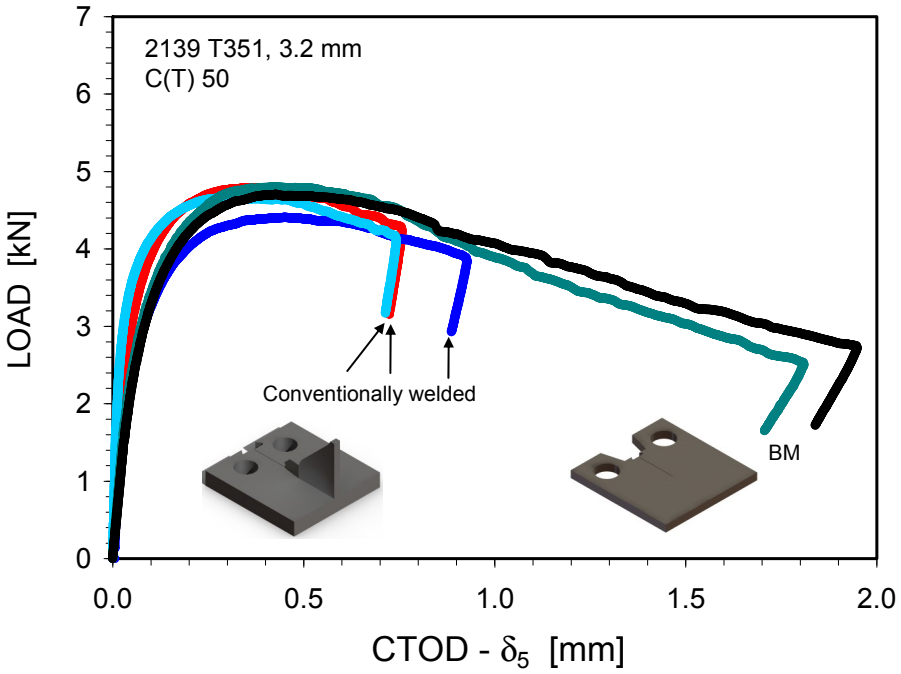

Figure 5.11: The load-CTOD δ_5 diagrams of base metal and conventionally welded C(T) 50 specimens containing part of the clip. The specimens were unloaded at various locations.

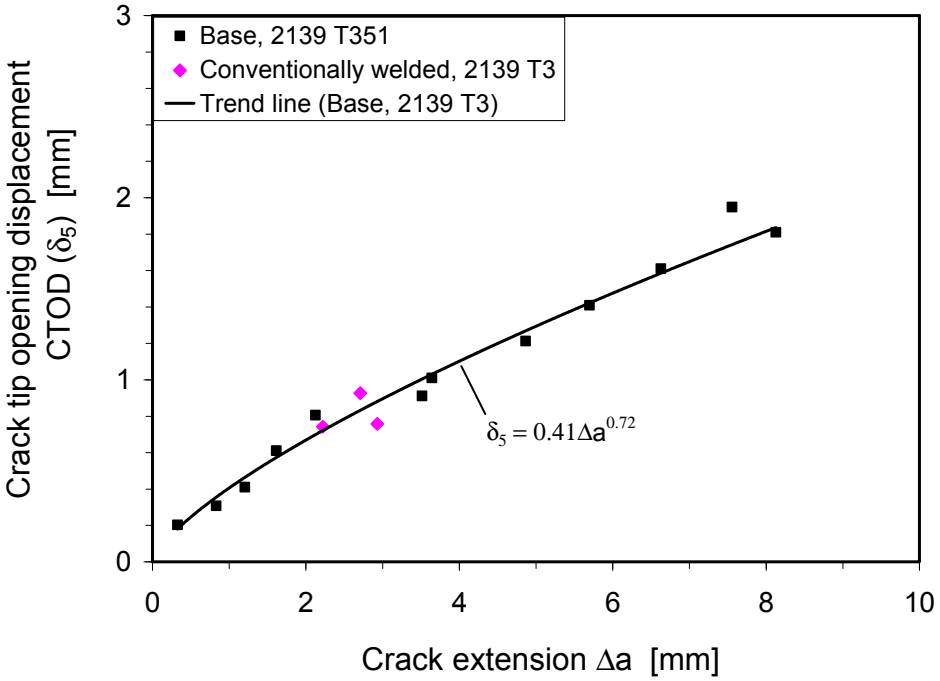

Figure 5.12: CTOD (δ5) crack resistance curve of 3.2 mm 2139 T351 base metal and three welded specimens showing that weld specimen results are in good agreement with the base metal results. The curve is expressed in terms of equation $\delta_5 = f(\Delta a)$.

5.2 Residual stress distribution of welds determined by neutron diffraction

Residual stresses are very effective on fatigue behaviour of the welded components. To investigate the evolution of the residual stresses and their effects on the FCP behaviour of the skin-clip joints, the residual stress distributions were determined for a variety of materials, heat treatment conditions, geometries (plain or pocketed) and welding configurations (in which the positions of run-ins and run-outs change relative to the weld geometry).

5.2.1 Small sample

To establish the residual stress measurement methodology, a small sample with dimensions of 160 × 275 mm^2 was selected as shown in Figure 3.1. The rolling direction was parallel to the welding direction. The measurements were performed throughout the scan lines transverse to the weld line at mid-clip, run-in and run-out locations at the mid-thickness of the base plate (Figure 5.13).

Furthermore, the investigation was extended to determine the variation of the residual stress distribution around run-in and run-outs. The results are discussed in [14]. Former was located 5 mm to run-in and latter the same distance to run-out. Other than the residual stress determination at each locations, the results show that weld free locations (5 mm away from run-in and run-out) possess lower stresses than the run-in and run-out locations.

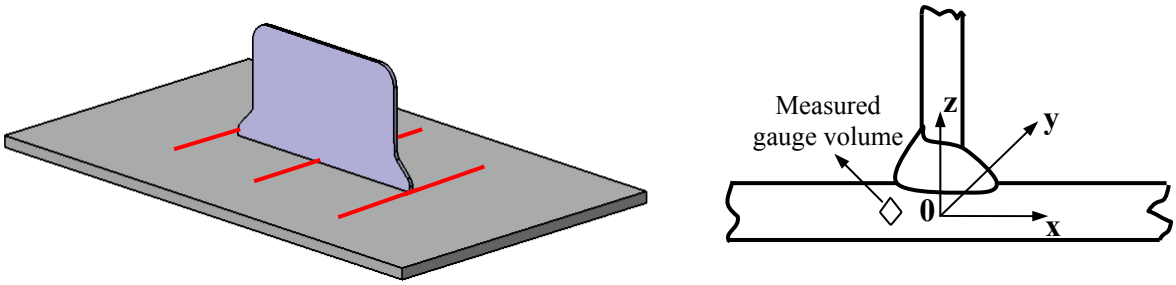

Figure 5.13: Drawings showing a) measurement scan lines on the small specimen and b) the zero position for the measurement in the base plate.

5.2.2 Large sample: M(T) 400 panels

Residual stress determination for the M(T) 400 panels with a size of 400×625 mm^2, and a 4.5 mm thick AA 6156 material of T4 and T6 conditions and a 3.2 mm thick AA 2139 material of T351 condition, which were conventionally welded to an AA6013 T6 clip was conducted. This size of the panel was chosen to enable fatigue crack propagation tests on a measured sample. The measurement was performed as it is described for the small sample and in section 3.3.

5.2.3 Effect of heat treatment on σ_{res}

Al-alloys 6156 could be welded either the naturally aged T4 or artificially aged T6 heat conditions. It was of interest to establish possible effect of heat condition of the panels (prior to the welding process) on the residual stress evolution. Hence, to determine the effect of heat treatment applied to the panels prior to welding, residual stress determinations for a T4 and T6 base panel – which were welded conventionally – were performed.

Residual stress distributions at the mid-clip position of the conventionally welded M(T) 400 plain panels of 6156 T4 and T6 materials are illustrated in Figure 5.14. The welded T6 panel possessed higher tensile longitudinal residual stresses than the T4 panel with the peak stress of about 210 MPa and 150 MPa respectively. Tensile transverse stresses exist with a peak value of around 60 MPa for both welded panels. The distribution of tensile longitudinal residual stresses at the mid-clip position of the welded T4 base panel shows broader pattern compared to that of the T6 base panel. The difference between T4 and T6 is due to the differences in tensile strength properties of these heat conditions where T6 has higher yield strength than T4 condition.

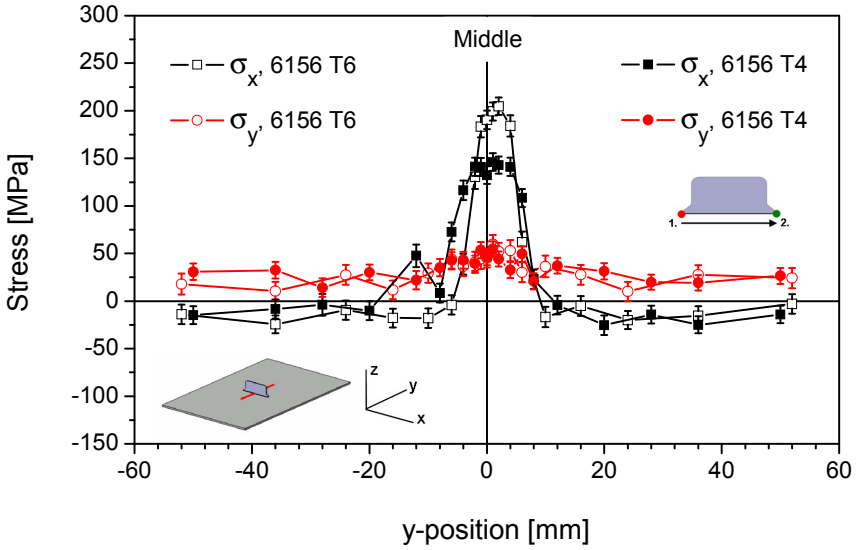

Figure 5.14: Residual stress distributions at the mid-clip locations of the 4.5 mm thick AA 6156 T4 and AA 6156 T6 plain panels. The welding was performed conventionally.

Tensile longitudinal and compressive transverse stresses occured at run-in location (Figure 5.15) in both welded panels. These residual stress values of T6 panel are lower in longitudinal direction and higher compressive in transverse direction compared to residual stresses of welded T4 panel. The peak compressive transverse stress value for the welded T6 base panel is approximately 100 MPa.

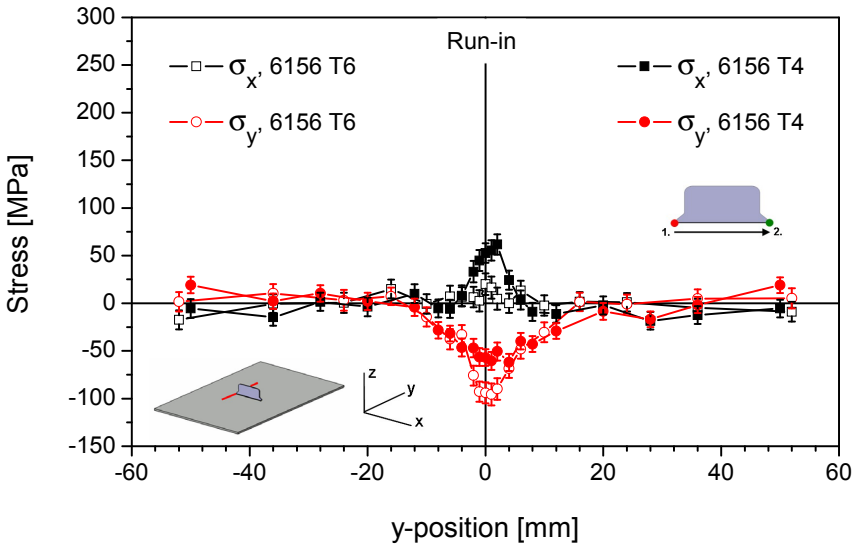

Figure 5.15: Residual stress distributions at the run-in locations of the 4.5 mm thick AA 6156 T4 and AA 6156 T6 plain panels. The welding was performed conventionally.

Figure 5.16 demonstrates the residual stress distributions at run-out location of the welded T4 and T6 panels. Similar to mid-clip position, high tensile longitudinal stresses were found for both welded panels with a peak stress value of around 150 MPa. Except one measurement-point in the region of the middle of the weld seam, slightly compressive transverse residual stresses were determined for the welded T6 panel with a peak value of about 50 MPa. However, tensile transverse residual stresses were determined for welded T4 panel with a peak stress value of approximately 70 MPa.

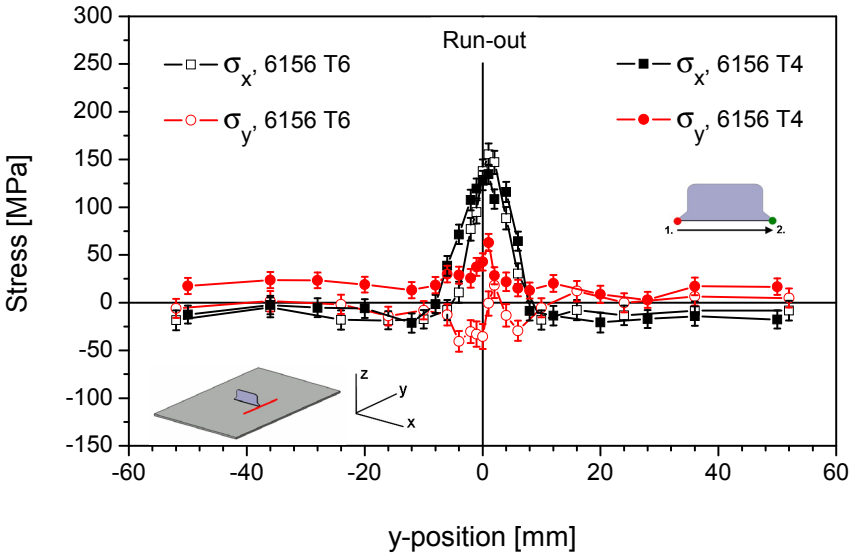

Figure 5.16: Residual stress distributions at the run-out locations of the 4.5 mm thick AA 6156 T4 and AA 6156 T6 plain panels. The welding was performed conventionally.

In the longitudinal direction, tensile residual stresses were measured for mid-clip, run-in and run-out locations. Remarkably lower tensile longitudinal residual stresses were measured at run-in locations compared to run-out and mid-clip locations for the both welded panels. It can be concluded that the clip welding of Al-alloy 6156 in T6 heat condition leads to higher residual stress development compared to welding performed in T4 condition due to the higher tensile strength of the Al-alloy in T6 condition (see Figure 5.20). Obviously, lower residual stress state of T4 will further be beneficial for the structure with respect to fatigue performance. However, the final use of the Al-alloy 6156 is T6 condition. Nevertheless, the decision on the T4 or T6 condition will require other issues (such as strength) to be considered. It can be concluded that higher tensile longitudinal stresses were determined at mid-clip and run-out positions of both T4 and T6 panels in comparison to those at run-in. Transverse stresses are tensile at mid-clip positions of both panels, which are tensile at run-out position of T4 panel and compressive (except one measurement point) at run-out position of T6 panel. At run-in position of both panels compressive transverse stresses exist. These results can be explained by higher constraint evolution at the open part (run-out) weld joint compared to the welded part (run-in area) left behind as welding progresses towards the run-out location. An increase of constraint imposed to the part ahead of the welding pool by the rigidity of the welded part behind leads to an increase of the tensile residual stresses at the final location of the welding process, whereas the same process creates compressive transverse residual stresses at the beginning location of the welding process.

The difference between start and end locations of the clip welds with respect to the evolved residual stress states is important. This new knowledge observed for welded panels leads to a possibility for "local engineering" of the residual stress state which is important for the fatigue crack initiation and propagation at the critical locations such as run-ins and run-outs with higher stress-concentrations.

The residual stress measurements at different locations of the short distance clip weld show that the higher stresses at run-out location need to be modified or reduced. Therefore, investigations were focussed to modify the welding procedure by changing the positions of the start (run-in) and end (run-out) of the welding process. By doing this, it was expected to modify the residual stress distribution at the critical locations, which will contribute to the improvement of the damage tolerance behaviour of the components which have welded clips.

Needless to say that residual stresses could be modified by post weld heat treatment, but this option includes an additional process and should be conducted only if no other means are available to reduce tensile residual stresses.

5.2.4 Effect of Al-alloy grade on σ_{res}

To determine the possible effect of material grade, residual stresses were also determined for a cold worked and naturally aged 3.2 mm thick AA 2139 T351 M(T) 400 panels (which was welded conventionally). This relatively new alloy was also welded in an identical manner as AA 6156, however the thickness of the 6156 alloy was 4.5 mm.

The residual stresses of the AA 2139 T351 and AA 6156 T4 plain panels show similar distributions at mid-clip (Figure 5.17), run-in (Figure 5.18), and run-out (Figure 5.19) locations. The 2139 alloy at the mid-clip position exhibits slightly higher longitudinal tensile stresses reaching up to about 160 MPa, which is approximately 150 MPa for the 6156 alloy (Figure 5.17). As noticed from Figure 5.19, the 2139 alloy has also a close longitudinal tensile stress peak value with 140 MPa at the run-out position to 6156 alloy which has a peak value of about 130 MPa. Transverse tensile residual stresses for both alloys are again very close to each other for mid-clip and run-out locations.

The difference seems to be higher for run-in locations of both alloys. Figure 5.18 indicates around 120 MPa tensile longitudinal stress peak value for 2139 alloy with about –25 MPa compressive transverse stresses, which are around –60 MPa and –65 MPa respectively for the 6156 alloy. However, the existence of higher tensile longitudinal stresses at run-out than run-in location and tensile transverse stresses at run-out and compressive transverse stresses at run-in location for 2139 alloy also confirm the case for the 6156 alloy. The variations in residual stresses can be attributed to the higher strength of the 2139 T351 alloy compared to 6156 T4 (see Figure 5.20), resulting in higher residual stresses.

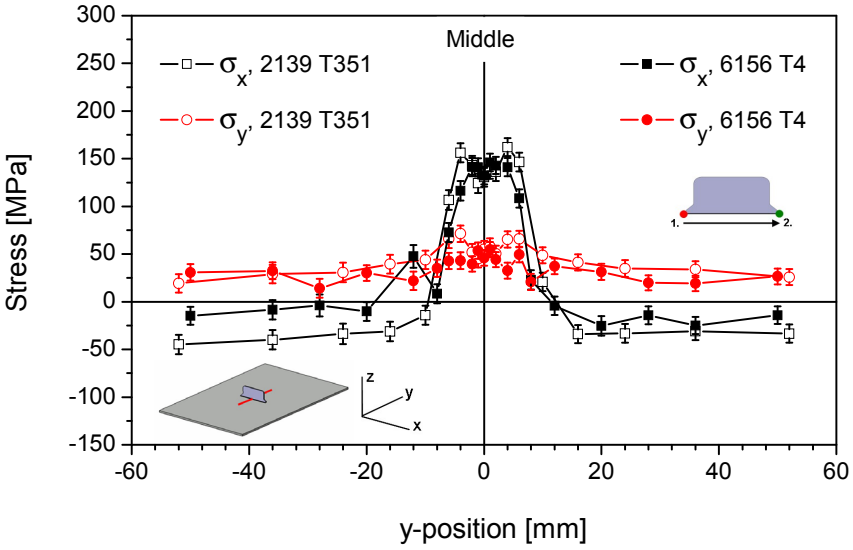

Figure 5.17: Residual stress distributions at the mid-clip locations of the 4.5 mm thick AA 6156 T4 and 3.2 mm thick AA 2139 T351 plain panels. The welding was performed conventionally.

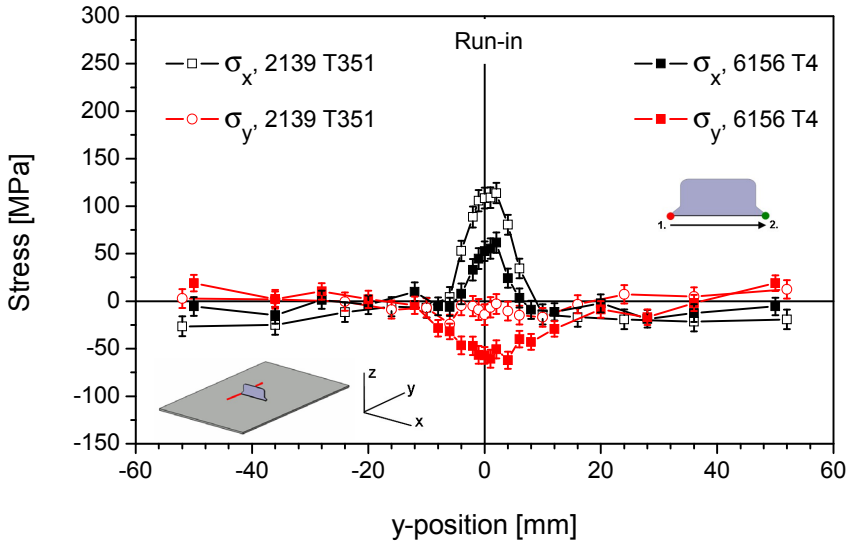

Figure 5.18: Residual stress distributions at the run-in locations of the 4.5 mm thick AA 6156 T4 and 3.2 mm thick AA 2139 T351 plain panels. The welding was performed conventionally.

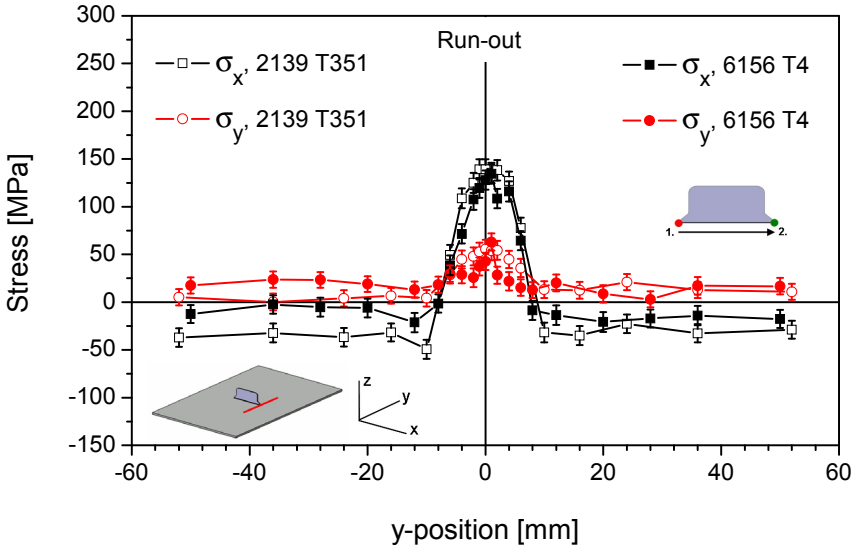

Figure 5.19: Residual stress distributions at run-out locations of the 4.5 mm thick AA 6156 T4 and 3.2 mm thick AA 2139 T351 plain panel. The welding was performed conventionally.

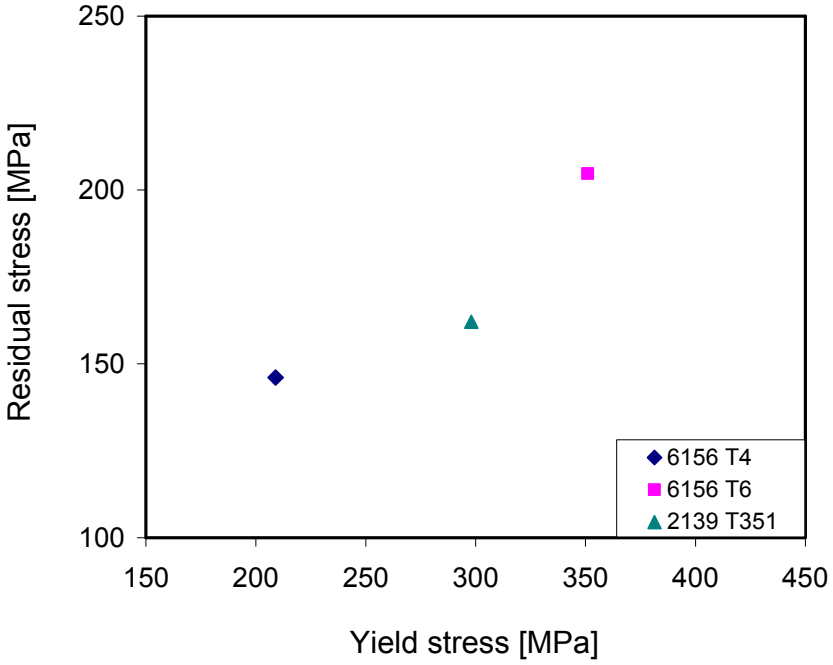

Figure 5.20: Comparison of the 6156 T4, 6156 T6 and 2139 T351 materials in terms of the residual stress of the conventionally welded panels and yield stress of the base panels**.**

5.2.5 Effect of pocketing on σ_{res}

To understand the effect of pocketing (i.e thickness reduction in skin, see Figure 3.3) on residual stress development, pocketed panels with 11 mm socket width (width of thick skin area under the clip) of each selected material were produced. It is expected that, machining of the pockets prior to welding can have an effect on residual stress evolution because of geometry change. This effect was investigated for AA 6156 T6 material and AA 2139 T351 material. The effect of machining after welding on residual stress redistribution was investigated for AA 6156 T4 material.

5.2.5.1 AA 6156 T6 base panel

Residual stress distributions of the 6156 T6 plain panel and the pocketed panel with 11 mm socket width, which was machined before welding, at the mid-clip location are presented in Figure 5.21. As compared to the plain panel of the same material, the pocketed panel exhibited slightly higher longitudinal residual stresses. The nature of the longitudinal distribution in the pocketed case is somewhat different, which displays broader tensile stress distribution with double peak values of approximately 230 MPa at a distance of ±4 mm. The peak value for the 6156 T4 panel is about 210 MPa. The transverse residual stress peak value is about 50 MPa, which is comparable to those for the plain panel.

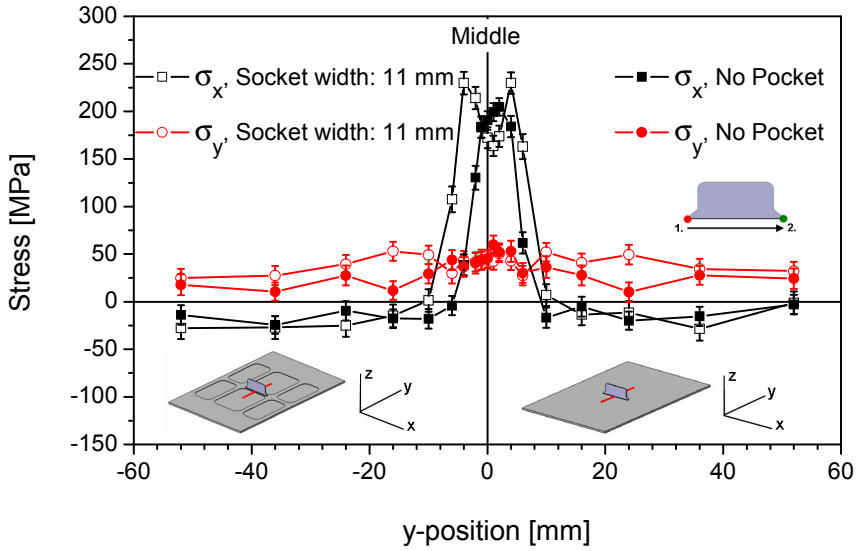

Figure 5.21: Residual stress distributions at the mid-clip locations of the 4.5 mm thick AA 6156 T6 plain panel and pocketed panel with 11 mm socket width, which were welded conventionally.

Faintly higher tensile longitudinal residual stress distributions are determined along the run-in position in the related pocketed panel (Figure 5.22) with a peak value of around 70 MPa with respect to those in the plain panel with approximately 20 MPa peak value. Pocketing also cause a broader residual stress distribution and lowers the compressive transverse stresses to a value of about –75 MPa which is around –100 MPa in the plain panel.

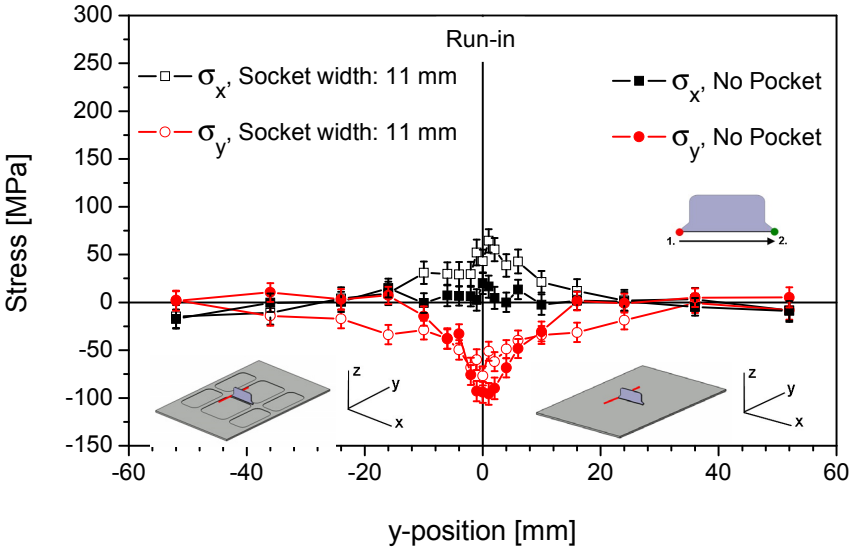

Figure 5.22: Residual stress distributions at the run-in locations of the 4.5 mm thick AA 6156 T6 plain panel and pocketed panel with 11 mmsocket width, which were welded conventionally

At run-out position of the pocketed panel, there exist around 150 MPa of peak tensile longitudinal stress (Figure 5.23), which is almost the same for that of plain panel. However, transverse stresses are tensile around the weld zone with a peak value of about 60 MPa in the pocketed case rather than compressive, which is the case for the HAZ region of plain panel. Broadening of the residual stress distribution is also observed at run-out position of the pocketed panel.

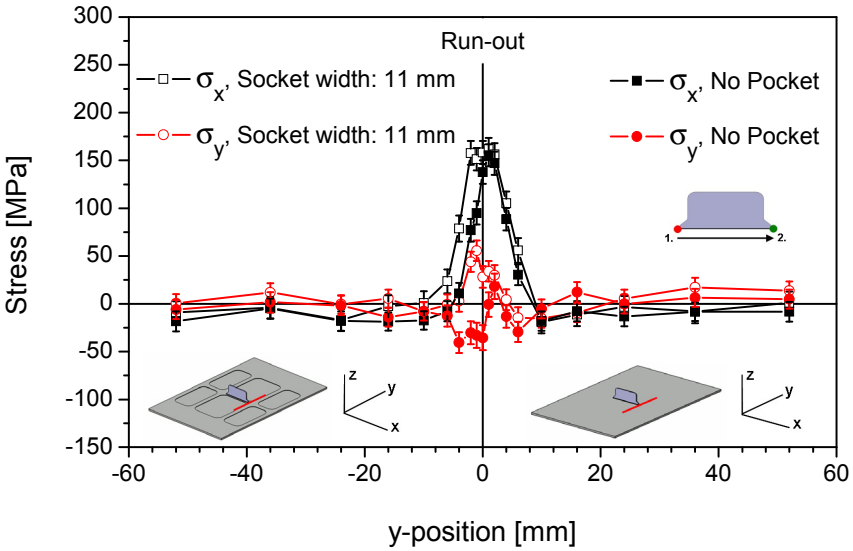

Figure 5.23: Residual stress distributions at the run-out locations of the 4.5 mm thick AA 6156 T6 plain panel and pocketed panel with 11 mm socket width, which were welded conventionally.

5.2.5.2 AA 6156 T4 base panel

The residual stress distribution of the 6156 T4 welded plain panel and pocketed panel with 11 mm socket width – which was machined after welding – show no significant differences at mid-clip locations of the welded panels (see Figure 5.24). The only difference is that the longitudinal peak stress value of the pocketed panel is about 20 MPa lower than the plain panel. This result is in contradiction with the results for the welded pocketed T6 panel – which was machined before welding – (Figure 5.21), where the pocketed panel exhibited slightly higher tensile longitudinal residual stresses and a broader distribution compared to the plain panel. In addition, no significant relaxation of residual stresses was observed after machining of the welded panel in contrary that was known from the literature. Obviously, 11 mm socket width is not narrow enough to relax the residual stresses of the weld.

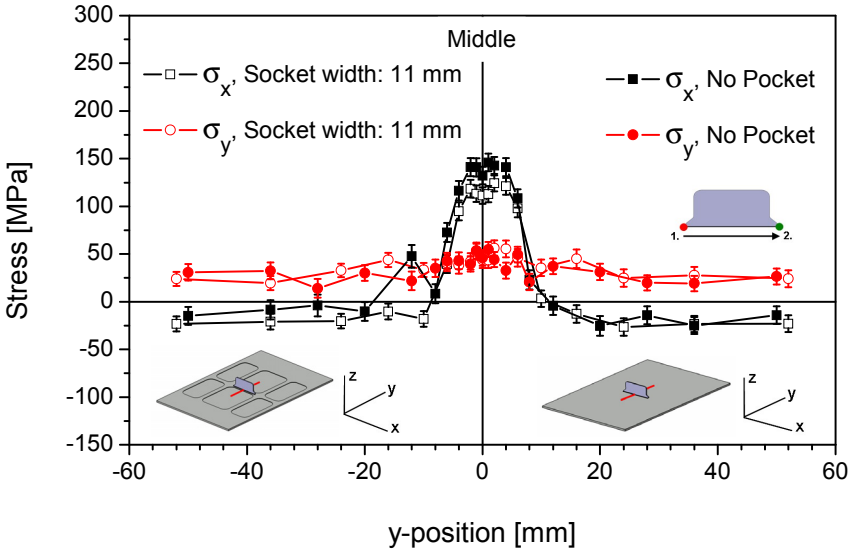

Figure 5.24: Residual stress distributions at the mid-clip locations of the 4.5 mm thick AA 6156 T4 plain panel and pocketed panel with 11 mm socket width, which were welded conventionally.

Residual stresses at the run-in and run-out locations of the plain and pocketed panels are plotted in Figures 5.25 and 5.26, respectively. Comparison of the pocketed panel with the plain panel shows that there is no significant difference between both. However, for the machined panel, slightly lower compressive transverse stresses at run-in location were determined.

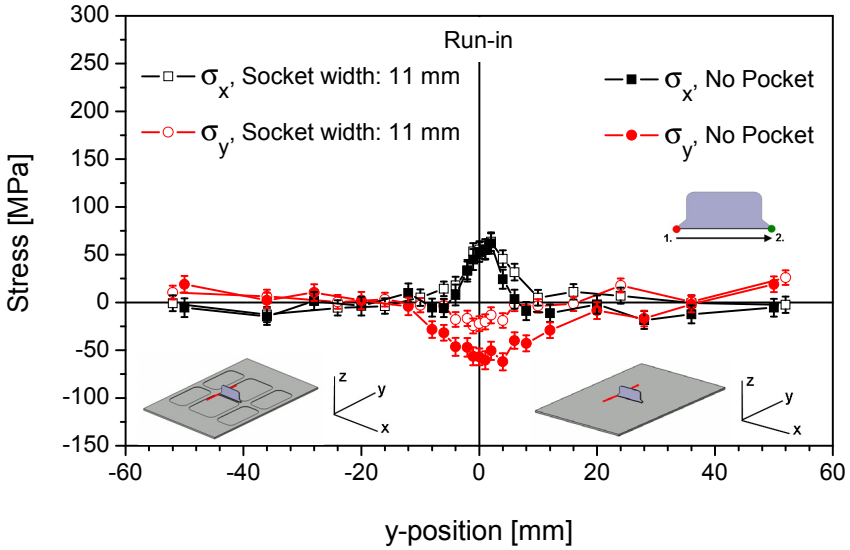

Figure 5.25: Residual stress distributions at the run-in locations of the 4.5 mm thick AA 6156 T4 plain panel and pocketed panel with 11 mm socket width, which were welded conventionally.

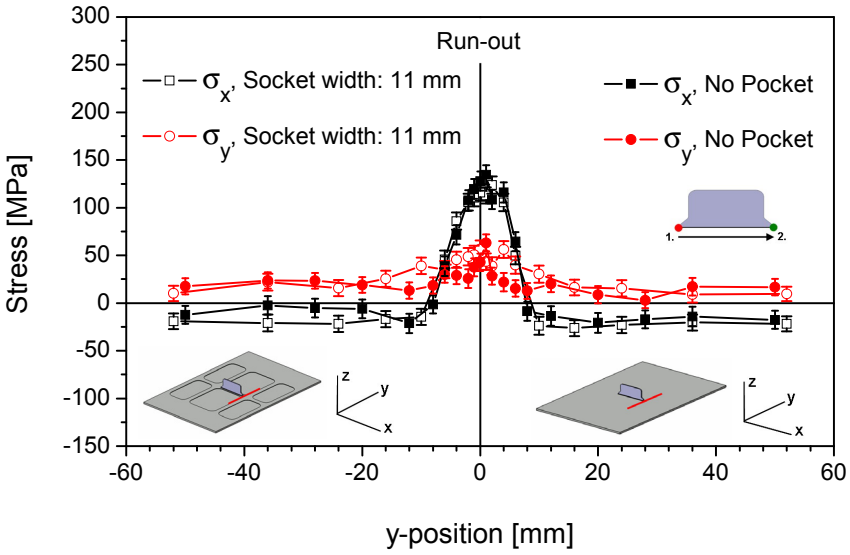

Figure 5.26: Residual stress distributions at the run-out locations of the 4.5 mm thick AA 6156 T4 plain panel and pocketed panel with 11 mm socket width, which were welded conventionally.

5.2.5.3 AA 2139 T351 base panel

For the 2139 T351 alloy panel with pocket (machining was applied before welding) with 11 mm socket width, only measurements at mid-clip and run-out locations were carried out. As in the case for 6156 T4 alloy, there is no considerable diversity of the residual stresses between plain panel and machined panel, see Figures 5.27 and 5.28 except for three measurement points at the middle of the weld seam of the pocketed panel. The reason could be the existence of microstresses.

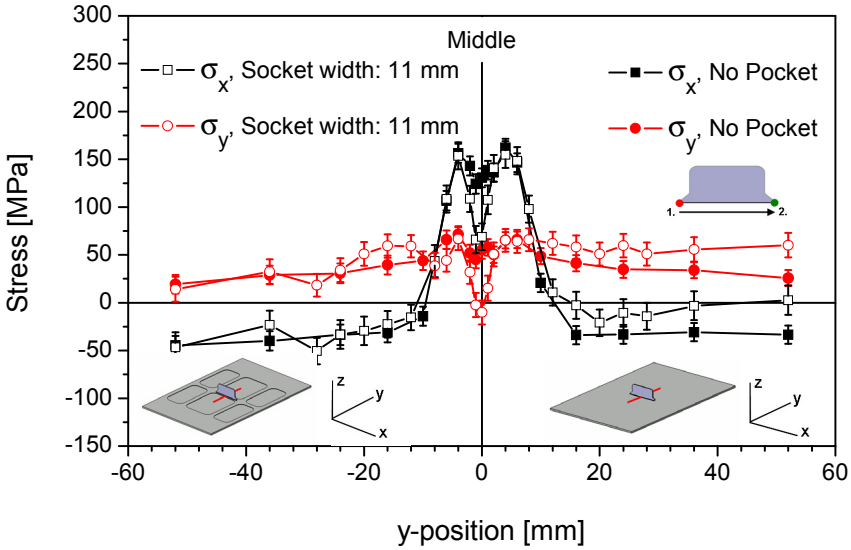

Figure 5.27: Residual stress distributions at the mid-clip locations of the 3.2 mm thick AA 2139 T351 plain panel and pocketed panel with 11 mm socket width, which were welded conventionally.

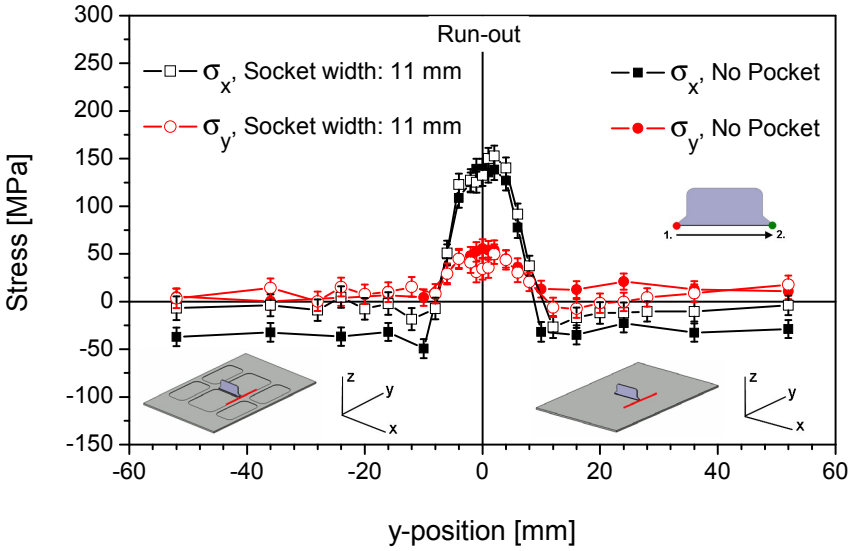

Figure 5.28: Residual stress distributions at the run-out location of the 3.2 mm thick AA 2139 T351 plain panel and pocketed panel with 11 mm socket width, which were welded conventionally.

5.2.6 Effect of socket width on σ_{res}

The width oft he thick skin region can influence the stress state oft he panel. Since the pocketing effect with 11 mm socket width was similar for the different heat conditions and materials, the effect of the socket width on residual stresses was investigated only for the panel of the 6156 T4 material for simplicity. The second socket width variable is chosen to be 20 mm. The panel with 20 mm socket width was also machined after welding like the one with socket width of 11 mm.

The comparison of residual stress distributions at the mid-clip positions between the plain panel and pocketed panel with socket width of 20 mm are given in Figure 5.29 and between pocketed panels with socket widths of 11 mm and 20 mm in Figure 5.30. These diagrams show no significant difference in the maximum longitudinal tensile stresses for the plain and pocketed panels with 11 mm and 20 mm socket width. Peak value varies within a range of 130-150 MPa. Similarly, the transverse residual stresses at the mid-clip positions exhibit the peak value of about 70 MPa for all three panels.

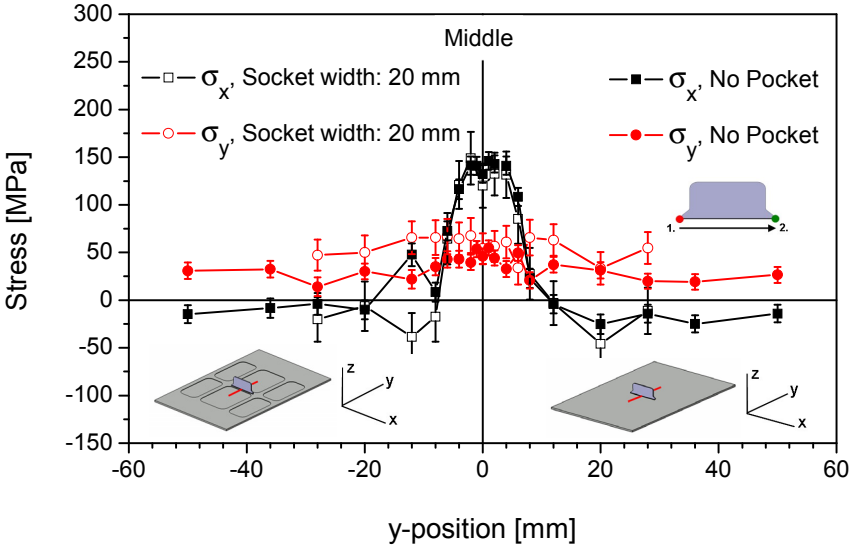

Figure 5.29: Residual stress distributions at the mid-clip locations of the 4.5 mm thick AA 6156 T4 plain panel and pocketed panel with 20 mm socket width, which were welded conventionally.

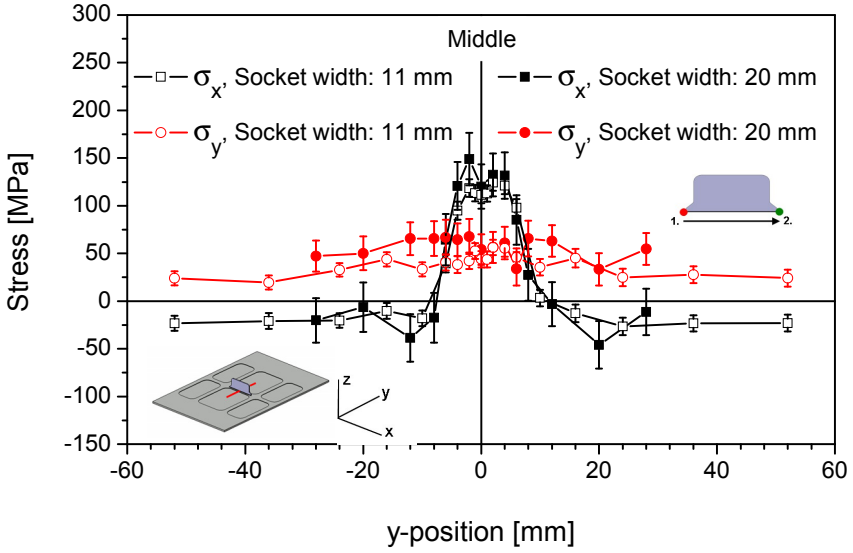

Figure 5.30: Residual stress distributions at the mid-clip locations of the 4.5 mm thick AA 6156 T4 pocketed panels with 11 mm and 20 mm socket width, which were welded conventionally

Figures 5.31 and 5.32 demonstrate residual stresses at run-in and run-out locations of the plain panel and pocketed panel with 20 mm socket width, respectively. The comparison of the residual stresses at run-in locations between pocketed panels with two different socket widths is given in Figure 5.33 and those at run-out locations is shown in Figure 5.34, correspondingly. Similarly to the plain and pocketed panel with 11 mm socket width, there exist longitudinal tensile stresses with peak value of about 70 MPa at run-in and 140 MPa at run-out locations. Similarly, transverse stress values of the pocketed panel with 20 mm socket width are very close to the results of the plain and pocketed panel with narrower socket width.

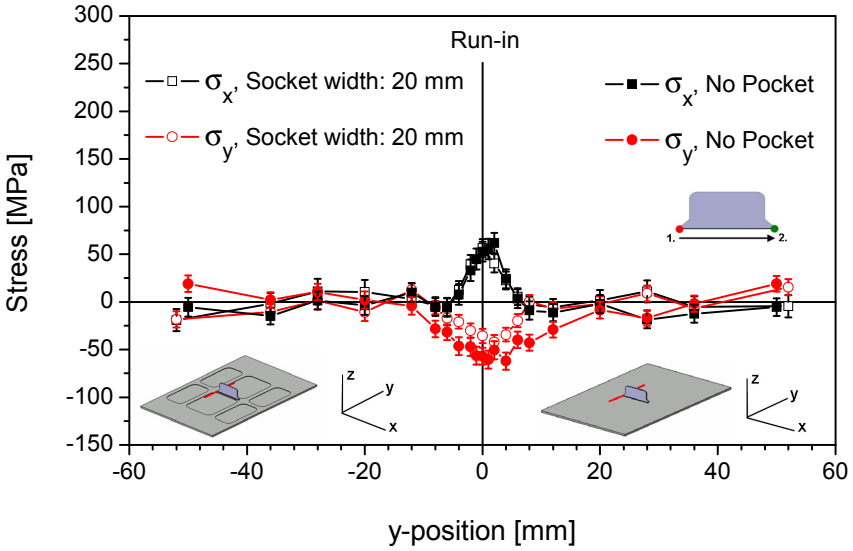

Figure 5.31: Residual stress distributions at the run-in locations of the 4.5 mm thick AA 6156 T4 plain panel and pocketed panel with 20 mm socket width, which were welded conventionally.

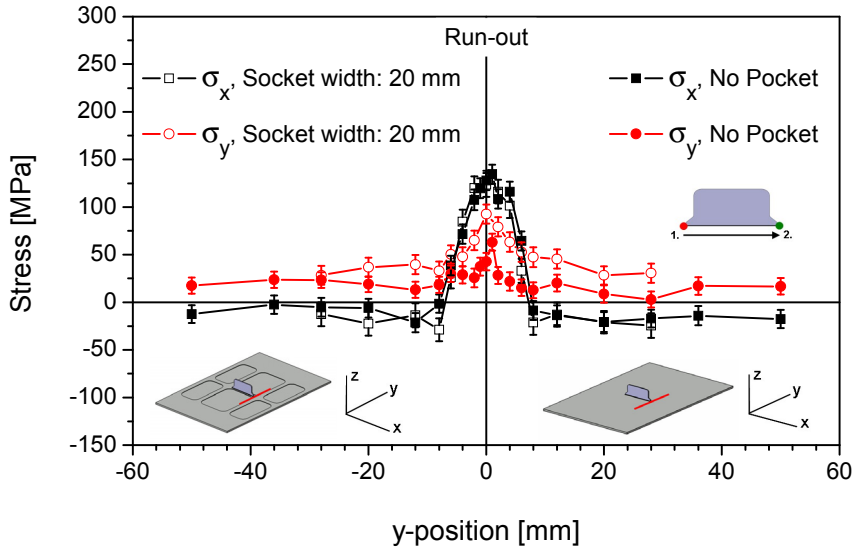

Figure 5.32: Residual stress distributions at the run-out locations of the 4.5 mm thick AA 6156 T4 plain panel and pocketed panel with 20 mm socket width, which were welded conventionally.

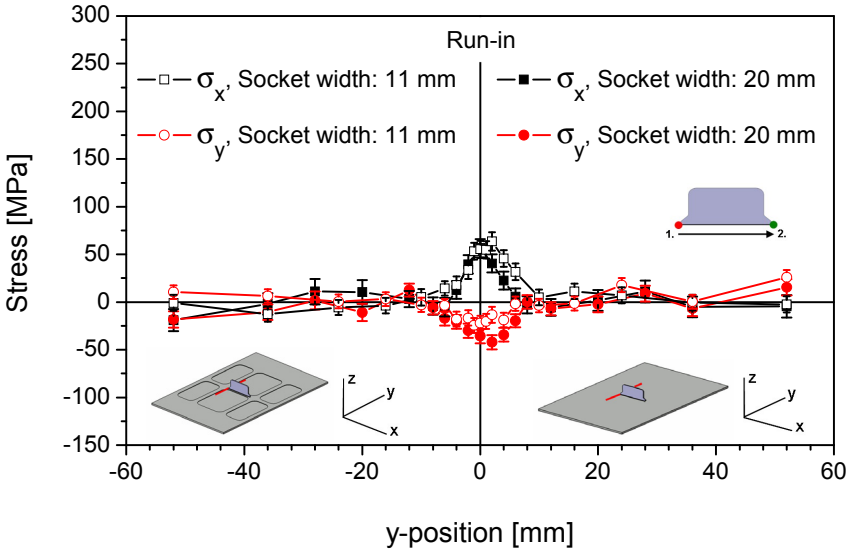

Figure 5.33: Residual stress distributions at the run-in locations of the 4.5 mm thick AA 6156 T4 pocketed panels with 11 mm and 20 mm socket width, which were welded conventionally.

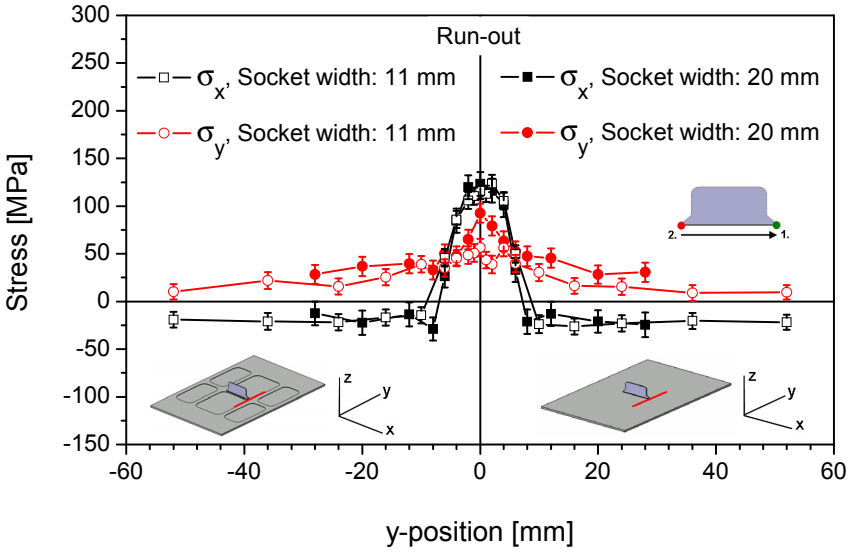

Figure 5.34: Residual stress distributions at the run-out locations of the 4.5 mm thick AA 6156 T4 pocketed panels with 11 mm and 20 mm socket width, which were welded conventionally.

The results have shown that by reducing the socket width from 20 mm to 11 mm, no significant effect was observed both in longitudinal residual stresses (σ_x) and in transverse stresses (σ_y) in the base panel.

5.2.7 Effect of welding type on σ_{res}

The effect of welding type (welded panels with two run-outs and welded panels with two run-ins) on residual stresses developed was experimentally determined in the framework of a Diploma Thesis [128]. All welded plain and pocketed panels were 6156 T6 material with 11 mm socket width. The machining was performed before welding for each panel.

5.2.7.1 Welding type with two run-outs

Residual stress distributions at the mid-clip location of the conventionally welded plain panel and welded plain panel, which contains two run-outs are given in Figure 5.35. Since this location is in fact run-in positions in this welding type, we should compare the residual stress distributions both with that of mid-clip position (Figure 5.35) and run-in position (Figure 5.36) of the conventionally welded plain panel. The peak longitudinal tensile stress value of the two-run-outs welded panel is approximately 170 MPa at the mid-clip position, which is lower than that of mid-clip position of the conventionally welded panel (around 200 MPa), but much higher than that of run-in position of the conventionally welded panel (about 25 MPa). We can correlate this to heat build-up around the welded zone owing to reheating of the run-in for the welded panel which contains two run-outs (see section 3.2, the comparison of TC 10–1 of Figure 3.7 and TC 10–3 of Figure 3.8). The states of the transverse residual stresses at the mid-clip position of the two run-outs welded panel are very similar to that at run in position of the conventionally welded panel, which are both compressive. However, the peak residual stress value is around –25 MPa for the former, and –100 MPa for the latter, which is also probably caused by reheating. Conversely, the transverse residual stresses at the mid-clip position of the conventionally welded panel are tensile with a peak value of about 50 MPa.

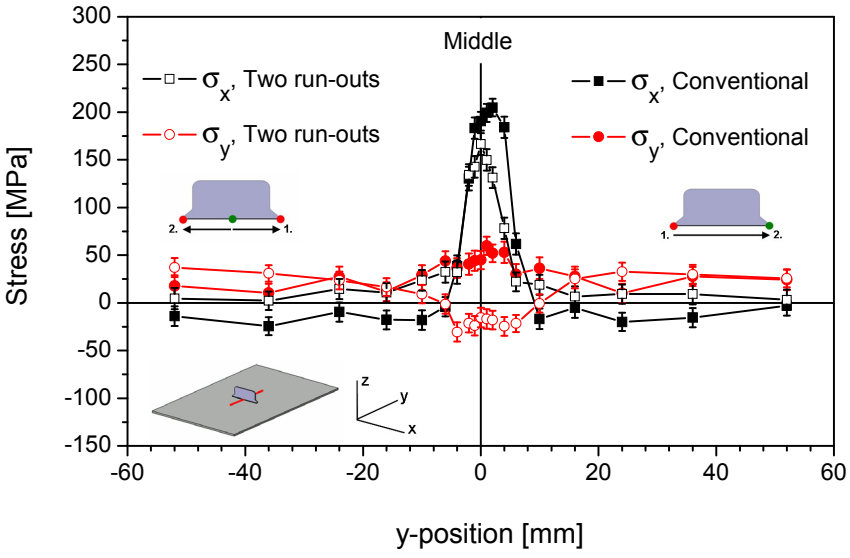

Figure 5.35: Residual stress distributions at the mid-clip locations of the 4.5 mm thick AA 6156 T6 conventionally welded plain panel and welded plain panel which contains two run-outs (the mid-clip position is in fact the run-in position in this welding type).

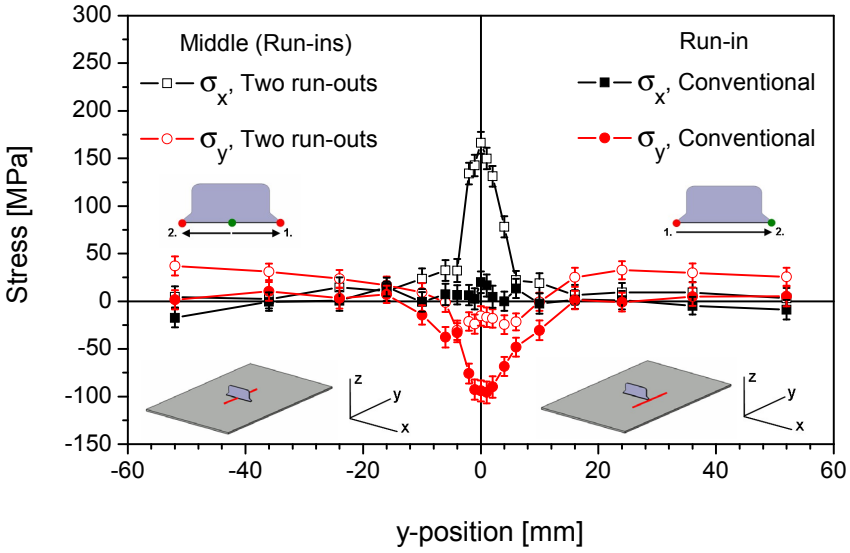

Figure 5.36: Residual stress distributions at the run-in locations of the 4.5 mm thick AA 6156 T6 conventionally welded plain panel and welded plain panel which contains two run-outs (the run-in position is located at the run-in position in this welding type).

At the first run-out position of the two run-outs welded plain panel, tensile longitudinal stresses occurred with a peak stress value of about 175 MPa, which is almost the same for run-out position of the conventionally welded plain panel (Figure 5.37). Whereas low tensile transverse residual stresses (with a peak value of about 30 MPa) exist at the first run out position of the panel with two run-outs, except one measurement point, slightly compressive residual stresses were determined in the conventionally welded panel, at the run-out position. Figure 5.38 shows the residual stress distributions at the run-out position of the conventionally welded plain panel and second run-out position of the two run-outs welded plain panel. Somewhat lower longitudinal residual stresses occur at the second run-out position with a peak value of around 150 MPa compared to the first run-out position. On the contrary, compressive transverse residual stresses were defined at the second run-out position of the two run-outs welded panel with a peak value of approximately –75 MPa. This behaviour can be attributed to occurrence of the smooth temperature gradient at the second run-out position due to preheating during welding of the first part of the clip (see Figure 3.8, TC 10–6 and 10–7).

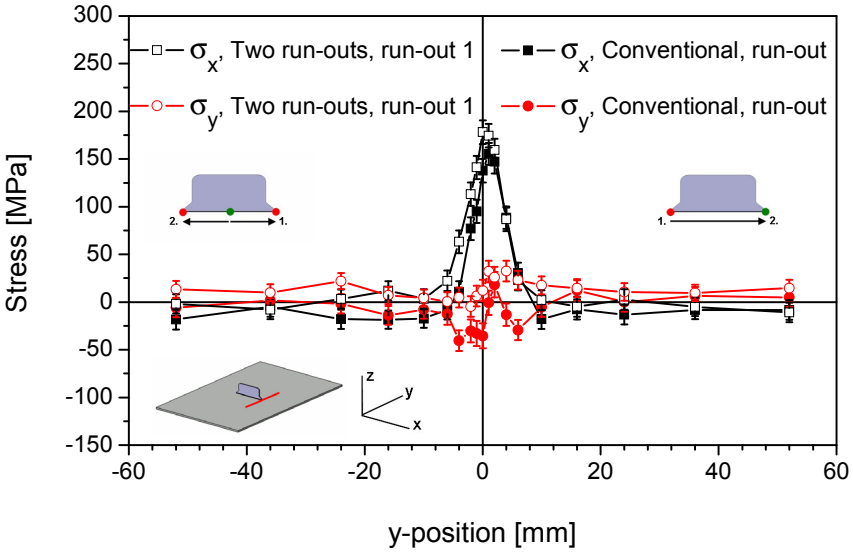

Figure 5.37: Residual stress distributions at the run-out location of the conventionally welded plain panel and at the first run-out location of the welded plain panel which contains two run-outs (panel thickness and material for both welded panels is 4.5 mm thick AA 6156 T6).

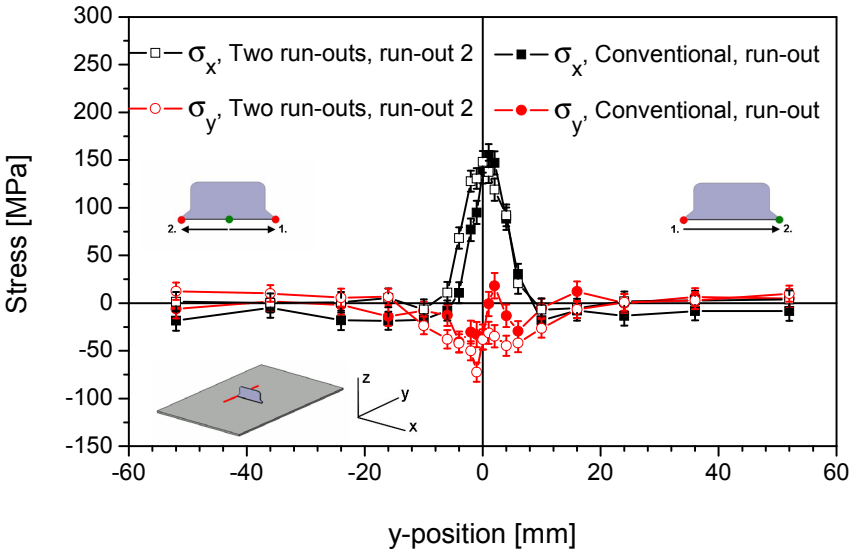

Figure 5.38: Residual stress distributions at the run-out location of the conventionally welded plain panel and at the second run-out location of the welded plain panel which contains two run-outs (panel thickness and material for both welded panels is 4.5 mm thick AA 6156 T6).

The evaluation of the residual stresses at the mid-clip position of the pocketed welded panel (which were machined before welding) of the two run-outs type with respect to plain welded panel of the same type (Figure 5.39) give the similar results, however tensile longitudinal stress peak is to some extend lower for the pocketed case, which is about 150 MPa. In transverse direction compressive residual stresses in the pocketed panel are slightly higher with a peak value of around –50 MPa. As in the case for conventionally welded panel (Figure 5.21), stress distribution in the pocketed panel of the two run-outs welded type shows broadening both for longitudinal and transverse directions.

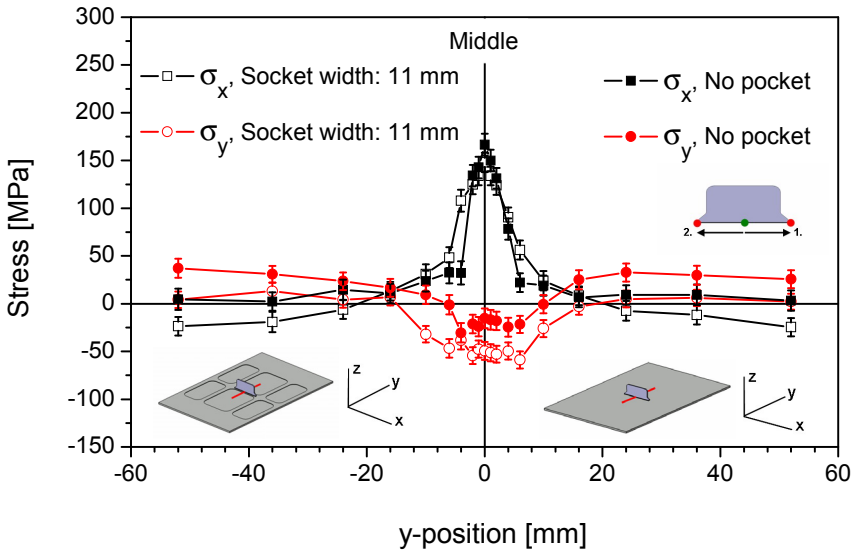

Figure 5.39: Residual stress distributions at the mid-clip locations (run-in position in this welding type) of the 4.5 mm thick AA 6156 T6 plain panel and pocketed panel with 11 mm socket width, which contains two run-outs.

Both at two run-out positions (Figures 5.40 and 5.41), there exist a peak tensile longitudinal stress of around 130 MPa for the welded pocketed panel, which were 175 and 150 MPa at first and second run-out positions of the plain panel, respectively. This difference can be explained by rapid conduction of heat for the pocketed panel due to thinner areas around weld region, which result in less temperature gradient. Transverse stresses are much alike in the pocketed and plain case. Again we observe broader stress distribution profiles at these locations for the pocketed welded panel with two run-outs as in the case for the conventionally welded pocketed panel (Figure 5.23).

These results clearly show that two run-out welds where they correspond to the clip ends develop favourable (compressive) transverse residual stresses at mid-clip and second run-out locations and low (approximately 30 MPa) transverse tensile stresses at the first run-out location.

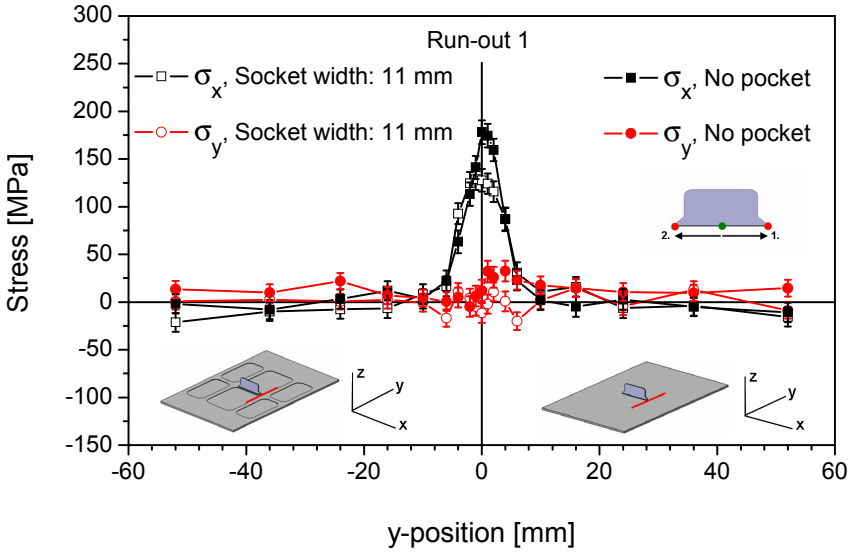

Figure 5.40: Residual stress distributions at the first run-out of the 4.5 mm thick AA 6156 T6 plain panel and pocketed panel with 11 mm socket width, which contains two run-outs.

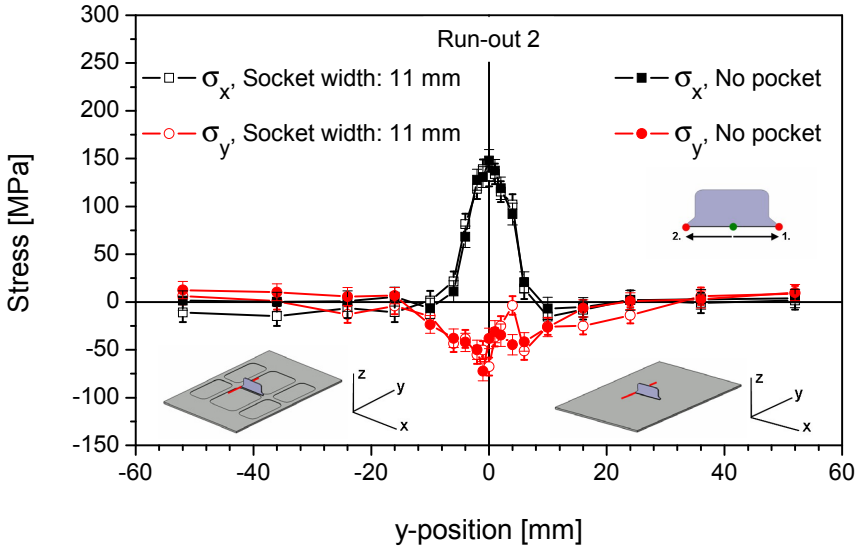

Figure 5.41: Residual stress distributions at the first run-out of the 4.5 mm thick AA 6156 T6 plain panel and pocketed panel with 11 mm socket width, which contains two run-outs.

5.2.7.2 Welding type with two run-ins

The mid-clip position of the 4.5 mm thick 6156 T6 welded plain panel containing two run-ins exhibits considerably higher tensile longitudinal stresses with a peak value of approximately 225 MPa, compared to conventionally welded plain panel (Figure 5.42) and welded panel with two run-outs (Figure 5.43). Peak residual stresses exist at the heat affected zones of the two run-ins welded panel. The mid-clip position of the two run-ins welded panel type is the run-out position of the process, which is the run-in position of the process for the two run-outs welded panel type. In this case, we should judge the residual stresses existing in the mid-clip position of the two run-ins welded panel regarding run-out locations of the conventionally welded (Figure 5.44) and two run-outs welded (Figures 5.45 and 5.46) panel. The longitudinal residual stresses in the mid-clip position of the two run-ins welded panel are extensively higher than run-out locations of both panels, which were conventionally and two-run-outs welded panel. In transverse direction, very high tensile residual stresses arise at the mid-clip position of the two run-ins welded panel with a peak value of about 150 MPa, which is the third times the peak stress value of the mid-clip position of the conventionally welded panel. Transverse stresses at the run-out position of the conventionally welded panel were compressive, excluding one measurement point. Additionally, these were slightly tensile for the first run-out position of the two-run-outs welded panel and significantly compressive for the second run-out position. Higher residual stresses occurrence in the two-run-ins welded panel at the mid-clip position, both in longitudinal and transverse directions can be caused by excessive heat developed during welding of second part of the clip (see section 3.2, the comparison of TC 10–3 of Figure 3.9 to TC 10–6 of Figures 3.7 and 3.8).

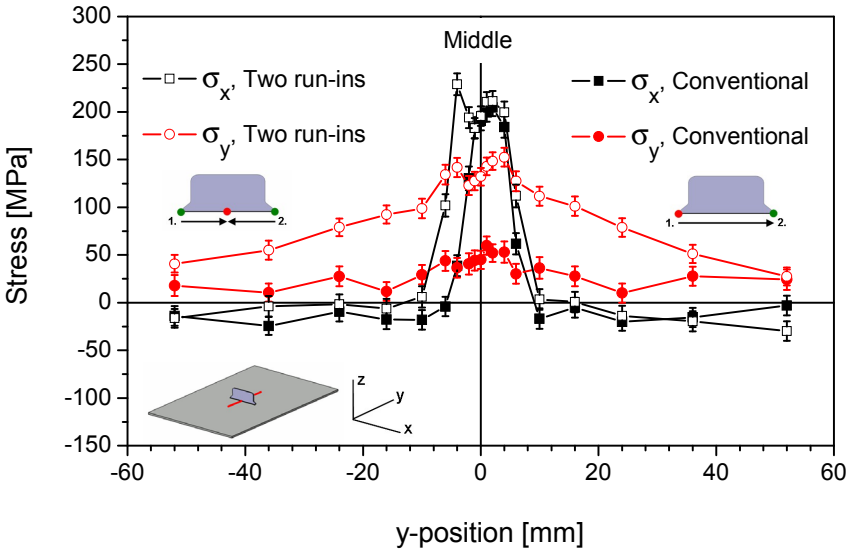

Figure 5.42: Residual stress distributions at the mid-clip positions of the 4.5 mm thick AA 6156 T6 conventionally welded plain panel and welded plain panel with two run-ins (the mid-clip position is in fact the run-out position in this welding type).

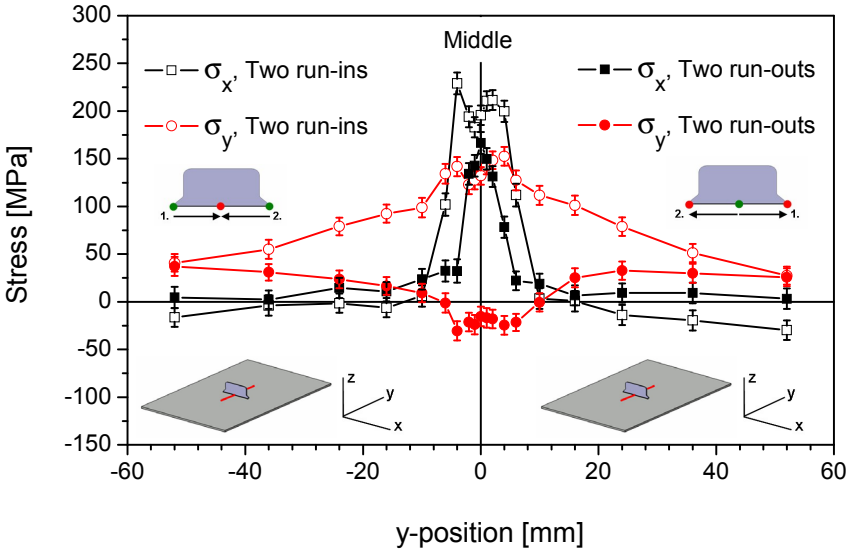

Figure 5.43: Residual stress distributions at the mid-clip positions of the 4.5 mm thick AA 6156 T6 welded plain panels with two run-outs (the mid-clip position is in fact the run-in position in this welding type) and with two run-ins (the mid-clip position is in fact the run-out position in this welding type).

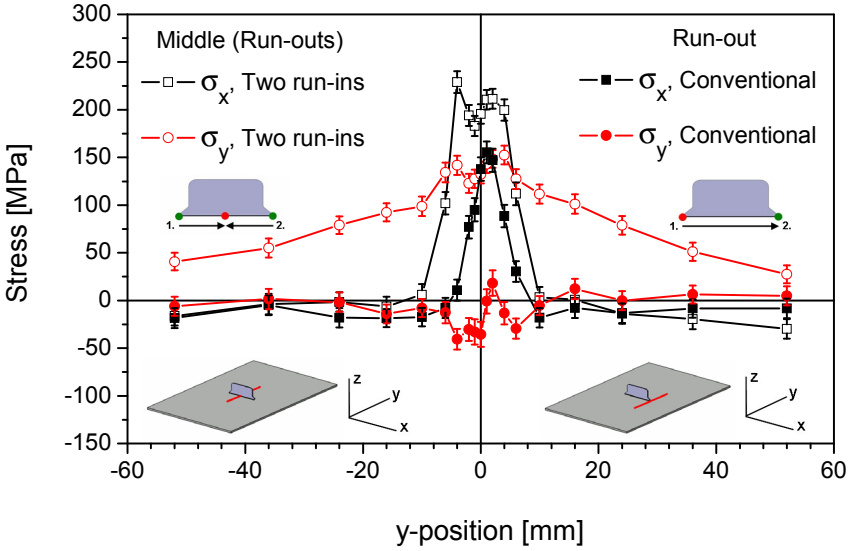

Figure 5.44: Residual stress distributions at the run-out positions of the 4.5 mm thick AA 6156 T6 conventionally welded plain panel, and welded plain panel with two run-ins (the run-out position is at the mid-clip position in this welding type).

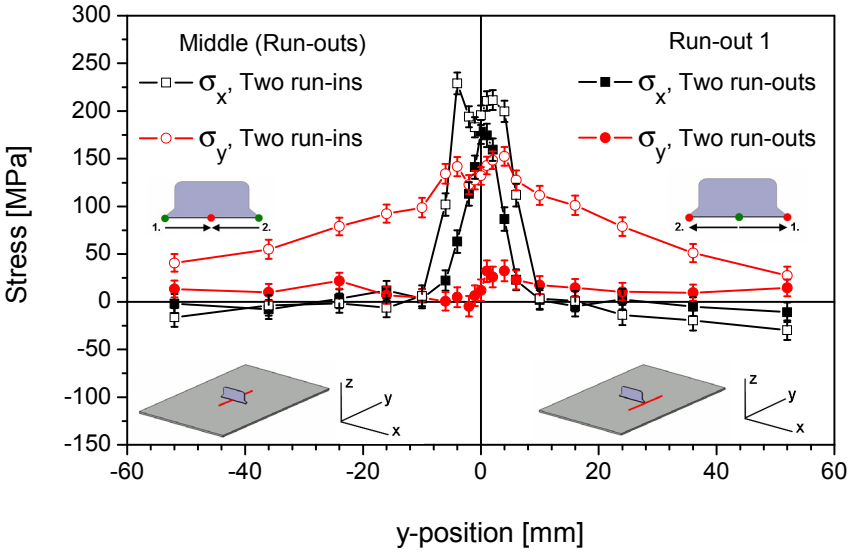

Figure 5.45: Residual stress distributions of the 4.5 mm thick AA 6156 T6 plain panels; at the first run-out position of the welded panel with two run-outs and at the run-out position of the welded panel with two run-ins (the run-out position is at the mid-clip position in this welding type).

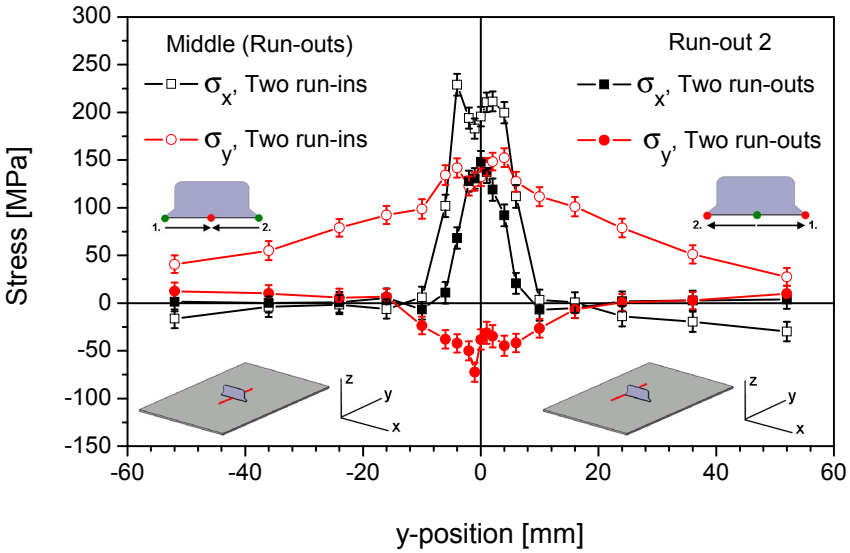

Figure 5.46: Residual stress distributions of the 4.5 mm thick AA 6156 T6 plain panels; at the second run-out position of the welded panel with two run-outs and at the run-out position of the welded panel with two run-ins (the run-out position is at the mid-clip position in this welding type).

The residual stress distributions at the run-in position of the conventionally welded plain panel are compared to those at the first run-in position of the welded plain panel with two run-ins in Figure 5.47 and second run-in position in Figure 5.48. Residual stresses at the first run-in position are rather comparable with that at run-in position of the conventionally welded plain panel. Longitudinal stresses in the conventionally welded panel were slightly tensile (about 20 MPa), on the other hand in the two run-ins panel at the first run-in location the peak tensile stress value is about 60 MPa. Though the distribution of transverse stresses at the first run-in location of the two run-ins panel is considerably wider than that at run-in position of the conventionally welded panel, the peak compressive stress value in both is equal with approximately –100 MPa. At the second run-in position of the two run-ins welded

panel, the peak tensile longitudinal stress value is almost doubled with near to 100 Mpa compared to the first run-in position. The compressive peak stress value is nearly equal but located in the HAZ region. In the welded zone lower compressive transverse residual stresses occur with a value of around –25 MPa. The residual stress distribution of the two run-outs welded plain panel at the mid-clip position, which is the run-ins positions are compared to those at the first and second run-in positon of the two run-ins welded plain panel in Figures 5.49 and 5.50, respectively. Run-in position (mid-clip) of the two run-outs welded panel exhibits higher tensile longitudinal stresses with a peak value of almost 160 MPa and lower compressive transverse stresses with a peak value of around –40 MPa. This is most probably caused by excessive heat occurred at this position due to reheating (see Figure 3.8, TC 10–3 and 10–4).

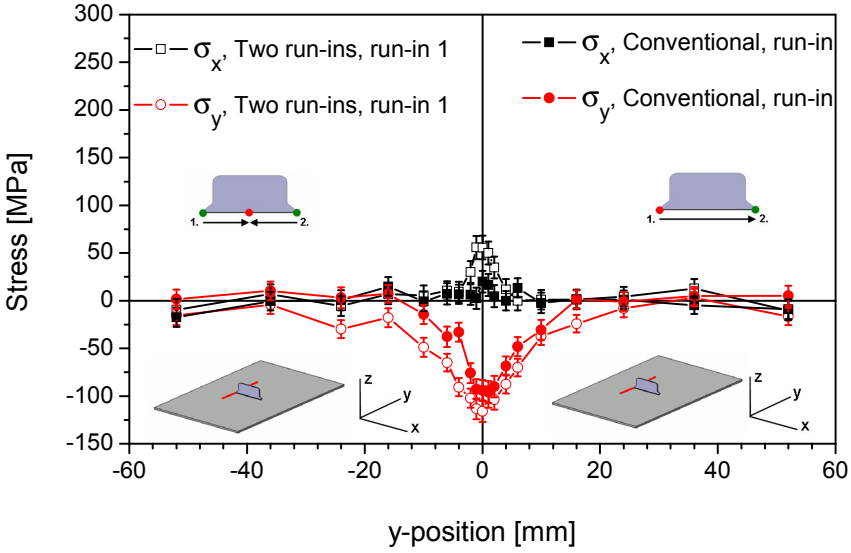

Figure 5.47: Residual stress distributions at the run-in position of the 4.5 mm thick AA 6156 T6 conventionally welded plain panel, and at the first run-in position of the welded plain panel with two run-ins.

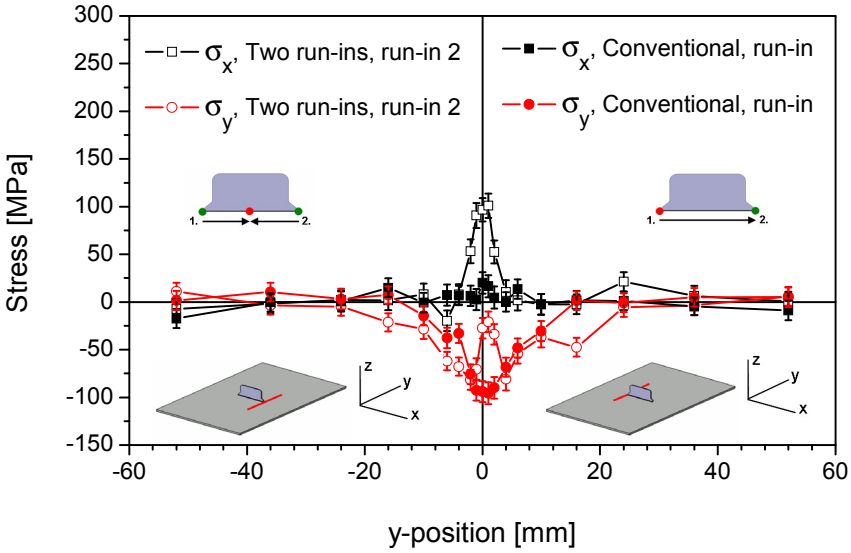

Figure 5.48: Residual stress distributions at the run-in position of the 4.5 mm thick AA 6156 T6 conventionally welded plain panel, and at the second run-in position of the welded plain panel with two run-ins.

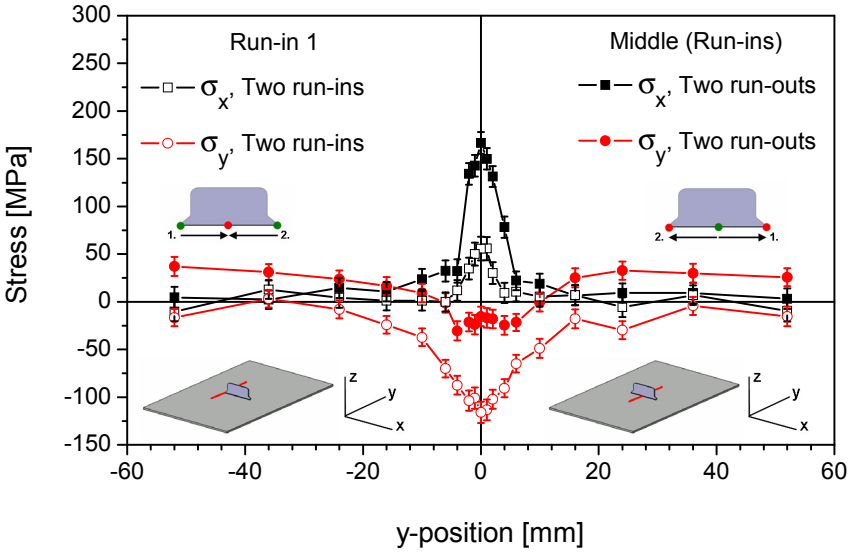

Figure 5.49: Residual stress distributions of the 4.5 mm thick AA 6156 T6 plain panels; at the run-in position of the welded panel with two run-outs (the run-in position is at the mid-clip position in this welding type) and at the first run-in position of the welded panel with two run-ins.

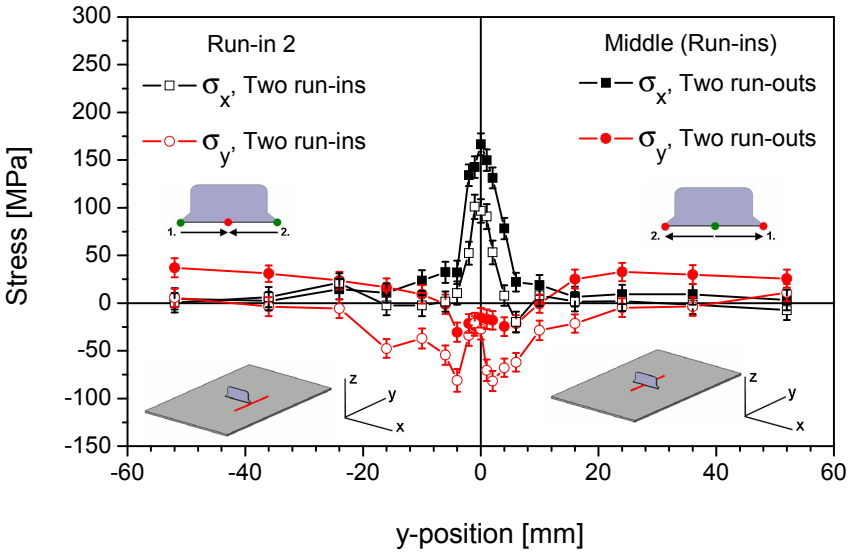

Figure 5.50: Residual stress distributions of the 4.5 mm thick AA 6156 T6 plain panels; at the run-in position of the welded panel with two run-outs (the run-in position is at the mid-clip position in this welding type) and at the second run-in position of the welded panel with two run-ins.

In Figure 5.51, residual stress distributions at the middle location (which is in fact run-out positions) of the 6156 T6 pocketed panel (which were machined before welding) with two run-ins, are plotted. The distribution of longitudinal and transverse stresses are very identical to that in the plain panel having the peak tensile longitudinal stress value of around 250 Mpa and the peak tensile transverse stress of about 150 MPa.

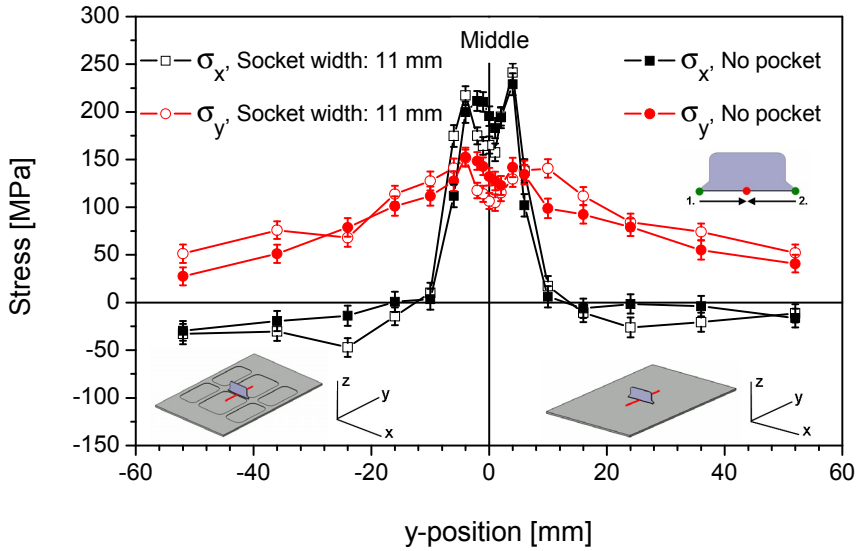

Figure 5.51: Residual stress distributions at the mid-clip location (run-out position in this welding type) of the 4.5 mm thick AA 6156 T6 plain panel and pocketed panel with 11 mm socket width, which contain two run-ins.

The first run-in position of the pocketed panel (Figure 5.52) exhibit very similar residual stress distribution like the one without pocket with a tensile longitudinal peak value of about 60 MPa and with a compressive peak value of around –100 MPa. At the second run-in position of the pocketed panel (Figure 5.53), tensile longitudinal stress and compressive transverse stress distributions and peak values are also very close to that of plain panel, except the existence of lower compressive transverse stresses in the fusion zone of the plain panel.

As a conclusion, these results obviously revealed the fact that having run-ins at the clip ends created low tensile longitudinal stresses and high transverse compressive stresses at the clip ends. However, having run-outs at mid-clip position created high tensile longitudinal and transverse stresses at this position. Although high residual stresses evolved at mid-clip region due to two run-outs at the same location, achieving lower residual stresses at clip ends is also an important gain with respect to fatigue performance of the welded clip-skin system.

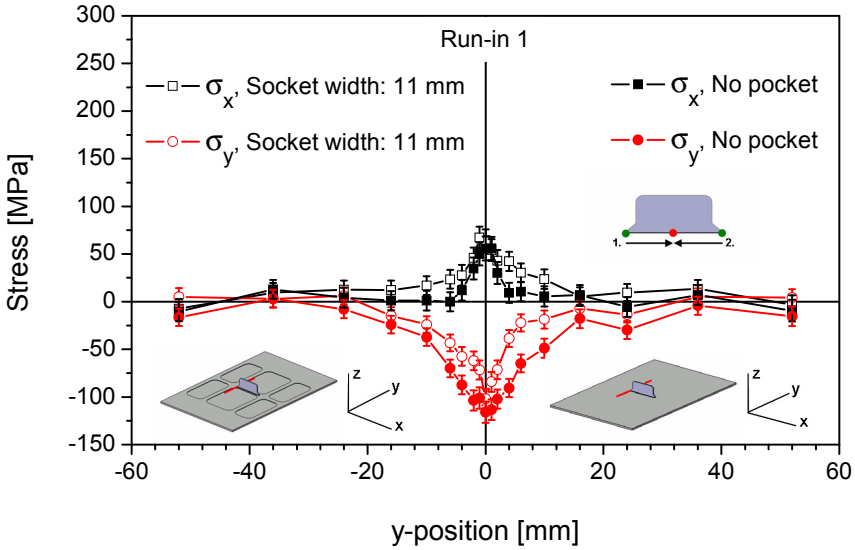

Figure 5.52: Residual stress distributions at the first run-in locations of the 4.5 mm thick AA 6156 T6 plain panel and pocketed panel with 11 mm socket width, which contains two run-ins.

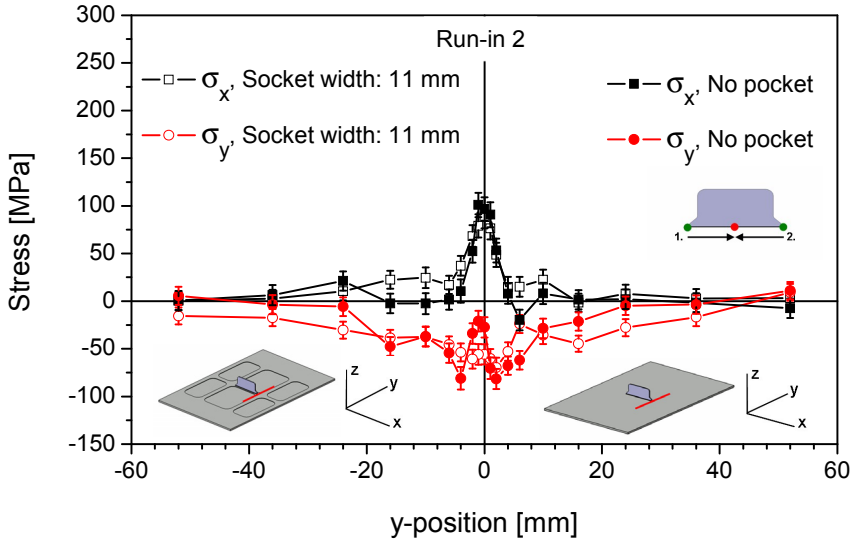

Figure 5.53: Residual stress distributions at the second run-in locations of the 4.5 mm thick AA 6156 T6 plain panel and pocketed panel with 11 mm socket width, which contains two run-ins.

5.3 Comparison of FE simulation and experimental residual stress results

Finite element analysis for residual stress estimations was performed using the SYSWELD code. Material databases for heat treatable Al-Mg-Si alloys were used that were contained in the SYSWELD package. The heat source was fitted to reproduce the weld bead visible in a macrograph. Additionally, predicted temperature profiles were compared with measured ones that were obtained with thermocouples mounted close to a weld (section 4.5).

In fact, the neutron diffraction measurement results give the average stress results in a defined gauge volume. To be able to compare the simulation results with experimental results, simulated stress curves were taken from the end limits and middle of this gauge volume from the same location of the base panel as in the experiment and interpolated to give the final stress curve.

5.3.1 Effect of heat treatment on σ_{res}

5.3.1.1 AA 6156 T4 base panel

The stress (von Misses) contour of conventionally welded 6156 T4 is given in Figure 5.54 which reveals the different stress distribution along mid-clip, run-in and run-out positions.

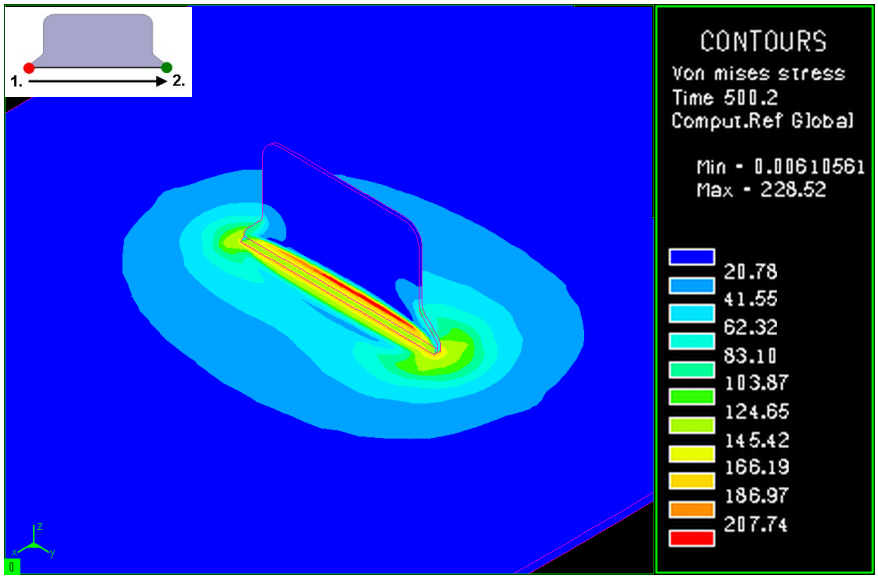

Figure 5.54: Von Misses residual stress distribution in the conventionally welded 6156 T4 panel.

The comparison of the simulation (Pre) and experimental (Exp) residual stress results at mid-clip location of the base and in the clip are given in Figure 5.55 and at run-in and run-out locations in Figures 5.56 and 5.57 respectively for the conventionally welded plain samples. They show good agreement particularly for the transverse stresses at all three locations. Although simulation results for the longitudinal stresses were higher than the experimental results, distributions of the stresses were similar in all three locations. Since the melted zone in the thermal simulation fits very well with the macrograph of the weld (see Figure 4.3), the reason for the difference lies probably in the meshing, which should refined in the weld region. The simulated stresses in the through thickness (z) direction are very close to zero at

each locations, so the plane stress assumption used in calculation of the experimentally measured residual stresses is confirmed.

Since welding was applied for all type of welded panels from one side only (positive y - axis side), the simulated and the measured residual stress distributions are not symmetrical with respect to the zero y - axis, as we can see from Figures 5.55a, 5.56 and 5.57.

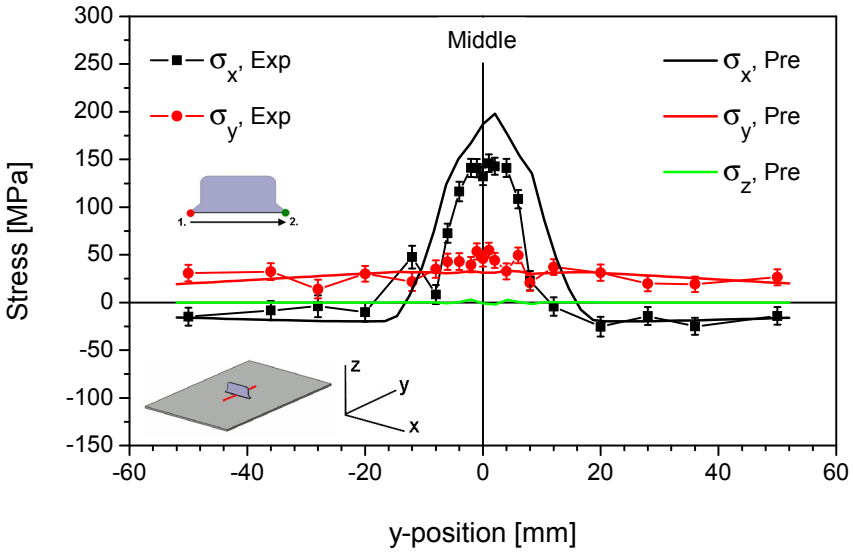

a)

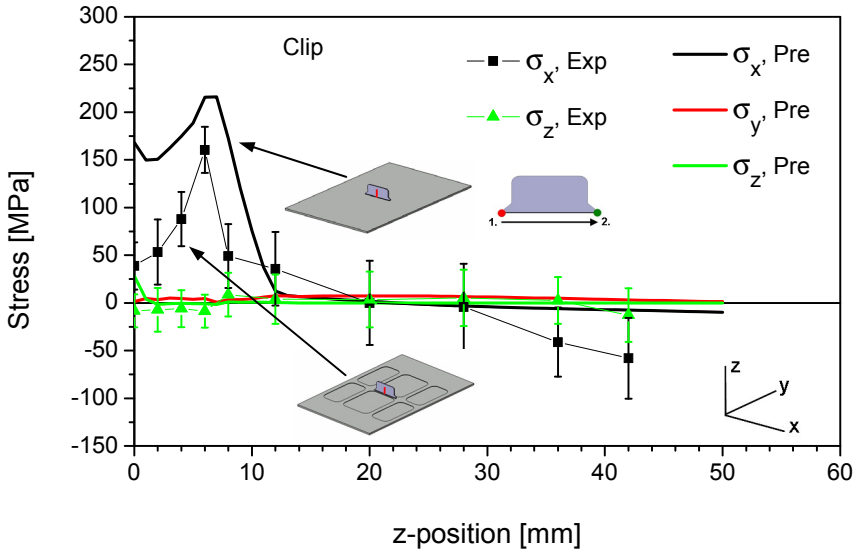

b)

Figure 5.55: Comparison of FE simulation and experimental residual stress distributions a) at the mid-clip location of the 4.5 mm thick AA 6156 T4 plain panel b) in the clip (experimental results of the clip is available only for pocketed panel with 20 mm socket width of the same material).

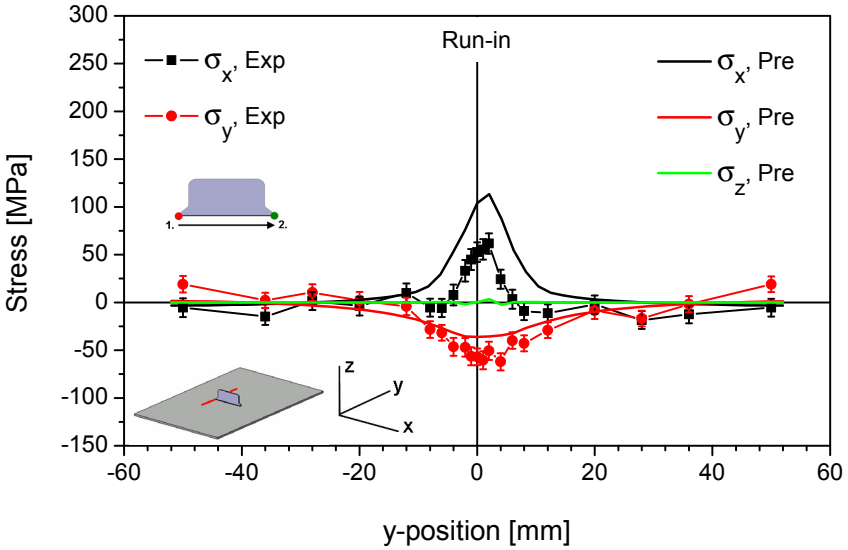

Figure 5.56: Comparison of FE simulation and experimental residual stress distributions at the run-in locations of the 4.5 mm thick AA 6156 T4 plain panel.

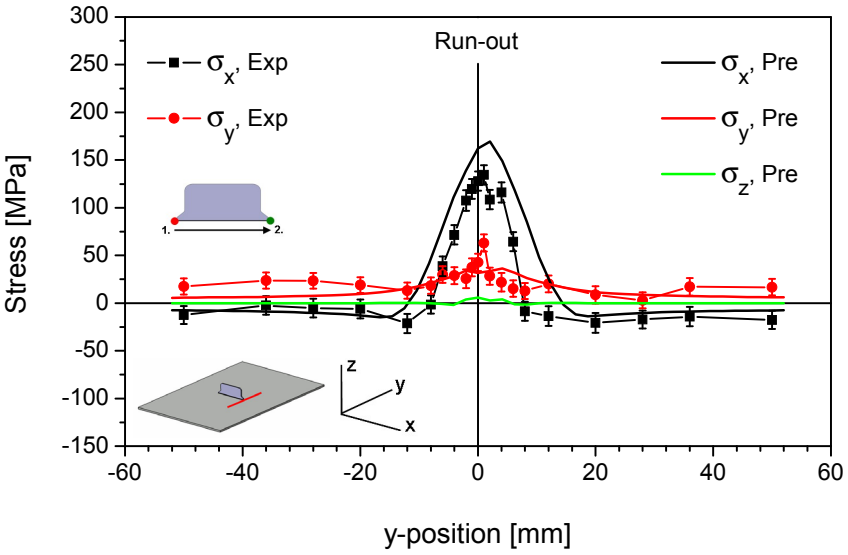

Figure 5.57: Comparison of FE simulation and experimental residual stress distributions at the run-out locations of the 4.5 mm thick AA 6156 T4 plain panel.

5.3.1.2 AA 6156 T6 base panel

The stress contour of conventionally welded 6156 T6 (Figure 5.58) resembles like the one for welded 6156 T4 panel (Figure 5.54). The main differences are narrower stress distribution around the weld and higher residual stresses existing in the welded T6 panel.

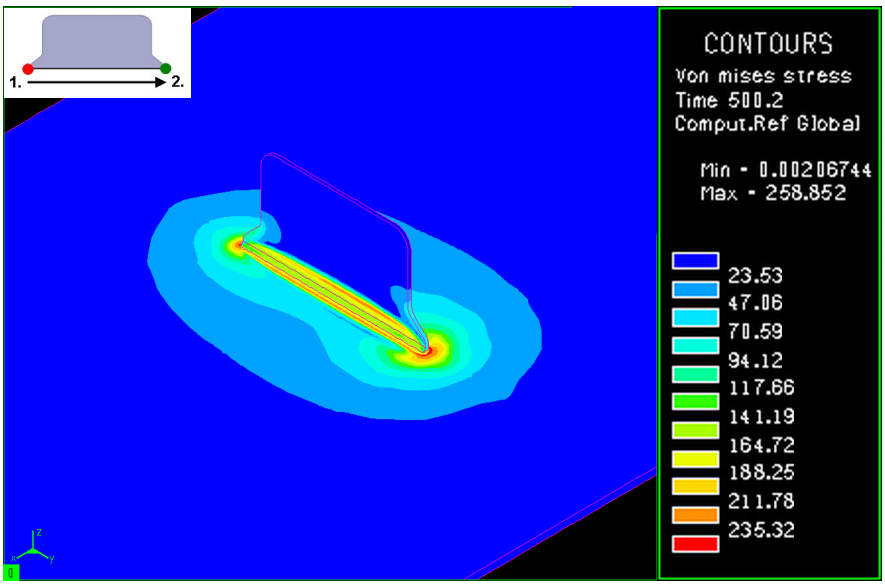

Figure 5.58: Von Misses residual stress distribution in the conventionally welded 6156 T6 panel.

The simulated and experimentally determined residual stress distributions of the conventionally welded 6156 T6 panel at mid-clip, run-in and run-out locations are given in Figures 5.59, 5.60 and 5.61, respectively. As compared to T4 material, narrower residual stress distribution and higher peak stress values exist at all three locations around the weld in the T6 panel which is also the case for the experimental results at mid-clip and run-out locations. However, the measured tensile residual stresses at run-in location of T6 panel are much lower than the simulated stresses in the longitudinal direction and higher compressive in the transverse direction. The measured and simulated residual stresses show consistency for T4 panel (Figure 5.55), it must be the case for T6 panel as well. The reason for this difference should be the microstresses existing in the T6 panel which also explains the measured transverse compressive stresses at run-out location.

Figure 5.62 compares the 6156 T4, 6156 T6 and 2139 T351 material in terms of the yield stress of the base materials and measured and simulated peak longitudinal residual stress values of each conventionally welded panel. As the strength of the materials increases, the peak value of the residual stresses occurring during the welding increases.

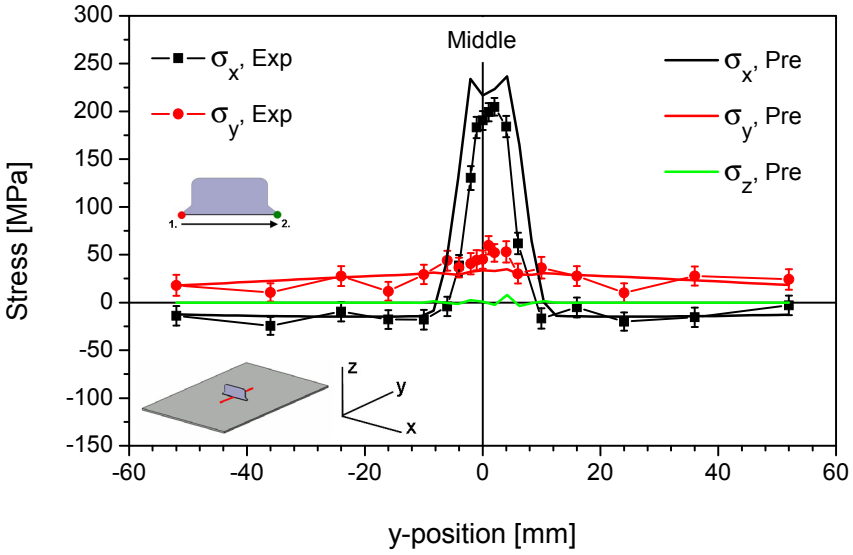

Figure 5.59: Comparison of FE simulation and experimental residual stress distributions at the mid-clip location of the 4.5 mm thick AA 6156 T6 plain panel.

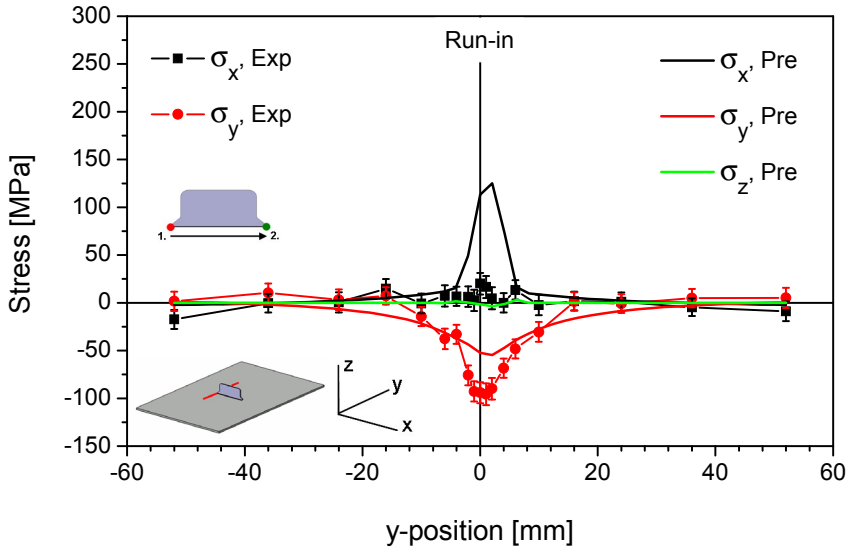

Figure 5.60: Comparison of FE simulation and experimental residual stress distributions at the run-in locations of the 4.5 mm thick AA 6156 T6 plain panel.

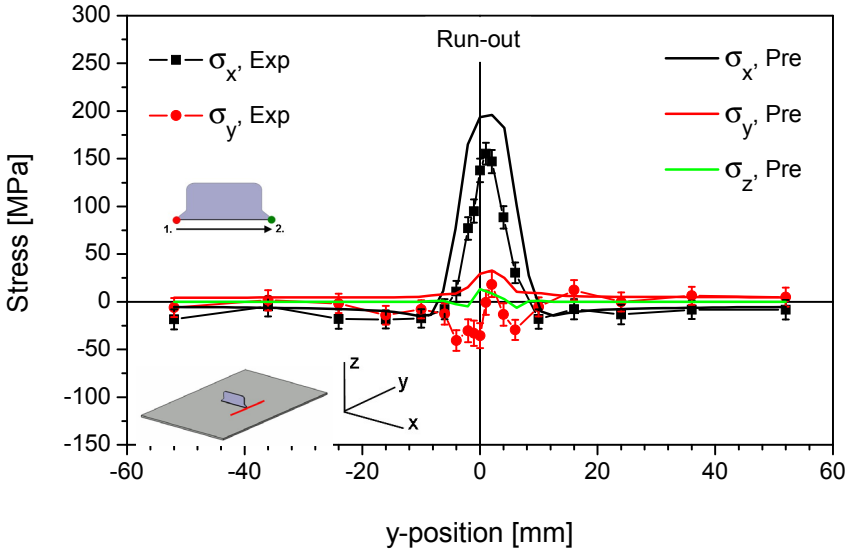

Figure 5.61: Comparison of FE simulation and experimental residual stress distributions at the run-out locations of the 4.5 mm thick AA 6156 T6 plain panel.

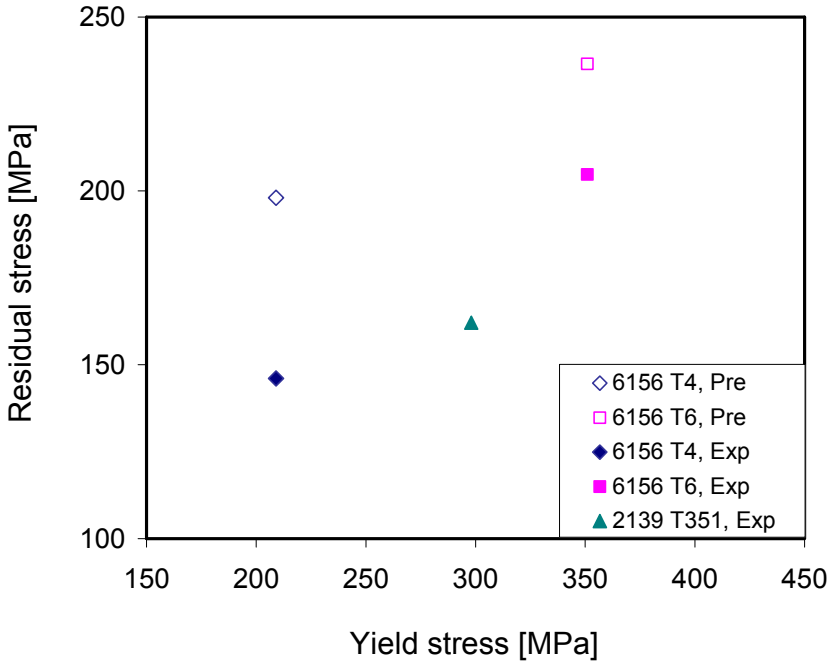

Figure 5.62: Comparison of the 6156 T4, 6156 T6 and 2139 T351 materials at mid-clip location in terms of the peak longitudinal residual stress values of the conventionally welded panels and yield stress of the base panels**.**

5.3.2 Effect of welding type on on σ_{res}

5.3.2.1 Welding type with two run-outs

Figure 5.63 shows the stress contour of the welded 6156 T6 panel containing two run-outs. A remarkable asymmetric distribution along each run-out positions exist. At the second run-out position, a narrower distribution exists and slightly lower residual stresses were calculated compared to the first run-out position, see Figures 5.65 and 5.66.

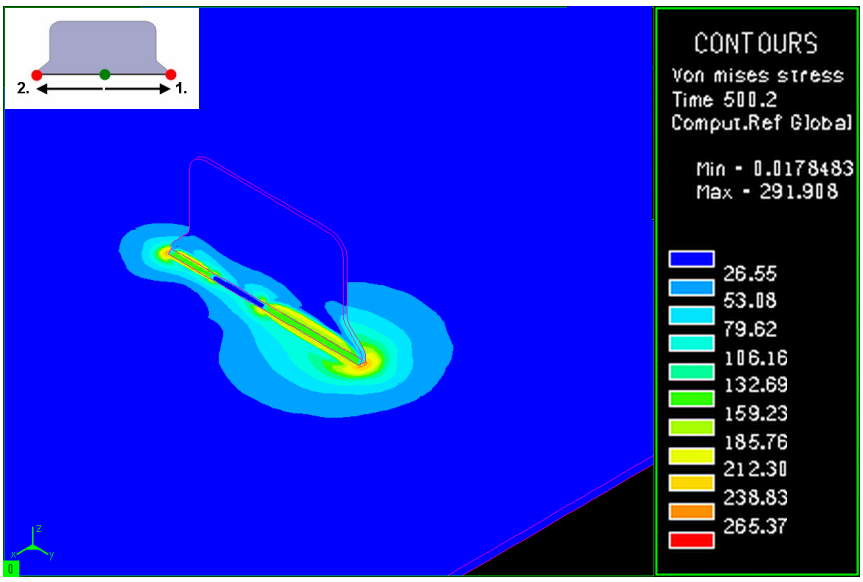

Figure 5.63: Von Misses residual stress distribution in the welded 6156 T6 panel with two run-outs.

The comparison of the simulation and experimental results at mid-clip position is demonstrated in Figure 5.64. Simulation predicts lower tensile longitudinal peak stress values however there exists a good consistency predicting compressive transverse stresses.

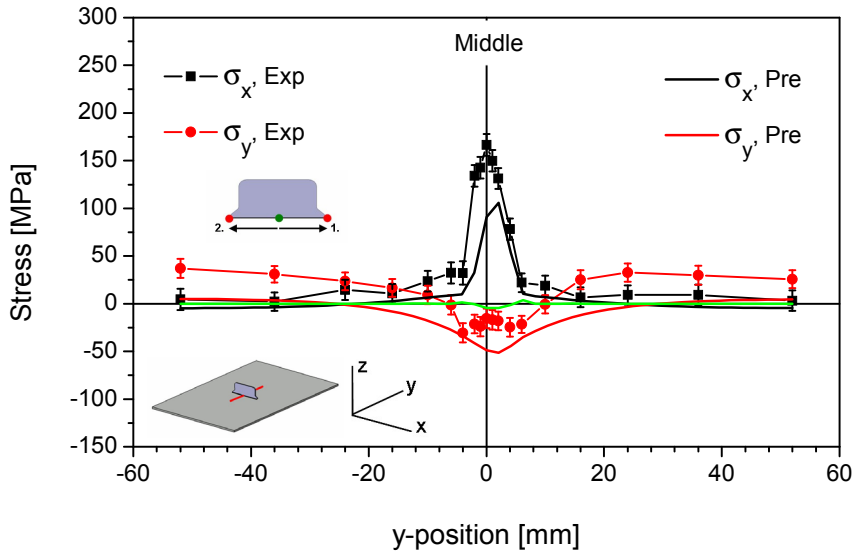

Figure 5.64: Comparison of FE simulation and experimental residual stress distributions at the mid-clip location of the 4.5 mm thick AA 6156 T6 welded plain panel with two run-outs.

The residual stress results at the first and second run-out positions are shown in Figures 5.65 and 5.66 respectively. There exists a perfect fit between simulated and measured results in the longitudinal direction. However, the simulated stresses in transverse direction are close to zero for both positions which were tensile with approximately 30 MPa peak value at the first run-out position and compressive with a value of about –70 MPa at the second run-out position.

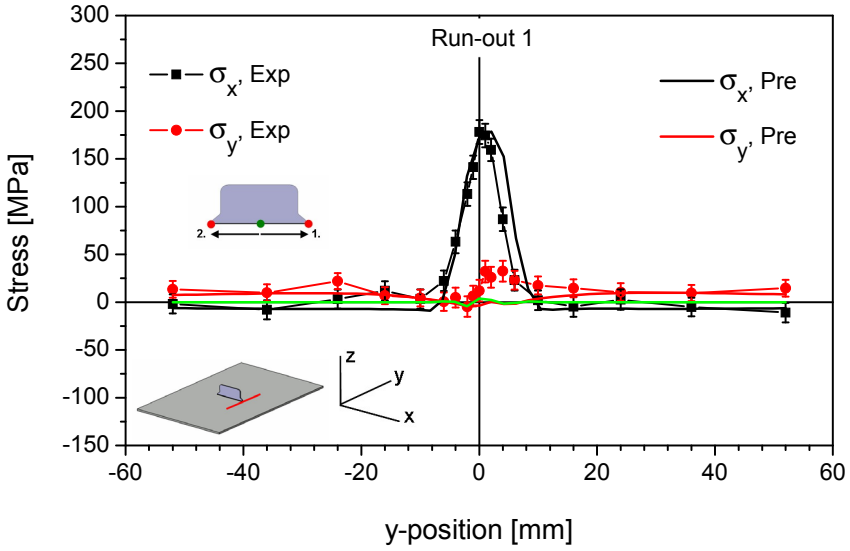

Figure 5.65: Comparison of FE simulation and experimental residual stress distributions at the first run-out location of the 4.5 mm thick AA 6156 T6 welded plain panel with two run-outs.

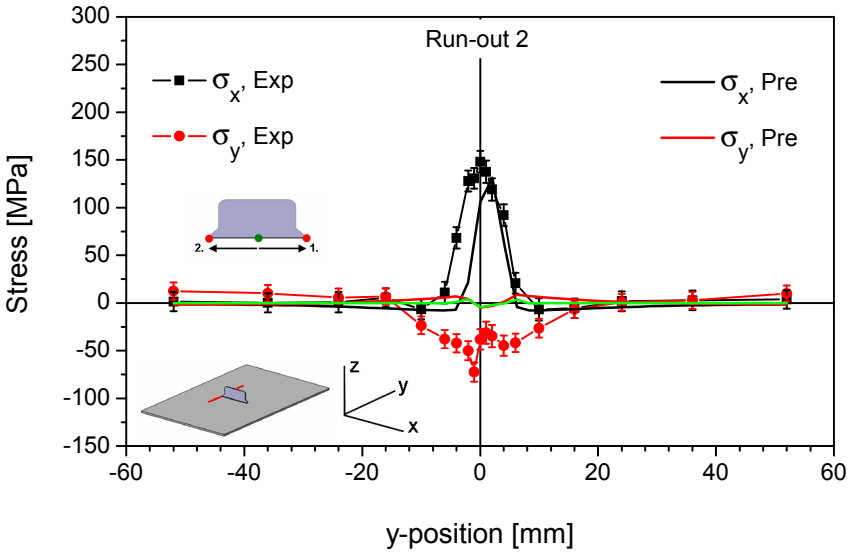

Figure 5.66: Comparison of FE simulation and experimental residual stress distributions at the second run-out location of the 4.5 mm thick AA 6156 T6 welded plain panel with two run-outs.

5.3.2.2 Welding type with two run-ins

The stress contour of welded 6156 T6 panel with two run-ins (Figure 5.67) differs both from the conventional one (Figure 5.58) and welded panel with two run-outs (Figure 5.63) which also confirms the different residual stress occurence during different welding processes. A broad residual stress distribution on the mid-clip position is remarkable, see comparative results in Figure 5.68. There exists a very good correlation between the simulated and measured results in longitudinal direction with a peak value of about 230 MPa. Both methods result in tensile residual stresses in transverse direction. However, maximum values of experimental and simulation results are different. The peak measurement residual stress value is around 150 MPa that is higher than twice the simulation value of about 60 MPa.

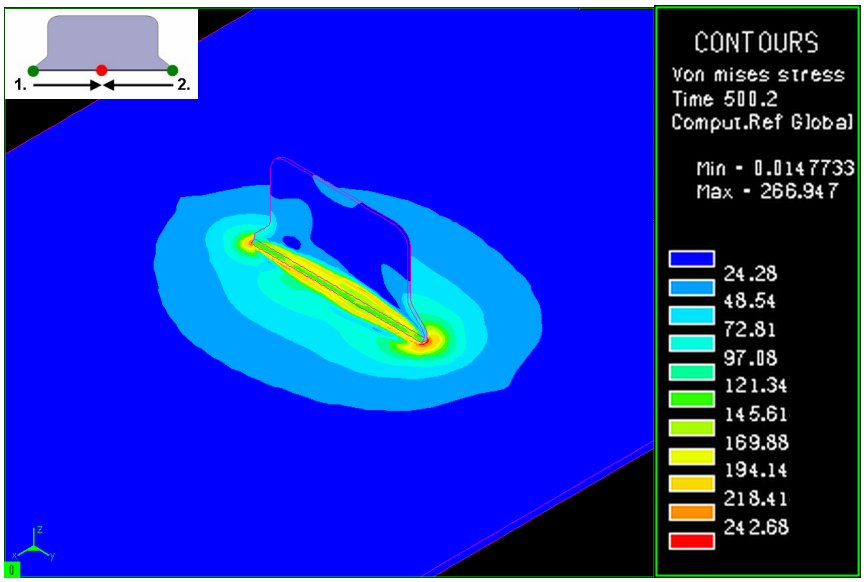

Figure 5.67: Von Misses residual stress distribution in the welded 6156 T6 panel with two run-ins.

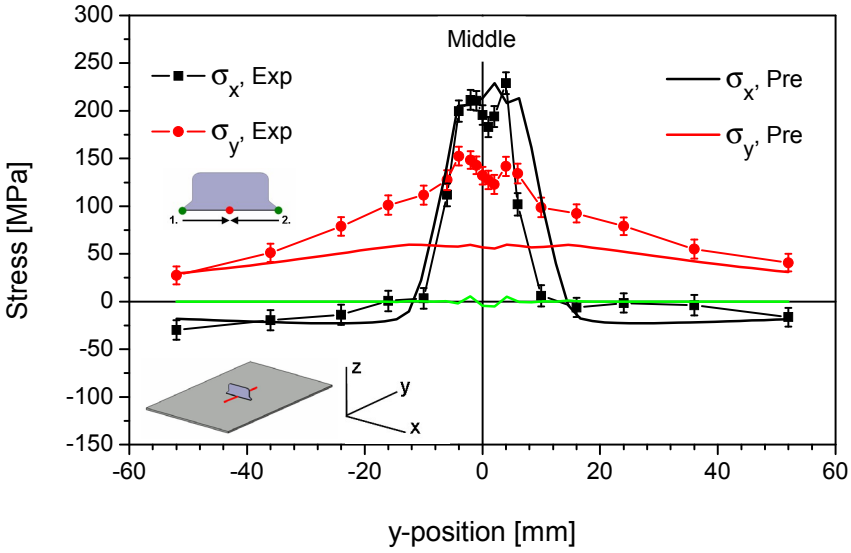

Figure 5.68: Comparison of FE simulation and experimental residual stress distributions at the mid-clip location of the 4.5 mm thick AA 6156 T6 welded plain panel with two run-ins.

Although the simulation and the measurement show differences, bot methods verify higher tensile longitudinal and lower compressive transverse stresses at the second run-in position (Figure 5.69) compared to the first run-in position (Figure 5.70).

It can be concluded that the established FE model enables qualitative predictions for residual stress states in more complicated geometries resembling panels used for aircraft production and for different welding sequences.

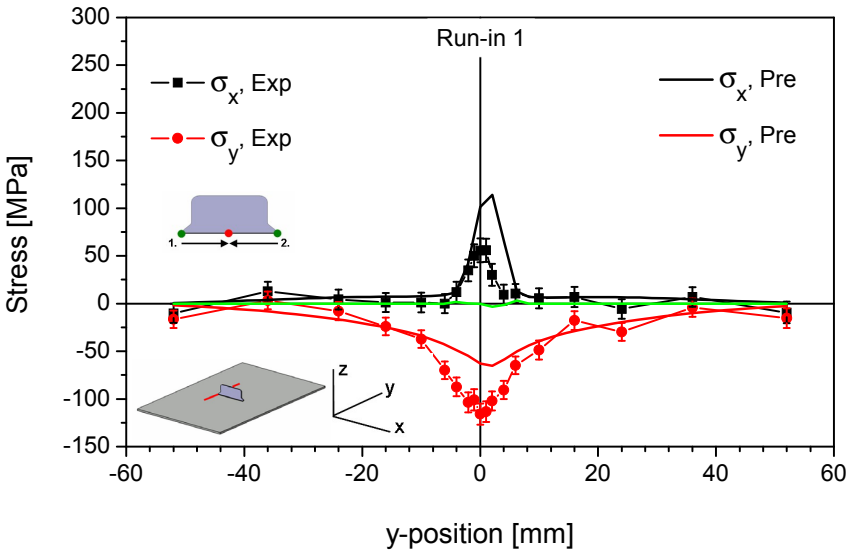

Figure 5.69: Comparison of FE simulation and experimental residual stress distributions at the first run-in location of the 4.5 mm thick AA 6156 T6 welded plain panel with two run-ins.

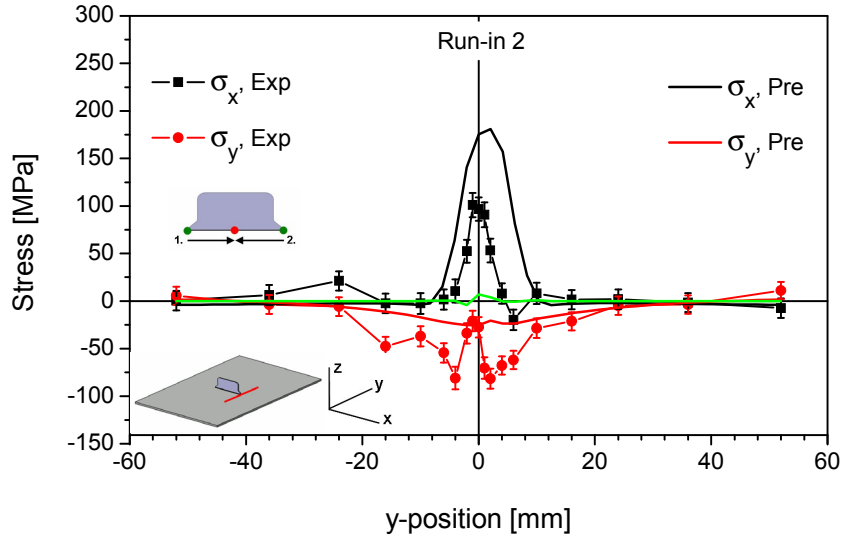

Figure 5.70: Comparison of FE simulation and experimental residual stress distributions at the second run-in location of the 4.5 mm thick AA 6156 T6 welded plain panel with two run-ins.

5.4 Fatigue crack propagation (FCP) behaviour of clip welds with different residual stress states

Fatigue crack propagation (FCP) tests were performed at a stress ratio of $R = 0.1$ under constant-amplitude tensile loading, with a maximum applied load of 61 MPa. The initial central notch ($2a_0$) (Figure 3.22a), was introduced at the mid-clip position adjacent to the weld toe on the root side (the rear side of the one-sided weld) and the crack was running parallel to the clip. The crack propagation length Δa, was measured on the polished specimen surface (back side) using a travelling optical microscope on both sides (right and left sides). An average of both measurements was used to construct the FCP vs. crack length curves. The aim was to analyse the effect of residual stress state of the "one-bay crack" panel on fatigue crack propagation behaviour.

5.4.1 FCP behaviour of plain panels

Fatigue crack propagation (FCP) results of M(T) 400 base panels are presented in terms of da/dN vs. ΔK for different types of Al alloys in Figure 5.71. The central parts of the curves in Figure 5.71 are approximately straight lines, and for these central regions we can use Paris-Erdogan equation [144], [145] in which crack growth rate is a function of ΔK together with two material constants;

$$\frac{da}{dN} = C(\Delta K)^m \quad , \qquad 5.1$$

where C and m are material constants. For the 6xxx series Al- alloy materials the exponent m takes values from $m = 2$ to $m = 3$, which can also be found in the literature [146]. Another empirical parameter, C, varies over a wide range. Using physical considerations, one might propose a connection between C and other material properties. For example, relationships were proposed such as $C \approx (\sigma_U K_{IC})^{-2}$ and $C \approx (E\varepsilon_U K_{IC})^{-2}$ for the moderate stresses. Here σ_U and ε_U are ultimate tensile stress and strain. In general, both C and m depend on the stress ratio $R = K_{\min} / K_{\max}$.

Equation 5.1 presents the relationship between the crack growth rate da/dN and the stress intensity factor range ΔK. The constants C and m were determined for each material by means of the curve fitting of the experimental data, which were plotted in the log-log scale (Figure 5.71) and given in Table 5.1. However, these values were obtained for the moderate crack growth rate region, such as $da/dN \approx 10^{-8}...10^{-4}$ m/cycle.

FCP results of the same panels are also given in terms of da/dN vs. half crack length in Figure 5.72, as well as in terms of crack length vs. cycles (Figure 5.73). The FCP rate of the 6156 T4 panel is rather comparable to that for the 2139 T351 panel. Since both panels were not subjected to aging, they were expected to have similar FCP behaviour. To differentiate FCP behaviour between aged panel and panel without aging, results of the 6156 T4 and T6 were compared. Up to around 14 mm half crack length, the FCP rate of the 6156 T4 panel is higher than that for the 6156 T6 panel, however as the crack propagates further, the FCP rate of the former becomes lower than that for the latter.

A typical a vs. N curves of the corresponding base metal panels are illustrated in Figure 5.73. 2139 T351 panel has a fatigue life of approximately 430,000 cycles, while both 6156 T4 and T6 panel have slightly higher values.

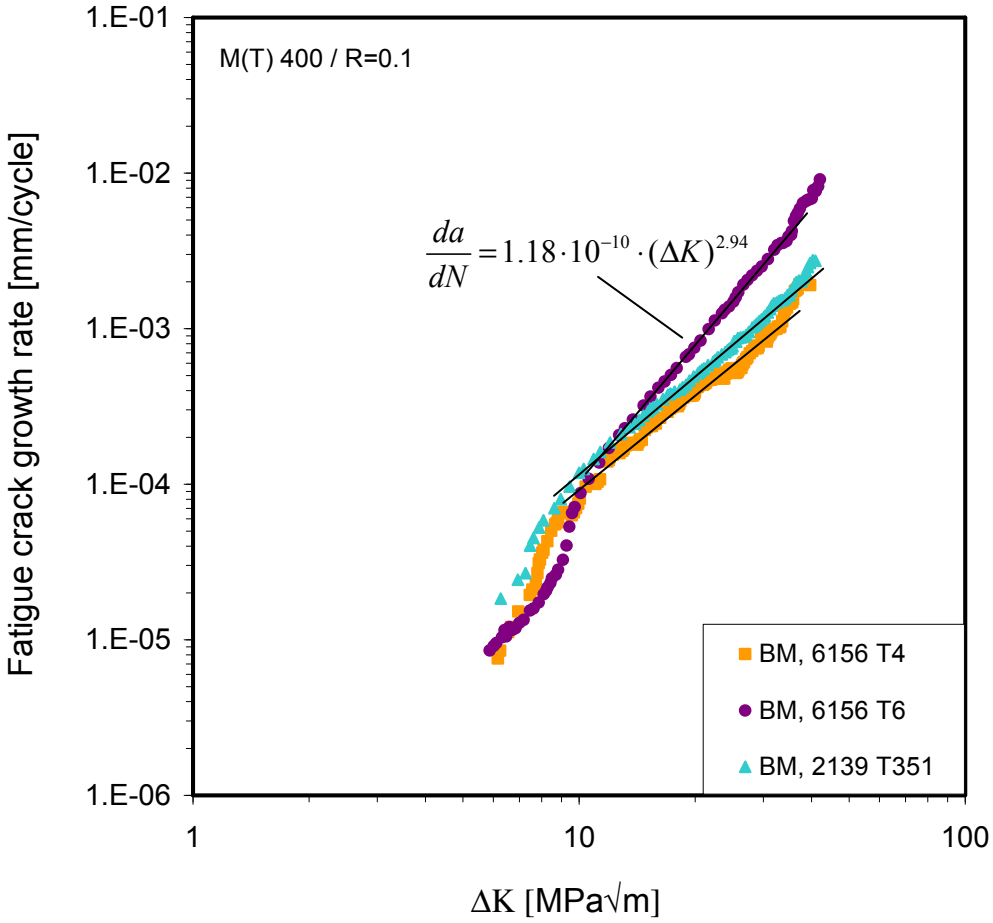

Figure 5.71: Fatigue crack growth rates plotted against ΔK of plain base metal (BM) panels of 6156 T4, 6156 T6 and 2139 T351 materials. As an example, one curve-fit of the Paris eqn. is shown for 6156 T6 alloy.

Table 5.1: Material type, applied heat treatment and material constants m and C, which were defined in the Paris-Erdogan (Equation 5.1).

Material	Heat Treatment	Aging Process	m	$C \times 10^{10}$
6156	T4	-	1.87	1.43
6156	T6	190°C, 4 hours	2.94	1.18
2139	T351	-	2.07	1.02

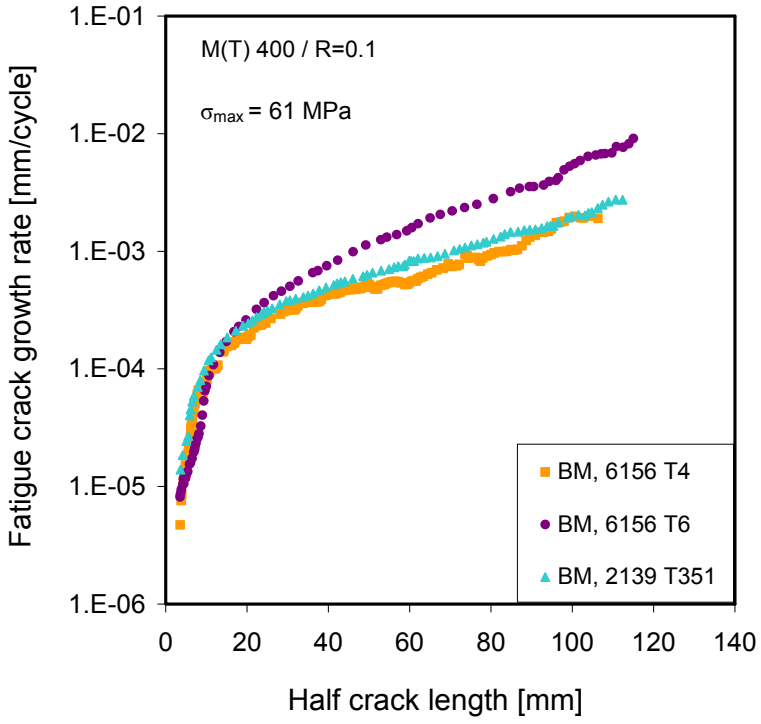

Figure 5.72: Comparison of fatigue crack growth rates plotted against half crack lengths of plain base panels of 6156 T4, 6156 T6 and 2139 T351 materials.

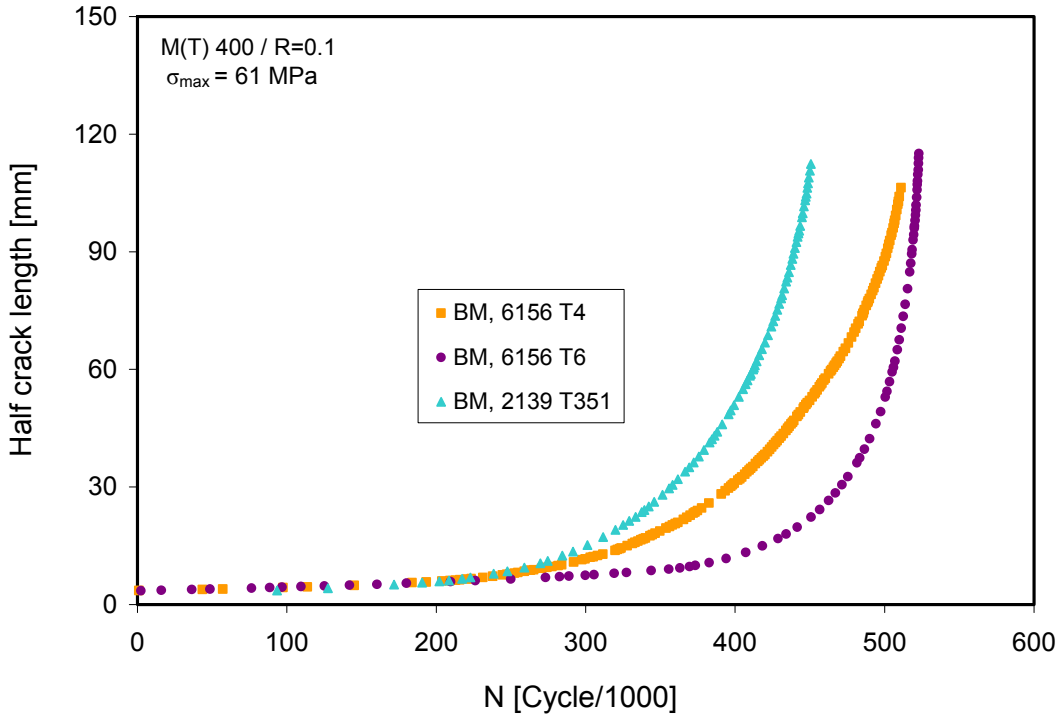

Figure 5.73: Comparison of the fatigue lives of the plain base panels of 6156 T4, 6156 T6 and 2139 T351 materials.

The FCP results in terms of da/dN vs. half crack length of the conventionally welded panels and base metal panels are illustrated for both 6156 T4 and T6 materials in Figures 5.75 and 5.76 respectively. The vertical line at the 60 mm crack length defines the location where fatigue crack reaches the clip ends. Welded panels showed high FCP behaviour with respect to the base metal panels at the first 60 mm (where clip weld is available in the welded panels). However, the crack propagation in the welded panels slowed down as crack entered to the base metal region of the clip welded panel. The reasons for the apparently faster FCP rates in the weld areas of both clip welded panels than in the base panel are the unfavourable weld microstructure (reduced strength due to dissolved precipitates [34]), high stress concentration of the T-joint geometry and tensile residual stresses in the direction of the applied load. However, as cracks approach the clip ends, crack retardation occurred abruptly in the welded panels. For larger crack lengths, FCP curves of welded clip panels tend to show properties similar to those of the base metal panel since the crack tip in the welded panels were sufficiently away from the weld area.

To determine the geometry effect on the crack propagation curves, the structural stress distribution consisting of the summation of the membrane and bending stress portions (excluding nonlinear notch stress portion) was calculated for both base panel and T-joint geometry by ABAQUS assuming linear elastic material behaviour (Figure 5.74). A coarse mesh finite element model was used in the simulation, whis is necessary for structural stress analysis. The stress distribution was linearised over plate thickness through the red line shown in Figure 5.74 where the initial notch was introduced for the FCP tests. For further information refer to Radaj et al. [147]. The maximum stress values calculated were 62.8 MPa for the base panel and 65.1 MPa for the T-geometry. Using the equation 5.1 the da / dN values of the base panel were recalculated considering for the maximum structural (geometric) stresses and and plotted with red points in Figure 5.75 for 6156 T4 material and Figure 5.76 for T6 material. As can be seen from these figures the geometry shows negligible effect on FCP behaviors.

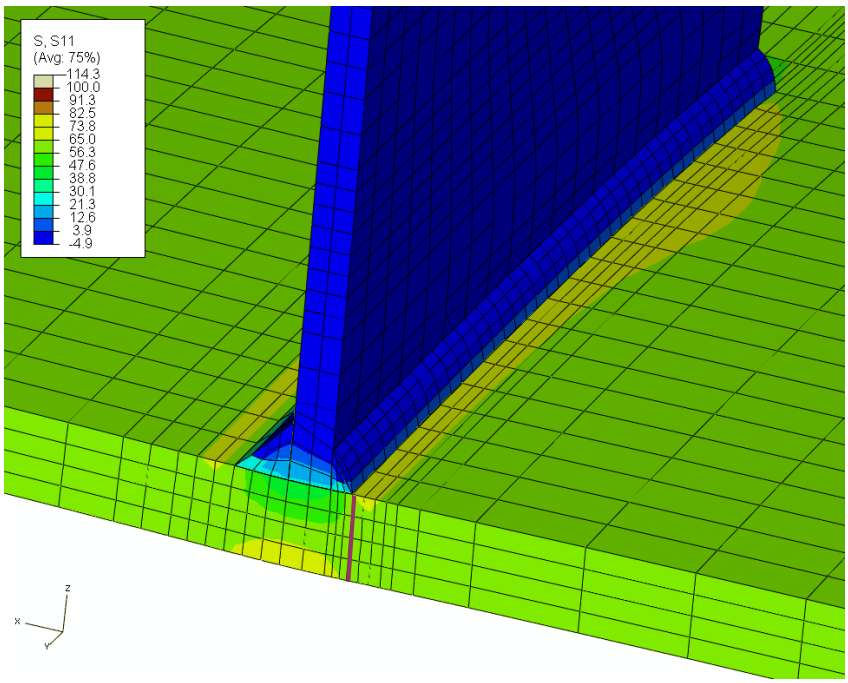

Figure 5.74: The calculated structural stress distribution fort the T-joint geometry.

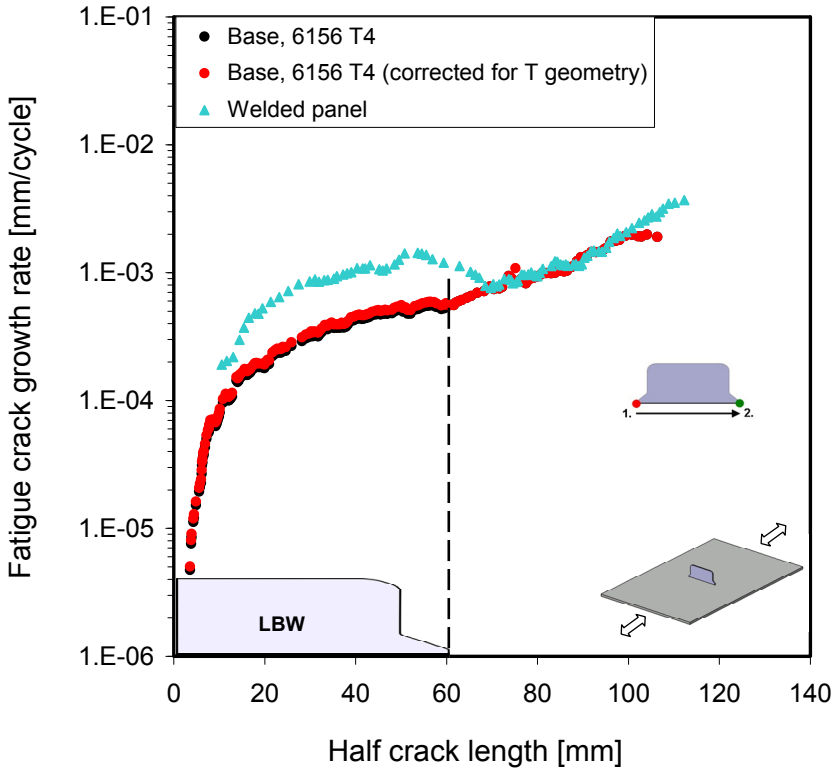

Figure 5.75: Fatigue crack growth rates plotted against half crack lengths of 6156 T4 plain base and welded panel. The weld was made with conventional procedure.

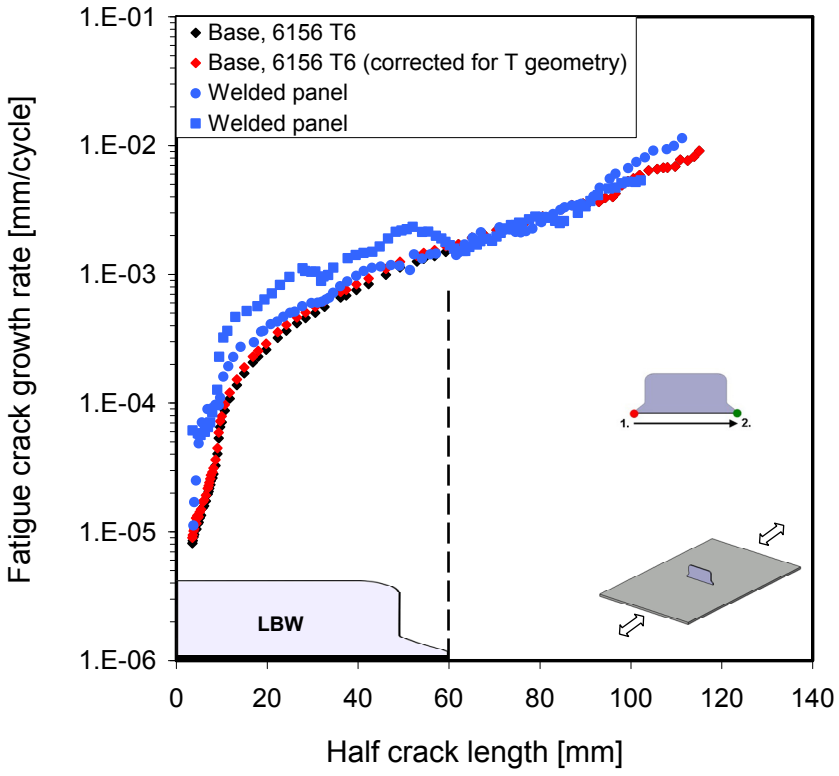

Figure 5.76: Fatigue crack growth rates plotted against half crack lengths of 6156 T6 plain base and welded panels. The weld was made with conventional procedure.

5.4.2 Effect of heat treatment on FCP behaviour

The effect of the applied heat treatment on the FCP rates of the clip welds were investigated on AA 6156 T4 and T6 material.

The FCP results in terms of da/dN vs. half crack length of the conventionally welded panels and base metal panels are illustrated for both 6156 T4 and T6 materials in Figure 5.77. The difference between FCP rates of the welded 6156 T4 panel and T4 base panel within 60 mm is relatively higher than that for the T6 panel. The comparison of the fatigue lives of the conventionally welded plain panels of 6156 T4 and T6 with respect to their base panels is illustrated in Figure 5.78. There are no significant differences in total fatigue lives of 6156 T4 and T6 panels. However, the welded panels have remarkably short fatigue lives (about 230,000 cycles) compared to base panels (500,000 cycles). Residual stresses are adding up to the acting stresses during crack growth, so that they are very effective in shortening of total fatigue lives. In order to find out the state of the residual stresses along the clip welds, the transverse residual stresses (σ_y) were determined at the mid-clip position through the scan lines perpendicular to the weld line of the 4.5 mm thick 6156 T4 and T6 material and are compared in Figure 5.79. The distributions of the residual stresses for both materials are very similar to each other, which will contribute to the acting stresses equally. Although, measured peak values of the transverse residual stresses are not too high (approximately 40-50 MPa), still these tensile stresses are increasing the crack tip stresses which contribute to the higher crack growth rates of the cracks propagating along the clip weld seams. Additionally, weld microstructure, which has inherently lower FCP properties than the base metal, contributes to the overall reduction of the FCP-lives of the panels as shown in Figure 5.78. However, the presence of the tensile residual stresses could play a major role and efforts should be made to control and modify these stresses.

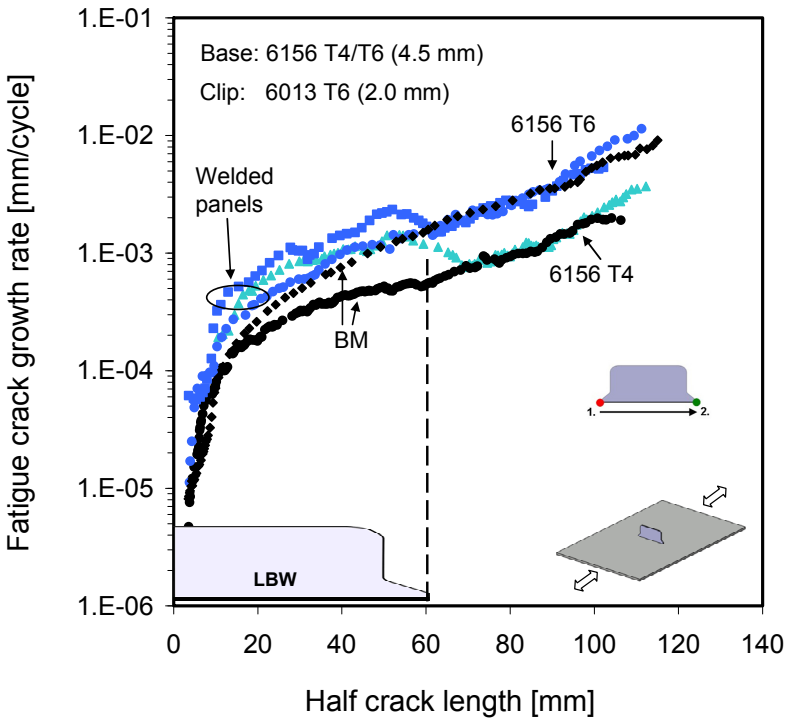

Figure 5.77: Fatigue crack growth rates plotted against half crack lengths of 6156 T4 and 6156 T6 plain base and welded panels. The weld was made with conventional procedure.

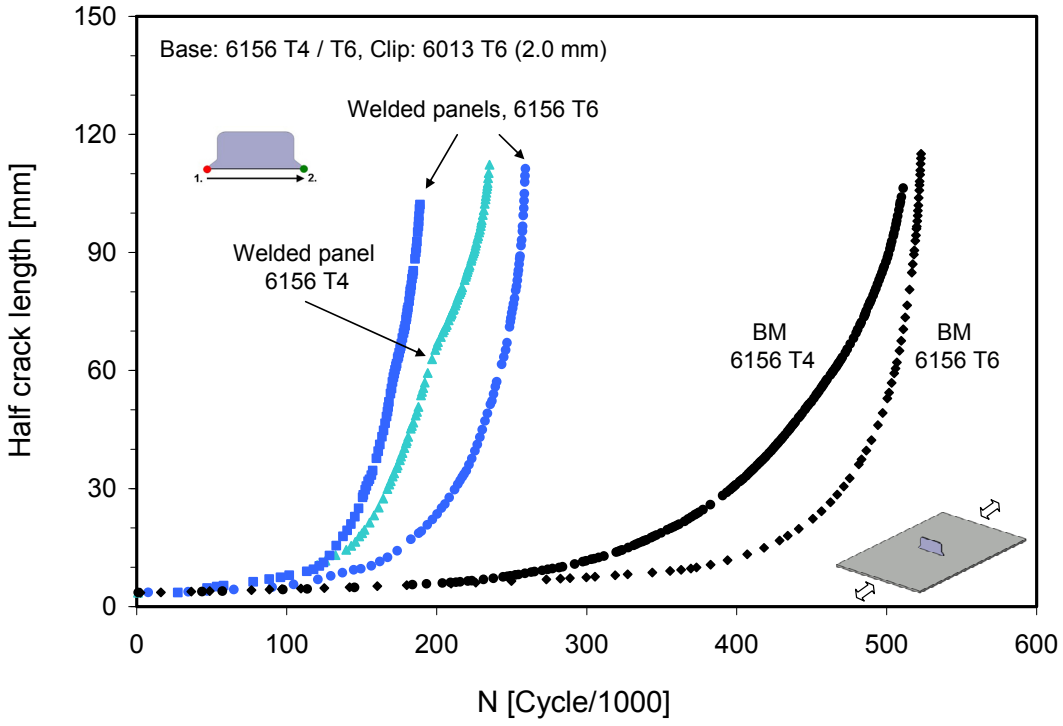

Figure 5.78: Comparison of the fatigue lives of the conventionally welded plain panels of 6156 T4 and 6156 T6 with respect to their base panels.

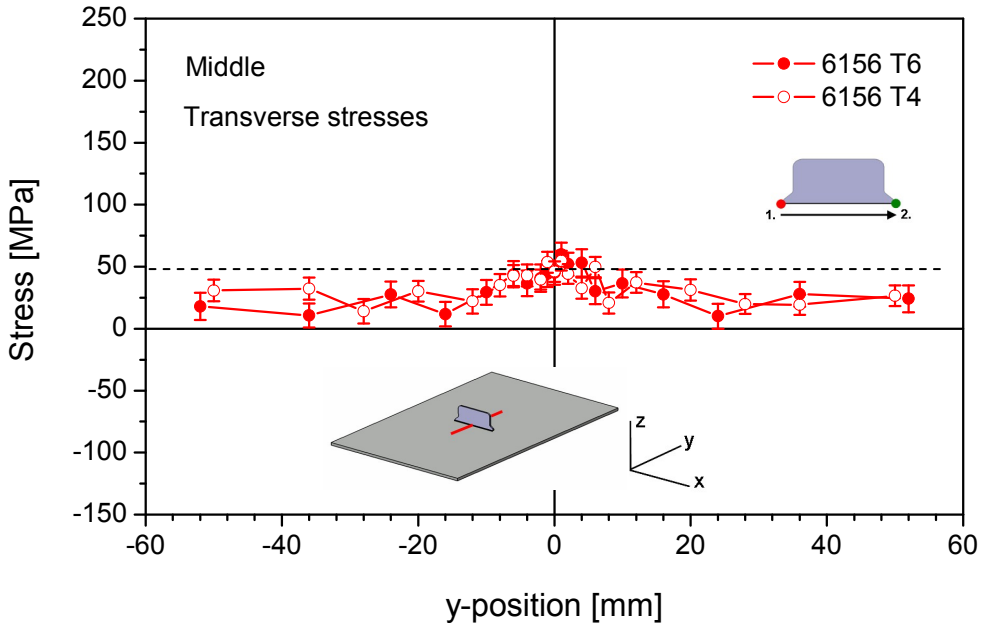

Figure 5.79: Transverse residual stress distributions at the mid-clip position of the conventionally welded plain panels of 6156 material (4.5 mm); solid points show that for the T6-artificially aged panel and empty points show that for the T4-naturally aged panel.

5.4.3 Effect of material on FCP behaviour

The effect of the material on FCP behaviour of the welds was determined by conducting FCP tests on the conventionally welded 2139 T351 panels and the base metal panel. The composition of this material differs from 6156 as given in Table 3.1. The FCP results of the conventionally welded 6156 T4 and 2139 T351 plain panels and respective base panels are shown in Figure 5.80. The comparison of FCP rates of the two welded 2139 T351 panels and a base metal show slight differences than what was obtained for 6156 T4 material, both naturally aged. The difference in FCP rates between the welded 2139 panels and the base panel within the clip is higher compared to that for 6156 panel. Although the thickness of the 2139 panels (3.2 mm) and 6156 panels (4.5 mm) are not identical, the applied maximum stresses are the same for both, which enables to make the comparison between these alloys.

The fatigue lives of welded panels of both materials are demonstrated in Figure 5.81, including base metal panels. 6156 welded panel with a fatigue life of about 230,000 cycles and base panel with 510,000 cycles posses slightly higher fatigue lives compared to 2139 panels, of which welded panels have around 120,000 to 180,000 and base panel has approximately 450,000 cycles. However, the reason cannot be explained by residual stress distributions of the materials (Figure 5.82), which exhibit close peak values. As it can be seen from Figure 5.71 representing da/dN vs. ΔK, the FCP behaviour of the 6156 T4 and 2139 T351 base panels follow the same trend and any abnormality leading to deviation from the linear Paris regime was also not observed.

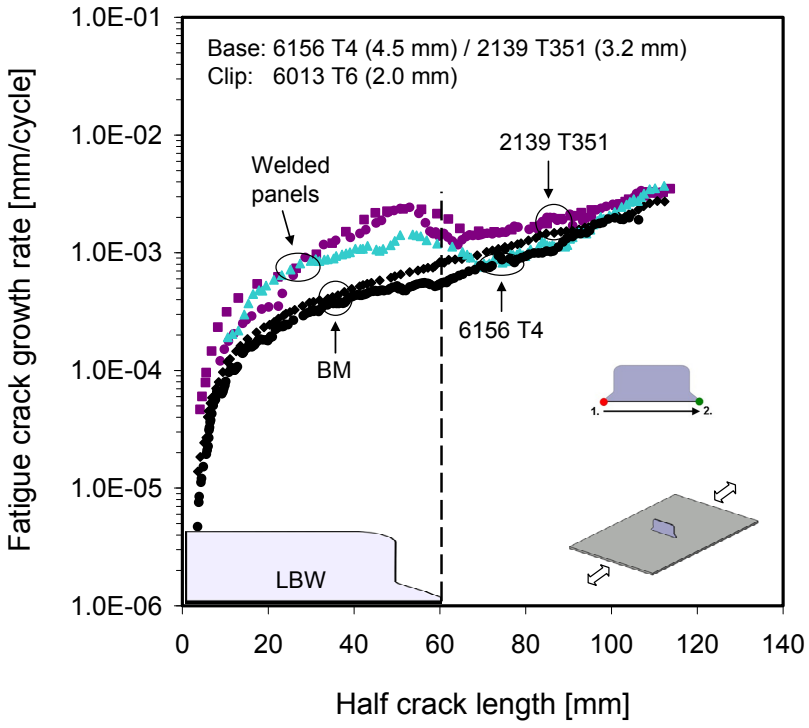

Figure 5.80: Fatigue crack growth rates plotted against half crack lengths of 2139 T351 and 6156 T4 plain base and welded panels. The welds were made with conventional procedure.

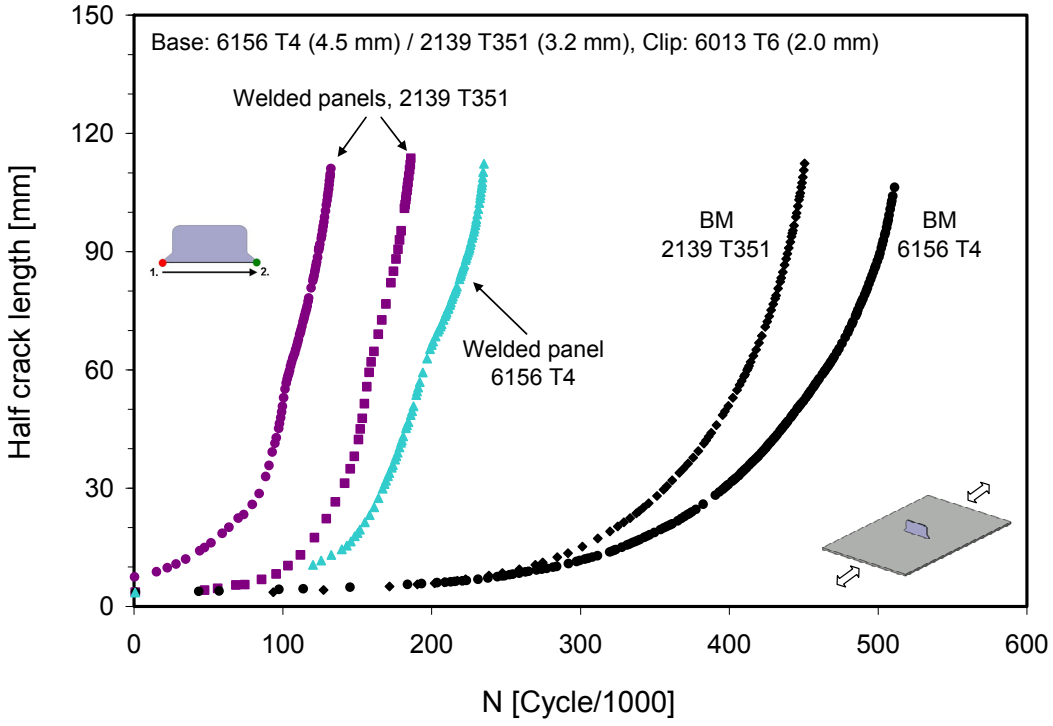

Figure 5.81: Comparison of the fatigue lives of the conventionally welded plain panels of 6156 T4 and 2139 T351 with respect to their base panels.

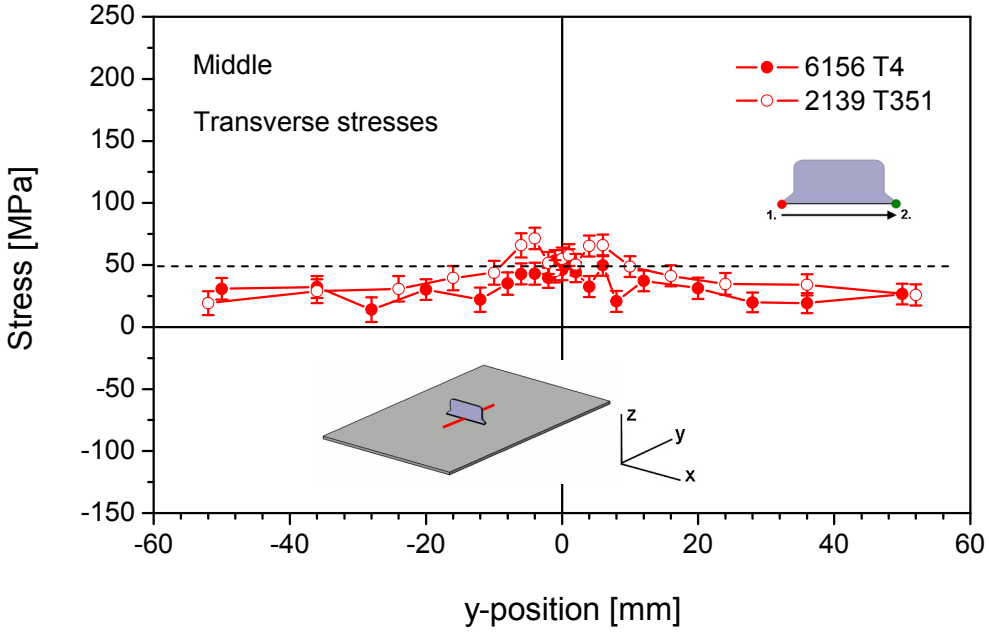

Figure 5.82: Transverse residual stress distributions at the mid-clip position of the conventionally welded plain panels; solid points show that for the 6156 T4 material and empty points show that for the 2139 T351 (both naturally aged).

5.4.4 Effect of pocketing on FCP behaviour

5.4.4.1 AA 6156 T6 base panel

Currently, it is general practise to introduce so-called “pockets” in to the skin areas (between stringers and clips) of the fuselage in order to reduce the weight of the structure. Moreover, the thicker socket area, where welded clip was placed, provides local strengthening to the welded locations, due to the strength undermatching nature of the weld joints, Figures 5.5 – 5.7. The effects of pocketing and the resulting redistribution of residual stresses on the FCP properties of the 6156 T6 clip welds were investigated, and results are presented in this section. The socket width of the pocketed panel is 11 mm in this case.

FCP rates of the welded pocketed panels should be compared to the pocketed base panels. For that reason, the pocketed base panel of 4.5 mm thick 6156 T6 material with 11 mm socket width was tested with a same applied stress value that was applied to the plain base panel having the same thickness.

Conventionally welded panels without and with pocketing were tested on 4.5 mm thick Al-alloy 6156 T6. Higher FCP rates of the welded panels with and without pockets can again be observed within the 60 mm compared to their respective base panels, see Figure 5.83. Reproducible da/dN vs. a curve for each welded pocketed panel was obtained. However, one of the welded plain panels has higher FCP rates in the weld area than that observed for the second welded plain panel.

Fatigue life curves of panels with and without pockets in comparison with their base panels are given in Figure 5.84. Since reduced thicknesses weren’t considered for the applied stress of the welded pocketed panels, the comparison of the fatigue lives between the plain and pocketed panel is not possible. That figure only reveals that lower fatigue life difference exists between the pocketed welded panels and pocketed base panel compared to the difference between the welded plain panel and its base metal panel. The residual stress distributions of the welded plain (solid symbols) and pocketed (empty symbols) panels, which are very similar and tensile for both welded panel geometries, Figure 5.85.

The deviation of crack paths from the weld seam, as the crack propagated further (Figure 5.99b), which is caused by the presence of stress riser effect of the pocket edges [148], explains the reason for close fatigue lives and FCP rates of the welded pocketed panels and pocketed base panel.

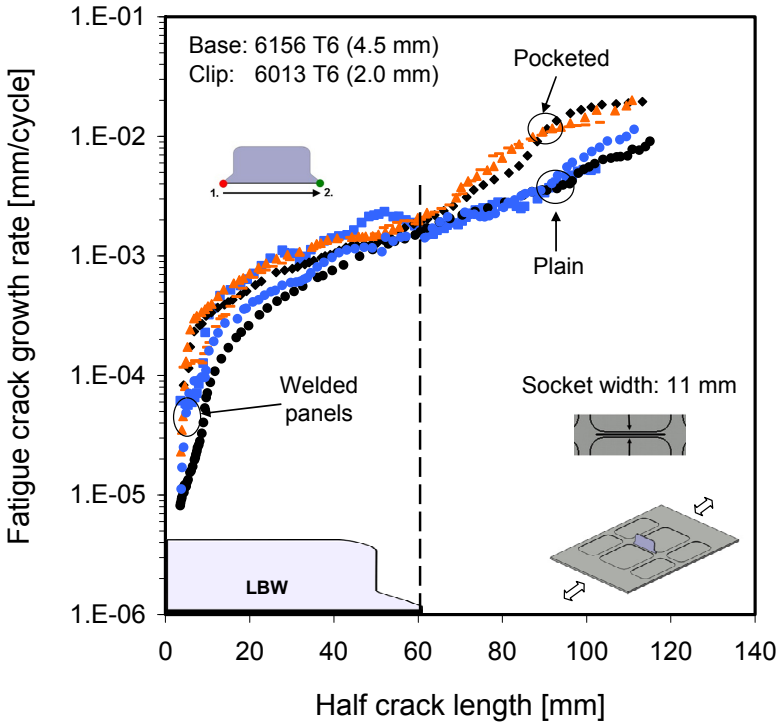

Figure 5.83: Fatigue crack growth rates plotted against half crack lengths of 6156 T6 plain base and welded panels and 6156 T6 pocketed base and welded panels with 11 mm socket width. The weld was made with conventional procedure.

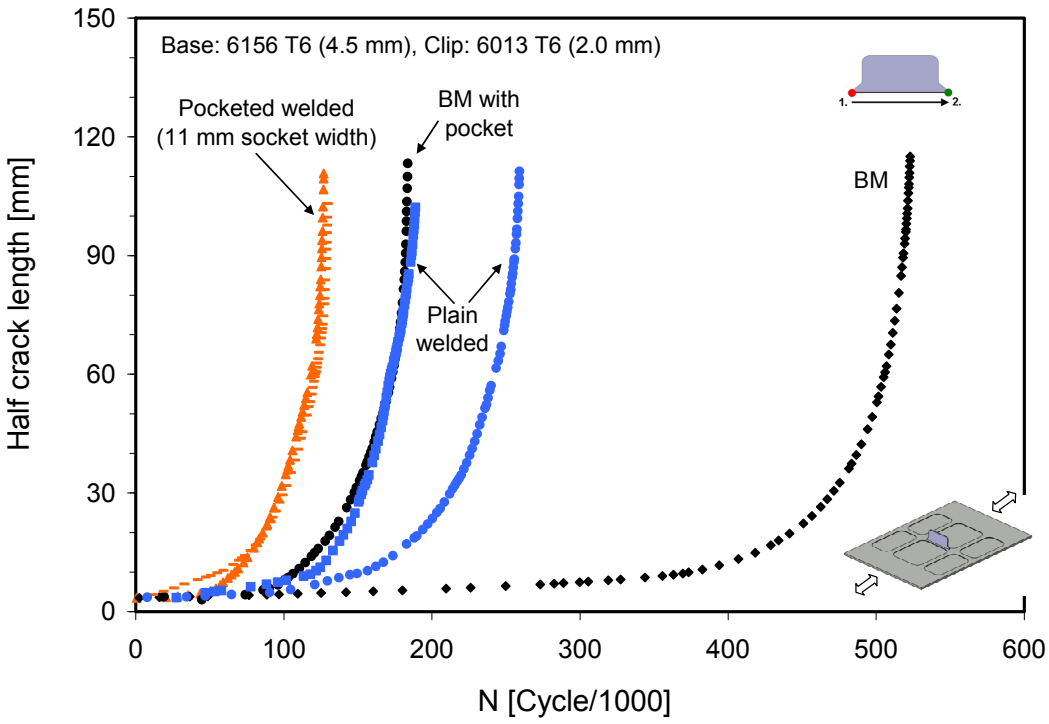

Figure 5.84: Comparison of the fatigue lives of the welded plain panel and pocketed panel with 11 mm of socket width (all welded conventionally) with respect to the plain and pocketed base panels.

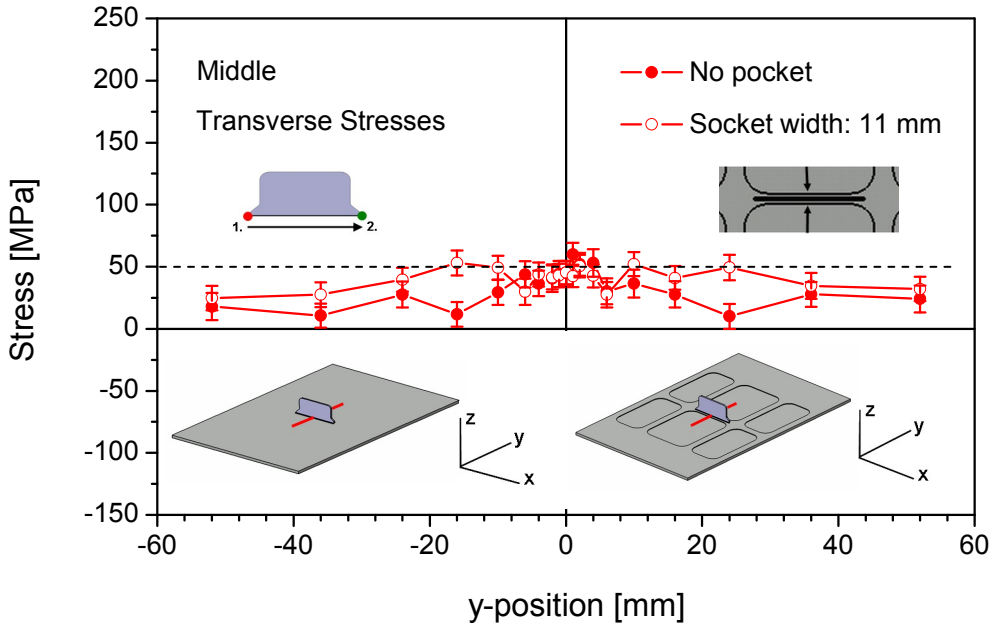

Figure 5.85: Transverse residual stress distributions at the mid-clip position of the conventionally welded 6156 T6 panels (4.5 mm); solid points show that for the plain panel and empty points show the results of the pocketed panel with 11 mm socket width.

5.4.4.2 AA 6156 T4 base panel

In Figure 5.86, comparison of the FCP rates of the plain and pocketed welded panels and plain and pocketed base panels of 6156 T4 material is given. 11 mm socket width was kept for the pocketed panel of this material.

Similar to 6156 T6 material, the FCP rates of the welded pocketed 6156 T4 material in the weld area are slightly faster than the pocketed base panel, however the welded plain panel exhibits more faster FCP rates than plain base panel. The fatigue lives of welded plain panel and even pocketed base panel remain in the scatter band of three welded pocketed panels (Figure 5.87). Residual stress values of the plain and pocketed panels of 6156 T4 are also very close to each other as can be seen from Figure 5.88.

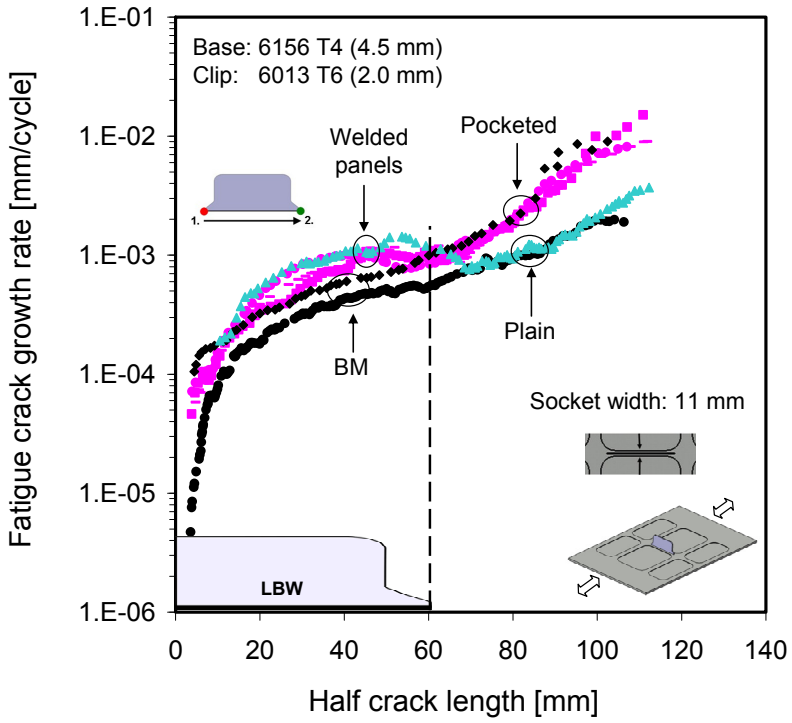

Figure 5.86: Fatigue crack growth rates plotted against half crack lengths of 6156 T4 plain base and welded panels and 6156 T4 pocketed base and welded panels with 11 mm socket width. The weld was made with conventional procedure.

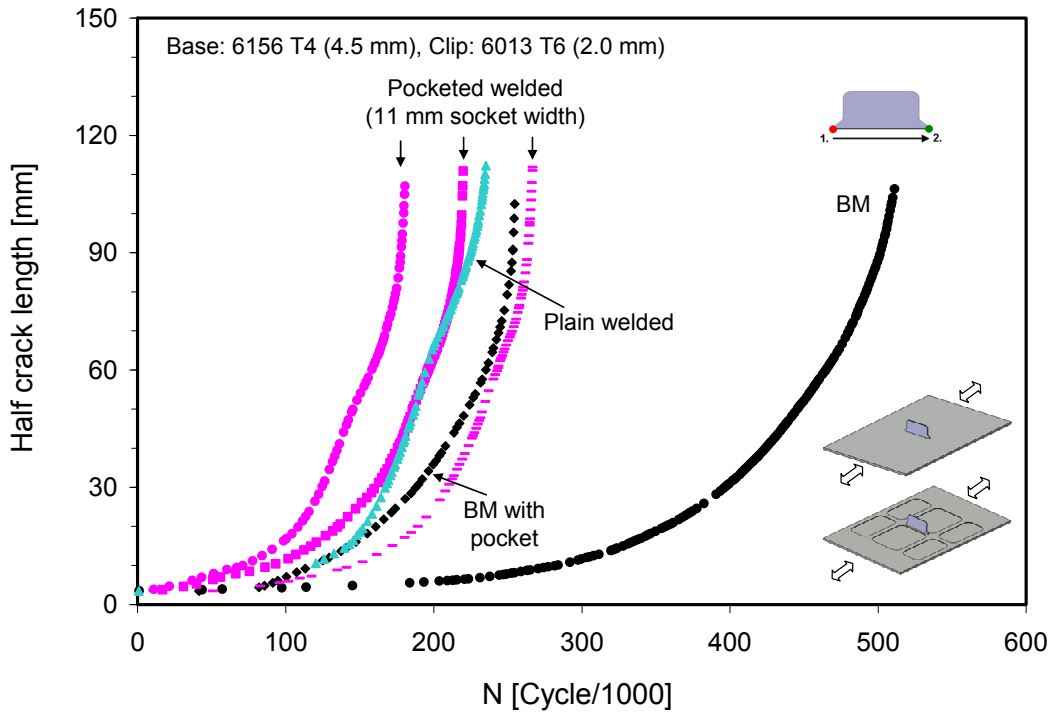

Figure 5.87: Comparison of the fatigue lives of the plain panel and pocketed panels with 11 mm socket width (all welded conventionally) with respect the plain and pocketed base panels.

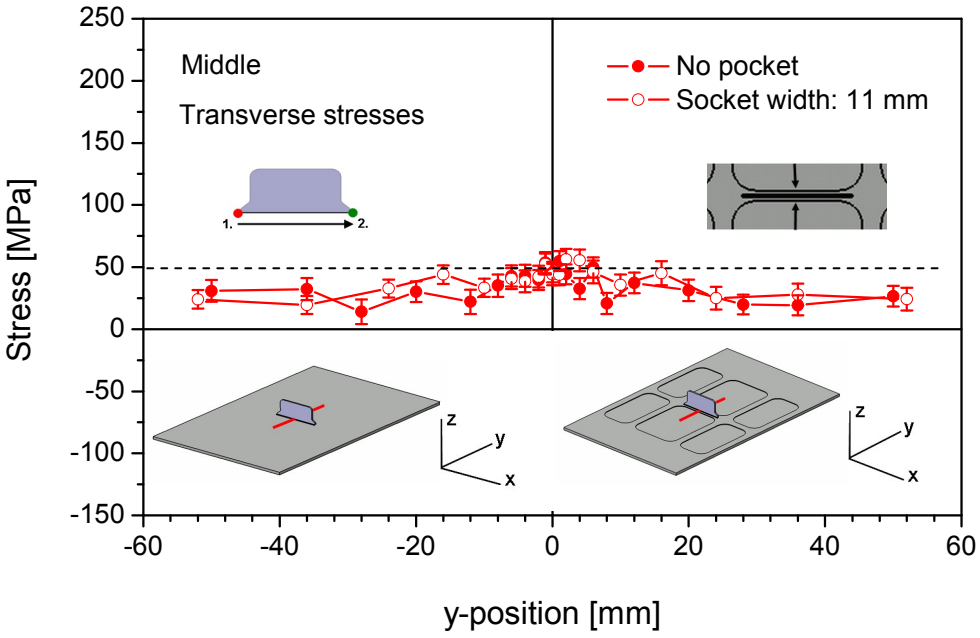

Figure 5.88: Transverse residual stress distributions at the mid-clip position of the conventionally welded 6156 T4 panels (4.5 mm); solid points show that for the plain panel and empty points show that for the pocketed panel with 11 mm socket width.

5.4.4.3 AA 2139 T351 base panel

Since the pocketing effect on the base panel was investigated for the 6156 T4 and T6 materials, FCP behaviour of the 2139 T351 pocketed base panel was not investigated. The FCP rates of the welded plain and pocketed panels were shown in Figure 5.89 compared with the plain base panel. As can be expected, the welded panels have higher FCP rates in the weld zone of the clip compared to the plain base panel.

Fatigue lives of three welded pocketed panels with 11 mm socket width remain in the range of lives of two welded plain panels, which were between 130,000 and 190,000 cycles, see Figure 5.90. There exist similar residual stress distributions of the welded plain and pocketed panels except for mid-location of the weld, which make the same contribution to the acting stresses (Figure 5.91).

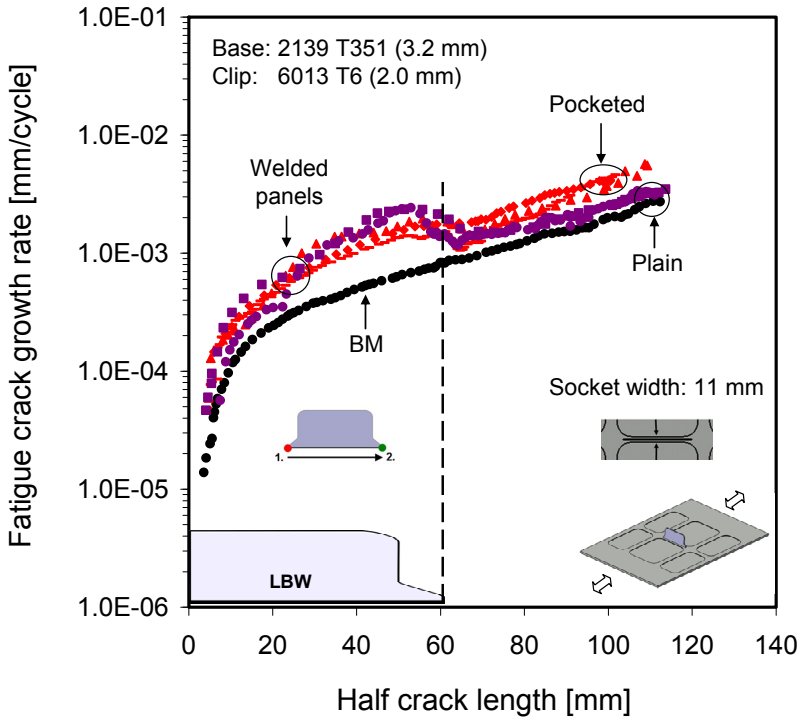

Figure 5.89: Fatigue crack growth rates plotted against half crack lengths of 2139 T351 plain base and welded panels and 2139 T351 pocketed base and welded panels with 11 mm socket width. The weld was made with conventional procedure.

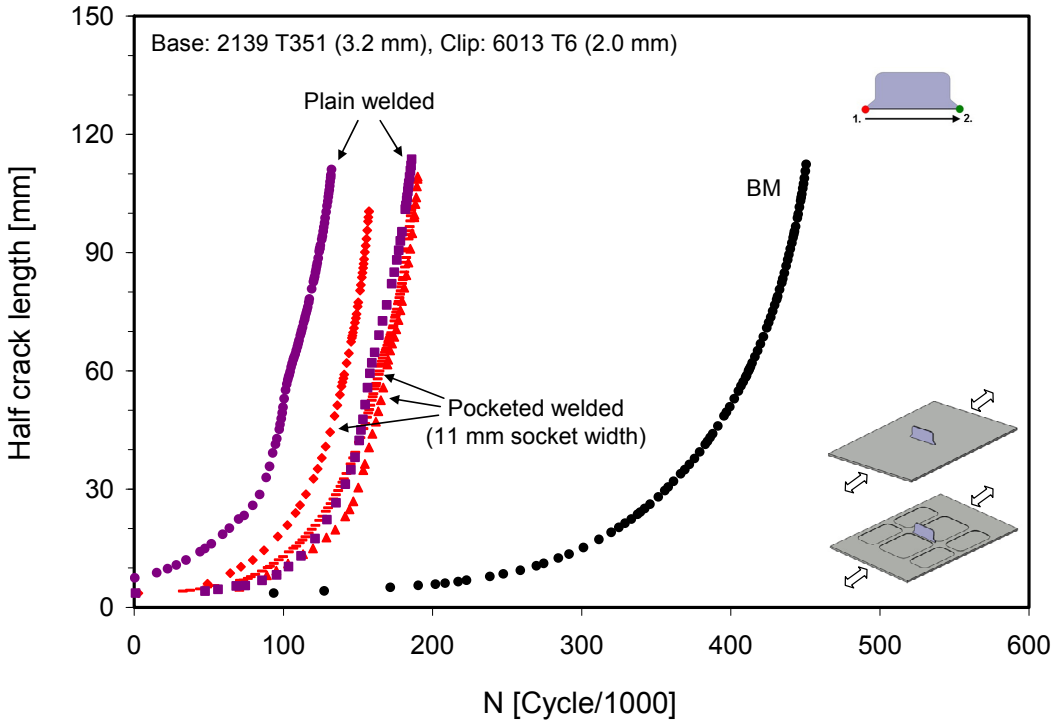

Figure 5.90: Comparison of the fatigue lives of the plain panels and pocketed panels with 11 mm socket width (all welded conventionally) with respect to the plain base panel.

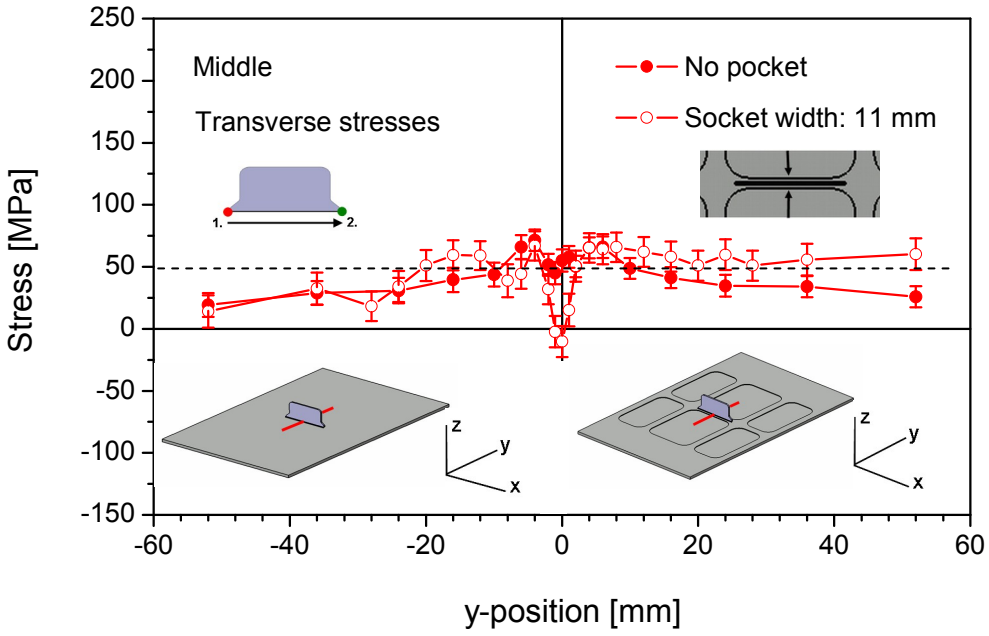

Figure 5.91: Transverse residual stress distributions at the mid-clip position of the conventionally welded 2139 T351 panels (3.2 mm); solid points show that for the plain panel and empty points show that for the pocketed panel with 11 mm socket width.

5.4.5 Effect of socket width on FCP behaviour

Socket width refers to the distance between the edge of the pockets (machined area), the region where the clip located. Since machining can cause redistribution of residual stresses, socket width variation can result in different residual stress state at the vicinity of the clip of the welded panel. Moreover, the socket width may affect the path of the propagated crack, by means of the degree of deviation from the clip weld seam. In order to investigate socket width effect on the FCP state, to find optimum design (with respect to both FCP rate and crack path deviation), two different socket widths were used for the pocketed panels, 11 mm and 20 mm.

5.4.5.1 AA6156 T4 base panel

The FCP results of the pocketed base panels of 4.5 mm thick 6156 T4 material with 11 mm and 20 mm socket width are demonstrated in Figure 5.92. Crack growth rates of both pocketed panels with different socket widths are very close to each other after half crack length reached to 10 mm. In the first 10 mm, FCP rate of the pocketed base panel with 11 mm socket width is somewhat higher compared to that of the pocketed base panel with 20 mm socket width. This leads to slightly lower fatigue life of the previous (250,000 cycles) with respect to the last (290,000 cycles) (Figure 5.93).

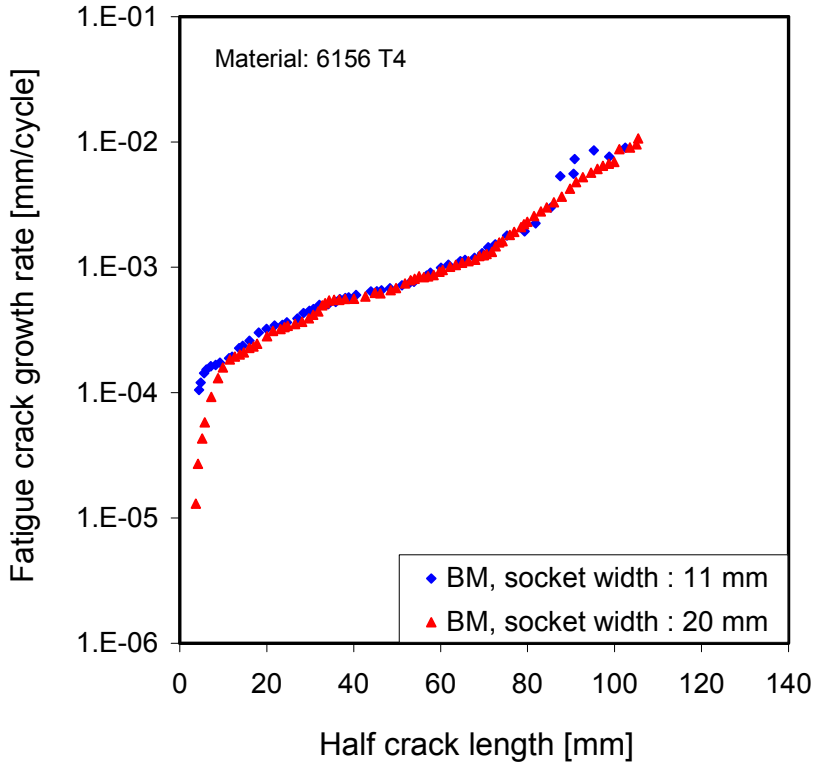

Figure 5.92: Comparison of the fatigue crack growth rates plotted against half crack lengths of pocketed base panels with 11 mm and 20 mm socket widths (both without welding).

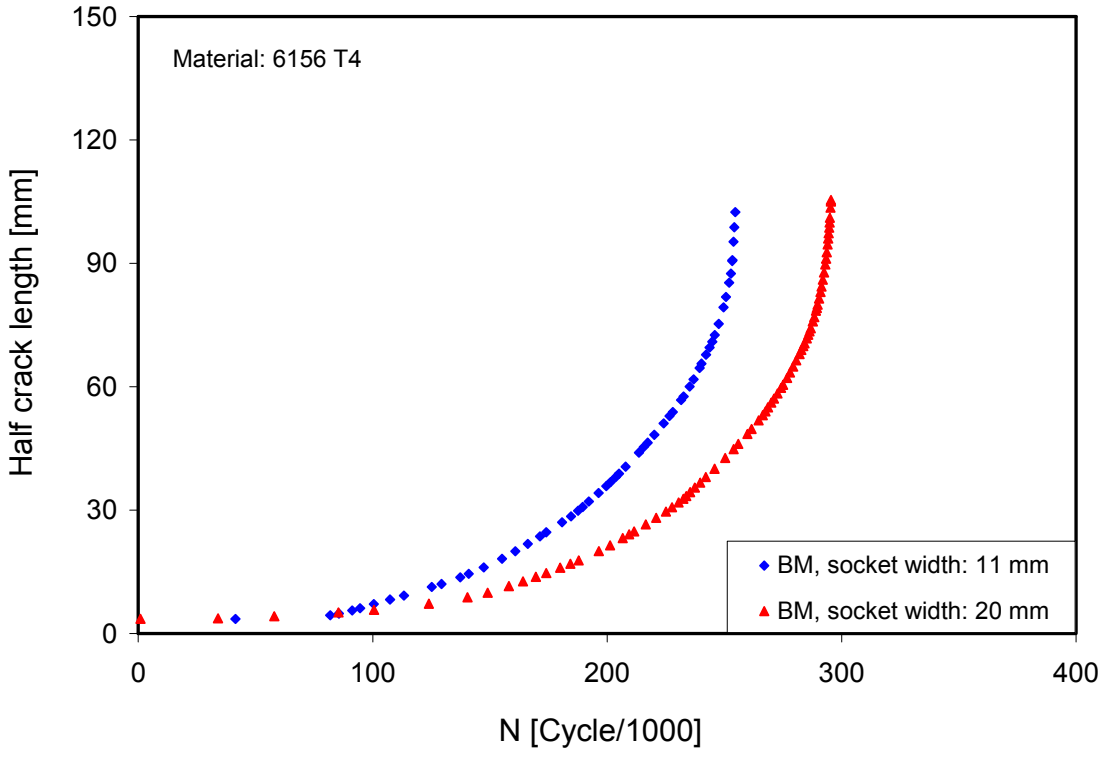

Figure 5.93: Comparison of the fatigue lives of 6156 T4 pocketed base panels with 11 mm and 20 mm socket widths (both without welding).

Crack growth rates of the conventionally welded 6156 T4 panels with socket widths of 11 mm and 20 mm are presented in Figure 5.94. Whereas, the FCP rates were similar up to clip ends for corresponded welded panels, panels with 20 mm of socket width exhibit more crack retardation compared to the panel with 11 mm of socket width. Earlier crack path deviation, which also occurred to a greater degree were observed in the welded panel with narrower socket. The crack is growing in the base metal and there is slight retardation as the crack approaches the location of clip end. This also explains the higher fatigue life of one of the welded panels with a narrower socket width (Figure 5.95). However, the reverse is true for the base panels with a pocket, meaning fatigue life of the panel with wider socket width is higher due to the much thicker area around the crack. Figure 5.96 indicates very similar transverse residual stress distributions for the welded panels with 11 and 20 mm socket widths.

Obviously, wider socket width of 20 mm provides more effective "shielding" by evolution of favourable stress distribution at the vicinity of the clip weld. Both panel results (with and without clip) with 20 mm socket width indicate that these panels exhibit slightly better FCP performance than 11 mm socket width. It should however be noted that narrower socket width could provide easier crack path deviation into the base metal and hence can improve FCP performance of the welded clip system. The balance between these two aspects could further be optimised by FE analysis.

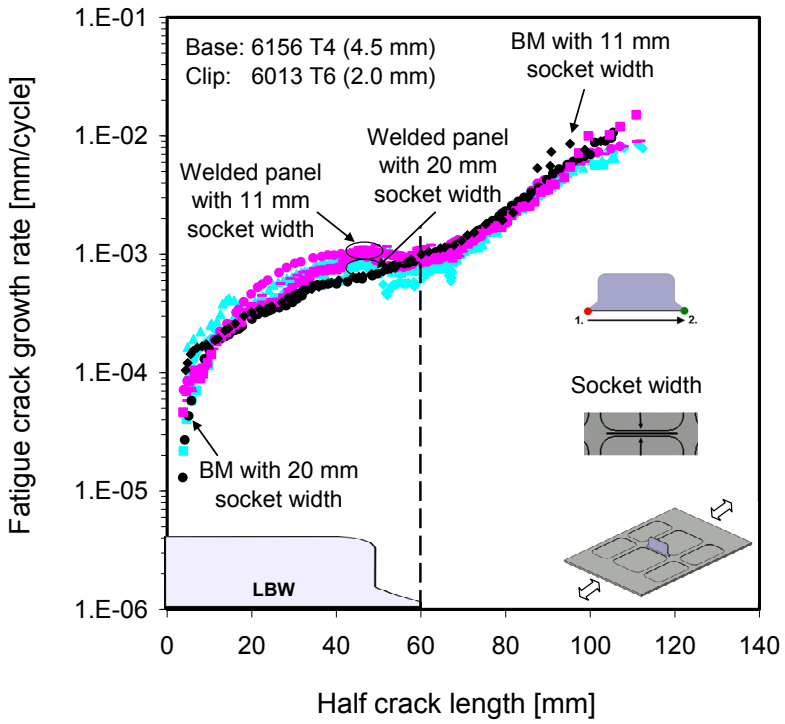

Figure 5.94: Fatigue crack growth rates plotted against half crack lengths of the 6156 T4 pocketed base and conventionally welded panels with both 11 mm and 20 mm socket widths.

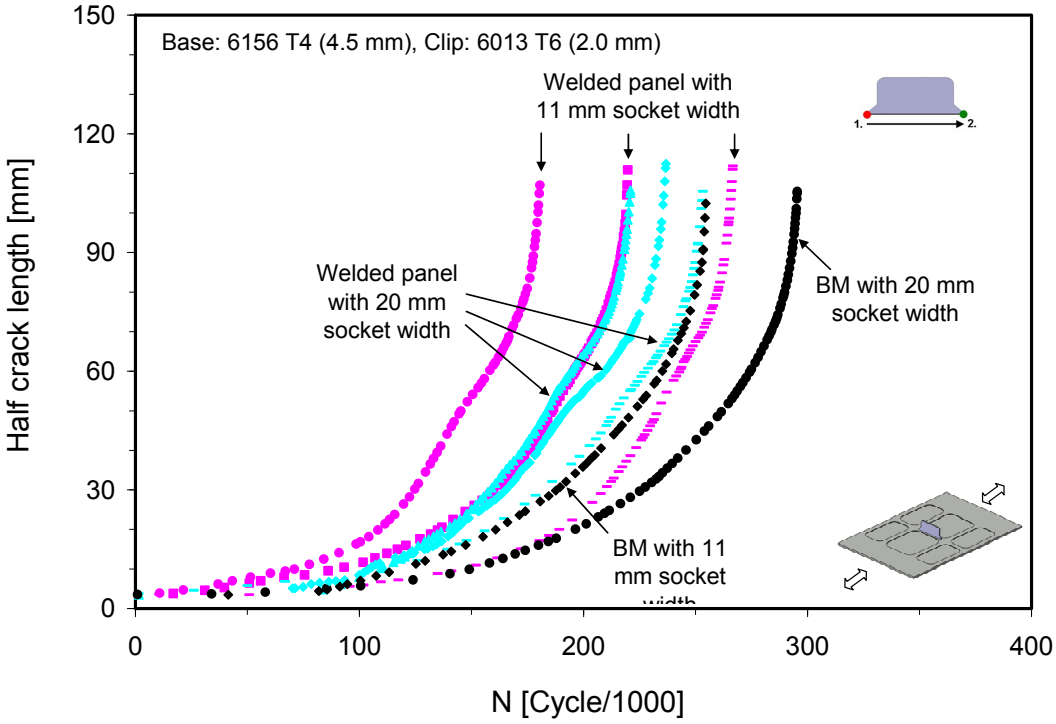

Figure 5.95: Comparison of the fatigue lives of the conventionally welded pocketed panels with 11 mm and 20 mm socket widths with respect to the pocketed base panels with 11 mm and 20 mm socket widths.

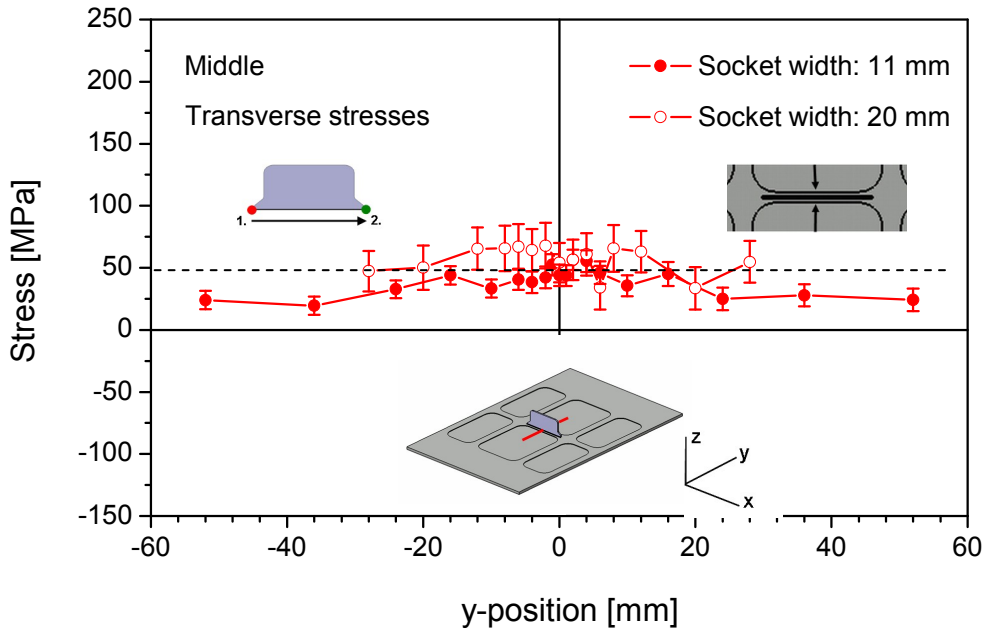

Figure 5.96: Transverse residual stress distributions at the mid-clip position of the conventionally welded 6156 T4 panels (4.5 mm); solid points show that for the pocketed panel with 11 mm of socket width and empty points show that for the pocketed panel with 20 mm of socket width.

5.4.5.2 AA 2139 T351 base panel

The FCP behaviour of the welded pocketed panel of 2139 T 351 material with 20 mm socket width (Figure 5.97) is similar to that for the welded pocketed panel with 11 mm, which also have close fatigue lives (Figure 5.98).

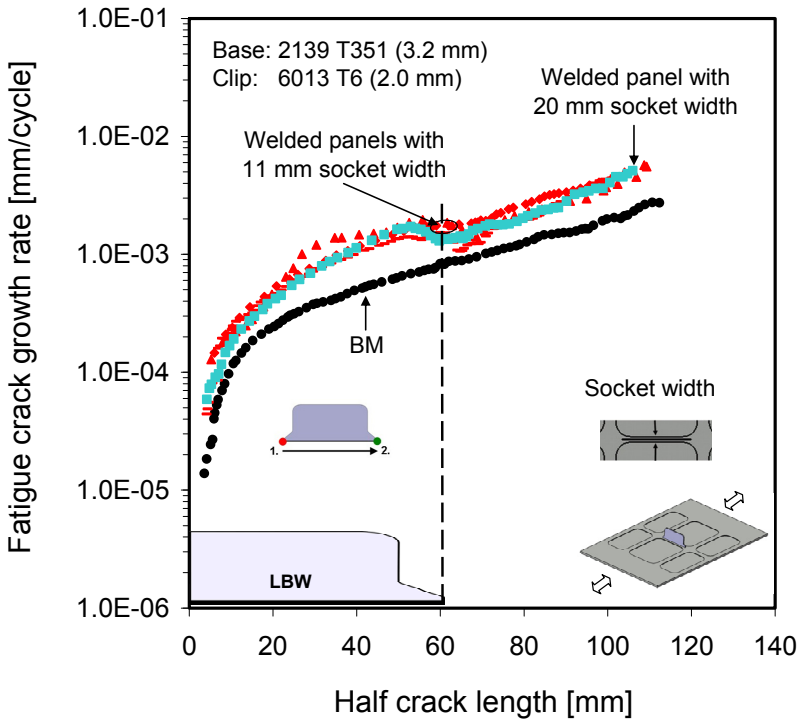

Figure 5.97: Fatigue crack growth rates plotted against half crack lengths of the 2139 T351 plain base panel and conventionally welded pocketed panels with 11 mm and 20 mm socket widths.

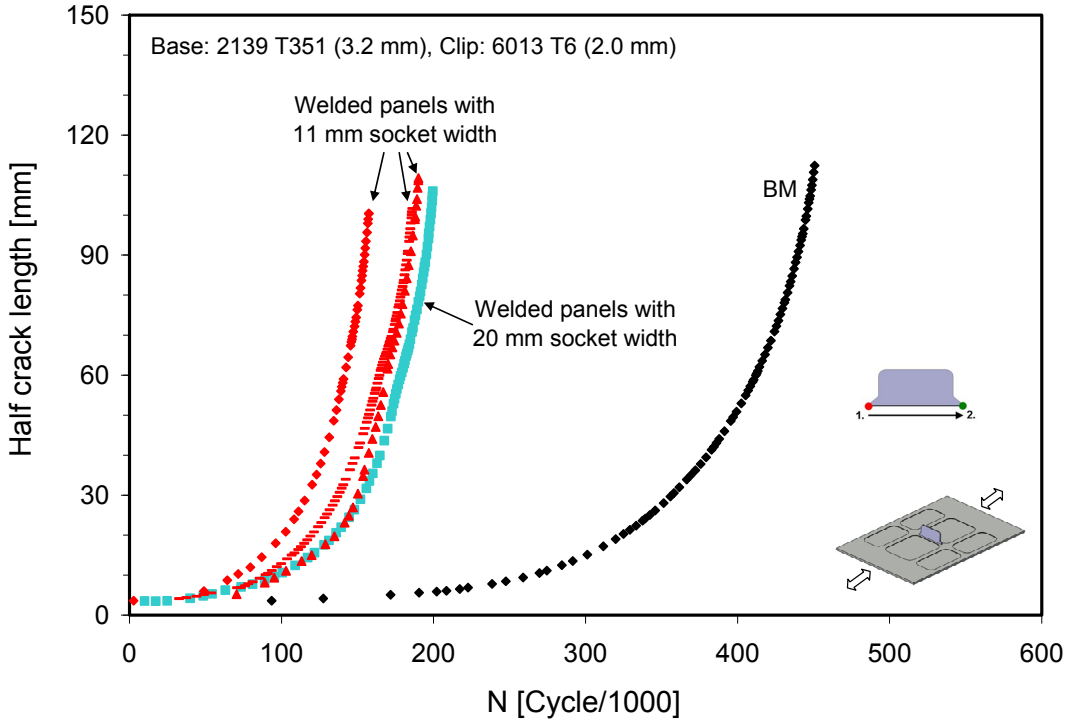

Figure 5.98: Comparison of the fatigue lives of the conventionally welded pocketed panels with 11 mm and 20 mm socket widths with respect to the plain base panel.

5.4.6 Crack propagation path

Crack propagation path observations in the weld vicinity have been made to compare the panels and panel geometry. Generally, crack path deviation occurred in pocketed panels with both socket widths (towards the thinner skin area, see Figures 5.99b and 5.99c), whereas the crack path followed the weld toe in plain panels (Figure 5.99a). The crack locations on tested panels were examined by conducting post-test-sectioning, and Figure 5.101a shows the crack location when the crack propagates through the mid-clip area of the pocketed panel with 20 mm socket width. The crack path deviation into the base metal, towards the clip end is shown in Figure 5.101b, although a rather unfavourable weld root causes high stress concentration.

The presence of geometrical variations and hence local stress distribution will eventually affect the crack path. Therefore, the panels were carefully examined with respect to crack path developments. Only three examples are shown to make generalized statements with respect to plain and pocketed panel comparison.

a)

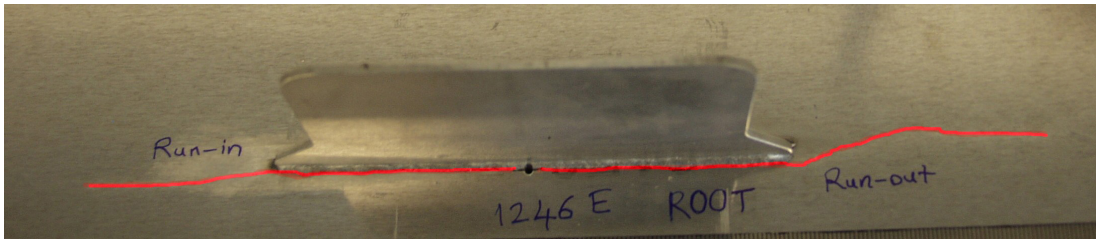

b)

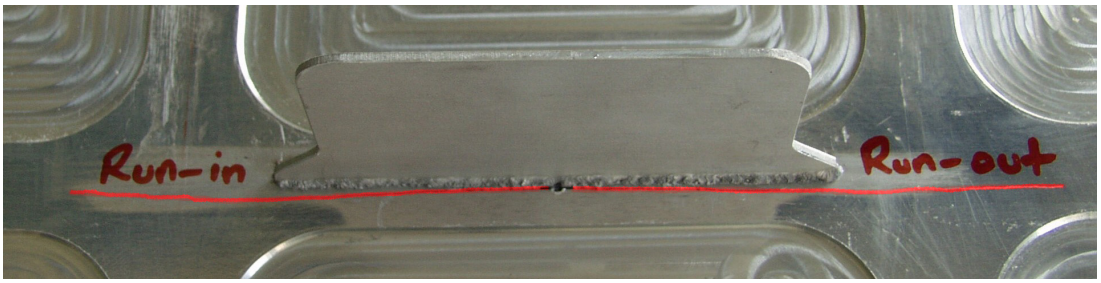

c)

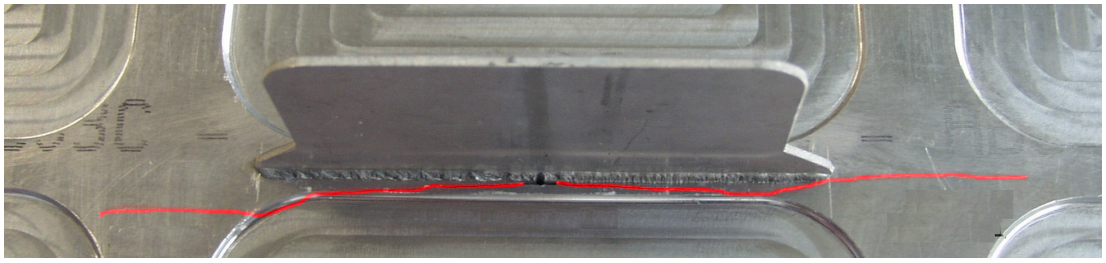

Figure 5.99: Crack propagation paths of a a) 6156 T4 plain panel, b) 6156 T4 pocketed panel with 11 mm socket width, c) 6156 T4 pocketed panel with 20 mm socket width.

a)

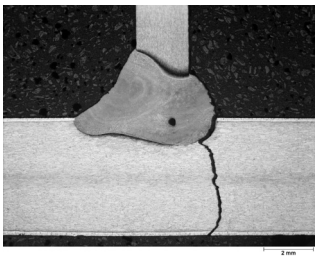

b)

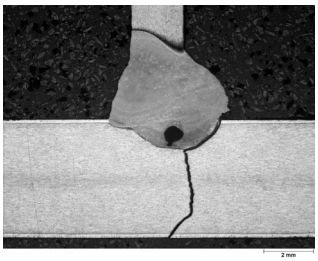

Figure 5.100: Macro-sections for the crack propagation paths in a 6156 T4 plain panel; a) at 7.5 mm away from mid-clip position b) about 7.5 mm distance towards to the clip end.

a)

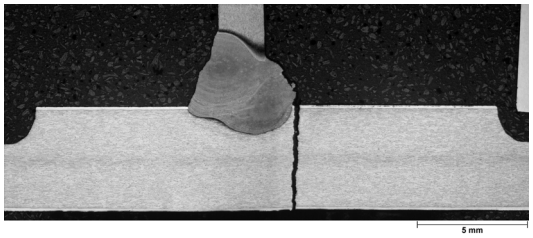

b)

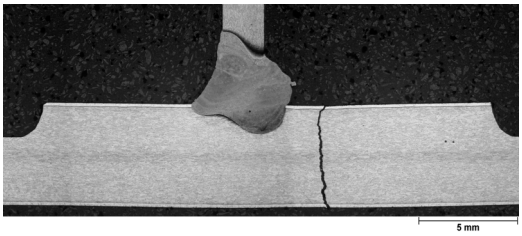

Figure 5.101: Macro-sections for the crack propagation paths in a 6156 T4 pocketed panel with 20 mm socket width (shown in Figure 5.99c), a) at 7.5 mm away from mid-clip position b) about 7.5 mm distance towards to the clip end.

5.4.7 Effect of welding type on FCP behaviour

5.4.7.1 Comparison between conventional and two run-out welds

FCP results are presented in terms of da/dN vs. crack length as well as in terms of crack length vs. cycles to demonstrate the effect of welding types on the FCP adjacent to the clip welds made on two Al-alloys.

5.4.7.1.1 AA 6156 T6 Material

FCP results of 4.5 mm thick 6156 T6 plain panels welded conventionally and having a welded clip with two run-outs (Figure 3.4b) and the plain base panel are given in Figure 5.102. The FCP rates of the weld seams of the welded clips are higher than the base panel for both type of welded panels, however the initial propagation part of the crack in the welded panel with two run-outs was slower than the conventionally welded panel. Fatigue lives of the corresponding welded panels with both welding types and base panel are given in Figure 5.103, again confirming the longer fatigue lives of the welded panels with two-run-outs than the conventionally welded panels. Furthermore, one of the welded panels with two run-outs has even slightly better fatigue life compared to the base panel. These results reveal that different constraint conditions develop during the welding of the clips, contributing to the evolution of different residual stress distributions. This leads to different fatigue crack propagation behaviours, since residual stresses are strongly affecting the acting crack tip stresses. It is prooved that residual stresses redistribute as crack grows with a decreasing peak value [44]. In this study, it is shown that the geometry effect on crack propagation behaviour of the welded panels was negligible (Figure 5.75 and 5.76). It can be seen from half crack length vs. cycle graphics (Figures 5.103, 5.106, 5.109 and 5.112) that as the half crack length reaches to about 10 mm slopes of the curves of the welded panels become rather equal. From these three findings it can be concluded that, the residual stresses either relieve or the increasing stress intensity of the growing crack dominates as crack length reaches to some extent.

The effectiveness of the two run-outs welding procedure for the clip welding is now confirmed for 4.5 mm 6156 Al-alloys. The next step of the investigations to confirm these results by investigating the residual stresses of these welds will be discussed below.

Figure 5.104 shows transverse residual stresses (σ_y) of the 4.5 mm thick Al-alloy 6156 T6. The conventionally welded clip, of which residual stress distribution are shown as solid symbols, revealed that residual stress components are tensile, whereas the welded panel with a clip having two run-outs, of which residual stress distribution are indicated by empty symbols showed compressive transverse residual stresses. The better fatigue performance (Figure 5.103) of the welded panels with a clip having two-run-outs are obviously due to the presence of compressive transverse residual stresses in the vicinity of the weld seam (on-going area). This is an important finding for development of damage tolerant welded clips.

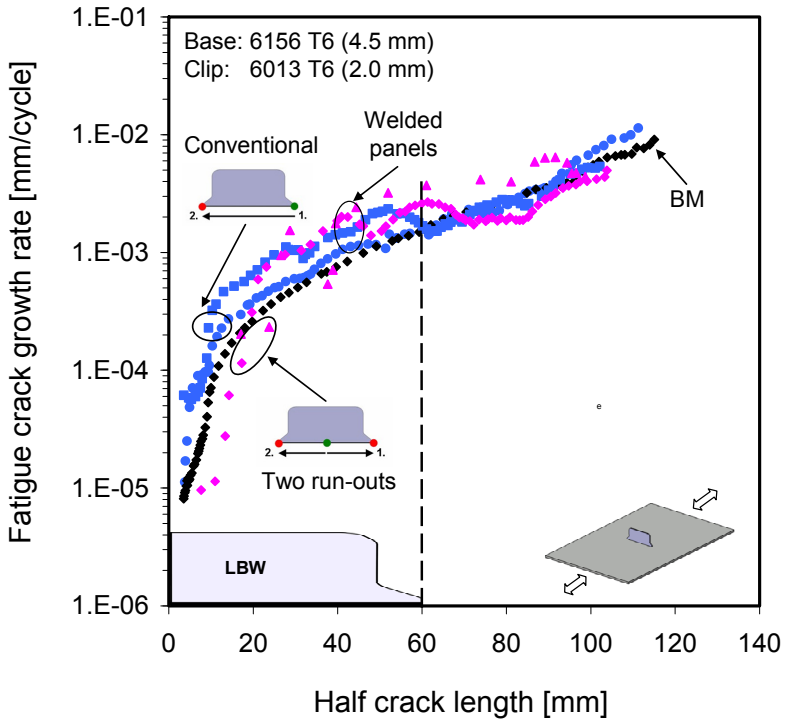

Figure 5.102: Fatigue crack growth rates plotted against half crack lengths of the plain base panel, conventionally welded panels and welded panels containing two run-outs.

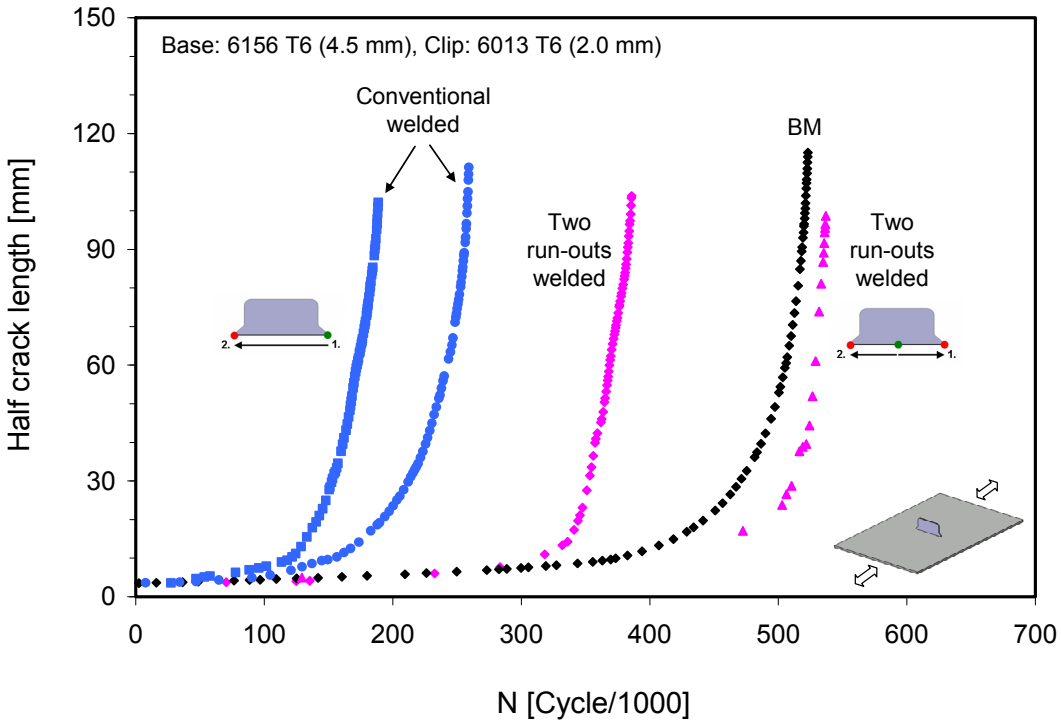

Figure 5.103: Comparison of fatigue lives of the plain base panel, conventionally welded panels and welded panels with two run-outs.

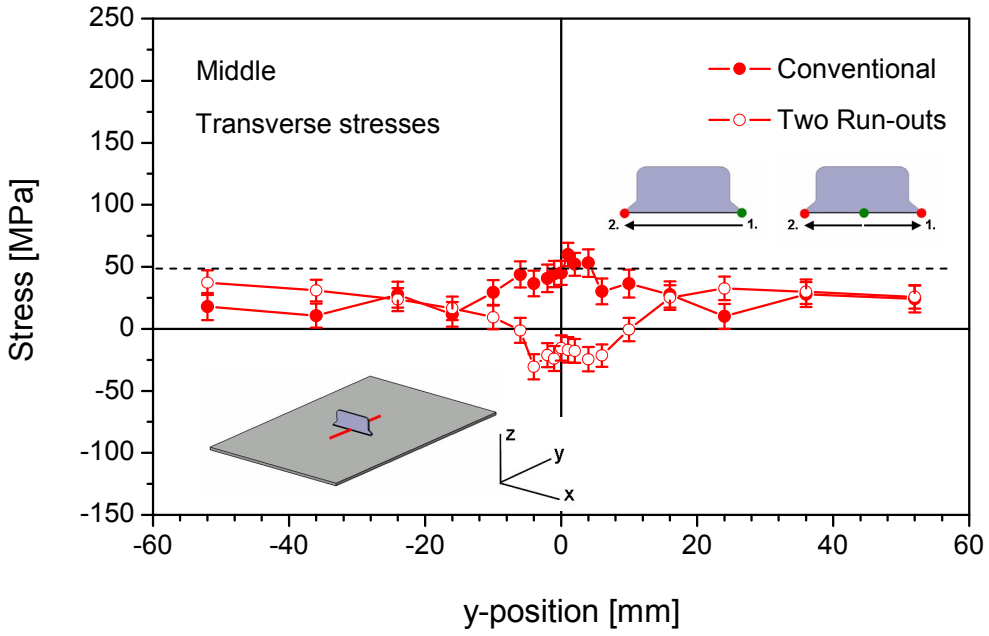

Figure 5.104: Transverse residual stress distributions at the mid-clip position of the welded plain panels of 6156 T6 material (4.5 mm); solid points show that for the conventionally welded panel and empty points show that for the welded panel containing two run-outs.

The welded pocketed panel with two run-outs (with 11 mm socket width) exhibits lower FCP rates until crack reaches to the clip ends, then it shows higher rates compared to the pocketed base panel, see Figure 5.105. This wasn't observed for the conventionally welded pocketed panel (Figure 5.105). The fatigue lives of the discussed panels, pocketed base panel, conventionally welded pocketed panels and also two other welded pocketed panels with two run-outs are plotted in Figure 5.106. The fatigue life of the welded pocketed panel with two run-outs is also more than three fold of the pocketed base panel and almost four fold of the conventionally welded pocketed panels. This behaviour is due to the presence of the compressive transverse stresses of the welded pocketed panel with clip containing two run-outs (see Figure 5.107).

As discussed above, the FCP performance of the welded clip panels with two run-outs clearly show the significant effect of the transverse residual stresses at the clip weld area. Furthermore, selection of the welding procedure, as demonstrated, produce favourable residual stresses which could provide improved damage tolerance performance of the welded clip system.

These results are obviously very promising to show the possibility of "residual stress control" and hence fabricate "inherently better" welded clip-skin components for future airframes.

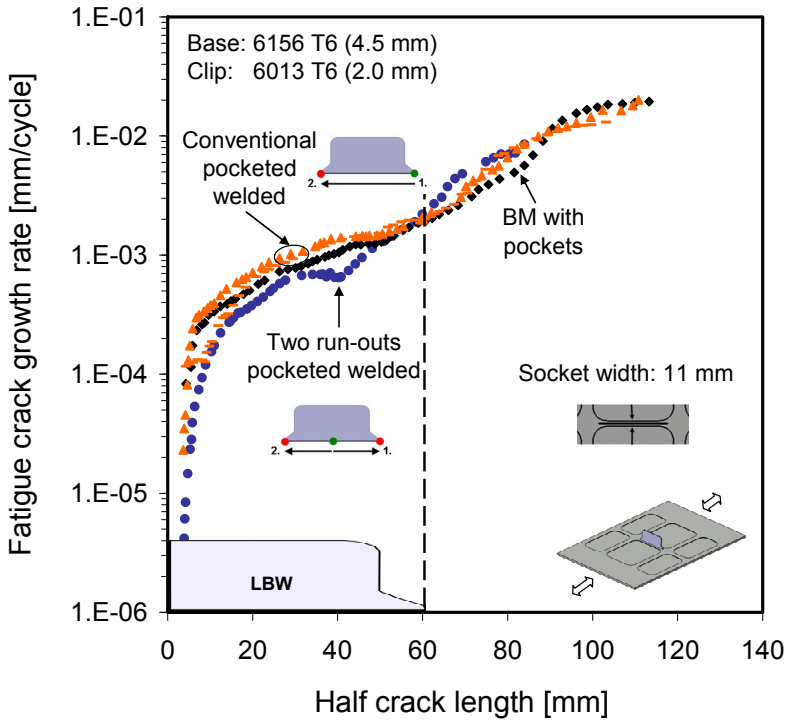

Figure 5.105: Fatigue crack growth rates plotted against half crack lengths of the pocketed base panel, conventionally welded pocketed panels and welded pocketed panel containing two run-outs. Socket widths for all are 11 mm.

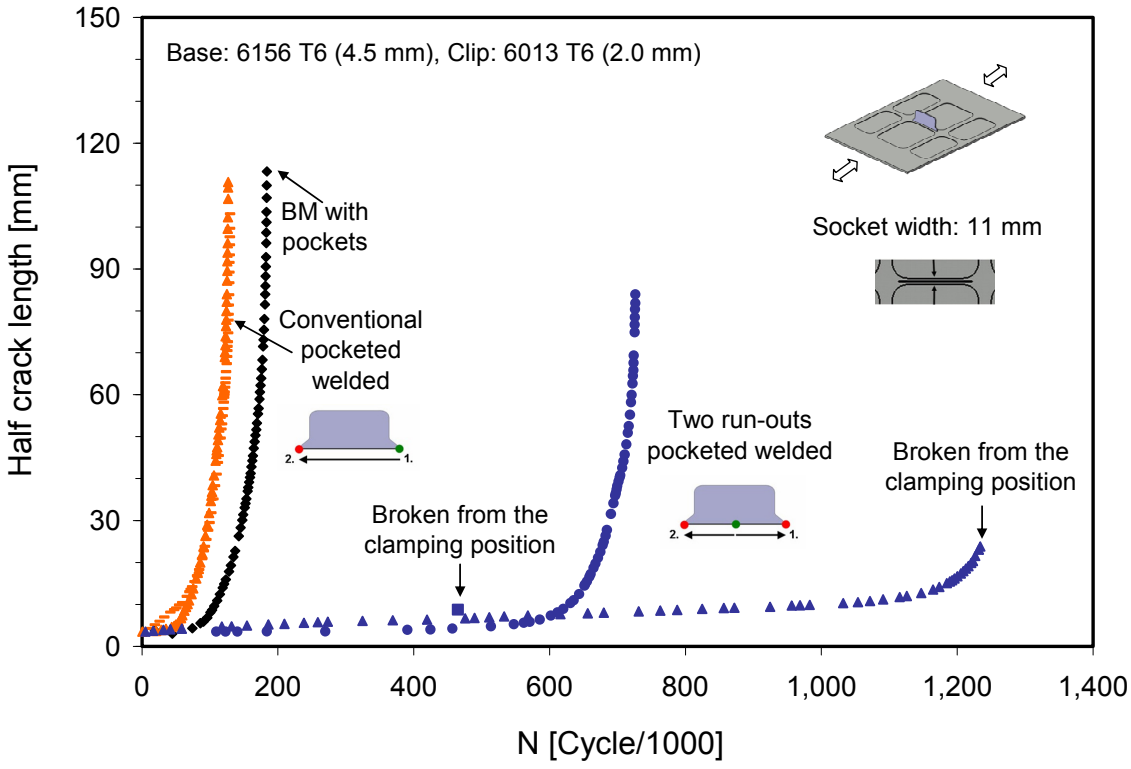

Figure 5.106: Comparison of fatigue lives of the pocketed base panel, conventionally welded panels and welded panels with two run-outs. Socket widths for all are 11 mm.

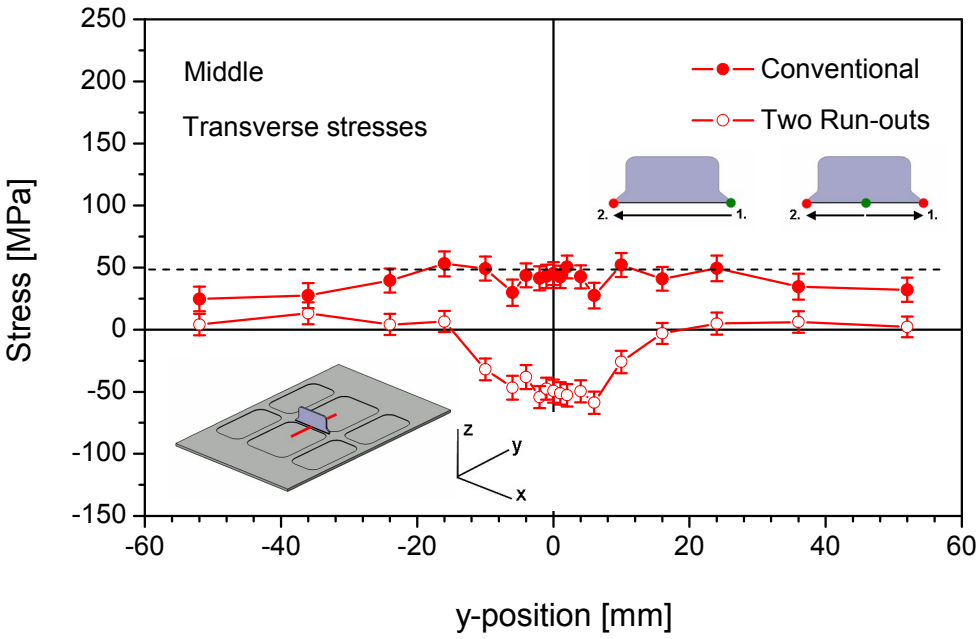

Figure 5.107: Transverse residual stress distributions at the mid-clip position of the welded pocketed panels of 6156 T6 material (4.5 mm) with 11 mm of socket width; solid points show that for the conventionally welded panel and empty points show that for the welded panel containing two run-outs.

5.4.7.2 Comparison between conventional and two run-in welds

The results of FCP tests of 4.5 mm thick 6156 T6 panels welded conventionally and having a welded clip with two run-ins (Figure 3.4c) and the base metal panel are shown in Figure 5.108. Similar to conventionally welded panels, welded clip panel with two run-ins exhibits a higher FCP rate than plain base metal panel. Again, a sudden drop in FCP rate was observed for the weld configuration with two run-ins when the crack tip approaches the clip ends which correspond to run-ins and they exhibit compressive transverse residual stresses. This drop could be associated with the presence of compressive residual stresses. In fact, it was expected that run-in and run-out locations (clip end locations) would have a negative effect on the FCP behaviour since these locations exhibit high stress concentration and poorer weld qualities than the on-going areas of the clip welds. However, the results obtained from 6156 T6 Al-alloy welded in three different welding procedures did not show any negative effect of the clip-ends on the FCP rates. On the contrary, drops of FCP rates at the vicinity of the run-in type of clip ends were observed. If the clip ends contain run-outs, a drop in the FCP rates was not specifically observed as shown in Figures 5.102 and 5.105. Therefore, it is appropriate to interpret the drop at the end of clips due to compressive transverse residual stresses present at those regions.

Fatigue life curves (a vs. N) of conventionally welded and welded clip panel with two run-ins are compared in Figure 5.109 and show that the panel with clip weld with two run-ins exhibits the shortest fatigue life, even less than the conventionally welded clip panel. Figure 5.110 shows the residual stress results obtained for the conventionally welded panel (solid symbols) and panel with a clip having two-run-ins (empty symbols). Higher transverse residual stresses (σ_y) were measured in two run-ins clip panel, this, in turn, strongly deteriorated the FCP performance of the panel, as shown in Figure 5.109. It is obvious that

transverse residual stresses are the main stress component which acts in addition to the applied stresses for the crack configuration investigated in this study. Hence, the highest tensile transverse stresses evolved during the laser welding of clips with two run-ins (welding starting at the clip ends and ending at the mid-clip location), and this configuration exhibited the shortest fatigue life due to the high tensile transverse residual stresses developed at mid-part of the clip weld. The superimposition of run-outs on both half of the clip welds results highest measured transverse tensile residual stresses at the mid-clip location (Figure 5.110) which leads to shortest fatigue life as shown in Figure 5.109.

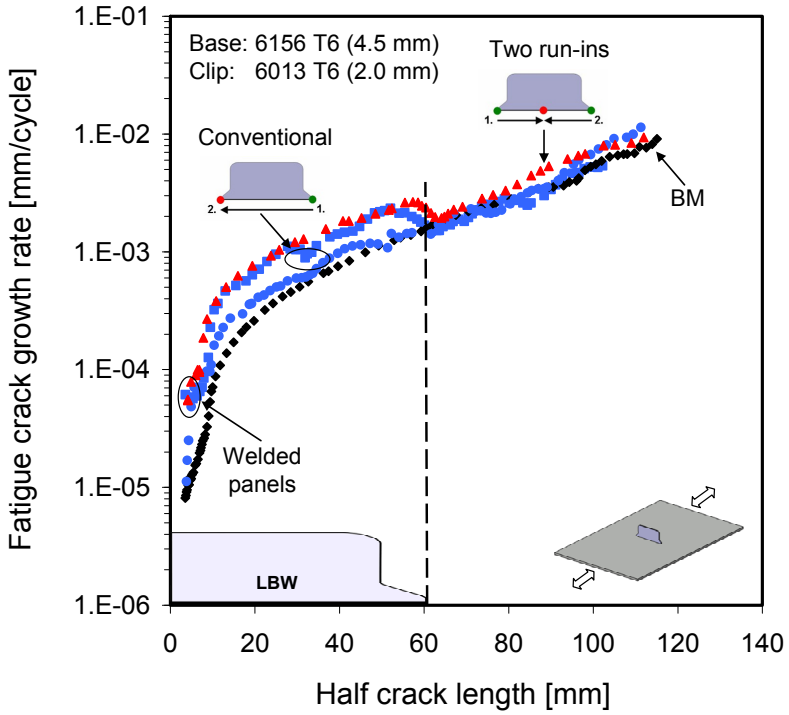

Figure 5.108: Fatigue crack growth rates plotted against half crack lengths of the plain base panel, conventionally welded panels and welded panel containing two run-ins.

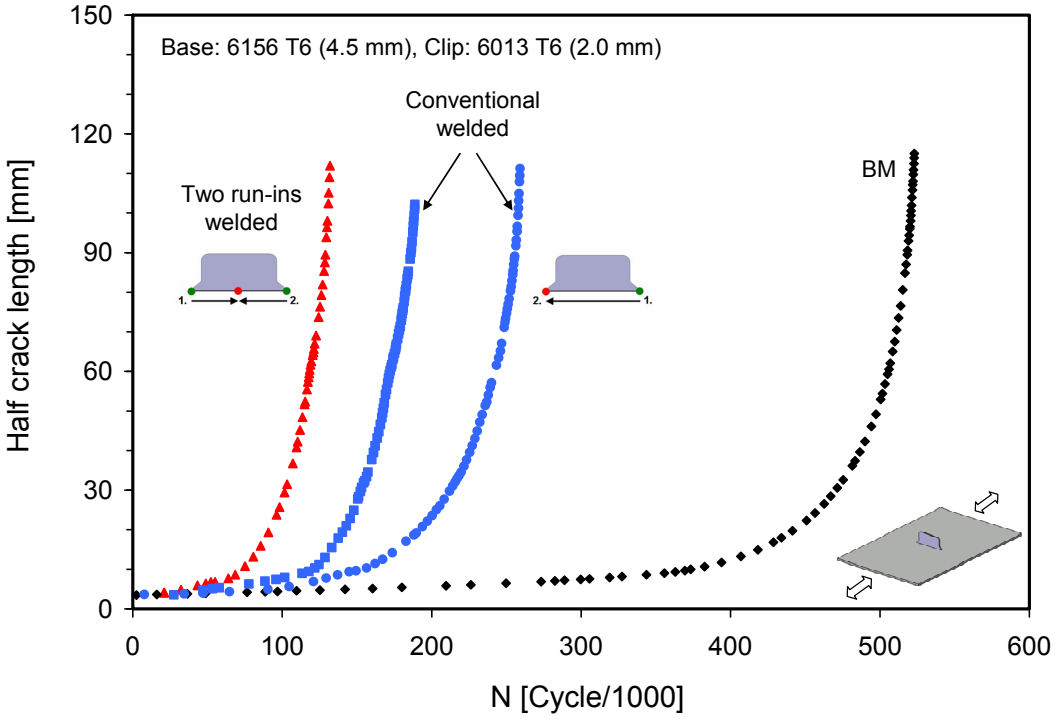

Figure 5.109: Comparison of fatigue lives of the plain base panel, conventionally welded panels and welded panel with two run-ins.

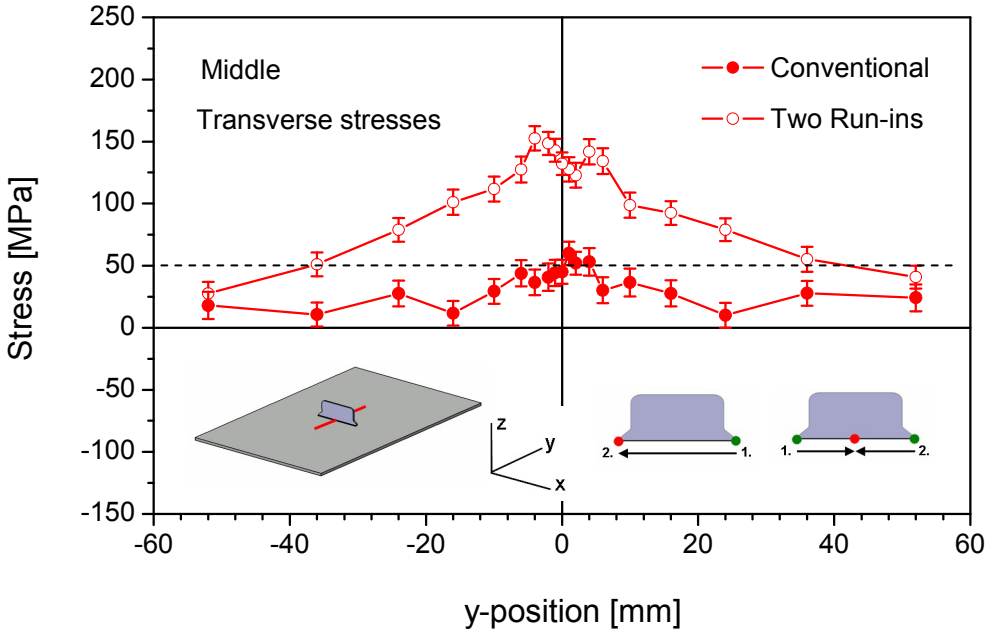

Figure 5.110: Transverse residual stress distributions at the mid-clip position of the welded plain panels of 6156 T6 material (4.5 mm); solid points show that for the conventionally welded panel and empty points show that for the welded panel containing two run-ins.

In addition to the plain panels discussed above, three pocketed clip panels with two run-ins (with 11 mm socket width) were tested. FCP results of the conventionally welded pocketed panels and welded pocketed panels with two run-ins with respect to the pocketed base metal panel are illustrated in Figure 5.111. The welded panels with two run-ins show slightly higher FCP rates compared to the base panel. As crack propagated through the clip ends sudden drop of propagation rates were observed due to the presence of the compressive residual stresses at the run-in locations. For the conventionally welded pocketed panels, FCP rates were also slightly higher in the weld and base region, slightly slowing down as crack approaches to the clip ends as compared to the pocketed base panel.

The comparison of the fatigue lives of the conventionally welded and two run-ins welded pocketed panels are shown in Figure 5.112 with respect to the pocketed base panel. The fatigue lives of each welded panel with both configurations are very close to each other with an average about 130,000 cycles, however pocketed base panel has a fatigue life of around 180,000 cycles.

The residual stress distribution of both welded configuration for the pocketed panels are shown in Figure 5.113. As in the case of plain panels of the same weld configurations, both have tensile residual stresses, however weld configuration with two run-ins has much higher residual stresses with about 150 MPa peak value being three fold of the conventional type. The reason why much higher residual stresses were not so effective in the pocketed case is the deviation of the crack path from the weld region into the socket area.

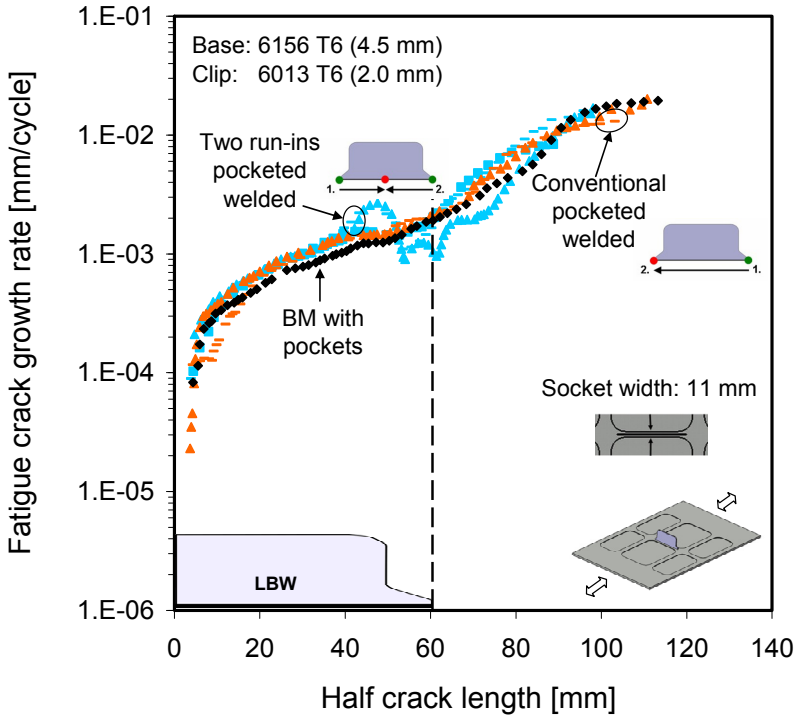

Figure 5.111: Fatigue crack growth rates plotted against half crack lengths of the pocketed base panel, conventionally welded pocketed panel and welded pocketed panel containing two run-ins. Socket widths for all are 11 mm.

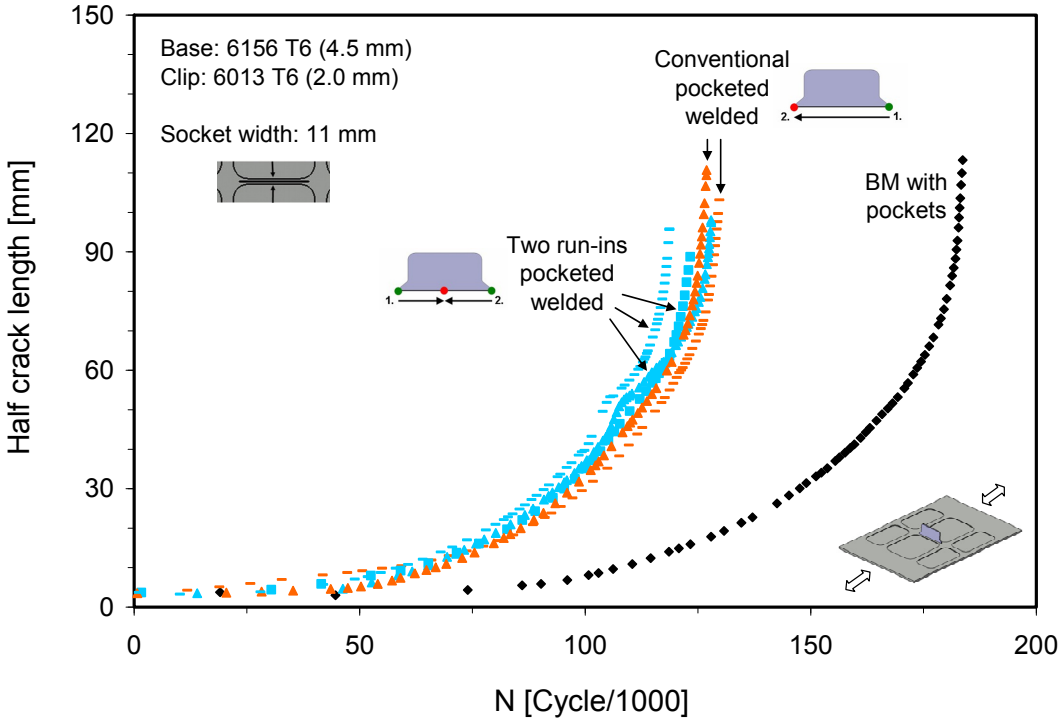

Figure 5.112: Comparison of fatigue lives of the pocketed base panel, conventionally welded panels and welded panels with two run-ins. Socket widths for all are 11 mm.

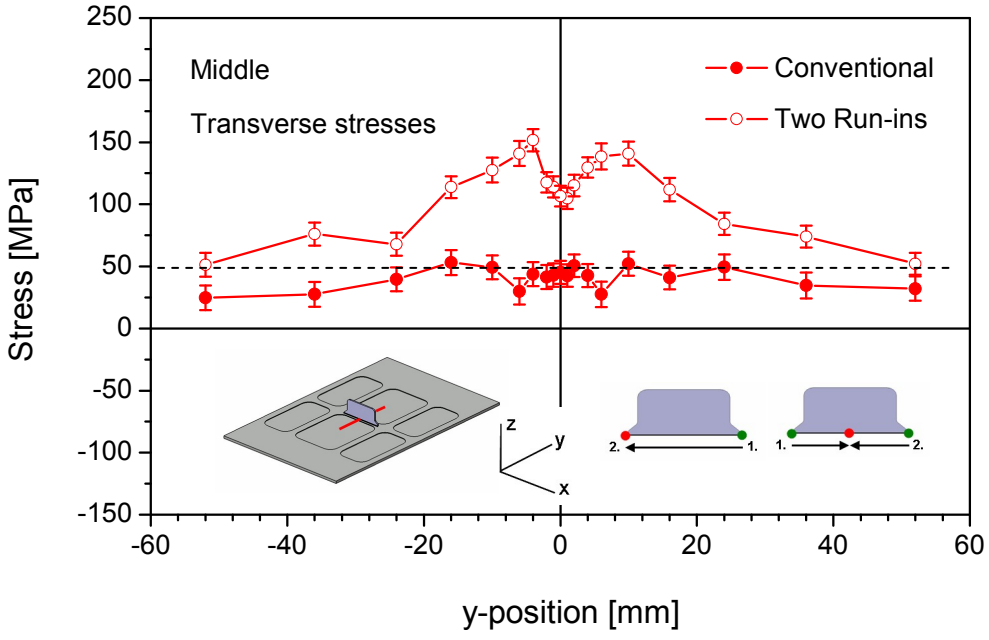

Figure 5.113: Transverse residual stress distributions at the mid-clip position of the welded pocketed panels of 6156 T6 material (4.5 mm) with 11 mm of socket width; solid points show that for the conventionally welded panel and empty points show that for the welded panel containing two run-ins.

6 Conclusions

A systematic investigation to clarify the residual stress effects on the fatigue crack propagation (FCP) behaviour of the laser beam welded "clip-skin" T-joints of Al-alloy airframe structure has been performed. Both experimental (neutron diffraction) and FE-simulation (SYSWELD) works have been conducted to determine the residual stress state of the clip welds. The welding types were changed to improve residual stress state at the mid-clip regions where the crack propagates along the clip welds. Since both ends of the clip welds have been considered as critical locations due to geometric reasons, an effort was made to improve residual stress states even at these locations.

A "One-bay-crack" (crack between two stringers) configuration was adopted to study the FCP behaviour (crack growing towards stringers along the clip) of the welded clips. Therefore, residual stress control at mid-clip region was equally important as the clip ends. Residual stress measurements were conducted using the neutron diffraction method on all type of welds and geometries at "run-in", "run-out" and "mid-clip" positions in the base plate. Residual stresses were determined only experimentally for the local joint geometry modifications (socket-pocket). Simulations were conducted on all three types of clip welds of plain panels.

Fatigue crack propagation analysis has been carried out to determine the effect of three different welding types (and hence their residual stresses) on the FCP behaviour. Furthermore, local joint geometry modifications (socket-pocket) have been introduced to check the crack path development along the weld seam.

These investigations have been carried out on three different weld types – in which the location of the "start" and "end" positions changes – namely;

- Conventionally welded clip,
- Clip with two run-outs,
- Clip with two run-ins.

The main out comes of this study are summarised under two main areas of the investigations, namely residual stresses and fatigue crack propagation as following.

Residual Stresses

Depending on the welding types, residual stress states of the welds show changes at different locations (run-in, run-out and mid-clip).

Compared to conventionally welded panel, the mid-clip position of the conventionally welded panel possesses higher tensile longitudinal residual stresses than that at the run-in position (also mid-clip position) of the welded panel with two run-outs. Moreover, there exist tensile transverse residual stresses in the conventionally welded panel in that position, but compressive stresses were determined for welded panel with two run-outs.

In the case of welding where run-ins are located at the clip ends, the run-out position is the mid-clip position. The mid-clip position of the conventionally welded panel possesses comparable tensile longitudinal stresses as run-out position of the welded panel with two run-ins. In addition, much higher tensile transverse residual stresses occurred for the latter.

After giving detailed description of the evolved residual stress states of each group of panels one may highlight the significance of the results as following:

- For the loading and geometry of the panel considered in this study, transverse residual stresses are significant with respect to damage tolerance performance of the panels,
- The transverse residual stress state along the clip weld needs to be controlled, or modified and if possible to generate high compressive stresses,
- This could be achieved by welding type of "two run-outs at mid-clip".

The pocketing with 11 mm socket width only shows an effect as leading to broader residual stress distributions if the machining applied before welding. Machining after welding doesn't cause any significant effect which is contrary to the literature. Obviously, the 11 mm socket width is not enough distance to the weld to affect the residual stress state. The socket widths variety of 11 and 20 mm also do not significantly affect the residual stress states.

The effect of heat treatment (prior to welding) on the residual stress has also been investigated. The results indicated that the tensile longitudinal residual stresses determined for T4 material are lower around the weld zone at mid-clip position and higher at run-in position in comparison to T6 material. Tensile transverse residual stresses occurred in the T4 material at run-out position, as being slightly compressive in the T6 material. For all positions, there exist broader residual stress distributions in the T4 material.

In order to determine the residual stress states of panels at different locations (mid-clip, run-in and run-out), analyses by numerical simulation of LBW processes were performed for all three types of the welded 6156 M(T) plain panels using commercial FE code SYSWELD.

Temperature field measurements were conducted and experimental results were compared with the thermal simulation results for the conventionally welded panel. Both results show some discrepancies. The simulated residual stress results were compared to the experimental measurements and they show good agreement particularly for the conventional welded panels in the transverse direction at all three locations.

Although simulation results for the longitudinal stresses were higher than experimental results (due to higher temperatures exposed in the simulation compared to experimental conditions), distributions of the stresses were similar in all three locations. The reason for the difference lies in the meshing, which should be refined further within the weld area. The simulated stresses in the through thickness (z) direction are very close to zero confirming the validity of plane stress assumption used for calculation of measured residual stresses. There exist asymmetric stress distributions at run-in and run-out locations as also measured by experiments, which was caused by constraint/stiffness increase as welding proceeds. Simulations were also successful for the two run-outs and two run-ins welded panels which could qualitatively predict different residual stress occurrence at different locations as the welding process changes. These results could lead to the use of process simulation with SYSWELD for the further geometry and process variations which minimizes the experimental work.

In summary;

- Compressive transverse residual stresses were only determined for clip weld having two run-outs at mid-clip position. This will have a significant impact on the fatigue crack propagation behaviour of the cracked panels,
- FE simulation results show good qualitative correlation with experimental results,
- No significant effect of pocketing and socket width variation was detected on the residual stress state of the conventionally welded panel.

Fatigue Crack Propagation

Fatigue crack propagation (FCP) of notched middle tension panels with single central clip were tested under constant amplitude cyclic loading. The crack growth and crack path development were carefully monitored to capture any possible effect of the welding process, residual stress state and local geometry of the weld seam area.

The FCP results of M(T) 400 base panels for different aluminium alloys are presented in terms of da/dN vs. ΔK and the central parts of the curves were almost straight which enable the application of Paris-Erdogan law given in equation 5.1, and the material constants are determined.

Increasing the tensile transverse stresses in the weld area, as in the welded panel with two run-ins decreased the fatigue life. Having compressive transverse stresses in the weld, as in the welded panel with two run-outs increased the fatigue life more than two fold compared to the conventionally welded panels. For sake of clarity to demonstrate the relationship between transverse residual stress states and FCP performance some diagrams are reproduced here;

- Panels having two run-ins at mid-clip position, showed higher compressive residual stresses and hence higher fatigue life (improved damage tolerance), see Figures 6.1a and 6.1b.
- Panels having two run-outs at clip centre, showed high tensile transverse stresses and hence exhibit shorter fatigue crack propagation life, see Figures 6.2a and 6.2b.
- Hence, it is recommended to start welding at the mid-clip position towards clip ends in two steps to produce compressive residual stresses along the weld seam which will lead to higher damage tolerance for the case of "one-bay-crack" panel analysis.

In the case of pocketing (11 mm and 20 mm socket width), crack path deviation to the base metal was observed due to the remote stress elevation in the pocket areas. The deviation was more pronounced for the narrower socket width of 11 mm.

Effect of heat treatment, material change, pocketing and socket width on FCP behaviour are investigated. No significant effects are determined, since similar transverse residual stresses exist for the compared cases. However, for all cases, the FCP rates of the cracks propagating through weld regions are higher than that of the crack growing in the parent metal. Similarly, the fatigue lives of the propagating crack of the welded panels are much lower than that of the base panel if no compressive transverse stresses present.

Limited numbers of FCP tests for stringer welded panels were also conducted. The results demonstrated that higher FCP rates occurred in the clip weld region is due to the weld quality and residual stress state.

In summary;

- Clip weld with two run-outs possesses highest fatigue lives compared to other two welding types due to compressive residual stresses in the applied load direction,
- No significant effect of pocketing was determined on FCP behaviour of the conventionally welded panels. However, narrow socket width of 11 mm enabled the increase in crack path deviation from the weld seam to the base metal part compared to the 20 mm socket width.

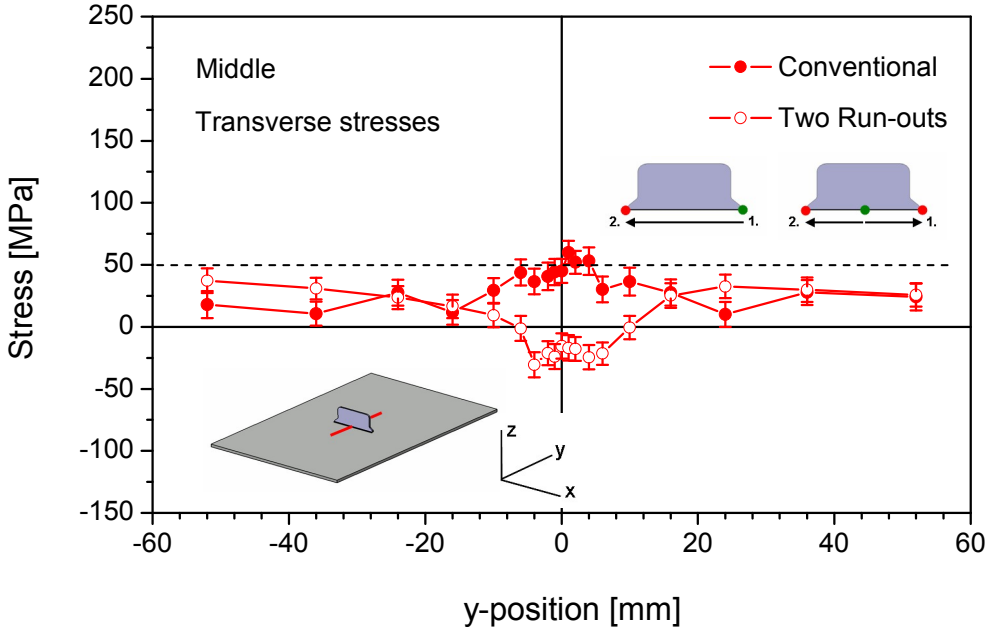

a)

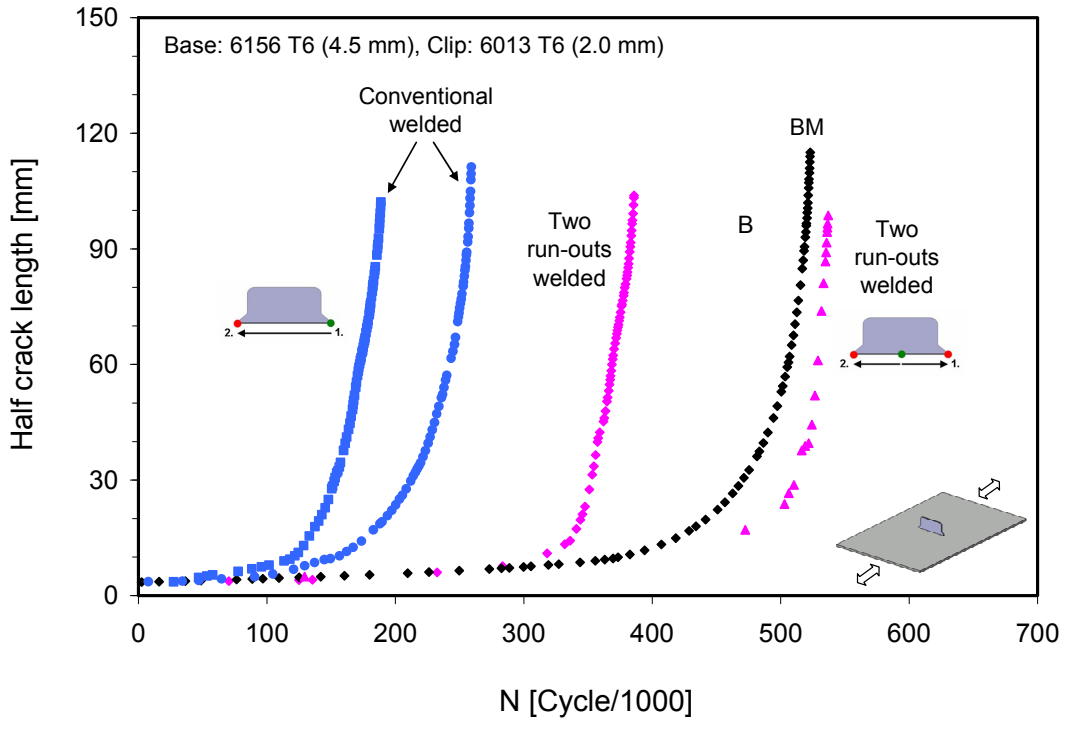

b)

Figure 6.1: Comparison of the a) transverse residual stresses b) fatigue lives of the conventional and two run-outs weld panels (see also Figures 5.102 and 5.103).

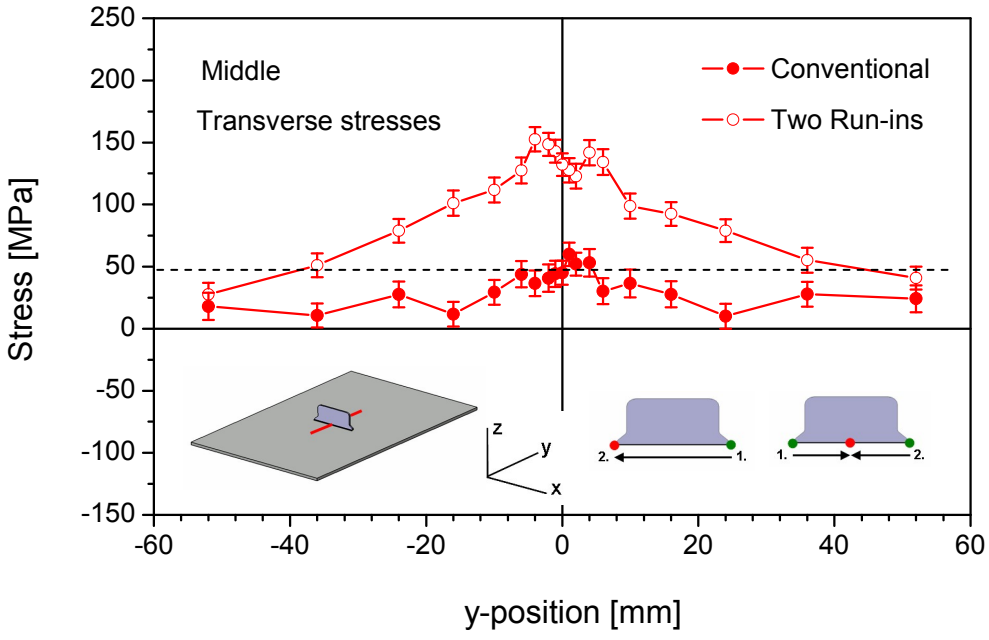

a)

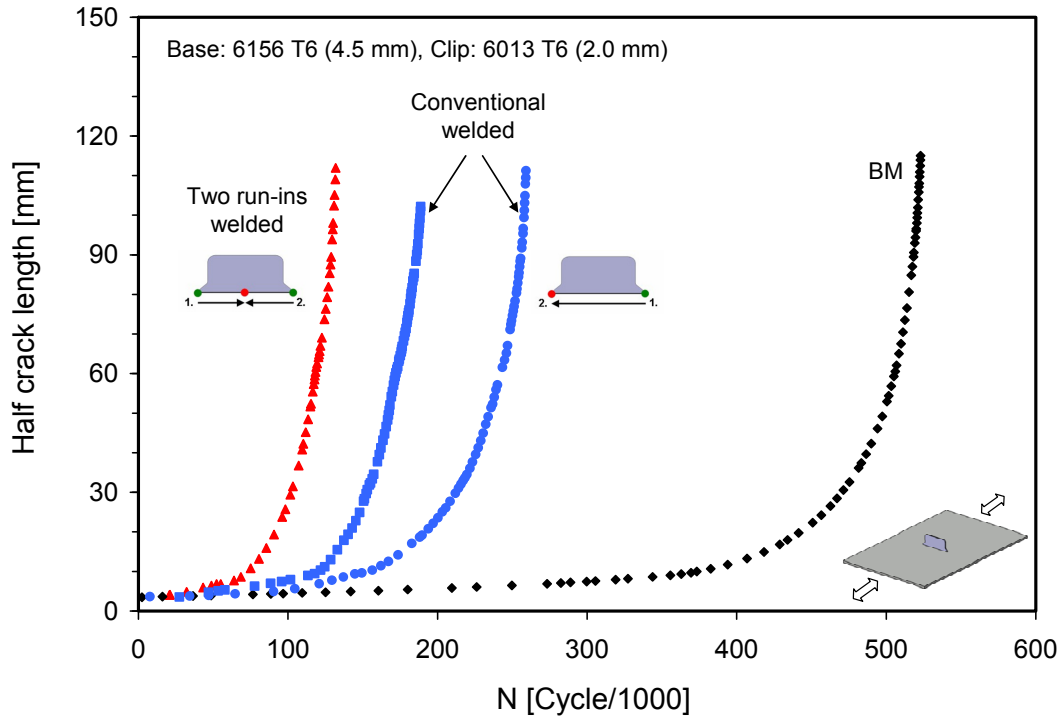

b)

Figure 6.2: Comparison of the a) transverse residual stresses b) fatigue lives of the conventional and two run-ins weld panels (see also Figures 5.108 and 5.109).

7 Outlook

Within this dissertation, smaller (400mm wide) clip welded panels were investigated to develop a basic understanding of the optimum technology as well as correlation between FCP and residual stresses. Real airframe structures contain welded stiffeners as shown in Figures 7.1 and 7.2. Therefore, R&D activities could be conducted by changing the clip design and having stiffened panels and investigating damage tolerance behaviour of the welded flat-panel systems as shown in Figure 7.2.

For this purpose, residual stress determination around the weld regions of the stringer and clip welded panel is planned. Further process optimization for the clip welding by new clip design (Figure 7.1) and 4-stringer and 3-clip welded panels (Figure 7.2) will be also investigated. Experimental residual stress measurements FE-simulation with SYSWELD will be performed and FCP behaviour will be studied together with residual stress effects.

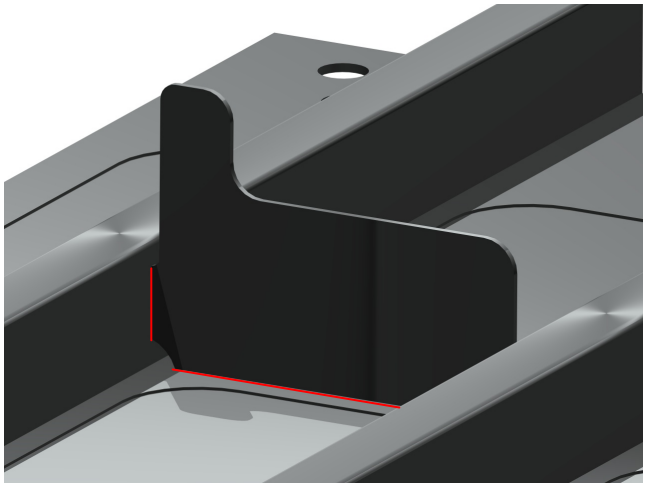

Figure 7.1: Schematic representation of the welded new clip design of the stringer panel.

Figure 7.2: Schematic representation of the multi-clip and -stringer welded panel.

8 References

[1] K. H. Rendings, "Aluminium Structures – Used in Aerospace – Status and Perspectives", Materials Science Forum (ICAA5), Vol. 242, pp. 11-24, 1997.

[2] B. Irving, "Why Aren't Airplanes Welded", Welding Journal, 76(1):31-42, 1997.

[3] Proceeding of the GKSS/TWI Workshop on Friction Stir Welding, GKSS Research Center, Geesthacht, Germany, 3rd May1999.

[4] D. Lohwasser, "Welding of Airframes by FSW", TWI, 3rd International Symposium on Friction Stir Welding, Kobe, Japan, 27–28 September 2001.

[5] R. Braun, C. Dalle-Donne, G. Staniek, "Laser Beam and Friction Stir Welding of 6013-T6 Aluminium Alloy Sheet", Material-wissenschaft und Werkstofftechnik, Vol. 31, pp. 1017–1026, 2000.

[6] N. Sekhar and P. Milton, "Distorting the Truth – A Novel Manufacturing Route for Aluminium Alloy Stiffened Panels", TWI Bulletin, Vol. 42, No. 5, Sept/Oct 2001.

[7] W. V. Vaidya, K. Angamuthu, M. Koçak, "Effect of Load Ratio and Temper on Fatigue Crack Propagation Behaviour of Al-alloy 6056", Fatigue 2002, Proceeding of 8th International Conference, Stockholm, Sweden, AF Blom, Ed, EMAS, UK, pp. 1467-1474, 2002.

[8] F. Lefebvre and I. Sinclair, "Micromechanical Aspects of Fatigue in MIG Welded Aluminium Airframe Alloy, Part 2: Short Fatigue Crack Behaviour", Materials Science and Engineering, A 407 pp. 265-272, 2005.

[9] E. Seib, M. Koçak, "Fracture Analysis of Strength Undermatched Welds of Thin-walled Aluminium Structures using FITNET Procedure", International Journal – Welding in the World, Vol. 49, No. 58, pp. 11–21, IIW Doc. X-1577-2005.

[10] E. Seib, "Residual Strength Analysis of Laser Beam and Friction Stir Welded Aluminium Panels for Aerospace Applications", PhD thesis, Technical University Harburg-Hamburg (TUHH), Germany, 2005.

[11] L. Tsay, Y. P. Shan, Y. H. Chao, W. Shu, "The Influence of Porosity on the Fatigue Crack Growth Behaviour of Ti-6Al-4 Laser Welds", Journal of Material Science, Vol. 41, No. 22, pp.7498 – 7505(8), 2006.

[12] M. Koçak, E. Seib, A. Motarjemi, "Treatments of Structural Welds using FITNET Fitness-for-service Assessment Procedure", International Journal Welding in the World, Vol. 51, No. 5/6-2007, pp. 106, IIW-1768-2006.

[13] E. Seib, M. Koçak, V. Uz, "Fracture analysis of thin-walled laser beam and friction stir welded Al-alloys using FITNET FFS procedure", Proceeding of the International Conference FITNET 2006, 17-19 May 2006, Amsterdam, The Netherlands, ISBN 978-3-00-021084-6, Ed. by M. Koçak, GKSS, Geesthacht, Germany, 2007.

[14] F. S. Bayraktar, P. Staron, M. Koçak and A. Schreyer, "Residual Stress Analysis of Laser Welded Aluminium T-Joints Using Neutron Diffraction", Materials Science Forum, Vols. 524-525 pp. 419-424, 2006.

[15] P. Staron. U. Cihak, H. Clemens, M. Stockinger, F. S. Bayraktar, M. Koçak, A. Schreyer, "Diffraction-based Residual Stress Analysis Applied to Problems in the Aircraft Industry", Advanced Engineering Materials, 9, No. 8, pp. 627–638, 2007.

[16] F. S. Bayraktar, P. Staron, M. Koçak and A. Schreyer, "Analysis of Residual Stress in Laser Welded Aerospace Aluminium T-joints by Neutron Diffraction and Finite Element Modelling", Materials Science Forum, Vols. 571–572 pp. 355–360, 2008.

[17] W. Machold, P. Staron, F. S. Bayraktar, S. Riekehr, M. Koçak, A. Schreyer, "Influence of the Welding Sequence on Residual Stresses in Laser Welded T-joints of an Airframe Aluminium Alloy", Materials Science Forum, Vols. 571–572 pp. 375-380, 2008.

[18] A. Paul and T. DebRoy, “Heat Transfer and Fluid Flow in Laser Melted Weld Pools”, TWR, pp. 29–33, 1986.
[19] J. O. Milewski, T. M. Mustaleski, “Modeling of Laser Energy Concentration in Narrow Gap Joints”, TWR, pp. 437–441, 1998.
[20] S. Tsukamoto, K. Hiraoka, Y. Asai and H. Irie and M. Oguma, “Characterization of Laser Induced Plasma in CO_2 Laser Welding”, TWR, pp. 431–436, 1998.
[21] K. Kazemi and J. A. Goldak, “Numerical Simulation of Laser Full Penetration Welding”, Computational Materials Science, Vol. 44, pp. 841–849, 2009.
[22] J. P. Reynolds, H. W. Kerr, P. J. Fehrenbach, L. Bourque and R. D. Davidson, “Cracking in Pulsed Laser Welds in Nickel-based Alloys, Stainless Steels, and their Combinations”, TWR, pp. 325–329, 1986.
[23] V. P. Kujanpää, “Hot Cracking of Laser and Electron Beam Welds in X20CrMoV121 Heat-Resisting Steel”, TWR, pp. 735–738, 1998.
[24] M. M. Biela, H. W. Kerr and D. C. Weckman, “Effects of Process Variables on Cracking of Pulsed Laser Welds in Inconel 600”, TWR, pp. 769–774, 1998.
[25] M. Shibahara, S. Itoh, H. Serizawa and H. Murakawa, “Numerical Prediction of Welding Hot Cracking Using Three-Dimensional FEM with Temperature Dependent Interface Element”, Welding in the World, Journal of the International Institue of Welding, Vol. 49, No. 11/12, ISSN 0043-2288, 2005 and 58th Annual Assembly of IIW, Prague, 10–15 July, 2005.
[26] S. Katayama, N. Seto, M. Mizutani and A. Matsunawa, “Keyhole Dynamics and Porosity Formation during Laser Welding”, Proceeding of the 7th International Symposium, JWS, Kobe, pp. 555–560, 2001.
[27] I. Kawaguchi, G. Arakane, H. Honda and S. Tsukamoto, “Suppression of Porosity Formation in High Power Laser Welding”, Proceeding of the 7th International Symposium, JWS, Kobe, pp. 591–596, 2001.
[28] J. M. Vitek, Y. S. Iskander, E. M. Oblow, S. S. Babu and S. A. David, “Neural Network Modeling of Pulsed-Laser Weld Pool Shapes in Aluminum Alloy Welds”, TWR, pp. 442–448, 1998.
[29] J. G. Blauel and W. Burget, “Mechanics and Materials Behaviour of Laser Beam Welded Joints in Aluminium”, Proc. of the 7th Int. Symp., JWS, Kobe, 2001.
[30] B. R. Leigh, C. Poon, H. W. Kerr, W.H.S. Lawson and N. Ferguson, “An Evaluation of the Physical Properties of Nd:YAG Laser Welded High Strength 6000 Series Aluminium Alloys”, ICAS Congress, 2002.
[31] R. Braun, G. Roth, J. Arnold, “Nd:YAG Laser Beam Welding of 6013 Aluminium Alloy Sheet Using Different Filler Powders”, Materials Science Forum, Vols. 396–402, pp. 1691–1696, 2002.
[32] R. Braun, “Laser Beam Welding of 6013 Aluminium Alloy Sheet”, Aluminium, Vol. 80, No. 4, pp. 304–308, 2004.
[33] R. Braun, “Nd: YAG Laser Butt Welding of AA6013 Using Silicon and Magnesium Containing Filler Powders”, Materials Science and Engineering A, Vol. 426, pp. 250–262, 2006.
[34] W. V. Vaidya, M. Koçak, E. Seib, H. Assler and J. Hackius, “Mechanical Behaviour of Laser Beam and Friction Stir Welded Aluminium Alloys for Airframes”, 57th Annual Assembly of the International Institute of Welding, International Conference on “Technical Trends and Future Prospectives of Welding Technology for Transportation, Land, Sea, Air and Space”, Osaka, Japan, July 15–16, 2004.
[35] E. Cicală, G. Duffet, H. Andrzejewski, D. Grevey and S. Ignat, “Hot Cracking in Al–Mg–Si Alloy Laser Welding – Operating Parameters and Their Effects”, Materials Science and Engineering A, Vol. 395, pp. 1–9, 2005.

[36] D. Fabrègue, A. Deschamps, M. Suery and J. M. Drezet, “Non-isothermal Tensile Tests During Solidification of Al–Mg–Si–Cu Alloys: Mechanical Properties in Relation to the Phenomenon of Hot Tearing”, Acta Materialia, Vol. 54, pp. 5209–5220, 2006.

[37] D. Fabrègue, A. Deschamps, M. Suéry and H. Proudhon, “Two- and Three-dimensional Characterizations of Hot Tears in a Al–Mg–Si alloy Laser Weld”, Scripta Materialia, Vol. 59, pp. 324–327, 2008.

[38] D. Fabrègue, A. Deschamps, M. Suéry, “Influence of the Silicon Content on the Mechanical Properties of AA6xxx Laser Welds”, Materials Science and Engineering A, Vol. 506, pp. 157–164, 2009.

[39] A. Ancona, P. M. Lugara, D. Sorgente and L. Tricarico, “Mechanical Characterization of CO_2 Laser Beam Butt Welds of AA5083”, Journal of Materials Processing Technology, Vol. 191, pp. 381–384, 2007.

[40] J. M. Sánchez-Amaya, T. Delgado, L. González-Rovira and F. J. Botana, “Laser Welding of Aluminium Alloys 5083 and 6082 under Conduction Regime”, Applied Surface Science, Vol. 255, pp. 9512–9521, 2009.

[41] Z. Li and S. L. Gobbi, “Laser Welding for Lightweight Structures”, Journal of Materials Processing Technology, Vol. 70, pp. 137–144, 1997.

[42] E. Schubert, M. Klassen, I. Zerner, C. Walz and G. Sepold, “Light-weight Structures Produced by Laser Beam Joining for Future Applications in Automobile and Aerospace Industry”, Journal of Materials Processing Technology, Vol. 115, pp. 2–8, 2001.

[43] L. Edwards, “Influence of Residual Stress Redistribution on Fatigue Crack Growth and Damage Tolerant Design”, Materials Science Forum, Vols. 524–525, pp. 363–372, 2006.

[44] K. Müller, J. P. Bergmann and H. W. Bergmann, “Residual Stress Measurements on Laser Beam Welds in Aluminium by X-Ray Diffraction Methods”, Zeitschrift Metallkunde, Vol. 92, No. 3, pp. 253–259, 2001.

[45] P. Staron, W. V. Vaidya, M. Koçak, J. Homeyer and J. Hackius, “Residual Stresses in Laser Beam Welded Butt Joints of the Airframe Aluminium Alloy AA6056”, Materials Science Forum, Vols. 524–525, pp. 413–418, 2006.

[46] P. V. Ramana, G. M. Reddy, T. Mohandas and A. V. S. S. K. S. Gupta, “Microstructure and Residual Stress Distribution of Similar and Dissimilar Electron Beam Welds – Maraging Steel to Medium Alloy Medium Carbon Steel”, Materials and Design, Vol. 31, pp. 749–760, 2010.

[47] G. Bruno, A. Carrado, B. Dunn, F. Fiori, E. Girardin, T. Pirling and F. Rustichelli, “Neutron Diffraction Measurements for the Determination of Residual Stress in Ti6Al4V Welded Plates”, Materials Science Forum, Vols. 347–349, pp. 684–689, 2000.

[48] S. V. Pearce, V. M. Linton and E. C. Oliver, “Residual Stress in a Thick Section High Strength T-butt Weld”, Materials Science and Engineering A, Vol. 480, pp. 411–418, 2008.

[49] S. Ganguly, M. E. Fitzpatrick and L. Edwards, “Comparative Neutron and Synchrotron X-Ray Diffraction Studies to Determine Residual Stress on an As-Welded AA2024 Plate”, Materials Science Forum, Vols. 490–491, pp. 223–228, 2005.

[50] S. Ganguly, V. Stelmukh, L. Edwards and M. E. Fitzpatrick, “Analysis of Residual Stress in Metal-inert-gas-welded Al-2024 Using Neutron and Synchrotron X-ray Diffraction”, Materials Science and Engineering A, Vol. 491, pp. 248–257, 2008.

[51] M. Ya, P. Marquette, F. Belahcene and J. Lu, “Residual Stresses in Laser Welded Aluminium Plate by Use of Ultrasonic and Optical Methods”, Materials Science and Engineering A, Vol. 382, pp. 257–264, 2004.
[52] G. Albertini, G. Bruno, B. D. Dunn, F. Fiori, W. Reimers, J.S. Wright, “Comparative Neutron and X-ray Residual Stress Measurements on Al-2219 Welded Plate” Materials Science and Engineering A, Vol. 224, p. 157–165, 1997.
[53] R. A. Owen, R. V. Preston, P. J. Withers, H. R. Shercliff and P. J. Webster, “ Neutron and Synchrotron Measurements of Residual Strain in TIG Welded Aluminium Alloy 2024”, Materials Science and Engineering A Vol. 346, pp. 159–167, 2003.
[54] M. Kartal, M. Turski, G. Johnson, M. E. Fitzpatrick, S. Gungor, P. J. Withers and L. Edwards, “Residual Stress Measurements in Single and Multi-pass Groove Weld Specimens Using Neutron Diffraction and Contour Method”, Materials Science Forum, Vols. 524–525, pp. 671–676, 2006.
[55] M. N. James, P. J. Webster, D. J.Hughes, Z. Chen, N. Ratel, S. P. Ting, G. Bruno and A. Steuwer, “Correlating Weld Process Conditions, Residual Strain and Stress, Microstructure and Mechanical Properties for High Strength Steel–The Role of Neutron Diffraction Strain Scanning”, Materials Science and Engineering A, Vol. 427, pp. 16–26, 2006.
[56] S. F. Estefen, T. Gurova, X. Castello and A. Leontiev, “Surface Residual Stress Evaluation in Double-electrode Butt Welded Steel Plates”, Materials and Design, Vol. 31, pp. 1622–1627, 2010.
[57] J. Goldak, A. Chakravarti, and M. Bibby, “A New Finite Element Model for Welding Heat Sources”, Metallurgical Transactions B, Vol. 15B, pp. 299–305, June 1984.
[58] E. Beyer: Schweißen mit Laser, ISBN 3-540-52674-9, Springer, 1995.
[59] J. Goldak, B. Patel, M. Bibby and J. Moore, Computational Weld Mechanics, June 1985.
[60] J. Goldak, A. Oddy, M. McDill, A. Chakravarti, M. Bibby and R. House, “Progress in Computing Residual Stress and Strain in Welds”, ASM International, 8605–008, pp. 523–527, 1986.
[61] J. Goldak, M. McDill, A. Oddy, R. House, X. Chi and M. Bibby, “Computational Heat Transfer for Weld Mechanics”, ASM International, 8605–001, pp. 15–20, 1986.
[62] D. H. B. Mok and R. J. Pick, “Finite Element Study of Residual Stresses in a Plate T-joint Fatigue Specimen”, I Mech E, Vol. 204, pp. 127–134, 1990.
[63] J. Cañas, R. Picón, F. París, A. Blazquez and J. C. Marín, “A Simplified Numerical Analysis of Residual Stresses in Aluminum Welded Plates”, Computers & Structures, Vol. 58, No. 1, pp. 59–69, 1996.
[64] M. Zain-ul-Abdein, D. Nelias, J.-F. Jullien, D. Deloison, “Prediction of Laser Beam Welding-induced Distortions and Residual Stresses by Numerical Simulation for Aeronautic Application”, Journal of Materials Processing Technology, Vol. 209, pp. 2907–2917, 2009.
[65] S. Sarkani, V. Tritchkov and G. Michaelov, “An Efficient Approach for Computing Residual Stresses in Welded Joints”, Finite Elements in Analysis and Design, Vol. 35, pp. 247–268, 2000.
[66] S.- H. Kim, J.- B. Kim, W.- J. Lee, “Numerical Prediction and Neutron Diffraction Measurement of the Residual Stresses for a Modified 9Cr-1Mo Steel Weld”, Journal of Materials Processing Technology, Vol. 209, pp. 3905–3913, 2009.
[67] A. Wu, S. Syngellakis and B. G. Mellor, “Finite Element Analysis of Residual Stresses in a Butt Weld”, Proceedings of the 7th Postgraduate Conference in Engineering Materials, pp. 37–38, 2001.

[68] A. Wu, S. Syngellakis and Brian Mellor, “Finite Element Prediction of Residual Stresses in a Fillet Welded T-joint”, 6th International Trends in Welding Research Conference Proceedings, 15–19 April 2002, Pine Mountain, GA, ASM International, 2003.

[69] L. Li, W. Renfu, X. Gang and M. Xiangjun, “Numerical Simulation on Residual Stress Distribution of the Pipe-plate Welding”, Key Engineering Materials, Vols. 417–418, pp. 937–940, 2010.

[70] L. K. Keppas, D. E. Katsareas, R. C. Wimpory, N. K. Anifantis and A. G. Youtsos, “Letterbox Type Repair Weld Finite Element Simulation and Residual Stress Prediction”, Materials Science Forum, Vols. 524–525, pp. 445–450, 2006.

[71] S. A. A. A. Mousavi, “Experimental and Numerical Analyses of Residual Stress Distributions in TIG Welding Process for 304L Stainless Steel”, Journal of Materials Processing Technology, Vol. 208, pp. 383–394, 2008.

[72] R. V. Preston, H. R. Shercliff. P. J. Withers and S. Smith, “Physically-based Constitutive Modelling of Residual Stress Development in Welding of Aluminium Alloy 2024”, Acta Materialia, Vol. 52, pp. 4973–4983, 2004.

[73] H. Cramer, A. Lechner, H. E. Chalandar, T. N. Nitschke-Pagel, D. Kosteas und C. Radlbeck, “Calculation and Measurement of Residual Stresses in Aluminium Welded Joints”, Welding and Cutting, Vol. 6, No. 6, pp. 342–347, 2007.

[74] T. L. Teng, C. P. Fung, P. H. Chang and W. C. Yang, “Analysis of Residual Stresses and Distortions in T-joint Fillet Welds”, International Journal of Pressure Vessels and Piping, Vol. 78, pp. 523–538, 2001.

[75] Chin-Hyung Lee, Kyong-Ho Chang, “Three-dimensional Finite Element Simulation of Residual Stresses in Circumferential Welds of Steel Pipe Including Pipe Diameter Effects”, Materials Science and Engineering A, Vol. 487, pp. 210–218, 2008.

[76] K. R. Dowse and C. E. Richards, “Fatigue Crack Propagation through Weld Heat Affected Zones”, Metallurgical Transactions, Vol. 2, pp. 599–603, February 1971.

[77] D. Benoit, H. P. Lieurade and M. Truchon, “A Study of the Propagation of Fatigue Cracks in the Heat–affected Zones of Welded Joints in E 36 Steel”, European Offshore Steels Research Seminar; Cambridge, England, VI/P13, Vol. 27–29, pp.1–7, November 1978.

[78] J. E. M. Braid and J. F. Knott, “Fatigue Crack Propagation in the Vicinity of Weld-Deposits in High-strength, Structural Steel”, F. Fatigue Resistance of Welded Joints, IIW, XIII–1014–81, pp. 2061–2069, 1981.

[79] H. P. Lieurade, “Fatigue in Welded Constructions”, Bulletin Technique Du Rureau Veritas, pp. 281–302, Oktober 1985.

[80] Y. Itoh, “Fatigue Life Prediction for GMA Welded Butt Joints in a C-Mn-Si Steel”, Welding Research Supplement, pp. 50–56, February 1987.

[81] T. M. Roberts, A. W. Davies and K. M. Holford, “Structural Integrity of Welded Steel Structures”, Key Engineering Materials, Vols. 167–168, pp. 142–151, 1999.

[82] T. Y. Oh, Y. K. Kwon, C. J. Lee and D. S. Kwak, “The Characteristics of Fatigue Strength in Laser Tailored Welded Blanking Sheet Metal”, Key Engineering Materials, Vols. 183–187, pp. 1321–1326, 2000.

[83] M. Nakajima, M. Akita, K. Tokaji and Y. Takai, “Fatigue Behaviour of Welded Joints in a Ferritic Stainless Steel SUS444”, 11th International Conference on Fracture, Turin, Italy, March 20–25, 2005.

[84] S. Hong, S. Kim, C. G. Lee and S. J. Kim, “Fatigue Crack Propagation Behaviour of Friction Stir Welded Al–Mg–Si alloy”, Scripta Materialia, Vol. 55, pp. 1007–1010, 2006.

[85] S. J. Hong, S. S. Kim, C. G. Lee and S. J. Kim, “Fatigue Crack Propagation Behaviour of Friction Stir Welded 6061-T651 Al Alloy”, Solid State Phenomena, Vols. 124–126, pp. 1321–1324, 2007.

[86] W. V. Vaidya, M. Horstmann, E. Seib, K. Toksoy and M. Koçak, “Assessment of Fracture and Fatigue Crack Propagation of Laser Beam and Friction Stir Welded Aluminium and Magnesium Alloys”, Advanced Engineering Materials, Vol.8, No. 5, ISSN 1438-1656, pp. 399–406, May 2006.

[87] P. M. G. P. Moreira, A. M. P. de Jesus, A. S. Ribeiro and P. M. S. T de Castro, “Assessment of the Fatigue Behaviour of Friction Stir Welded Joints: Aluminium Alloy 6082-T6”, Key Engineering Materials, Vols. 348–349, pp. 209–212, 2007.

[88] V. Balasubramanian, V. Ravisankar and G. M. Reddy, “Influences of Pulsed Current Welding and Post Weld Aging Treatment on Fatigue Crack Growth Behaviour of AA7075 Aluminium Alloy Joints”, International Journal of Fatigue, Vol. 30, pp. 405–416, 2008.

[89] B. Zhang and T. Moan, “Analysis of Fatigue Crack Propagation in Typical Welded Joints of FPSOS”, Proceedings of OMAE2005, 24th International Conference on Offshore Mechanics and Arctic Engineering, Halkidiki, Greece, June 12–17, 2005.

[90] D. Fersini and A. Pirondi, “Analysis and Modelling of Fatigue Failure of Friction Stir Welded Aluminum Alloy Single-lap Joints”, Engineering Fracture Mechanics, Vol. 75, pp. 790-803, 2008.

[91] R. John, K. V. Jata, K. Sadananda, “Residual Stress Effects on Near-threshold Fatigue Crack Growth in Friction Stir Welds in Aerospace Alloys”, International Journal of Fatigue Vol. 25, pp. 939-948, 2003.

[92] S. Kim, C. G. Lee, and S.-J. Kim, “Fatigue Crack Propagation Behaviour of Friction Stir Welded 5083-H32 and 6061-T651 Aluminium Alloys”, Materials Science and Engineering A, Vol. 478, pp. 56–64, 2008.

[93] G. Pouget and A. P. Reynolds, “Residual Stress and Microstructure Effects on Fatigue Crack Growth in AA2050 Friction Stir Welds”, International Journal of Fatigue, Vol. 30, pp. 463–472, 2008.

[94] L. Fratini, S. Pasta, A. P. Reynolds, “Fatigue Crack Growth in 2024-T351 Friction Stir Welded Joints: Longitudinal Residual Stress and Microstructural Effects”, International Journal of Fatigue, Vol. 31, pp. 495–500, 2009.

[95] R. Galatolo and A. Lanciotti, “Fatigue Crack Propagation in Residual Stress Fields of Welded Plates”, International Journal of Fatigue, Vol. 19, No. 1, pp. 43–49, 1997.

[96] C. D. M. Liljedahl, M. L. Tan, O. Zanellato, S. Ganguly, M. E. Fitzpatrick and L. Edwards, “Evolution of Residual Stresses with Fatigue Loading and Subsequent Crack Growth in a Welded Aluminium Alloy Middle Tension Specimen”, Engineering Fracture Mechanics, Vol. 75, pp. 3881–3894, 2008.

[97] C. D. M. Liljedahl, J. Brouard, O. Zanellato, J. Lin, M. L. Tan, S. Ganguly, P. E. Irving, M. E. Fitzpatrick, X. Zhang and L. Edwards, “Weld Residual Stress Effects on Fatigue Crack Growth Behaviour of Aluminium Alloy 2024-T351”, International Journal of Fatigue, Vol. 31, pp. 1081–1088, 2009.

[98] C. Lachmann, Th.Nitschke-Pagel and H. Wohlfahrt, “Characterisation of Residual Stress Relaxation in Fatigue Loaded Welded Joints by X-Ray Diffraction and Barkhausen Noise Method”, Materials Science Forum, Vols. 347–349, pp. 374–380, 2000.

[99] S. Sarkani, G. Michaelov and D. P. Kihl, “Stochastic Fatigue Damage Accumulation in a T-welded Joint Accounting for the Residual Stress Fields”, International Journal of Fatigue, Vol. 23, pp. 71–78, 2001.

[100] B. C. Goo, S. Y. Yang and D. H. Lee, "A Study on the Effect of Welding Residual Stress on Fatigue Behaviour by Finite Element Analysis", Key Engineering Materials, Vols. 270–273, pp. 2296–2301, 2004.
[101] B. C. Goo, S. Y. Yang and J. W. Seo, "Fatigue Life Evaluation Model for Welded Joints with Residual Stresses", Key Engineering Materials, Vols. 297–300, pp. 762–767, 2005.
[102] B. C. Goo, S. Y. Yang and D. H. Lee, "A Simple Strain-Life Approach for the Fatigue Life Evaluation of Welded Joints with Residual Stresses", Key Engineering Materials, Vols. 306–308, pp. 127–132, 2006.
[103] E. Gonçalves and M. A. C. Gonzales, "Residual Stresses Behaviour under Fatigue Crack Cyclic Loading: a Finite Element Analyses", 11th International Conference on Fracture–Turin (Italy), March 20–25, 2005.
[104] D. Fabrègue, A. Deschamps and M. Suéry, "Influence of the Silicon Content on the Mechanical Properties of AA6xxx Laser Welds", Materials Science and Engineering A, Vol. 506, pp. 157–164, 2009.
[105] P. Staron, H.-U. Ruhnau, M. Marmotti, P. Mikula, R. Kampmann, "The New Diffractometer ARES for the Analysis of Residual Stresses" Physica B, Vol. 276–278, pp. 158–159, 2000.
[106] A. J. Allen, M. T. Hutchings, C. G. Windsor and C. Andreani, Advances in Physics, 1985, Vol. 34, No. 4, pp. 445–473, 1985.
[107] B. Clausen, T. Lorentzen, T. Leffers, "Self-consistent Modelling of the Plastic Deformation of F.C.C. Polycrystals and its Implications for Diffraction Measurements of Internal Stresses", Acta Materialia, 1998, Vol. 46 pp. 3087–3098.
[108] H. G. Priesmeyer, eds. M. T. Hutchings and A. D. Krawitz, NATO ASI series, Vol. E216, pp 277–284, 1992.
[109] E. O'Brien, Proc. of the Sixth Int. Conf. on Residual Stresses, ICRS-6, IOM Communications Ltd., 13, London, UK, 2000.
[110] M. Hutchings, P. Withers, T. Holden, T. Lorentzen, CRC Press Taylor & Francis Group, UK, 2005.
[111] A. D. Krawitz, R. A. Winholtz, "Use of Position-dependent Stress-free Standards for Diffraction Stress Measurements", Materials Science and Engineering, Vol. A185, pp. 123-130, 1994.
[112] A. Stacey, H.J. Macgillivary, G.A. Webster, P.J. Webster, K.R.A. Ziebeck, "Measurement of Residual Stresses by Neutron Diffraction", Journal of Strain Analysis, Vol. 20, No. 2, p. 93–100, 1985.
[113] A. Pyzalla, "Determination of the Residual Stress State in Components using Neutron Diffraction", Source: J. Neutron Research, Vol.8. pp. 187–213, 2000.
[114] P. Staron, U. Cihak, H. Clemens, M. Stockinger, F. S. Bayraktar, M. Koçak, A. Schreyer, "Diffraction-Based Residual Stress Analysis Applied to Problems in the Aircraft Industry", Advanced Engineering Materials, Vol. 9, No. 8, 2007.
[115] U. Cihak, P. Staron, W. Marketz, H. Leitner, J. Tockner and H. Clemens, "Residual Stresses in Forged IN718 Turbine Discs", Zeitschrift für Metallkunde, Vol. 95, No. 7, pp. 663–668, 2004.
[116] P. Staron, M. Koçak and S. Williams, "Residual Stresses in Friction Stir Welded Al Sheets", Applied Physics A, Vol. 74, pp. 1161–1162, 2002.
[117] P. Staron, M. Koçak, S. Williams, "Residual Stress Distributions in Friction Stir Welded Al Sheets Determined by Neutron Strain Scanning", 6th International Trends in Welding research Conference Proceedings, pp. 253-256, April 15–19, 2002, Pine Mountain, GA, ASM International, 2003.

[118] P. Staron, M. Koçak, S. Williams, A. Wescott, Physica B, "Residual Stress in Friction Stir-welded Al Sheets", Vol. 350, p. 491–493, 2004.
[119] L. Pintschovius, V. Jung, E. Macherauch and O. Vöhringer, "Residual Stress Measurements by means of Neutron Diffraction", Materials Science and Engineering, Vol. 61, p. 43–50, 1983.
[120] Cedric Gasqueres, Christine Sarrazin-Baudoux, Jean Petit, David Dumont, "Fatigue Crack Propagation in an Aluminium Alloy at 223 K", Scripta Materialia Vol. 53, pp. 1333–1337, 2005.
[121] F. S. Silva, "The Importance of Compressive Stresses on Fatigue Crack Propagation Rate", International Journal of Fatigue, 27, 1441–1452, 2005.
[122] J. A. Bannantine, J. J. Comer, J. L. Handrock, "Fundamentals of Metal Fatigue Analysis", Prentice Hall, Inc, NJ, 1990.
[123] S. C. Chapra and R. P. Canale, "Numerical Methods for Engineers: With Personal Computer Applications", McGraw-Hill, New York, 1985.
[124] ASTM International, Standard Test Method for Measurement of Fatigue Crack Growth Rates, Designation: E 647 – 05, pp. 692–736.
[125] J. M. Bergheau, "Contributions of Numerical Modelling to the Optimisation of Welding Processes", Welding International, Vol. 19, No. 12, pp. 956–966, 2005.
[126] S. A. Tsirkas, P. Papanikos, Th. Kermanidis, "Numerical Simulation of the Laser Welding Process in Butt-joint Specimens", Journal of Materials Processing Technology, Vol. 134, pp. 59–69, 2003.
[127] S. A. Tsirkas, P. Papanikos, K. Pericleous, N. Strusevich, F. Boitout and J. M. Bergheau, "Evaluation of Distortions in Laser Welded Shipbuilding Parts using Local–global Finite Element Approach", Science and Technology of Welding and Joining, Vol. 8, No. 2, pp. 79–88, 2003.
[128] W. Machold, Diploma Thesis, "Residual Stress Analysis of Laser Beam Welded Aluminium T-joints for the Airframes", University of Hamburg, 2007.
[129] Von Mises R., "Mechanik der Festen Korper im plastisch deformablen Zustand", Göttin. Nachr. Math. Phys., Vol. 1, pp. 582–592, 1913.
[130] E. A. Starke, Jr and J. T. Staley, "Application of Modern Aluminum Alloys to Aircraft, Progress in Aerospace Sciences", Vol.32, pp. 131–172, 1996.
[131] M. V. Uz, Master Thesis at TUHH Hamburg-Harburg, "Investigation on Fracture Behaviour of Laser Beam Welded Aerospace Aluminium Alloy", 2005.
[132] B. R. Leigh, C. Poon, H. W. Kerr, W.H.S. Lawson, N. Ferguson, "An Evaluation of the Physical Properties of Nd: YAG Laser Welded High Strength 6000 Series Aluminum Alloys", ICAS Congress, pp. 4102.1-12, 2002.
[133] C. A. W. Olea, L. Roldo, J. F. dos Santos, T. R. Strohaecker, "A Sub-structural Analysis of Friction Stir Welded Joints in an AA6056 Al-alloy in T4 and T6 Temper Conditions", Materials Science and Engineering A, Vol. 454–455, pp. 52–62, 2007.
[134] M. Cabibbo, H.J. McQueen, E. Evangelista, S. Spigarelli, M. Di Paola, A. Falchero, "Microstructure and Mechanical Property Studies of AA6056 Friction Stir Welded Plate", Materials Science and Engineering A, Vol. 460–461, pp. 86–94, 2007.
[135] F. Delmas, M.J. Casanove, P. Lours, A. Couret, A. Coujou, "Quantitative TEM Study of the Precipitation Microstructure in Aluminium Alloy Al(MgSiCu) 6056 T6", Materials Science and Engineering A, Vol. 373, pp. 80–89, 2004.
[136] B. Heinz and B. Skrotzki, "Characterization of a Friction-Stir-Welded Aluminium Alloy 6013", Metallic Materials Transaction B, 33B, p.489–498, 2002.
[137] S. Kou, Welding Metallurgy, John Wiley & Sons Inc., Second Edition, 2002.

[138] C. Huang and S. Kou, “Liquation Mechanisms in Multicomponent Aluminum Alloys during Welding”, Welding Journal, pp. 211–222, Oktober 2002.
[139] M. Koçak and W. V. Vaidya, “Laser Beam and Friction Stir Welding of Aluminium Alloys: Process-Property-Performance (3P) Relationship”, Laserstrahlfügen: Prozesse, Systeme, Anwendungen, Trends, (Strahltechnik, Band 19), G. Sepold, T. Seefeld, (eds.), BIAS Verlag, Bremen, pp. 225–235, 2002.
[140] M. V. Uz, Project work at TUHH Hamburg-Harburg, “Fracture Behaviour Characterisation of Laser Beam Welded Aluminium Alloy AA6056”, 2004.
[141] Dawes, M. G. S. A. Karger and J. Przydatek, “Fracture Toughness of Friction Stir Welds in 2014A”, 7075 and 5083 Aluminium Alloys”, TWI Report, 77381.01/99/1045.03, TWI, March 2000.
[142] Von Strombeck A., G. Cam, J. F. dos Santos, V. Ventzke and M. Koçak, “A Comparison between Microstructure, Properties and Toughness Behaviour of Power Beam and Friction Stir Welds in Al-alloys”, Aluminium 2001, eds., S. K. Das, J. G. Kaufmann and T. J. Lienert, TMS, pp. 249–264, 2001.
[143] P. Hornet, M. Koçak, S. Hao, B. Petrovski, A. Cornec and K. H. Schwalbe, “CTOD (δ5) estimate on Tension Loaded Wide Plates by Using the Engineering Treatment Model (ETM)”, DVM-Arbeitskreis “Bruchvorgänge”, 26. Vortragsveranstaltung, Magdeburg, F.R.G., 22–23. 02 1994.
[144] P. C. Paris and F. Erdogan, “A Critical Analysis of Crack Propagation Laws”, Journal of Basic Engineering, Vol. 85, pp. 528–534, 1960.
[145] V. V. Bolotin, Mechanics of Fatigue, CRC Press LLC, 1999.
[146] F. Bergner, G. Zouhar and G. Tempus, “The Material-dependent Variability of Fatigue Crack Growth Rates of Aluminium Alloys in the Paris Regime”, International Journal of Fatigue, Vol. 23, pp. 383–394, 2001.
[147] D. Radaj, C. M. Sonsino and W. Fricke, “Fatigue Assessment of Welded Joints by Local Approaches”, CRC Press Boca Raton Boston New York Washington, DC, Woodhead Publishing in Materials.
[148] S. Daneshpour, M. Koçak, F. S. Bayraktar, S. Riekehr, “Damage Tolerance Analyses of Laser Welded “Skin-Clip” Joints for Aerospace Applications”, to be published at IIW, Doc. X -1643- 08 / Doc. XIII – 2239 – 08, 2008.

RESUME

Personal Information

Name:	Funda Seniz Bayraktar
Date of Birth:	22 November 1972
Nationality:	German
Marital Status:	Married
e-mail address:	funda.bayraktar@t-online.de
Tel No:	+49 (0) 174 476 30 29
Contact address:	Am Büchenbergskamp 3, 21039 Börnsen, Germany

Education and Employment Summary

8/2011 – Present: Stress Engineer – EADCO European Aerospace Design Consultants, on behalf of Premium Aerotec GmbH, Hamburg, Germany

4/2008 –11/2011: PhD. Study – Technical University Hamburg Harburg, Germany

3/2010 – 07/2011: Fatigue and Damage Tolerance Engineer – STEGMANN Aircraft Maintenance GmbH, on behalf of AIRBUS Operations GmbH, Bremen, Germany

3/2008 – 2/2010 Researcher – GKSS Research Centre, Germany – Institute of Materials Research – Materials Mechanics Section – Joining and Assessment Department

3/2005 – 3/2008 Researcher – GKSS Research Centre, Germany – Institute of Materials Research – Neutron and Synchrotron Scattering – Structure Research for New Materials Department

1/1996 – 2/2002: Process Engineer – ORS Middle East Bearing Industry, Turkey

10/1994 – 1/1998: Master of Science Degree

Metallurgical and Materials Engineering Department

Middle East Technical University (METU), Ankara –Turkey

10/1989 – 7/1994: Bachelor of Science Degree

Metallurgical Engineering Department

Middle East Technical University (METU), Ankara –Turkey

9/1978 – 6/1989: First, secondary and high school education, Ankara – Turkey